J. Bangladesh Acad. Sci. Volume 50, Issue 1, March 2026

ISSN 2224-7270 (Online), 0378-8121 (Print)

Journal of Bangladesh Academy of Sciences is published four times a year (March, June, September and December comprising one volume) in English. Original research articles, review articles, and short communications of all branches of Science and Technology are considered for publication in this journal. Review articles are generally by invitation.

Disclaimer

The opinions, analysis and conclusions expressed or implied in this journal are those of the authors and do not represent the views of Bangladesh Academy of Sciences.

Submission

All correspondence regarding contributions for publication in the journal should be addressed to the *Editor, Journal of Bangladesh Academy of Sciences* <jbas.editor@yahoo.com>. Authors should consult the contributor's guideline at the back of the journal before submitting their manuscripts.

Published by

Bangladesh Academy of Sciences, National Science and Technology Complex, Agargaon, Dhaka-1207.

Design and Printed by

Sucharu Desktop Publishing, 1/E/1, Paribagh, Dhaka-1000, Bangladesh

Annual Subscription: Tk. 500.00 (Bangladesh); US $ 60.00; £ 21.50 plus postage.

Single Copy: Tk. 250.00 (Bangladesh); US $ 30.00; £ 11.25 plus postage.

Obituary

Dr. Kazi M. Badruddoza
(1927-2023)

Dr. Kazi M. Badruddoza was born on first January 1927 in the village of Toldanga Gobindragonj, district Giabandha. His father was Kazi Badiuzzaman and mother Jamila Khatun.

Dr. Kazi M. Badruddoza has a illustrious professional career. He completed Bachelor of Agriculture degree from Bengal Agriculture Institute in 1948, now Sher-e-Bangla Agricultural University. Master of Agriculture degree from Dhaka University in 1952. After doing PhD from Louisiana State University of USA in 1956, Dr. Badruddoza did post doctoral research in genetics from Lund University of Sweden and gained advanced knowledge in plant breeding and genetics. After graduation from Bengal Agriculture Institute, he started his career as Research Assistant at the Agricultural Research Laboratory in Pakistan. He held many executive positions, such as Executive Director, Pakistan Agricultural Research Council, Executive Vice-Chairman, Bangladesh Agricultural Research Council, Founding Director, Bangladesh Agricultural Research Institute (BARI), Chief Research Advisor, Government of Vietnam etc. He initiated corn (maize) improvement research in 1950s and introduced wheat production in Bangladesh.

Dr. Badruddoza has established Bangladesh Agricultural Research Institute (BARI), a multi-crop research institute with several regional stations in 1976 and had been its founder Director. Subsequently, he strengthened and reorganized Bangladesh Agricultural Research Council (1983-84) as an apex body for agricultural research in Bangladesh. He contributed to reorganization and establishment of National Agricultural Research System (NARS) encompassing all agriculture sub-sectors. He has also contributed in establishing the Postgraduate Studies in Agriculture (IPSA) in 1983 which eventually developed into Agricultural University. He has largely contributed in developing research infrastructures to facilitate generation of improved technologies Bangladesh has now the proud of achieving self-sufficiency in agricultural production.

Dr. Badruddoza contributed in reorganizing and strengthening of Pakistan Agricultural Research Council (1960-1970) and Strengthening of the Council of Agricultural Science and Technology in Vietnam (1985-1988) and Institute of Genetics Research in Hanoi, Vietnam in 1985.

He played significant roles as member of the Agricultural Resource Coordination Board of Pakistan (1964-1971), Member of the central Cotton Committee of Pakistan (1968), Member of the Pakistan American Joint Agricultural Evaluation Team (1968), Member of the Board of Governors, Bangladesh Rice research Institute (1974-1985), Member of the Advisory Board of the Bangladesh Atomic Energy Commission (1080-1984). Dr. Badruddoza has numerous publications in many national and international Journals.

In addition, he wrote many books, book chapters, reports and prepared many national policy papers in agriculture.

Significant Award/Honor Received:

In recognition of professional accomplishments and glorious contributions in agricultural research and development, Dr. Badruddoza was adorned with many prestigious national and international awards and honor. Followings are the important awards and honor he received:

Tamgha-e-Imtiaz(TI) and *Tamgha-e-Pakistan* (TP) national awards from the Government of Pakistan in 1968 and 1969; Zebunnesa-Kazi Mahbubullah Gold Medal in 1982; Made Scientist Emeritus for the National Agricultural Research System (NARS) by the Government of Bangladesh in 1985; Certificate of appreciation by the Government of the United States of America in 1985 for decades of leadership of Dr. Badruddoza to BARC and the NARS in Bangladesh; Krishibid Institution Gold Medal in 1991; D.Sc. (Honoris Causa) degree by the Viswa Unnyayan Samsad, Independence Award (2012), the highest level national award by the Government of Bangladesh; and Channel i-Standard Chartered Bank Agro Award 2020 for lifetime achievement in agricultural research and development. Besides, he also received awards and honor from Bangladesh Horticulture Society, DeshBandhu Chittaranjan Das Research Council, Plant Breeding and Genetic Society of Bangladesh, Abu Hossain Sarker Memorial Trust, Bangladesh Academy of Agriculture, Dr. M.O. Gani Memorial Gold Medal by Bangladesh Academy Sciences and Research Development Foundation.

Dr. Badruddoza had been and has been a Fellow/member of numerous national and international prestigious professional bodies and societies in many of which he served and is serving as chairman, coordinator and other roles. He was the founder member of Regional Co-ordination Center for Research and Development of Coarse Grains, Pulses, Roots and Tuber Crops (CGPRT), in the Humid Tropics of Asia and the Pacific, Bogor, Indonesia; Founder Trustee, International Services for National Agricultural Research (ISNAR,), Hague, Netherlands, (1979-1984); member, Advisory Committee of Tropical Products Institute (TPI), London (1977-1979); member, International Federation for Agricultural Research and Development (IFARD); member, Consultation Group of Agricultural Information Bank Asia (AIBA); member of the Task Force constituted by the Consultative Group on International Agricultural Research (CGIAR); and member, Quinquennial Review Team of the International Rice Research Institute (IRRI), Manila, Philippines (1987). He was the first Chairman of the Agricultural Group of the South Asian Association for Regional Cooperation (SAARC).

At home, he was the President, Bangladesh Association for the Advancement of Science; Chairman, Bangladesh Milk Producers Co-operative Union Ltd (Milk-Vita); Director, Board of Management, Bangladesh Bank; Chairman, International Life sciences Institute, Bangladesh; Member of the Syndicates/Senates of the major Universities of Bangladesh; and currently, is the President of Bangladesh Academy of Agriculture and Fellow of Bangladesh Academy of Sciences.

Dr. Kazi M. Badruddoza passed away on 30 August, 2023 at his Uttara residence in Dhaka. May Allah (SWT), the most Merciful, grant him Zannatul Ferdous. Ameen.

- Zahurul Karim

J. Bangladesh Acad. Sci. 47(2); 139-154: December 2023 DOI:https://doi.org/10.3329/jbas.v47i2.67992

Journal of Bangladesh Academy of Sciences

Journal homepage: http://www.bas.org.bd/publications/jbas.html

Review Article

Ethnomedicinal uses, phytochemistry, pharmacology and toxicological aspects of genus *Wendlandia*: an overview

Md. Jamal Hossain, Fahamida Maliha, Md. Bappy Hawlader, Mamtaz Farzana[1] and Mohammad A. Rashid[1*]

Department of Pharmacy, School of Pharmaceutical Sceinces, State University of Bangladesh, Dhanmondi, Dhaka, Bangladesh

ARTICLE INFO

Article History

Received: 13 June 2023
Revised: 10 October 2023
Accepted: 18 October 2023

Keywords: *Wendlandia*, Phytoconstituents, Ethnomedicinal, Antioxidant, Food supplement.

ABSTRACT

The genus *Wendlandia* includes around 70 species and is native to southeast Asia, northeast Africa, China, Australia, and Turkey. Mnay plant species of this genus have ethnomedicinal properties, which are used to deal various health complications, including dysentery, severe fever, cough, diabetes, hypertension, hyperlipidemia, constipation, and inflammation. This review sought to summarize details on the ethnomedicinal uses, phytochemical composition, safety aspects, and toxicology of *Wendlandia* species. Additionally, it covered the nomenclature, distribution, taxonomy, and botanical characteristics of this genus. Several electronic databases were used to retrieve the information, including Google Scholar, PubMed, Web of Science, Scopus, Science Direct, and Springer Link. The Plant List (www.theplantlist.org) was used for taxonomical authentications. SciFinder and PubChem were utilized for the verification of chemical structures and IUPAC (International Union of Pure and Applied Chemistry) name of the compounds. Numerous examinations of chemical constituents of the *Wendlandia* genus have identified approximately 60 essential plant compounds, such as iridoid glycosides, flavonoids, flavonoid glycosides, carotenoids, and triterpenes. Various research studies have showcased the therapeutic potential of *Wendlandia* species, highlighting their abilities in treating diabetes, combating oxidation, reducing inflammation, fighting microbes, lowering blood pressure, and potentially hindering cancer growth. The significance of *Wendlandia* in traditional medicine systems and its role as a valuable origin of impactful natural compounds are evident. This review provided scientific basis for future endeavors, including chemical investigations into already studied species and other less studied species of *Wendlandia* for finding future lead compounds.

Introduction

Currently, approximately 350,000 vascular plant species and 325,000 flowering plant species exist worldwide. However, only a tiny fraction, precisely 25,791 plants, less than 8% of the total, have been formally studied for their potential therapeutic uses (Antonelli et al., 2020). It is important to note that medicinal plants contain diverse bioactive phytochemicals, which can serve as valuable foundations for creating innovative medications (Bari et al., 2021). In recent times, synthetic chemical sources have taken over the pharmaceutical sector, and thus, the consumption of chemicals is rising at an alarming rate (Brishty et al., 2021). For ameliorating one disease, maybe today's functional chemical analog can create a dormant home for tomorrow's unknown illness. To escape this problem, using

*Corresponding author:<arpharm64@du.ac.bd>

[1]*Department of Pharmaceutical Chemistry, Faculty of Pharmacy, University of Dhaka, Dhaka, Bangladesh*

herbal medicine is a better choice. Herbal drugs derived from plant sources are being tremendously exploited to deal with various human diseases (Maryam et al., 2018; Rashid et al., 2023; Mitra et al., 2022). The genus *Wendlandia* is such an exclusive source of phytochemical value. This genus belongs to a widely distributed tropical family called Rubiaceae, encompassing around 13,200 species spread across 615 different genera. *Wendlandia* has different life forms: trees, shrubs, and herbaceous plants with annual and perennial life cycles (Xie et al., 2010). Approximately 50-70 species of this genus are located in the Indo-Malayan region (Choze et al., 2010). In the past, various mountain communities noticed that by using traditional medicinal practices, plants could effectively treat conditions such as ulcers, dysentery, athlete's foot, diabetes, whooping cough, bronchitis, asthma, migraines, and more. Further, researchers have an extensive focus on this genus. Some species of this genus *Wendlandia* are of miraculous importance and are used in the treatment of snake bites, scorpion stings, regulation of menses, securing the birth of male children, diarrhea and intestinal parasites, hypertension, cardiovascular dysfunctions, mental disturbs and alimentary disorders (Sindhe et al., 2015).

Wendlandia has bioactive molecules and the presence of diversified phytoconstituents such as; Ixoxide, Iridoid glycosides, diphenylpicrylhydrazyl (DPPH), hydroxyl radical, flavonoid, terpenes, triterpenes, beta carotene, lycopene, caffeic acid, rutin, procyanidin, catechin, myricyl stearate, stearic acid, D-mannitol, b -sitosterol, stigmasterol, and geniposidic acid etc. make this genus a tremendous medicinal value (Raju et al., 2014; Dinda et al., 2011; Inouye et al., 1988). These phytochemical molecules give a large variety of pharmacological activities like antimicrobial, antioxidant, antidiabetic, anticancer, anti-inflammatory, analgesic, antinociceptive, anti-asthmatic, insecticidal, and anti-mutagenic activity (Sindhe et al., 2015).

Considering the various activities of the genus *Wendlandia*, this review aimed to provide a comprehensive profile of the genus *Wendlandia*, focusing on its traditional uses, phytochemistry, pharmacological and toxicological properties.

Methodology

To acquire evidence for this review, we did a thorough literature search utilizing the Google Scholar and PubMed databases. The leading search terms were "*Wendlandia*," "*Wendlandia* species," "ethnopharmacology," "ethnobotany," "chemical constituents," "phytoconstituents," "biological activity," "pharmacological activity," "toxicology," and "safety." We also used additional academic platforms such as Google Scholar, PubMed, Web of Science, Scopus, Science Direct, and Springer Link to get the essential information. During the compilation and synthesis of material, the downloaded papers were thoroughly examined to determine the legitimacy and usefulness of their data. Information gathered from the chosen articles encompassed the names of reported plant species, the specific parts of plants examined, isolated phytochemicals from these species, pharmacological studies on each plant extract, the kinds of experiments conducted, the dosage or concentration used in these experiments, and relevant details on toxicity studies. The material retrieved was classified and reported in detail for each category. To authenticate the identity of the Gynura species mentioned in this review, the Plant List (ww.theplantlist.org) was employed. ChemDraw Ultra 7.0 was used to draw all the chemical structures, which were validated using SciFinder and PubChem.

Taxonomy and Distribution

Wendlandia genus comprises approximately 50-70 species, ranging from south-east Asia to north-east Africa, China, Australia and Turkey. Some representative species are shown in the Fig. 1. It is under the rubiaceae family, rubiaceae is the fourth largest angiosperm family in the world. Rubiaceae plants typically stand out due to their simple, opposite, or whorled leaves, paired interpetiolar stipules, and an ovary situated inferiorly (Ranjan and

Kumar, 2015). Schumann (1891) was the first to suggest the intragenic categorization of *Wendlandia*. He divided the genus into two sets based on the varying lengths of its species. This division failed to reflect the true relationship of the species of *Wendlandia*. Furthermore, Cowan (1932) divided *Wendlandia* by the characters of stigma, stamens and the feature of the stipules. The genus *Wendlandia* is popular in the hilly regions among the tribes of tropical & sub-tropical areas. As it is a forestry flowering plant, its culinary and medicinal uses make this genus significant from the Rubiaceae family (Choze et al., 2010). The scientific name, synonyms and distribution of the species have already been established with different previously accepted name within the genus. Notably, the original author names, original publication resources, accepted or synonymous plant name and the International Plant

Name Index (IPNI) identifier by the plant list (www.theplantlist.org). Raju et al., (2012) reported its tubular flower, evergreen woody trees protect the hilly soil from erosion and similarly useful for pollination by a wide array of pollinators including butterflies, beees, flies, wasps, moth etc (Xie et al., 2010). Because of the similarity of some species of *Wendlandia* like *Wendlandia formosana* is closely related to some phytoconstituents derived from *Angustifolia* (Choze et al., 2010). The complete taxonomical classification of the genus is given below:

Kingdom	**Plantae**
Subkingdom	**Viridiplantae**
Infrakingdom	**Streptophyta**
Division	**Embryophyta**
Subdivision	**Tracheophyta**
Division	**Spermatophytina**
Order	**Gentianales**
Family	**Rubiaceae**
Subfamily	**Ixoroideae**
Tribe	**Gardenieae**
Genus	***Wendlandia***

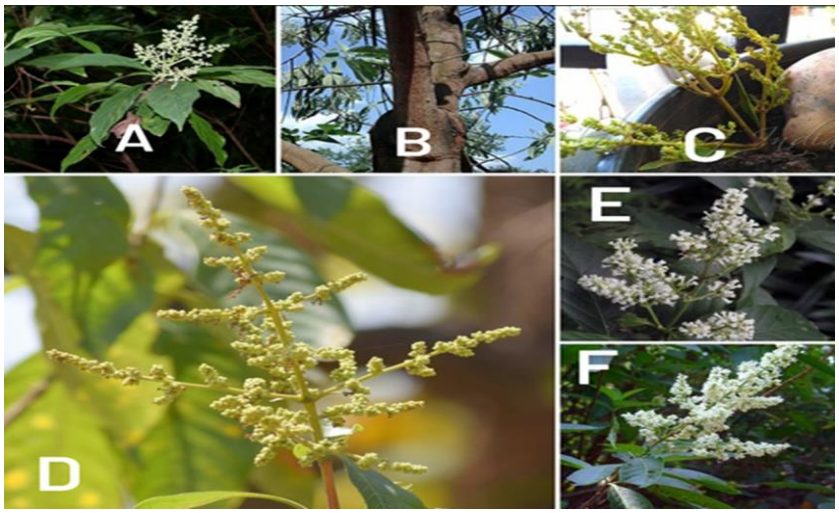

Fig. 1. (A) Wendlandia formosana, (B) Wendlandia heynei (C) Wendlandia glabrata (D) Wendlandia tinctoria (E) Wendlandia wallachii (F) Wendlandia thyrosoidea.

Ethnomedicinal Uses

Several *Wendlandia* species have a long history of use in traditional ethnomedicine to treat a range of ailment in India, Pakistan, Australia, Srilanka, Bangladesh, Japan, China, Turkey and the Southeast Asian regions including Vietnam, Malaysia, Thailand. A brief description about *Wendlandia* species and its reported activity is given below:

Wendlandia heyenei: The Rubiaceae family plant *W. heynei* (Schult.) Santapau and Merchant, popularly known as "Ukan Pansara," is abundantly spread in Rawalpindi, Kahuta, Panjar district, Pakistan (Maryam et al., 2018). Local populations utilize this plant to cure ulcers, swellings, wounds, diarrhoea, fever, urinary problems, skin illnesses, colds and coughs, and body pains (Khatoon and Irshad, 2016). The tree's fruits and barks are used to cure piles (Rawat et al., 2009). Furuncles and urinary diseases are treated with a bark paste. The powdered leaf extract has wound-healing effects, and the leaves and fruits' decoction are effective in amenorrhea, as an antispasmodic, and as a febrifuge (Ajaib et al., 2018). Its roots are utilized as an antidote to snake bite (Murthy et al., 1986). In India, *W. heynei's* bark is used to treat colds and high fevers.

Wendlandia exserta: *W. exserta* Roxb. DC., a member of the Rubiaceae family known regionally as chila/ratela/tikli, is widely distributed in the sub-Himalayan region, particularly in areas prone to landslides. It serves as a valuable source of fuelwood and yields small timber. This plant can potentially cover expansive areas, especially in regions susceptible to soil erosion (Dhiman and Gupta, 2009). The bark displays a reddish-brown hue. Its leathery leaves are arranged oppositely, broadly oval or lanceolate. The flowers, which are white and minute, grow in sessile clusters at the apex, forming pyramidal structures around 25cm long (Praveen et al., 2007). The leaves and fruit decoctions of Wendlandia exserta are utilized in treating conditions like amenorrhea, fever, spasms, and skin ailments such as eczema and scabies. Moreover, the flowers possess properties beneficial for purifying blood and are employed in managing joint infections (Shahzadi et al., 2018)

Wendlandia glabrata: Young sprouts of *Wendlandia glabrata* DC are used as functional foods in India's north-eastern region. This blooming plant from the Rubiaceae family is used to make the traditional salad Singju. The plant has qualities such as lowering obesity and managing blood sugar. It is also used to treat dysentery in addition to serving as an expectorant (Meetei and Singh, 2007). In hepatocytes and myoblast cells, extracts of *W. glabrata* suppress G-6-Pase and glucose absorption. This study revealed procyanidin A2 (PCA2) as a powerful anti-diabetic drug with significant aglucosidase inhibition. It has been shown that PCA2 lowers the amount of G-6-Pase protein and mRNA in diabetic mice while increasing glucose absorption in CC1 hepatocytes and C2 C12 myoblast cells (Sheikh et al., 2019). The fraction extracted from *W. glabrata*, rich in novel iridoid compounds, exhibited noteworthy potential in reducing blood glucose levels. It also effectively prevented hepatic gluconeogenesis conditions by significantly increasing the phosphorylation of AMP-activated protein kinase (AMPK) by approximately 1.4 to 1.7 times and downregulated key enzymes involved in gluconeogenesis, such as glucose-6-phosphatase (G6Pase) and phosphoenolpyruvate carboxykinase (PEPCK) (Sarma et al., 2022).

Wendlandia paniculata: *Wendlandia paniculata* (Roxb.) DC is an exceedingly uncommon species in Bangladesh, utilised by the Chakmas tribe in mountains regions. It is commonly used as a treatment for chest pain by rubbing the crushed leaves on the chest. The plant family Rubiaceae encompasses the flowering plant genus *Wendlanda*, distributed across regions spanning from tropical and subtropical Asia to Queensland and the northern parts of Africa. According to Hasan et al., 2021, these plants could serve as a promising source for hypoglycemic medications and possess anthelmintic properties, given the historical use of various plants and plant-derived substances in diabetes treatment. Herbs having hypoglycemic qualities promote insulin

release, enhance glucose uptake by adipose or muscle tissues, and inhibit glucose absorption from the digestive tract as well as hepatic glucose synthesis (Hui et al., 2009). Acute, chronic, visceral, inflammatory, and neuropathic pain are all possible (Masuda et al., 2017; Tamba et al., 2013). A quarter of all Americans, for example, suffer from chronic discomfort. With these numbers in its favour, pain has emerged as a global health problem and the leading cause of disability globally (Gedin et al., 2017).

Plants have long been used as analgesic agents in folk medicine (Ullah et al., 2015; Ayaz et al., 2016). The search for new bioactive molecules with analgesic effects in medicinal plants is intensifying. Diarrhoea is defined as a gastrointestinal disorder characterised by a rapid flow of gastric material through the gastrointestinal tract, leading to abnormal and frequent semi-solid or watery faecal discharge that occurs on average three times per day (Yakubu and Salimon, 2015; Vickers, 2017; Singh et al., 2012). Enteric pathogenic bacteria such as *Salmonella typhi*, *Shigella flexneri*, *Escherichia coli*, *Staphylococcus aureus*, *Vibrio cholerae*, and *Candida albicans* are common causes of diarrhoea in humans (Akinboro et al., 2007; Kitaoka et al., 2011).

Wendlandia tinctori: *Wendlandia tinctoria* var. *grandis* (Roxb.) DC. is a flowering plant that exhibits characteristics of both evergreen and deciduous plants. In the summer season, *W. tinctoria* plays a vital role by providing butterflies with an important nectar supply and serving as a pollen source for honey bees. *W. tinctoria* is commonly used by tribal communities to treat snakebite. It is also utilized to alleviate cramps in cholera patients. Previous research found that the stem of *W. tinctoria* contains stearic acid, geniposidic acid, d-mannitol, -sitosterol, myricyl stearate, and stigmasterol. According to earlier findings, the root of W. tinctoria contains a variety of iridoid glucosides, including 5-dehydro-8-epi-mussaenoside, 5-dehydro-8-epi-adoxosidic acid, wendoside, 8-epi-mussaenoside, and 10-O-dihydro feruloyldeacetyldaphylloside (Dinda et al., 2006; Dinda et al., 2011). Farzana et al. (2022) recently conducted a study where they identified a total of eight phenolic compounds in W. tinctoria. These compounds include liquiritigenin (1), naringenin (2), apigenin (3), kaempferol (4), glabridin (5), ferulic acid (6), 4-hydroxybenzoic acid (7), and 4-hydroxybenzaldehyde (8). Additionally, the study demonstrated that the stem extract of this plant species has antioxidant, hypoglycemic, and antidiarrheal properties (Farzana et al., 2022). The individual ethnomedicinal uses of the main *Wendlandia* species are summarized in Table 1.

Iridoid Glycoside

Iridoids are cyclopentanopyran-like monoterpenoids that exist in a broad range of animals and plants. They are generated biosynthetically from 8-oxogeranial. Iridoids are most often found in plants as glycosides, most of which are linked to glucose (Tundis et al., 2008). It has been regarded as defense chemicals against pathogens. Majority of *Wendlandia* species contain iridoid glycoside. From *Wendlandia formosana* this iridoid glycosides are elucidated Methyl deacetyl asperulosidate, 10-O-caffeoyl scandoside methyl ester, 6-methoxy scandoside methyl ester, 10-O-caffeoyl deacetyl dephylloside, 6-beta methoxy geniposide, 6-beta hydroxyl geniposide (Raju et al., 2011). In 2006 and 2011, Dinda et al. depicted the following compounds like: 8-epi-deoxyloganic acid, Deacetyl – daphylloside, Caffeoylmussaenosidic acid, Caffeoylmussaenosidic acid hexaacetate, Ixoside, Ixoside tetraacetate, 5-Dehydro-8-epi-adoxasidic Acid pentaacetate, 8-epi-mussaenoside, 8-epi-mussaenoside tetraacetate, 5-dehydro-8-epi-mussaenoside, 5-dehydro-8-epi-mussaenoside tetraacetate, 10-O-Dihydroferuloyldeaxetyldaphylloside, 10-O-

Table 1. General information, taxonomical distribution and ethnomedicinal uses of Genus *Wendlandia.*

Species (Accepted Name)	Synonyms	Plant Part Used	Geographical Locations	Ethnomedicinal Uses	References
Wendlandia paniculata (Roxb.) DC.	*Gardenia* burha Buch. -Ham. ex Wall. *Rondeletia paniculata* Roxb. *Wendlandia paniculata* var. genuina Valeton	Leaves	Northwestern Vietnam, western Africa, Southeast Asia, subtropical countries of East Asia and northern Australia.	Anti-diabetic property, anti-diarrheal effect, antinociceptive activity	Hasan et al., 2021
Wendlandia formosana Cowan	*Wendlandia formosana* subsp. *formosana*	Leaves, stem bark & wood	Indo Malayan region to China	Antioxidant, analgesic property	Delprete, 1999
Wendlandia tinctoria (Roxb.) DC.	*Wendlandia tinctoria* subsp. *Callitricha* (Cowan) W.C. Chen *Wendlandia tinctoria* subsp. *Floribunda* (Craib) Cowan *Wendlandia tinctoria* subsp. *Handelii* Cowan *Wendlandia tinctoria* subsp. *Intermedia* (F.C.How) W.C.Chen *Wendlandia tinctoria* subsp. *Orientalis* Cowan *Wendlandia tinctoria* var. *grandis* (Roxb.) DC.	Stem, root and bark	North-eastern states of India	Antidote to snakebite, antibacterial activity, antioxidant, hypoglycemic, and antidiarrheal properties	Raju et al., 2014; Farzana et al., 2022
Wendlandia glabrata DC.	*Rhombospora sumatrana* (Miq.) Miq. *Wendlandia glabrata* var. *glabrata* *Wendlandia sumatrana* Miq. *Wendlandia tenuiflora* Miq. Ex Hook.f.	Tender shoot	North-eastern states of India	Anti-hypoglycemic activity, reduce obesity, anti-diarrheal effect used in dysentery, act as expectorant	Sheikh et al., 2019
Wendlandia heynei (Schult). Santapau and Merchant	*Rodeletia cinerea* Wall. *Rodeletia exserta* Roxb. *Rodeletia heynei* Schult. *Rodeletia orissensis* Roth *Rodeletia thyrsiflora* Roth *Wendlanida cinerea* DC. *Wendlandia exserta* (Roxb.) DC.	Bark, leaves, root	Panjar, Kahuta, Rawalpindi district, Pakistan	Treatment of piles, furuncles, urinary infections, amenorrhea, febrifuge, antispasmodic activity, antioxidant, anti-inflammatory activity, antidote to snake bite, used in cold & high fever	Maryam et al., 2018
Wendlandia ligutroides (Boiss. & Hohen.) Blakelock	*Sestina kotschyi* (Boiss. & Hohen.) Chiov. *Sestina ligustroides* Boiss. & Hohen *Wendlandia Kotschyi* Boiss. & Hohen.	aerial parts (stems, leaves, and flowers)	North Iraq, Turkey	Antiprotozoal activity	Çalış et al., 2020
Wendlandia thyrosoidea (Roth) Steud.	*Canthium thyrsoidea* Roem. & Schult. *Canthium thyrsoideum* Schult. *Cupia thyrsoidea (Roth)* DC. *Ixora montana* Miq. ex Hook. f *Webera thyrsoidea* Roth *Wendlandia lawii* Hook.f. *Wendlandia montana* K. Schum. *Wendlandia notoniana* Wall. ex Wright & Arn. *Wendlandia thyrsoidea* var. lawii (Hook.f.) Cowan	Leaves	Central Western Ghats region of Chikkamagaluru, Karnataka, India	Antimicrobial, analgesic property	Vinu et al., 2021
Wendlandia wallichii (Wight and Arn)	*Wendlandia wallachii* var. *wallachii*	Leaves	North-eastern region in tropical Africa and Asia	Fat and fiber content used as common vegetable. Decrease the risk of constipation, lower diabetes, serum cholesterol level, heart diseases, breast and colon cancer, hypertension etc. High protein source used as a dietary element.	Chaudhuri et al., 2018
Wendlandia bicuspudata Wight & Arn	*Wendlandia notoniana* var. *bicuspudata* (Wight & Arn.) Hook.f. *Wendlandia notoniana* var. *zeylanica* Hook.f.	Wood	Hilly regions of Srilanka	Antioxidant activity	De Silva et al., 1987
Wendlandia exerta (Roxb.) DC.	Not available	Leaves	Pakistan Nepal, Indian	Antibacterial, anti-fungal, analgesic activity	Ajaib et al., 2018

Table 2. Phytoconstituents of Genus *Wendlandia*

Comp. No	Phytochemical class	Compounds	Sources	Plant part	Reference
1	Iridoid glycoside	Scandoside methyl ester	*W. formosana*, *W. bicuspudata* *W. ligustroides*	Stem, leaves & flowers	De silva et al., 1987, Moreina et al., 2010
2	Iridoid glycoside	Methyl deacetyl asperulosidate	*W. formosana*	Leaves	Raju et al., 2011
3	Iridoid glycoside	10-O-caffeoyl scandoside methyl ester	*W. formosana*, *W. tinctoria*	Leaves	Raju et al., 2011
4	Iridoid glycoside	6-methoxy scandoside methyl ester	*W. formosana*	Leaves	Raju et al., 2011
5	Iridoid glycoside	10-O-caffeoyl deacetyl dephylloside	*W. formosana*	Leaves	Raju et al., 2011
6	Diterpene alkaloid	Phytol	*W. formosana*	Leaves	Massey and Burton, 1990
7	Pentacyclic triterpenoid	Ursolic acid	*W. formosana*	Leaves	Raju et al., 2014
8	Iridoid glycoside	Gardenoside	*W. formosana* *W. ligustroides*	Stem, leaves & flowers	Inouye et al., 1988
9	Iridoid glycoside	Geniposidic Acid	*W. formosana*, *W. ligustroides*	Stem, leaves & flowers	Çalış et al., 2020; Tzakon et al., 2007
10	Iridoid glycoside	10-Deoxyloganic acid	*W. formosana*, *W. ligustroides*	Stem, leaves & flowers	Inoue et al., 1992; Takeda et al., 1996
11	Iridoid glycoside	6-beta methoxy geniposide	*W. formosana*, *W. ligustroides*	Stem, leaves & flowers	Raju et al., 2014
12	Iridoid glycoside	6-beta hydroxyl geniposide	*W. formosana*, *W. ligustroides*	Stem, leaves & flowers	Raju et al., 2014
13	Flavonoid glycoside	Rutin	*W. heynei*	Leaves	Maryam et al., 2018
14	Polyphenolic flavonoid	Catechin	*W. heynei*	Leaves	Maryam et al., 2018
15	Prsotacyanidin flavonoid	Procyanidin A2	*W. glabrata*	Tender shoot	Sheikh et al., 2019
16	Retinol	Beta carotene	*W. heynei*	Bark & leaves	Maryam et al., 2018
17	Flavonoid	Lycopene	*W. heynei*	Bark & leaves	Maryam et al., 2018
18	Polyphenolic flavonoid	7-Deoxygardoside	*W. formosana*, *W. ligustroides*	Stem, leaves & flowers	Bianco et al., 1986
19	Iridoid glycoside	8-epi-deoxyloganic acid	*W. ligustroides*	Stem, leaves & flowers	Nakamura et al., 2000; Murai et al., 1984; Teng et al., 2005
20	Iridoid glycoside	Deacetyl - daphylloside	*W. ligustroides*	Stem, leaves & flowers	Tzakou et al., 2007
21	Iridoid glycoside	8-epi-deoxyloganic acid deacetyl - daphylloside	*W. ligustroides*	Stem, leaves & flowers	Dinda et al., 2011
22	Iridoid glycoside	Caffeoylmussaenosidic acid	*W. tinctoria*	Stem	Dinda et al., 2011
23	Iridoid glycoside	Caffeoylmussaenosidic acid hexaacetate	*W. tinctoria*	Stem	Dinda et al., 2011
24	Iridoid glycoside	Ixoside	*W. formosana*	Leaves	Dinda et al., 2011
25	Iridoid glycoside	Ixoside tetraacetate	*W. formosana*	Leaves	Dinda et al., 2011
26	Iridoid glycoside	5-Dehydro-8-epi-adoxasidic Acid	*W. tinctoria*	Stem	Inouye et al., 1988
27	Iridoid glycoside	5-Dehydro-8-epi-adoxasidic Acid pentaacetate	*W. tinctoria*	Stem	Dinda et al., 2006
28	Iridoid glycoside	8-epi-mussaenoside	*W. tinctoria*	Stem	Dinda et al., 2006
29	Iridoid glycoside	8-epi-mussaenoside tetraacetate	*W. tinctoria*	Stem	Dinda et al., 2006
30	Iridoid glycoside	5-dehydro-8-epi-mussaenoside	*W. tinctoria*	Stem	Dinda et al., 2006

31	Iridoid glycoside	5-dehydro-8-epi-mussaenoside tetraacetate	*W. tinctoria*	Stem	Dinda et al., 2006
32	Iridoid glycoside	10-O-Dihydroferuloyldeaxetyldaphylloside	*W. tinctoria*	Stem	Dinda et al., 2006
33	Iridoid glycoside	10-O-Dihydroferuloyldeaxetyldaphylloside hexaacetate	*W. tinctoria*	Stem	Dinda et al., 2006
34	Iridoid glycoside	Wendoside	*W. tinctoria*	Stem	Dinda et al., 2006
35	Iridoid glycoside	Wendoside pentaacetate	*W. tinctoria*	Stem	Dinda et al., 2006
36	Iridoid glycoside	Aglucone Wendoside pentaacetate	*W. tinctoria*	Stem	Dinda et al., 2006
37	Iridoid glycoside	10-O-Caffeoyldeacetyldaphylloside	*W. tinctoria*	Stem	Dinda et al., 2006
38	Iridoid glycoside	8-α-dihydrogeniposide	*W. tinctoria*	Stem	Inouye et al., 1988
39	Iridoid glycoside	Semperoside	*W. tinctoria*	Stem	Dinda et al., 2006
40	Iridoid glycoside	10-O-Veratroyleranthemoside	*W. tinctoria*	Root	Dinda et al., 2011
41	Iridoid glycoside	10-O-Veratroyleranthemoside tetraacetate	*W. tinctoria*	Root	Dinda et al., 2011
42	Iridoid glycoside	Eranthemoside	*W. tinctoria*	Root	Dinda et al., 2011
43	Iridoid glycoside	10-O-trans-coumaroyleranthemoside	*W. tinctoria*	Root	Dinda et al., 2011
44	Terpene	Octa acyl lupeols	*W. formosana*	Stem	Delprete, 1999; Raju et al., 2004
45	Terpene	Deca acyl lupeols	*W. formosana*	Stem	Delprete, 1999; Raju et al., 2004
46	Coumarin	Coumarin	*W. formosana*	Stem	Canuto and Silveira, 2006
47	Flavonoid	Scopoletin	*W. formosana*	Stem	Ribeiro and Kaplan, 2002
48	Flavonoid	Kaempferol	*W. formosana*	Stem bark & Wood	Delprete, 1999
49	Flavonoid	Quercetin	*W. formosana*	Stem bark & Wood	Delprete, 1999
50	Flavonoid	Flavonol rutin	*W. formosana*	Stem bark & Wood	Delprete, 1999
51	Flavonoid	Myricitrin	*W. formosana*	Stem bark & Wood	Choze et al., 2010; Delprete, 1999
52	Triterpene	Pentacyclic triterpenes ursolic acid	*W. formosana*	Stem	Delprete, 1999; Raju et al., 2004
53	Phenolic compound	2-Methoxy-4-hydroxy-benzoic acid	*W. formosana*	Stem	Berretta, 2007
54	Flavonoid	Naringenin	*W. formosana*	Stem	Delprete, 1999
55	Iridoid Glycoside	6-O-methyl-Scandoside methyl ester	*W. ligustroides*	Stem, leaves & flowers	Machida et al., 2003
56	Iridoid Glycoside	6-O-methyl deacetyl–daphylloside	*W. ligustroides*	Stem, leaves & flowers	Machida et al., 2003
57	Iridoid Glycoside	Ixoroside	*W. tinctoria*	Stem	Inouye et al., 1988
58	Iridoid Glycoside	Iridodial	*W. tinctoria*	Stem	Inouye et al., 1988
59	Iridoid Glycoside	Gardenosidic acid	*W. tinctoria*	Stem	Inouye et al., 1988
60	Iridoid Glycoside	Ixoside 11-methyl ester	*W. tinctoria*	Stem	Inouye et al., 1988

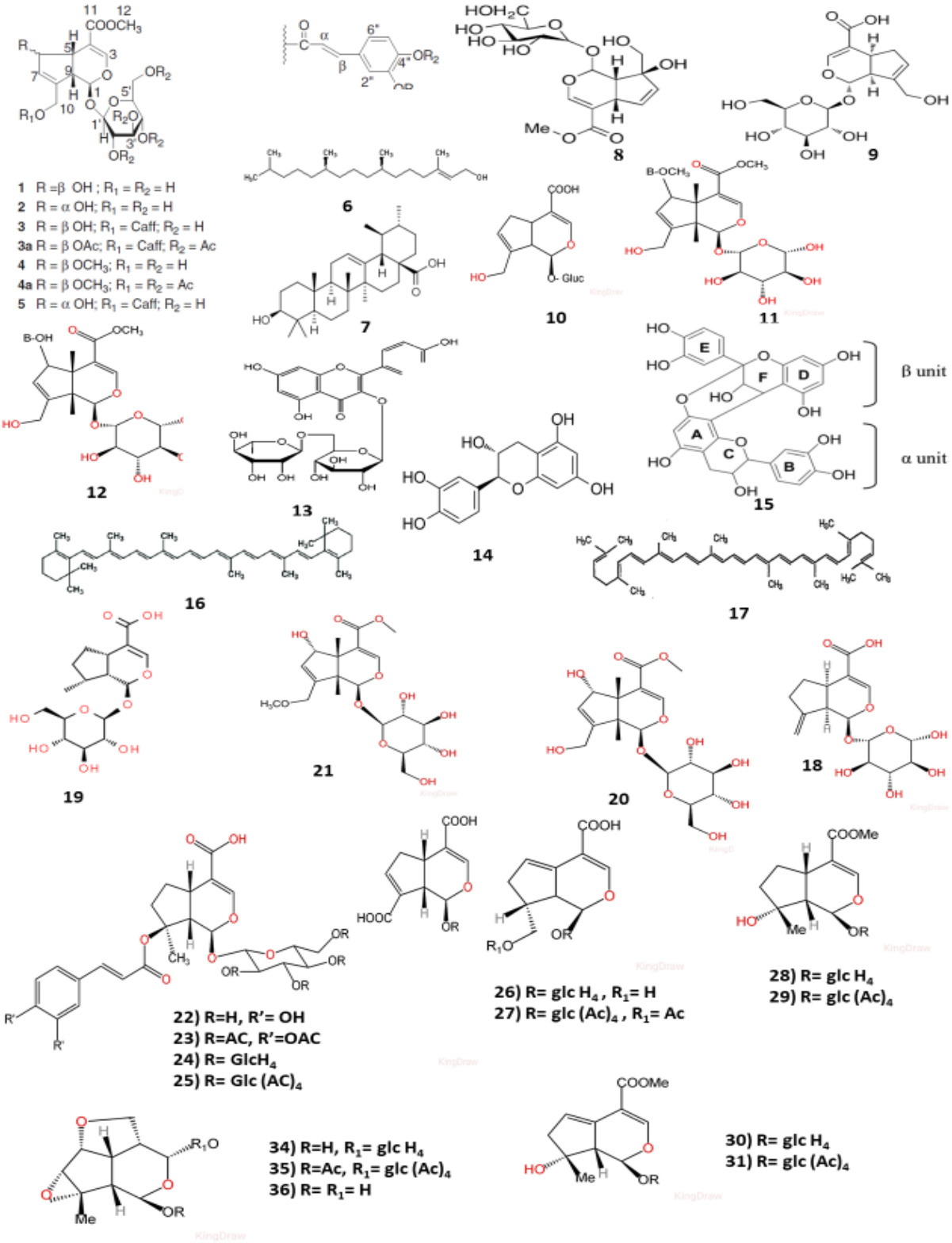

Fig. 2. The chemical structures of 60 phytocompounds of Genus *Wendlandia* listed in Table 2

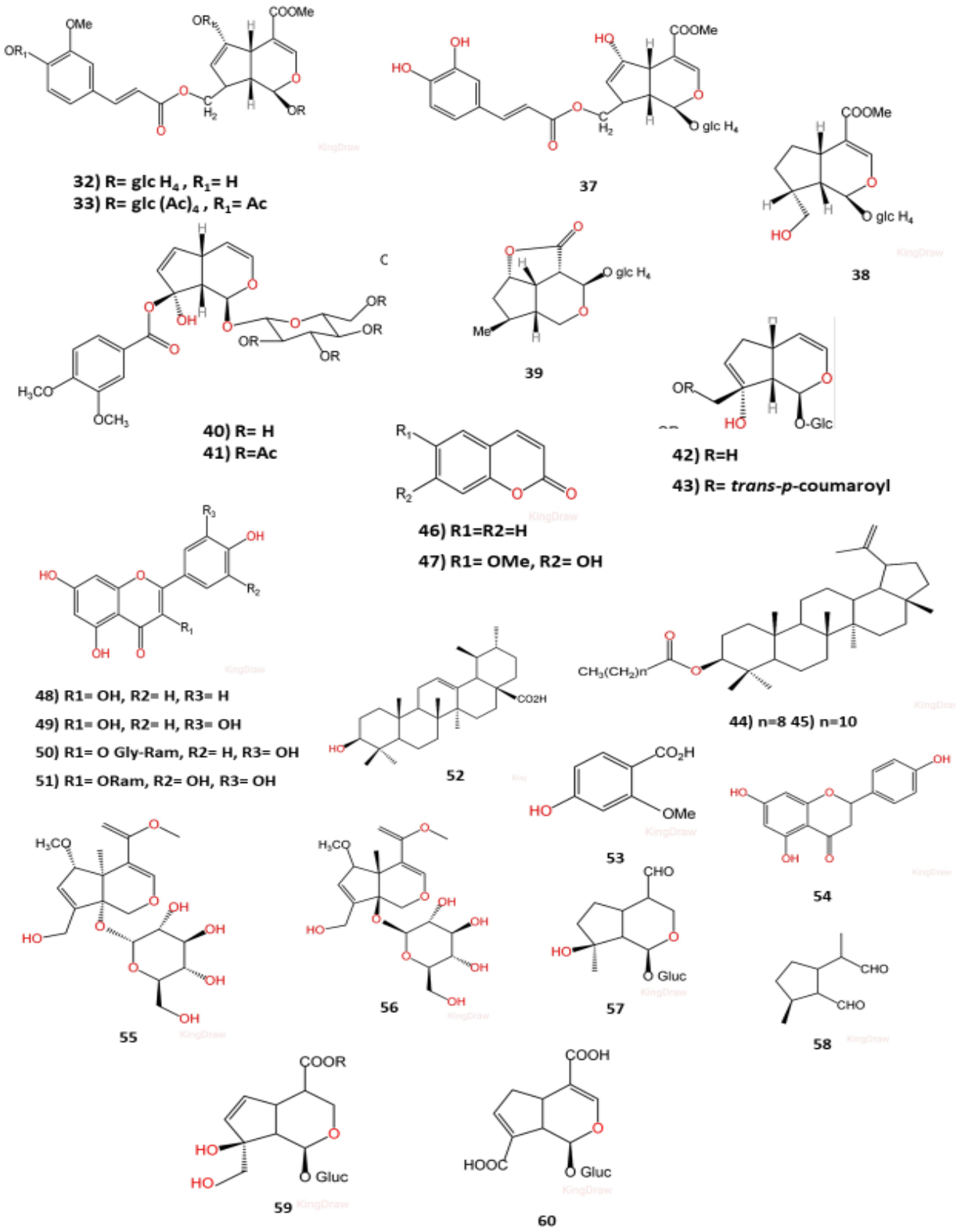

Fig. 2. The chemical structures of 60 phytocompounds of Genus *Wendlandia* listed in Table 2 (Continued)

Dihydroferuloyldeaxetyldaphylloside hexaacetate, Wendoside, Wendoside pentaacetate, Aglucone Wendoside pentaacetate, 10-O-Caffeoyldeacetyldaphylloside, Semperoside, 10-O-Veratroyleranthemoside, 10-O-Veratroyleranthemoside tetraacetate, Eranthemoside, 10-O-trans-coumaroyleranthemoside from *Wendlandia tinctoria* (Dinda et al., 2006; Dinda et al., 2011). Despite the inherent biological capability, the specific molecular mechanisms behind the impactful effects of iridoid glycosides remain unexplained. It is hypothesized that due to the presence of unstable aglycones resembling glutaraldehyde structures and possessing alkylating properties against nucleophilic residues in biomolecules, particularly amino acids, these compounds might induce protein denaturation in the cell wall of pathogens (Dinda et al., 2006; Dinda et al., 2011).

The main pharmacological effects of iridoid glycosides are antioxidant, anti-diabetic, anti-inflammatory, anti-obesity activities. Sheikh et al., (2019) reported α-glucosidase inhibitory activities of the methanol extract of shoots of *Wendlandia glabrata*. Alpha-glucosidase is considered for future lead molecules for type 2 diabetes. *Wendlandia* species have plenty source of α-glucosidase. That is why it has promising potential for postprandial management of DM type 2. Diabetes mellitus stems from irregular sugar metabolism due to insufficient insulin production or the body's resistance to insulin in target organs (Maiti et al., 2004). Despite the recognized therapeutic benefits of fruit-based remedies in traditional medicine for diabetes, developing economically viable natural treatments lags behind modern pharmaceuticals (Wadkar et al., 2008).

Dietary polysaccharides play a crucial role in generating blood glucose (Ghani, 2015). α-glucosidase, a key enzyme, is pivotal in transforming polysaccharides into monosaccharides. Hence, there's a pressing need to create food or herbal solutions and inhibitors that can slow down α-glucosidase activity, thereby managing post-meal blood sugar levels. Additionally, targeting glucose-6-phosphatase (G-6-Pase) holds promise in treating type 2 diabetes. G-6-Pase oversees the final step in generating glucose from gluconeogenesis and glycogenolysis. Studies suggest that reducing blood glucose involves curtailing hepatic glucose production by regulating G-6-Pase. Diabetic animals show elevated protein content and mRNA levels of G-6-Pase, contributing to heightened blood sugar. Therefore, G-6-Pase inhibitors are seen as potential means to lessen hepatic glucose output, making them an appealing therapeutic option for type 2 diabetes treatment.

Flavonoid

Flavonoids, a type of polyphenolic compounds present in plants, are frequently part of human diets. Chemically, they feature a basic structure composed of a 15-carbon skeleton comprising two phenyl rings and a heterocyclic ring (Mitra et al., 2022).

Wendlandia species are flowering plant, their leaves, root juice, flowers contain a rich source of flavonoid. *Wendlandia formosana* has rutin, catechin, procyanidin A2, lycopene, beta carotene, scopoletin, quercetin, myricitrin, naringenin flavonoids. Among these some are polyphenolic flavonoid, flavanone, carotenoids type. Flavonoids are thought to offer health advantages by affecting different cell pathways and acting as antioxidants. Rutin and catechins, among flavonoids, are the prevalent polyphenolic compounds in our diet and are widespread in plants (Spencer, 2008; Maryam et al., 2018; Sheikh et al., 2019; Bianco et al., 1986).

Flavonols, like quercetin, are the primary bioflavonoids and are also present everywhere, albeit in smaller amounts. Flavonoids are widely spread, diverse, and generally less toxic compared to other plant compounds like alkaloids (Eumkeb et al., 2010, Kumar et al., 2010). That is the reason for showing antioxidant and dietary supplement for mankind.

Flavonoids and saponins prevent the creation or release of prostaglandins, autocoids, and contractions caused by spasm-inducing agents, similarly affecting

movement and the release of fluids and electrolytes (Eumkeb et al., 2010, Kumar et al., 2010) while saponins may forestall the arrival of histamine (Wang et al., 2010). Polyphenols and tannins help fortify the lining of the intestines, reducing intestinal leakage, speeding up intestinal transit, and promoting a better equilibrium in water movement across the mucosal cells (Phoem et al., 2013).

Terpene

A terpene molecule is made up of 10 carbon atoms and must have a double bond. Terpene hydrocarbons are sensitive to heat and readily undergo oxidation. This is why citrus oils, rich in terpenes, are prone to these changes. *Wendlandia* have a small range of terpene like phytol, ursolic acid, acyl lupeol found in stem, bark of *Wendlandia formosana.* Ursolic acid is a substance with various chemical, biological, and physiological impacts. With the recent discovery of ursolic acid's anti-inflammation and anti-cancer effects via targeting signal pathways, particularly in preventing breast cancer, ursolic acid has gained attention (Venugopal and Liu, 2012). Ursolic acid is presently being tested on humans to treat cancer, tumors, and wrinkles (Sultana, 2011). Certain terpenes are believed to possess anti-inflammatory, antiseptic, antiviral, and antibacterial qualities. However, the essential oil's impact results from the collective physiological actions of its various components. Specific terpenes might exhibit analgesic effects or serve as stimulants. Some are known to prompt mucous secretion, making them effective decongestants. Throughout history, essential oils have found widespread use in medicinal practices (Nuutinen, 2018)

Toxicological profile

W. heynei methanol extract was found to protect the liver from damage caused by bisphenol A (BPA), suggesting its potential as a supportive treatment for drug-induced liver injury (Maryam et al., 2018). Conversely, a flavonoid called catechin from *W. formosana* was associated with the development of autoantibodies, leading to conditions like haemolytic anaemia and renal failure. This led to the removal of Catergen, a drug containing catechin used for treating viral hepatitis, from the market in 1985 (Mazuz wt al., 2023).

Future Perspective

There are available chemical substances in *Wendlandia* species that have biological properties for lowering serum glucose, controlling lipid profile, skin diseases, and regulating the menstruation cycle. Nowadays, convenient drugs are present in the market, but these drugs produce a wide range of cytotoxic side effects. In this review, *Wendlandia* species showed different phytoconstituents that can be used as drugs and dietary supplements. The presence of flavonoids and glycosides exerts antioxidant, anti-diabetic, and anti-inflammatory activities, making this genus a combined source of safe medicinal value. This review also manifested that screened phytochemicals and isolated compounds will be potential sources of the drug industry in the future to treat multiple diseases if analyzed.

Limitations

There are some limitations of the review. The review did not pay close attention to the stated phytoconstituents of the genus or their detailed mechanisms of action due to lack of enough evidences of exact mechanistic information.

Conclusion

Wendlandia, a genus with a rich traditional medicinal background, exerts diverse biological effects that align with its various therapeutic applications. Among *Wendlandia* species, certain species have broad spectrum of phyto-constituents and other reported as effective pharmacological effect. Behind in depth mechanism align with their pharmacokinetic profile study may be clarified further about it vast pharmacological action. Analyzing the chemicals in these compounds might lead to exciting possibilities for new medicines. Given the global revival of interest in herbal remedies, *Wendlandia* species offer a compelling option for various conditions like

diabetes, obesity, hypertension, inflammation, cancer, menstrual irregularities, skin issues, and related disorders. Moreover, some *Wendlandia* species are utilized as dietary supplements and are considered safe for occasional consumption. However, more research is needed to determine how effective and safe it is to consume these plants long-term.

References

Ajaib M, Ishtiaq S and Siddiqui MF. Comparative analgesic evaluation of *Himalrandia tetrasperma* and *Wendlandia exserta* of family Rubiaceae after induction of pain in mice. *Pak. J. Pharm. Sci*. 2018; 31(6): 2509-2514.

Akinboro A and Bakare AA. Cytotoxic and genotoxic effects of aqueous extracts of five medicinal plants on Allium cepa Linn. *J. Ethnopharmacol.* 2007; 112(3): 470-475.

Antonelli A, Smith RJ, Fry C, Simmonds MS, Kersey PJ, Pritchard HW, Abbo MS, Acedo C, Adams J, Ainsworth AM and Allkin B. *State of the World's Plants and Fungi* (Doctoral dissertation, Royal Botanic Gardens (Kew); Sfumato Foundation). 2020.

Ayaz M, Junaid M, Ullah F, Sadiq A, Subhan F, Khan MA, Ahmad W, Ali G, Imran M and Ahmad S. Molecularly characterized solvent extracts and saponins from Polygonum hydropiper L. show high anti-angiogenic, anti-tumor, brine shrimp, and fibroblast NIH/3T3 cell line cytotoxicity. *Front. Pharmacol.* 2016; 7: 74.

Bari MS, Khandokar L, Haque E, Romano B, Capasso R, Seidel V, Haque MA and Rashid MA. Ethnomedicinal uses, phytochemistry, and biological activities of plants of the genus *Gynura*. *J. Ethnopharmac*. 2021; 271: 113834.

Berretta AA. Fitoterapia como prática integrativa e complementar no SUS. II Semana Farmacêutica do HC. *Ribeirão Preto, Brasil*. 2007.

Bianco A, Passacantilli P, Righi G, Nicoletti M, Serafini M, Garbarino JA and Gambaro V. Iridoids in equatorial and tropical flora. 10. 7-deoxygardoside, a new acid iridoid glucoside from argylia-radiata. *Gazzetta Chimica Italiana*. 1986; 116(2): 67-8.

Brishty SR, Hossain MJ, Khandaker MU, Faruque MR, Osman H and Rahman SM. A comprehensive account on recent progress in pharmacological activities of benzimidazole derivatives. *Front. Pharmacol*. 2021; 12: 762807.

Çalış İ, Weas A, Yusufoğlu HS, Dönmez AA and Jensen SR. Iridoid glucosides from Wendlandia ligustroides (Boiss. &Hohen.) Blakelock. *Saudi Pharm. J*. 2020; 28(7): 814-818.

Canuto KM and Silveira ER. Constituintes químicos da casca do caule de Amburana cearensis AC Smith. *Química Nova*. 2006; 29: 1241-1243.

Chaudhuri K, Hasan SN, Barai AC, Das S, Seal T and Bag BG. Green synthesis of gold nanoparticles using Wendlandia wallichii, a potent wild edible plant consumed by the tribal of north-eastern region in India. *Pharmaceut. Innovat. J.* 2018; 7: 437-446.

Choze R, Delprete PG and Lião LM. Chemotaxonomic significance of flavonoids, coumarins and triterpenes of Augusta longifolia (Spreng.) Rehder, Rubiaceae-Ixoroideae, with new insights about its systematic position within the family. *Revista Brasileira de Farmacognosia*. 2010; 20: 295-299.

Cowan JM. The genus *Wendlandia*. Notes from the Royal Botanic Garden Edinburgh, 1932; 16: 233-314.

De Silva LB, Herath WH, Navaratne KM, Ahmad VU and Alvi KA. An iridoid glycoside from Wendlandia bicuspidata. *J. Nat. Prod.* 1987; 50(6): 1184.

Delprete PG. Rondeletieae (Rubiaceae): Part I (Rustia, Tresanthera, Condaminea, Picardaea, Pogonopus, Chimarrhis, Dioicodendron, Molopanthera, Dolichodelphys, and Parachimarrhis). *Flora Neotropica*. 1999:1-225.

Dhiman R and Gupta NK. Standardisation of the best season and auxin concentration for rooting of the

cuttings of *Wendlandia exserta* Roxb. DC.-a biofuel species of Himalayan region. *J Tree Sci*. 2009; 28: 41-49

Dinda B, Debnath S, Arima S, Sato N and Harigaya Y. Iridoid glucosides from *Wendlandia tinctoria* roots. *Chem. Pharm Bull*. 2006; 54(7): 1030-1033.

Dinda B, Debnath S, Banik R, Sato N and Harigaya Y. Iridoid glucosides from *Wendlandia tinctoria* roots. Nat. Prod. Commun. 2011; 6(6): 1934578X1100600601.

Eumkeb G, Sakdarat S and Siriwong S. Reversing β-lactam antibiotic resistance of Staphylococcus aureus with galangin from *Alpinia officinarum* Hance and synergism with ceftazidime. Phytomedicine. 2010; 18(1): 40-45.

Farzana M, Hossain MJ, El-Shehawi AM, Sikder MA, Rahman MS, Al-Mansur MA, Albogami S, Elseehy MM, Roy A, Uddin MA and Rashid MA. Phenolic constituents from *Wendlandia tinctoria* var. *grandis* (Roxb.) DC. Stem deciphering pharmacological potentials against oxidation, hyperglycemia, and diarrhea: phyto-pharmacological and computational approaches. *Molecules*. 2022; 27(18): 5957.

Gedin F, Skeppholm M, Burström K, Sparring V, Tessma M and Zethraeus N. Effectiveness, costs and cost-effectiveness of chiropractic care and physiotherapy compared with information and advice in the treatment of non-specific chronic low back pain: study protocol for a randomised controlled trial. *Trials*. 2017; 18: 1-2.

Ghani U. Re-exploring promising α-glucosidase inhibitors for potential development into oral anti-diabetic drugs: Finding needle in the haystack. *Eur. J Med. Chem*. 2015; 103: 133-162.

Hasan MM, Hossain MS, Taher MA and Rahman T. Evaluation of Analgesic, Antidiarrheal and Hypoglycemic Activities of *Wendlandia paniculata* (Roxb.) DC Leaves Extract using Mice Model. Toxicol. Int. 2021; 28(2): 155-163.

Hui H, Tang G and Go VL. Hypoglycemic herbs and their action mechanisms. *Chinese Med.* 2009; 4: 11

Inoue K, Ono M, Nakajima H, Fujie I, Inouye H and Fujita T. Radioimmunoassay of iridoid glucosides. I: General methods for preparation of the haptens and the conjugates with a protein of this series of glucosides. *Heterocycles (Sendai).* 1992; 33(2): 673-695.

Inouye H, Takeda Y, Nishimura H, Kanomi A, Okuda T and Puff C. Chemotaxonomic studies of rubiaceous plants containing iridoid glycosides. *Phytochemistry*. 1988; 27(8): 2591-2598.

Khatoon S and Irshad S. Bark drugs as Indian ethnomedicine–modern therapeutics and future prospects. Indian ethnobotany: emerging trends, Jain AK (Editor), *Scientific Publisher, Jodhpur, India*. 2016: 87-98.

Kitaoka M, Miyata ST, Unterweger D and Pukatzki S. Antibiotic resistance mechanisms of Vibrio cholerae. *J. Med. Microbiol.* 2011; 60(4): 397-407.

Kumar R, Sharma RJ, Bairwa K, Roy RK and Kumar A. Pharmacological review on natural antidiarrhoel agents. *Der Pharma Chemica*. 2010; 2(2): 66-93.

Machida K, Takehara E, Kobayashi H and Kikuchi M. Studies on the Constituents of Gardenia Species. III. New iridoid glycosides from the leaves of *Gardenia jasminoides* cv. *fortuneana* H ARA. *Chem. Pharm. Bull.* 2003; 51(12): 1417-9.

Maiti R, Jana D, Das UK and Ghosh D. Antidiabetic effect of aqueous extract of seed of *Tamarindus indica* in streptozotocin-induced diabetic rats. *J. Ethnopharmacol*. 2004; 92(1): 85–91.

Maryam S, Khan MR, Shah SA, Zahra Z, Batool R and Zai JA. Evaluation of anti-inflammatory potential of the leaves of *Wendlandia heynei* (Schult.) Santapau & Merchant in Sprague Dawley rat. *J. Ethnopharmacol.* 2019; 238: 111849.

Maryam S, Khan MR, Shah SA, Zahra Z, Majid M, Sajid M and Ali S. In vitro antioxidant efficacy

and the therapeutic potential of *Wendlandia heynei* (Schult.) Santapau & Merchant against bisphenol A-induced hepatotoxicity in rats. Toxicol. Res. 2018; 7(6): 1173-1190.

Massey KD and Burton KP. Free radical damage in neonatal rat cardiac myocyte cultures: effects of α-tocopherol, Trolox, and phytol. *Free Rad. Biol. Med.* 1990; 8(5): 449-458.

Masuda R, Ajimi J and Murata T. Pharmacotherapy for neuropathic pain in Japan. *J. Nippon Med. School*. 2017; 84(6): 258-267.

Mazuz E, Shtar G, Kutsky N, Rokach L, Shapira B. Pretrained transformer models for predicting the withdrawal of drugs from the market. *Bioinformatics*. 2023; 39(8): btad519.

Meetei SY and Singh PK. Survey for medicinal plants of Thoubal district, Manipur. *Flora Fauna.* 2007; 13(2): 355-358.

Mitra S, Lami MS, Uddin TM, Das R, Islam F, Anjum J, Hossain MJ and Emran TB. Prospective multifunctional roles and pharmacological potential of dietary flavonoid narirutin. *Biomed. Pharmacother*. 2022; 150: 112932.

Moreira VF, Oliveira RR, Mathias L, Braz-Filho R and Curcino Vieira IJ. New chemical constituents from Borreria verticillata (Rubiaceae). *Helvetica Chimica Acta*. 2010; 93(9): 1751-1757.

Murai F, Tagawa M, Damtoft S, Jensen SR and Nielsen BJ. (1R, 5R, 8S, 9S)-Deoxyloganic acid from Nepeta cataria. *Chem. Pharm. Bull*. 1984; 32(7): 2809-2814.

Murthy KS, Sharma PC and Kishore P. Tribal remedies for snakebite from Orissa. *Ancient Sci. Life*. 1986; 6(2): 122.

Nakamura M, Kido K, Kinjo J and Nohara T. Antinociceptive substances from *Incarvillea delavayi*. *Phytochemistry*. 2000; 53(2): 253-6.

Nuutinen T. Medicinal properties of terpenes found in Cannabis sativa and Humulus lupulus. *Eur. J. Med. Chem.* 2018; 157: 198-228.

Perveen AN and Qaiser MU. Pollen flora of pakistan-Liv. Rubiaceae. *Pak. J. Bot.* 2007; 39(4): 999-1015.

Raju AJ, Ramana KV and Lakshmi PV. *Wendlandia tinctoria* (Roxb.) DC.(Rubiaceae), a key nectar source for butterflies during the summer season in the southern Eastern Ghats, Andhra Pradesh, India. *J. Threatened Taxa.* 2011; 3(3): 1594-1600.

Raju AJ, Ramana KV and Rao NG. Psychophily and anemochory in *Wendlandia tinctoria* (Roxb.) DC. (Rubiaceae): a dry season blooming tree species in the dry deciduous southern eastern ghats forest, Andhra pradesh, India: psychophily and anemochory in *Wendlandia tinctoria*. Biological Sciences-PJSIR. 2012 Apr 27;55(1):1-9.

Raju AS and Ramana KV. Temporal dioecism, melittophily and anemochory of *Wendlandia glabrata* (Rubiaceae). *TAPROBANICA: J. Asian Biodiver.* 2014; 6(2): 83-89.

Ranjan V and Kumar A. Conspectus of family Rubiaceae in West Bengal, India. *Geophytology*, 2015; 45(2), pp. 161–174.

Rashid PT, Hossain MJ, Zahan MS, Hasan CM, Rashid MA, Al-Mansur MA and Haque MR. Chemico-pharmacological and computational studies of *Ophiorrhiza fasciculata* D. Don and *Psychotria silhetensis* Hook. f. focusing cytotoxic, thrombolytic, anti-inflammatory, antioxidant, and antibacterial properties. Heliyon. 2023; 9(9): e20100.

Rawat DS, Kharwal AD and Rawat S. Ethnobotanical studies on dental hygiene in district Hamipur, Himachal Pradesh (HP), India. *Ethnobot. Leaflets*. 2009; 2010(5): 4.

Ribeiro CV and Kaplan MA. Tendências evolutivas de famílias produtoras de cumarinas em Angiospermae. *Química Nova*. 2002; 25: 533-538.

Sarma P, Bharadwaj S, Swargiary D, Ahmed SA, Sheikh Y, Barge SR, Manna P, Talukdar NC, Bora J and Borah JC. Iridoid glycoside isolated from Wendlandia glabrata and the role of its enriched fraction in regulating AMPK/PEPCK/G6Pase signaling pathway of hepatic gluconeogenesis. *New J. Chem*. 2022; 46(27): 13167-13177.

Schumann K. Rubiaceae. *Die naturlichen Pflanzenfamilien*, 1891; 4: 1-156.

Shahzadi T, Riaz T, Abbasi MA, Mazhar F, Shahid M and Ajaib M. Wendlandia exserta: a pertinent source of antioxidant and antimicrobial agent. *Turkish J. Biochem.* 2018; 43(4): 456-463.

Sheikh Y, Chanu MB, Mondal G, Manna P, Chattoraj A, Deka DC, Talukdar NC and Borah JC. Procyanidin A2, an anti-diabetic condensed tannin extracted from *Wendlandia glabrata*, reduces elevated G-6-Pase and mRNA levels in diabetic mice and increases glucose uptake in CC1 hepatocytes and C1C12 myoblast cells. *RSC advances*. 2019; 9(30): 17211-17219.

Sindhe MA, Bodke YD and Kenchappa R. In vitro anthelmintic activity of *Wendlandia thyrsoidea* leaves extracts against *Pheretima posthuma*. *Int. J. Pharmacol.* 2015; 2(6): 1-4.

Singh Y, Lester M, Ng V and Miall L. 636 Premedication for Neonatal Intubation: Current Practice in the Tertiary Neonatal units in the United Kingdom. *Arch. Dis. Child.* 2012; 97(Suppl 2): A463.

Spencer JP. Flavonoids: modulators of brain function?. *British J. Nutr.* 2008; 99(E-S1): ES60-77.

Sultana N. Clinically useful anticancer, antitumor, and antiwrinkle agent, ursolic acid and related derivatives as medicinally important natural product. *J. Enz. Inhibit. Med. Chem.* 2011; 26(5): 616-642.

Takeda Y, Yagi T, Matsumoto T, Honda G, Tabata M, Fujita T, Shingu T, Otsuka H, Sezik E and Yesilada E. Nepetanudosides and iridoid glucosides having novel stereochemistry from *Nepeta nuda* ssp. *albiflora*. *Phytochemistry*. 1996; 42(4): 1085-1088.

Tamba BI, Leon MM and Petreus T. Common trace elements alleviate pain in an experimental mouse model. *J. Neuro. Res.* 2013; 91(4): 554-561.

Teng RW, Wang DZ, Wu YS, Lu Y, Zheng QT and Yang CR. NMR assignments and single-crystal X-ray diffraction analysis of deoxyloganic acid. *Mag Res. Chem*. 2005; 43(1): 92-96.

Tundis R, Loizzo MR, Menichini F, Statti GA and Menichini F. Biological and pharmacological activities of iridoids: recent developments. *Mini Rev. Med. Chem*. 2008; 8(4): 399-420.

Tzakou O, Mylonas P, Vagias C and Petrakis PV. Iridoid glucosides with insecticidal activity from *Galium melanantherum*. *Zeitschrift für Naturforschung C*. 2007; 62(7-8): 597-602.

Ullah R, Ahmad S, Atiq A, Hussain H, ur Rehman N, Abd Elsalam NM and Adnan M. Quantification and antibacterial activity of flavonoids in coffee samples. *African J. Trad. Complement. Alternat. Med.* 2015; 12(4): 84-86.

Venugopal R and Liu RH. Phytochemicals in diets for breast cancer prevention: The importance of resveratrol and ursolic acid. *Food Sci. Human Wellness.* 2012; 1(1): 1-3.

Vickers NJ. Animal communication: when i'm calling you, will you answer too?. *Curr. Biol.* 2017; 27(14): R713-R715.

Vinu K, Krishna V and Krishnappa M. Molecular identification and antibacterial activity of endophytic fungi Curvularia lunata in *Wendlandia thyrsoidea* (Roth) Steud. of central western Ghats region of Chikkamagaluru, Karnataka. *Int. J. Bot. Stud.* 2021; 6(4): 436-439.

Wadkar KA, Magdum CS, Patil SS and Naikwade NS. Antidiabetic potential and Indian medicinal plants. *J. Herb. Med. Toxicol.* 2008; 2(1): 45-50.

Wang GX, Han J, Zhao LW, Jiang DX, Liu YT and Liu XL. Anthelmintic activity of steroidal saponins from Paris polyphylla. *Phytomedicine*. 2010; 17(14): 1102-1105.

Xie P and Zhang D. Pollen morphology supports the transfer of Wendlandia (Rubiaceae) out of Rondeletieae. *Bot. J. Linnean Soc.* 2010; 164(2): 128-141.

Yakubu MT and Salimon SS. Antidiarrhoeal activity of aqueous extract of *Mangifera indica* L. leaves in female albino rats. *J. Ethnopharmacol.* 2015; 163: 135-141.

J. Bangladesh Acad. Sci. 47(2); 155-167: December 2023 DOI:https://doi.org/10.3329/jbas.v47i2.65837

Journal of Bangladesh Academy of Sciences

Journal homepage: http://www.bas.org.bd/publications/jbas.html

Research Article

Exogenous application of potassium fertilizer alleviates the detrimental effect of waterlogging on soybean

Mohammad Mohaddes Hossen, Md. Abdullah Al Mamun*, Md. Mizanur Rahman[1] and M. Abdul Karim

Department of Agronomy, Bangabandhu Sheikh Mujibur Rahman Agricultural University (BSMRAU), Gazipur, Bangladesh

ARTICLE INFO

Article History

Received: 30 April 2023
Revised: 16 July 2023
Accepted: 30 July 2023

Keywords: Greenness, Grain yield, Lodging, Productivity, Stress, Tolerant

ABSTRACT

A field trial was laid out to mitigate the detrimental consequences of waterlogging (WL) on morpho-physiology and productivity of soybeans through potassium (K) application. Soybean genotypes AGS383 and G00166 were tested against 4 days of WL at the flowering stage. The K fertilizer was applied as (i) basal (full dose) and (ii) basal (50%) + top dress (50%) after the termination of a flood. The experiment's results showed that the WL negatively affected leaf greenness, water and chlorophyll (Chl) content, plant height, nodule and pod production, and soybean seed yield. However, the split application of K fertilizer minimized the detrimental effect of WL in the case of AGS383. This genotype produced taller plants, contained more Chl and water, higher nodules, bold seeds, and accumulated higher amounts of mineral nutrients in their grains under WL condition with K as basal + top dress after the termination of a flood.

Introduction

Soybean (*Glycine max* L.), an important legume and oilseed crop, contains protein, oil, carbohydrate, Ca, P, and vitamins (Mannan and Mamun, 2018; Yasmin et al., 2022; Dola et al., 2022). Phenolics, vitamins, antioxidants, dietary fiber, flavonoids, minerals, pigments, protein, and carbohydrates can be obtained from plant sources (Fatema et al., 2023). It has good nitrogen (N)-fixing ability (17-127 kg N ha^{-1} $year^{-1}$), which plays an irreplaceable role in the sustainable agricultural system (Messina, 1997). Soybean seeds also contain macronutrients, minerals, vitamins, folic acids, and secondary metabolites (Saki and Kogiso, 2008). Consuming soybeans reduces cancer, cholesterol, osteoporosis, and heart disease (Birt et al., 2004). Due to its wide range of adaptability and commercial value,the role of soybean in oilseed production increased from 160 million (m) tons on 70 m ha in 1998 to 350 m tons on 125 m ha in 2018 worldwide (FAOStats, 2021).

In Bangladesh, it has been cultivated since early 1970s in the greater Noakhaliand the area under soybeancultivation has expandedtragicallyfrom only 5000ha in 2005 to 62508ha in 2018-2019 (BBS, 2020)in the districts of Bhola, Patuakhali, Faridpur, and even in the northernpart of Bangladesh. It is mostly sown in January and harvested in April (Akand et al., 2018). However, the crop suffers from excess soil moisture due to a change in rainfall pattern, which is the consequence of recent climate change. Cyclone *Nada* in early November of 2016 caused heavy rains, which delayed soybean sowing. Similarly, soybean was damaged due to heavy rains in April 2017. In 2020, cyclone Amphan hit the southern part of Bangladesh on 20th March and damaged standing crops seriously.

Waterlogging (WL) is a critical problem in some parts of Jashore, Satkhira, Khulna, Bhola, Patuakhali, and Faridpur districts of Bangladesh. Monsoon rains are

*Corresponding author: <aamamun@bsmrau.edu.bd>

[1]*Department of Soil Science, Bangabandhu Sheikh Mujibur Rahman Agricultural University (BSMRAU), Gazipur, Bangladesh*

responsible for WL in crop fields of these southern districts, which causes widespread damage to crops. The growth and development of soybean is restricted under WL condition. WL also causes chlorosis and stunting, resulting in yield loss of soybeans (Tewari and Arora, 2016). Soil WL primarily inhibits crop growth and yield by initiating hypoxia conditions (Yin et al., 2009). Under hypoxia conditions, the growth pattern of plants depends onspecies type and survival mechanism (Nagai et al., 2010). Abiotic stress deteriorates the productivity of crops by producing oxidative damage and the creation of reactive oxygen species (ROS), which eventually cause damage in membrane, DNA, and proteins, create an imbalance in nutrients, and attenuation of photosynthetic rates and change color pigments (Sarker and Oba, 2020). The plant under stress conditions has boosted enzymatic and non-enzymatic antioxidants to alleviate ROS (Hassan et al., 2022).

Linkemer et al. (1998) observed a 30% yield loss at the early growth stage and a 93% yield loss at the reproductive stage. The WL hindered growth, dry matter production, and pod formation, resulting in lower yield (Hasanuzzaman et al., 2016). It also inhibited photosynthesis by closing stomata, degrading Chl leaf senescence (Ahmed et al., 2013). WL at the vegetative stage caused a yield loss of up to 18% worldwide (Komatsu et al., 2013).

Nutrient element K has a significant role in increasing the tolerant capacity of plants against various environmental stresses. It helps the plants overcome stress, disease, and pest infestation and take balanced nutrients. Plants deficient in K cannot efficiently use water and other nutrients from soil or fertilizer and are less tolerant to stress conditions. Strategic application of K in plants before hypoxia conditions may alleviate nutrient deficiency and can recover from flood damage. It maintains cell turgidity, starch formation and translocation, synthesis of protein and water, and nutrient uptake. It enhances the photosynthesis, translocation of photosynthates and activates enzymes during nodulation (Divitoand Sadras, 2014). It improves productivity (Emmanuel et al., 2021) and grain quality through better uptake of N and P in plants. Under the WL conditions, K uptake is significantly reduced in plants due to root damage (Amin et al., 2017). Therefore, the exogenous application of K after the flood recession might recover the WL damage in soybeans. Keeping these above considerations in view, the present study has aimed to determine the morpho-physiological changes of soybean plants due to WL and to find out the effect of K application after the flood water recession on soybeans' yield performance.

Materials and Methods

Experimental site

An experiment was conducted at the agronomy research field of Bangabandhu Sheikh Mujibur Rahman Agricultural University (BSMRAU), Gazipur (24°09′ N and 90°26′ E), Bangladesh, from December 2019 to April 2020 (Rabi season). The experimental site was situated at an elevation of 8.4 m from the sea level.

The temperature of the site increases gradually from January to June. Total monthly precipitation was high during January and April, while the minimum was during December, February, and March (Fig. 1). Before experimentation, the soil was analyzed to determine its physicochemical properties of the soil.

Soil pH was measured with a glass electrode in a soil-water mixture with a ratio of 1:2.5 (w/v) (Kalra and Maynard, 1991). Soil organic matter was determined by the Wlkley-Black method (Walkley and Black, 1934); total soil N by the micro-Kjeldahl method (Yoshida et al., 1976);available P by Olsen method (Olsen et al., 1954); exchangeable K by NH_4O-AC extraction method (Helmke and Sparks, 1996); and available S ($CaCl_2$-S) was determined by extracting the soil with 0.15 $CaCl_2$ (Williams and Steinbergs, 1959).

The field contains 40%, 45%, and 15% clay, silt, and sand, respectively, and is classified as silty clay. The soil has pH 6.1, organic matter 1.20%, total N 0.11%, available P 7.21 ppm, exchangeable K 0.19 meq/100 g soil, and available S 11 ppm.

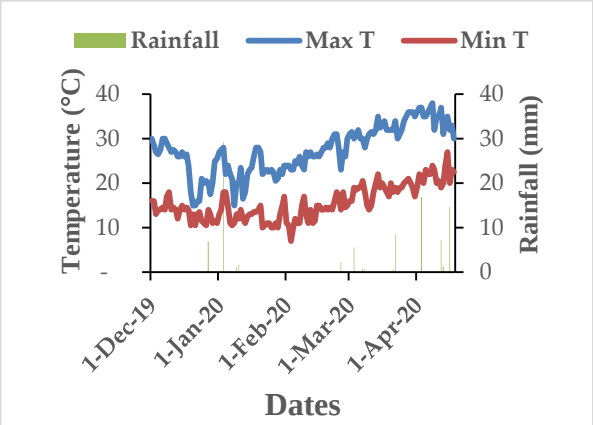

Fig. 1. Temperature and precipitation of the site during the experimental period

Cultural practice and experimental treatments combination

The site was prepared well before seed sowing. The soil was fertilized with urea, triple superphosphate, muriate of potash (MoP), gypsum, and zinc sulfate @ 60, 170, 100, 100, and 10 kg ha^{-1}, respectively. After application, they were incorporated into the soil.

The MoP was applied according to the treatment combination. The size of each plot was 3´4 m^2. Polythene was used to make a ridgearound the plot to restrict lateral water movement. The treatments were Factor A (soybean genotypes): i. AGS383 and ii. G00166, Factor B (WL): i. control (no water logging) and ii. WL for 4 days at the flowering stage), and Factor C (K application): i. basal (100%) and ii. basal (50%) + top dress (50%) after the termination of water logging. A randomized complete block design with three replications was used to conduct the experiment. AGS383 is a bold-grained and medium-statured soybean genotype. This genotype requires 100 to 105 days for maturity. Similarly, genotype G00166 is a short-stature and medium-grained genotype, which takes 80 to 85 days for maturity.

Sowing soybean seeds

Soybean seeds were sown manually in lines, maintaining 30´5 cm spacing. After sowing, the plots were lightly irrigated to confirm uniform seed germination. Thinning was done at the trifoliate leaf stage to maintain uniform and healthy crop growth. Weeding was done to keep the crop free from weeds and pulverized the soil crust for better aeration and conservation of soil moisture. Irrigation was done as and when necessary.

Creation of WL condition

The WL plots were surrounded by 30 cm deep polythene to hold water. The WLtreatment was created at the soybean's flowering stage (60 DAS). The height of flood water was 5 cm above the ground level. The treatments were continued for up to 4 days, and water was drained out. The air temperature was recorded during water logging period. As the duration of WL was 4 days, the measurement was taken from the second day. The data were taken twice daily (9 am and 4 pm).

Collection of leaf greenness, lodging, and growth data

After the termination of flood water, leaf greenness was determined following the method adopted by Akter et al. (2021). Lodging of plants after the recession of water was estimated based on visual observation following the standard evaluation system of IRRI (1988). Data were collected on plant height, soil plant analysis development (SPAD), leaf and stem dry matter (DM), and yield contributing characters were determined. A SPAD meter (model: SPAD-502, Minolta Co. Ltd., Japan) was used to record the SPAD value. A SPAD meter is a meter for determining leaf greenness. The measurements were taken after the recession of flood water. For each treatment, three plants were identified from each replication for taking the SPAD value. The uppermost fully expanded leaveswere selected for taking measurements. Three readings were taken at the basal, middle portion, and terminal part of the leaf and averaged. For growth and DM, estimation sampling was done after the termination of the WL condition. A 100 cm measuring scale was used to record plant height. The leaves $plant^{-1}$ was recorded from the average of five plants.

The leaf fresh weight (FW), turgid weight (TW), and dry weight (DW) were recorded.

To record DM of leaf, nodule and stem parts were dried at 70 °C for 72 h. Relative water content

(RWC) and water saturation deficit (WSD) were determined according to Sangakkara et al. (1996).

$$RWC = \frac{FW - DW}{TW - DW} \times 100$$

$$WSD = \frac{TW - FW.}{TW - DW.} \times 100$$

Harvesting and quantification of yield data

The crop was harvested at physiological maturity when the pods turned brownish and got hard. To record yield components, five plants were collected from each plot. The first and last rows of the plot were avoided to reduce the border effect. The pods were separated and counted. The pod having at least one seed was counted as a filled pod. The length of ten pods was measured, andthe mean value was recorded. After separating the seeds from the pods, they were counted by hand. The weight of 100-seed was recorded for each genotype treatment-wise. The grain and straw yield data were collected from the 1.8 m^2 area of each plot. After collecting plants, seeds were separated, air dried, weighted by an electrical balance, and converted to t ha^{-1} at 14% moisture. The N, P, and K were determined from the collected grain samples. The grain sample was dried at 70 °C for 72 hrs and ground by Wiley Mill. The ground sample was digested in concentrated H_2PO_4, and the micro Kjeldahl method determined the total N concentration (Yoshida et al., 1976). P and K concentrations were analyzed by digesting a 0.2 g grain sample with 6 ml of 5:2 HNO_3: $HClO_4$ (Yoshida et al., 1976). Grain and straw samples from each plot (200 mg) were taken and separately oven-dried at 65 °C overnight to grind in a grinding machine.

Statistical analysis

Recorded data were analyzed using the CropStat 7.2 statistical package program. The treatment means were separated following DMRT at a 5% probability level (Gomez and Gomez, 1984).

Results and discussions

Plant height and dry matter production at the flowering stage

The plant height of AGS383 was 64.66 cm when K was top dressed in control and 55.77 cm when K was applied basally under the WL condition (Table 1). However, the plant height of G00166 was 31.88 cm when K was top dressed in control and 27.86 cm when K was applied basally under the WL condition. Both testing genotypes produced comparatively taller plants when K was top-dressed. However, AGS383 produced long-stature plants as compared to G00166 genotype. The genetic difference was responsible for the different plant heights of the two genotypes. The WL-induced decrease in plant height was noted in soybeans (Mamun et al., 2022). Kim et al. (2018) reported that the reduction in plant height under WL conditions was probably due to oxygen deficiency, anaerobic conditions, less root activity, and inhibition of synthesis and transport of photosynthetic assimilates.

The leaf number of AGS383 was 36.67 $plant^{-1}$ when K was applied basally under the WL condition and 32.00 when K was applied top dressed in control (Table 1). However, the leaf number of G00166 was 58.66 $plant^{-1}$ when K was applied top-dressed under the WL condition and 49.66 when K was applied basally under the WL condition. Under the WL conditions, the leaves' dry matter of both genotypes was higher than the control conditions. The leaf's dry matter of AGS383 was 10.72 g when K was applied basally under the WL condition and 7.40 g when K was applied basally in control. However, the leaf's dry matter of G00166 was 6.88 g when K was applied top dressed in control and 6.07 g when K was applied basally in control. The number of leaves $plant^{-1}$ decreased due to the imposition of WL treatment. However,G00166 produced more leaves than AGS383 under both growing conditions. The WL induced several physiological disturbances in growth (Hasanuzzaman et al., 2016).

However, the application of K after the recession of flood water provokes the production of more leaves $plant^{-1}$ (Table 1). The supplementation of K increased

photosynthetic capacity and Chl content reported, resulting in more leaves plant^{-1}.

The nodules plant^{-1} of AGS383 was 39.66 when K was applied basally in control and 13.00 when K was applied basally under the WL conditions. However, the nodules plant^{-1} of G00166 was 24.33 when K was applied top dressed in control and 5.66 when K was applied basally under the WL conditions (Table 2). The nodule dry matter plant^{-1} of AGS383 was 0.29 g when K was applied top dressed in control and 0.06 g when K was applied basally under the WL conditions. However, the nodule dry matter plant^{-1} of G00166 was 0.32 g when K was applied top-dressed in control and 0.03 g when K was applied basally under the WL conditions.

The stem dry matter plant^{-1} of AGS383 was 6.04g when K was applied basally under the WL conditions and 4.71 g when K was applied basally in control. However, the stemdry matter plant^{-1} of G00166 was 3.09 g when K was applied top dressed in control and 2.68 g when K was applied basally in control. The nodule number drastically reduced under WL in both genotypes. However, the top dressing of K reduced the nodule production. The nodule production was reduced by 67 and 70% under basal K application, while 23 and 32% under a top dressing of K treatment in the case of AGS383 and G00166, respectively. The decrease in nodule production under the WL condition may be due to decreased oxygen transport and nutrition uptake and result in root destruction (Dennis et al., 2000).

Under hypoxia conditions, oxygen deficiency, anaerobic conditions, less root activity, and inhibition of synthesis and transport of photosynthetic assimilates are the probable causes of reduced nodule production. However, the top dressing of K fertilizer provoked the production of more nodules in soybean plants (Table 2).

Table 1. Effect of K application on growth of soybean at flowering stage

Soybean genotypes	Potassium application	Plant height (cm)		Leaves plant^{-1}		Leaf weight plant^{-1} (g)	
		Control	WL	Control	WL	Control	WL
AGS383	Basal	63.55^{a}	55.77^{a}	32.00^{b}	36.67^{b}	7.40^{a}	10.72^{a}
	Top dress	64.66^{a}	61.44^{a}	36.66^{b}	37.33^{b}	8.19^{a}	9.98^{a}
G00166	Basal	29.66^{b}	29.33^{b}	51.33^{a}	49.66^{a}	6.07^{b}	6.39^{b}
	Top dress	31.88^{b}	27.86^{b}	55.00^{a}	58.66^{a}	6.88^{b}	6.18^{b}

Similar letters in a column did not differ significantly at the 5% level. WL= Waterlagging.

Table 2. Effect of K application on dry matter production of soybean at flowering stage

Soybean genotypes	Potassium application	Nodule plant^{-1}		Nodule weight plant^{-1} (g)		Stem weight plant^{-1} (g)	
		Control	WL.	Control	WL.	Control	WL
AGS383	Basal	39.66^{a}	13.00^{b}	0.24^{abc}	0.06^{bc}	4.71^{a}	6.04^{a}
	Top dress	35.33^{a}	27.00^{b}	0.29^{ab}	0.11^{abc}	5.04^{a}	5.68^{a}
G00166	Basal	19.00^{b}	5.66^{b}	0.23^{abc}	0.03^{c}	2.68^{b}	2.75^{b}
	Top dress	24.33^{b}	16.33^{b}	0.32^{a}	0.22^{abc}	3.09^{b}	2.50^{b}

Similar letters in a column did not differ significantly at the 5% level. WL= Waterlagging

Leaf greenness and plant lodging after the termination of floodwater

Leaf greenness was observed 7 days after the termination of flood water. In the WL condition, leaf greenness was high in the case of G00166 with a top dressing of K fertilizer (Table 3). The lowest greenness was observed in AGS383 (5) when K was applied basally under the WL condition. AGS383 showed the highest lodging between the two genotypes under the WL condition with basal application of K fertilizer followed by a top dressing of K (Table 3). The lowest lodging was observed in the case of G00166 under the WL condition when K was top-dressed.

The soybean plants were sensitive to WL The symptom of leaf color varied from green to yellow within 4 days of WL stress. In WL condition, leaf greenness was high in G00166 with the dressing of K fertilizer. The greenness of adult leaves was significantly lower in WL condition. Fixing carbon by plant level is detrimental, leading to poorer growth (Zeng et al., 2013). The WL negatively affected soybean genotypes standing in nature. Among the genotypes, AGS383 (50%) showed the highest lodging, followed by G00166 (20%) with a top dressing of K fertilizer. The AGS383 is a taller genotype, while G00166 is a short-stature one. Taller soybean genotypes are more prone to lodging than shorter ones (Todaka et al., 2015).

Chlorophyll and relative water content at the flowering stage

Under both control and WL conditions, the Soil Plant Analysis Development (SPAD) of G00166 was higher than that of AGS383.

There was a general tendency of decreasing SPAD value due to WL irrespective of genotypes (Table 4). The SPAD of AGS383 was 34.86 when K was top-dressed in control. However, the SPAD of G00166 was decreased (35.66) when K was top dressed under the WL condition.

The Relative Water Content (RWC) did not show any clear trend due to the methods of the K application (Table 4). However, there was a general tendency of decreasing RWC due to WL irrespective of genotypes. The RWC of AGS383 was 81.92% when K was applied basally in control and 79.77% when K was applied basally under the WL condition. However, the RWC of G00166 was 83.33% when K was top-dressed in control and 70.88 when K was top-dressed under the WL condition. Under the WL conditions, the Water saturation deficit (WSD) of G00166 was higher than that of AGS383 in the case of both top-dressed and basally K applications. The WSD did not show any clear trend due to the methods of the K application. However, there was a general tendency to increase WSD due to WL irrespective of genotypes. The WSD of AGS383 was 20.23% when K was applied basally under the WL condition and 18.08% when K was applied basally in control. However, the WSD of G00166 was 29.12% when K was applied basally under the WL condition and 16.67% when K was top dressed in control.

Table 3. Effect of K application on leaf greenness and plant lodging of soybean after recession of flood water

Soybean genotypes	Potassium application	Leaf greenness score		Plant lodging score	
		Control	WL.	Control	WL
AGS383	Basal	2.0 (80)	5.0 (50)	0 (0)	5.0 (50)
	Top dress	1.0 (90)	4.0 (60)	0 (0)	3.5 (40)
G00166	Basal	2.0 (80)	4.0 (60)	0 (0)	2.7 (30)
	Top dress	1.0 (90)	3.0 (70)	0 (0)	1.0 (20)

Values within parentheses indicate percent greenness or lodging. WL= Waterlagging

The Chl content of the leaf is highly correlated with leaf greenness. The Soil Plant Analysis Development (SPAD) was measured 7 days after the recession of floodwater to observe the changes in Chl status in the leaves. Our result indicated that soybean leaf Chl content significantly decreased due to WL, resulting in leaf color variation. The general SPAD values were decreased due to 4-days WL Under the WL condition,G00166 had the highest SPAD, while AGS383 had the lowest during the measurement period. Under stress conditions, the Chl content was reduced compared to control (Ferdous et al., 2018).

Rocío et al. (2018) also observed a progressive decline in SPAD values of adult leaves under one week of WL.

This was also supported by the findings of Mondal (2013). The WL inhibits N absorption by the root system, resulting in decreased SPAD of the leaf (Bacanamwo and Purcell, 1999). Under the WL condition, AGS383 exhibited the highest RWC, while G00166 gave the lowest. Both genotypes showed numerically higher RWC under control than WL. It indicated that WL is detrimental to RWC in soybeans. However, the reduction of RWC of G00166 was much higher than that of AGS383 due to WL. It revealed that the RWC of AGS383was less affected by WL than G00166. Therefore, the absolute amount of plant water content decreased. G00166 exhibited the highest WSD under the WL. condition, while AGS383 gave the lowest one in control. Both genotypes showed numerically higher WSD under the WL conditions, indicating that the plants are subjected to a greater water deficit. Sterling et al. (2018) found that lodging occurs under the WL condition that hinders water uptake by soybeans. However, water and nutrient uptake by plants was disturbed under the WL conditions, resulting in higher WSD. (Dennis et al., 2000).

Production of pods and seeds plant^{-1}

The pod of AGS383 was 39.66 plant^{-1} when K was top dressed in control and 30.33 plant^{-1} when K was applied basally under the WL conditions. However, the pod plant^{-1} of G00166 was 45.00 when K was applied top-dressed in control and 32.00 when K was top-dressed under the WL conditions (Table 5). The pod length of AGS383 was 4.25 cm when K was applied basally under the WL condition and 3.94 cm when K was applied basally in control. However, the pod length of G00166 was 4.34 cm when K was top-dressed in control and 3.66 cm when K was applied basally under the WL condition (Table 5). The seed number of AGS383 was 2.73 pod^{-1} when K was applied basally under the WL condition and 2.65 pod^{-1} when K was top dressed in control. However, the seed plant^{-1} of G00166 was 2.73 when K was top-dressed in control and 2.00 when K was applied basally under the WL condition.

Table 4. Effect of K application on chlorophyll, RWC, and WSD of soybean at flowering stage

Soybean genotypes	Potassium application	SPAD value		RWC (%)		WSD (%)	
		Control	WL.	Control	WL.	Control	WL
AGS383	Basal	34.66^{b}	32.60^{b}	81.92^{a}	79.77^{ab}	18.08^{a}	20.23^{ab}
	Top dress	34.86^{b}	33.60^{b}	79.93^{ab}	81.01^{ab}	20.07^{ab}	18.99^{ab}
G00166	Basal	39.06^{ab}	39.97^{a}	76.05^{ab}	74.51^{ab}	23.95^{ab}	25.49^{ab}
	Top dress	41.36^{a}	35.66^{b}	83.33^{a}	70.88^{a}	16.67^{a}	29.12^{a}

Similar letters in a column did not differ significantly at the 5% level. SPAD = Soil Plant Analysis Development; RWC = Relative Water Content; WSD = Water Saturation Deficit. WL= Waterlagging.

The number of pods and seeds plant^{-1} are the yield contributing characteristics of soybean. In this study, the production of pods and their length were reduced due to WL in soybeans. Growth and pod formation weredisturbed under WL conditions (Ahmed et al., 2020; Islam et al., 2014; Sathi et al., 2022). However, the genotype G00166 produced more pods plant^{-1} and longer-sized pods when K was applied after the flood recession. This finding was similar to Vyas et al. (2007) and Alam et al. (2009).

Grain and straw yield of soybean

The 100-seed weight of AGS383 was 19.94 g when K was top-dressed under the WL condition and 14.34 g when K was top-dressed under the control (Table 6). However, the 100-seed weight of G00166 was 11.81 g when K was applied basally under the WL condition and 9.66 g when K was top dressed in control.

Under the flooded condition, the 100-seed weight of soybean was more than the control condition when K was both top dressed and basally applied. This finding did not match the findings of Ara et al. (2016), who found that 100-seed weight decreased when the plants were subjected to WL stress. Ahmed et al. (2013) reported that the individual seed weight of maize and soybean was increased by 8 and 4%, respectively, under heavier K application. It may be due to increased plant photosynthetic activity and sink capacity by applying K, as reported by Alam et al. (2009) and Ahmed et al. (2020). However, the seed size of AGS383 was bigger than G00166. The weight of individual seeds is a genetically regulated character, and AGS383 has a bigger-sized seed.

The seed yield of AGS383 was higher under control than WL conditions in both modes of K application. The seed yieldof AGS383 was 2.61 t ha^{-1} when K was top dressed under the control condition and 1.52 t ha^{-1} with basal K application in WL. However, the seed yieldof G00166 was higher at 1.40 t ha^{-1} when K was applied basally in control and 1.05 t ha^{-1} when K was top dressed under the WL. The straw yieldof AGS383 was 1.56 t ha^{-1} when K was applied basally under the WL condition and 1.43 t ha^{-1} with basal K application in control. However, the straw yieldof G00166 was 0.79 when K was top dressed under the WL condition and 0.72 t ha^{-1} when K was applied basally under the WL condition (Table 6). Under the WL conditions, grain yield was drastically reduced. The reduction of yield contributing characters under WL resulted in lower yield. The yield components of mungbean were also affected by WL, as reported by Islam et al. (2014), resulting in lower yield (Amin et al., 2017). However, the split application of K improved grain yield in the case of AGS383 under both growing conditions. In this experiment, AGS383 produced 2 and 15% higher grain under the control and WL conditions, respectively, when K was applied after the recession of flood water. It indicated that the detrimental effect of flooding K fertilizer can be reduced. This finding also agreed with the result of Vyas et al. (2007). Application of K increased test weight and grain yield (Uddin et al., 2013) because photosynthetic activity, translocation, and metabolism of carbohydrates are influenced by K (Lu et al., 2016). The genotype AGS383 yielded 1.43 and 1.45 t ha^{-1} straw in the K basal and split application, respectively, under control.

Table 5. Effect of K application on pod and seed production of soybean at harvest

Soybean genotypes	Potassium application	Pod plant^{-1}		Pod length (cm)		Seeds pod^{-1}	
		Control	WL	Control	WL	Control	WL
AGS383	Basal	34.00^{a}	30.33^{ab}	3.94^{a}	4.25^{bcd}	2.66^{ab}	2.73^{a}
	Top dress	39.66^{ab}	34.00^{ab}	4.04^{ab}	4.24^{bcd}	2.65^{ab}	2.60^{abc}
G00166	Basal	44.00^{ab}	37.66^{ab}	3.76^{ab}	3.66^{cd}	2.26^{bcd}	2.00^{d}
	Top dress	45.00^{ab}	32.00^{b}	4.34^{abc}	3.81^{d}	2.73^{a}	2.20^{cd}

Similar letters in a column did not differ significantly at the 5% level. WL= Waterlagging

Nutrient concentration in soybean grain

The WL can lead to nutrient deficiency, particularly in N, K, and P in various plant species. Soil WL causes a significant decrease in K uptake in plants due to reduced root activity (Amin et al., 2017) as a reason the plant shows wilting. In this experiment, both genotypes absorbed more nutrients under the WL condition than control (Table 7).

The N concentration in the grains of AGS383 was 6.48 and 6.61% under the WL condition when K was applied basally and top dress, respectively. This genotype accumulated 5.48 and 5.35% N in grain when K was top dressed. Under the control condition, the P concentration was 0.44 and 0.46% in AGS383, while 0.49 and 0.58% in G00166 when K was applied basally and top dressing, respectively. G00166 absorbed 3.22 and 3.13% K under WL and 2.75 and 3.05% under control with basal and split application of K fertilizer, respectively (Table 7). The application of K improved the total amount of N in plants, as reported by Ahmed et al. (2013). Fixed ammonium ions were released from the soil in the presence of K, which favors plants to accumulate a higher amount of N. Therefore, plants' N, P, and K content increased due to applying K (Ali et al., 2019). Board (2008) reported that the effects of WL on P were not mentionable. Energy is essential in the root system for the active transportation of different nutrients (Mohammadi, 2009).

Under drought or WL conditions, the energy in the root system is reduced, and transportation of N, P, and K is suppressed (Rima et al., 2019; Vodnik et al., 2009). N, P, and K concentrations were higher under the WL condition in both genotypes. The exogenous application of K fertilizer improves N uptake when plants are subjected to WL conditions (Elzenga and Veen, 2010). Under the WL condition, plant growth, pigment content, and nutrient uptake by roots improve when K is applied as a supplement (Solaiman et al., 2007).

Table 6. Effect of K application on grain and straw yield of soybean at harvest

Soybean genotypes	Potassium application	100-seed weight (g)		Grain yield (t ha^{-1})		Straw yield (t ha^{-1})	
		Control	WL	Control	WL	Control	WL
AGS383	Basal	14.36^{b}	19.76^{a}	2.56^{a}	1.52^{c}	1.43^{a}	1.56^{a}
	Top dress	14.34^{b}	19.94^{a}	2.61^{a}	1.75^{b}	1.45^{a}	1.44^{a}
G00166	Basal	10.13^{cd}	11.81^{c}	1.40^{c}	1.06^{d}	0.76^{b}	0.72^{b}
	Top dress	9.66^{d}	11.02^{cd}	1.08^{d}	1.05^{d}	0.73^{b}	0.79^{b}

Similar letters in a column did not differ significantly at the 5% level. HL = Waterlogging.

Table 7. Effect of K application on the nutrient accumulation in grain of soybean at harvest

Soybean genotypes	Potassium application	Nitrogen (%)		Phosphorus (P, %)		Potassium (%)	
		Control	WL	Control	WL	Control	WL
AGS383	Basal	5.48^{c}	6.48^{b}	0.44^{b}	0.53^{ab}	2.75^{d}	2.83^{cd}
	Top dress	5.35^{d}	6.61^{a}	0.46^{ab}	0.45^{ab}	2.95^{c}	2.73^{d}
G00166	Basal	4.85^{c}	5.07^{c}	0.49^{ab}	0.52^{ab}	2.75^{d}	3.22^{a}
	Top dress	4.79^{c}	5.29^{d}	0.58^{a}	0.57^{ab}	3.05^{b}	3.13^{a}

Similar letters in a column did not differ significantly at the 5% level. WL= Waterlagging

Conclusions

Flooding negatively affected leaf greenness, chlorophyll content, relative water content, plant height, nodule, pod number, and grain and straw yield of soybeans. The detrimental effect of flooding was minimal when potassium was applied 50% during final land preparation and 50% after the recession of flood water. It could be concluded that AGS383 could be cultivated as a relatively high-yielding soybean genotype in waterlogging conditions for 4 days following potassium application as 50% during final land preparation and 50% after the recession of flood water.

Acknowledgments

This research work was supported by BSMRAU, Gazipur 1706, Bangladesh.

Declaration of conflicting interest

The authors have no conflicts of interest to declare.

Author's Contributions

MAA Mamun contributed to the conceptualization, supervision, data analysis, and manuscript drafting; M.M. Hossen carried out the field experiment, collected data, and prepared the table and graphs; M.M. Rahman and M.A. Karim contributed to the methodology and editing of the manuscript.

References

Ahmed A, Aftab S, Hussain S, Nazir Cheema H, Liu W, Yang F and Yang W. Nutrient accumulation and distribution assessment in response to potassium application under maize–soybean intercropping system. *Agron*. 2020; 10(5): 725.

Ahmed F, Rafii MY, Ismail MR, Juraimi AS and Rahim HA. Waterlogging tolerance of crops: breeding, mechanism of tolerance, molecular approaches and future prospects. *Bio. Res. Int.* 2013; 963525:1-10.

Akand MMH, Mamun MAA, Ivy NA and Karim MA. Genetic variability of soybean genotypes under drought stress. *Ann. Bangladesh Agril.* 2018; 22(1): 79-93.

Akter M, Akter M, Mamun MAA and Karim MA. Waterlogging effect on short duration soybean genotypes: Phenology and greenness. *Ecol. J.* 2021; 3(2): 169-173.

Alam MR, Ali MA, Molla MSH, Momin MA and Mannan MA. Evaluation of different levels of potassium on the yield and protein content of wheat in the high Ganges River floodplain soil. *Bangladesh J. Agril. Res.* 2009; 34(1): 97-104.

Ali S, Hafeez A, Ma X, Tung SA, Chattha MS, Shah AN and Yang G. Equal potassium-nitrogen ratio regulated the nitrogen metabolism and yield of high-density late-planted cotton (*Gossypium hirsutum* L.) in Yangtze River valley of China. *Crop Prod.* 2019; 129: 231-241.

Amin MR, Karim MA, Khaliq QA, Islam MR and Aktar S. The influence of waterlogging period on yield and yield components of mungbean (*Vigna radiata* L. Wilczek). *The Agriculturis.* 2017; 15(2): 88-100.

Ara R, Mannan MA, Khaliq QA and Miah MU. Waterlogging tolerance of soybean. *Bangladesh Agron. J.* 2016; 18(2): 105-109.

Bacanamwo M and Purcell LC. Soybean dry matter and nitrogen accumulation responses to flooding stress, N sources and hypoxia. *J. Exp. Bot*. 1999; 50(334): 689-696.

BBS, Bangladesh Bureau of Statistics. Yearbook of Agricultural Statistics-2020. *Bangladesh Bureau of Statistics*, Ministry of Planning, Government of the People's Republic of Bangladesh. 2020.

Birt DF, Hendrich S, Alekel DL and Anthony M. Soybean and the prevention of chronic human disease. Soybeans: Improvement, production, and uses. 2004; 16: 1047-1117.

Board JE. Waterlogging effects on plant nutrient concentrations in soybean. *J. Plant Nut.* 2008; 31(5): 828-838.

Dennis ES, Dolferus R, Ellis M, Rahman M, Wu Y, Hoeren FU, Grover A, Ismond KP, Good AG and Peacock WJ. Molecular strategies for

improving waterlogging tolerance in plants. *J. Exp. Bot.* 2000; 51(342): 88-97.

Divito GA and Sadras VO. How do phosphorus, potassium and sulphur affect plant growth and biological nitrogen fixation in crop and pasture legumes? A meta-analysis. *Field Crops Res*. 2014; 156: 161-171.

Dola DB, Mannan MA, Sarker U, Mamun M.A.A., Islam T, Ercisli S, Saleem MH, Ali B, Pop OL and Marc RA. Nano-iron oxide accelerates growth, yield, and quality of glycine max seed in water deficits. *Front. Plant Sci.* 2022; 13: 992535.

Elzenga J.T.M. and van Veen H. Waterlogging and plant nutrient uptake. In Waterlogging signaling and tolerance in plants. *Springer, Berlin, Heidelberg*, 2010. p. 23-35.

Emmanuel OC, Akintola OA, Tetteh FM and Babalola OO. Combined application of inoculant, phosphorus and potassium enhances cowpea yield in savanna soils. *Agron*. 2021; 11(1):15.

FAO. World Food and Agriculture - Statistical Yearbook 2021. Rome, 2021.

Fatema MK, Mamun MAA, Sarker U, Hossain MS, Mia M.A.B., Roychowdhury R, Ercisli S, Alina Marc R, Babalola OO and Karim MA. Assessing morpho-physiological and biochemical markers of soybean for drought tolerance potential. *Sustainability*, 2023; 15(2): 1427.

Ferdous J, Mannan MA, Haque MM, Mamun MAA and Alam MS. Chlorophyll content, water relation traits and mineral ions accumulation in soybean as influenced by organic amendments under salinity stress. *Australian J. Crop Sci.* 2018; 12(12): 1806-1812.

Gomez KA and Gomez AA. Statistical procedure for agricultural research (2nd ed.). John Willey and Sons, *New York*. 1984; p. 680.

Hasanuzzaman M, Nahar K, Rahman A, Mahmud JA, Hossain MS and Fujita M. Soybean production and environmental stresses. In: *Environmental stresses in soybean production*. Academic Press. 2016. p. 61-102

Hassan J, Rajib M.M.R., Sarkar U, Akter M, Khan M, Khandaker S, Khalid F, Rahman G, Ercisli S and Muresan C. Optimizing textile dyeing wastewater for tomato irrigation through physiochemical, plant nutrient uses and pollution load index of irrigated soil. *Sci. Rep.* 2022; 12: 10088.

Helmke PA and Sparks DL. *Method of soil analysis. Part 3. Chemical Method*. Sparks DL, Page AL, Helmke PA, Loeppert RH, Soltanpour PN, Tabatabai MA, Johnston CT, . Sumner ME, eds.,Soil Science Society of America, Inc., American Society of Agronomy, Inc. 1996

IRRI. International Rice Research Institute. Standard Evaluation System for Rice, International Rice Research Institute, Los Banos, Philippines. 1988.

Islam MR, Akter N, Parvej SS and Haque KS. Growth and yield response of mungbean (*Vigna radiata* L. Wilczek) genotypes to wet puddling, flooding and saturated soil culture. *J. Plant Sci.* 2014; 2(6): 311-316.

Kalra YP and Maynard DG. *Methods manual for forest soil and plant analysis*. Forestry Canada, Northwest Region, Northern Forestry Centre, Edmonton, Alberta. Information Report NOR-X-319E. 1991; p.116.

Kim Y, Seo CW, Khan AL, Mun BG, Shahzad R, Ko JW and Lee IJ. Ethylene mitigates waterlogging stress by regulating glutathione biosynthesis-related transcripts in soybeans. *Bio Res*. 2018. 252312.

Komatsu S, Makino T and Yasue H. Proteomic and biochemical analyses of the cotyledon and root of flooding-stressed soybean plants. *PLOS One*, 2013; 8(6): e65301.

Linkemer G, Board JE and Musgrave ME. Waterlogging effects on growth and yield

components in late-planted soybean. *Crop Sci*. 1998; 38(6): 1576-1584.

Lu Z, Lu J, Pan Y, Lu P, Li X, Cong R and Ren T. Anatomical variation of mesophyll conductance under potassium deficiency has a vital role in determining leaf photosynthesis. *Plant Cell Env*. 2016; 39(11): 2428-2439.

Mamun MAA, Julekha, Sarker U, Mannan MA, Rahman MM, Karim MA, Ercisli S, Marc RA and Golokhvast KS. Application of potassium after waterlogging improves quality and productivity of soybean seeds. *Life.* 2022; 12(11): 1816.

Mannan MA and Mamun MAA. Selection of vegetable soybean suitable for Bangladesh through multivariate analysis. *Ann. Bangladesh Agril*,2018; 22(2): 51-57.

Messina MJ. Soyfoods: Their role in disease prevention and treatment. In: Soybeans, Springer, Boston, MA. Liu K (ed.), Chapman & Hill, 1997; pp 442-477.

Mohammadi GR. The effect of seed priming on plant traits of late-spring seeded soybean (*Glycine max* L.). *Am-Eu. J. Agric. Environ. Sci*. 2009; 5(3): 322-326.

Mondal RI. Agronomic research for enhancing sustainable crop production. 12th Conference of Bangladesh Society of Agronomy, 20-21 September, 2013.

Nagai K, Hattori Y and Ashikari M. Stunt or elongate? Two opposite strategies by which rice adapts to floods. *J. Plant Res*. 2010; 123(3): 303-309.

Olsen SR, Cole CV, Watanable FS and Dean LA. Estimation of available phosphorus in soils by extraction with sodium bicarbonate. *U.S. Dept. Agric. Circular No.* 939,1954; p.19.

Rima IA, Mannan MA, Mamun MAA and Kamal ZU. Morpho-physiological traits of soybean as affected by drought. *Bangladesh Agron. J.* 2019; 22(2): 41-54.

Rocío AP, Miralles DJ, Colmer TD, Ploschuk EL and Striker GG. Waterlogging of winter crops at early and late stages: impacts on leaf physiology, growth and yield. *Front. Plant Sci*. 2018; 9: 1863.

Sakai T and Kogiso M. Soy isoflavones and immunity. *J. Med. Inv*. 2008; 55(3&4): 167-173.

Sangakkara UR, Hartwig UA and Nosberger J. Soil moisture and potassium affect the performance of symbiotic nitrogen fixation in faba bean and common bean. *Plant Soil*. 1996; 184(1): 123-130.

Sarker U and Oba S. The response of salinity stress-induced A. tricolor to growth, anatomy, physiology, non-enzymatic and enzymatic antioxidants. *Front. Plant Sci.* 2020; 11: 559876.

Sathi KS, Masud AAC Falguni MR, Ahmed N, Rahman K and Hasanuzzaman M. Screening of soybean genotypes for waterlogging stress tolerance and understanding the physiological mechanisms. *Adv. Agric.* 2022; 1-14.

Solaiman Z, Colmer TD, Loss SP, Thomson BD and Siddique KHM. Growth responses of cool-season grain legumes to transient waterlogging. *Aus. J. Agril. Res*. 2007; 58(5): 406-412.

Sterling M, Baker C, Joseph G, Gillmeier S, Mohammadi MD, Blackburn G, Wyatt D, Berry P, Hatley D and Spink J. Mitigating yield losses due to lodging of cereal crops. In: *Proceedings of the International Workshop on Wind-Related Disasters and Mitigation.* Tohoku University, Sendai, Japan, 2018; 11-14 March, 2018.

Tewari S and Arora NK. Soybean production under flooding stress and its mitigation using plant growth-promoting microbes. *In: Environmental stress in soybean production*. 2016. Vol. 2. Academic Press/Elsevier Inc., New York. USA.

Todaka D, Shinozaki K and Yamaguchi-Shinozaki K. Recent advances in the dissection of drought-stress regulatory networks and strategies for development of drought-tolerant transgenic rice plants. *Front. Plant Sci.* 2015; 6: 84.

Uddin S, Sarkar M and Rahman M. Effect of nitrogen and potassium on yield of dry direct-seeded rice cv. NERICA 1 in aus season. *Intl. J. Agron. Plant Prod*. 2013; 4: 69-75.

Vodnik D, Strajnar P, Jemc S and Maček I. Respiratory potential of maize (*Zea mays* L.) roots exposed to hypoxia. *Environ. Exp. Bot.* 2009; 65(1): 107-110.

Vyas AK, Billore SD, Ramesh A, Joshi OP, Gupta GK, Sharma AN and Imas P. Role of potassium in balanced fertilization of soybean-wheat cropping system. In: *Proceedings of the Regional Seminar on Recent Advances in Potassium Nutrition Management for Soybean Based Cropping Systems*, 2008. National Research Center for Soybean, Indian Council of Agricultural Research (ICAR) Indore, India, 28-29 September, 2007.

Walkley A and Black I. An Examination of the Degtjareff Method for Determining Soil Organic Matter and a Proposed Modification of the Chromic Acid Titration Method. *Soil Sci.* 1934; 37(1): 29-38.

Williams CH and Steinbergs A. Soil sulphur fraction as chemical indices of available sulphur in soils. *Aust. J. Soil Res.* 1959; 10(3): 340-352.

Yasmin A, Mannan MA, Sarker U, Dola DB, Higuchi H, Ercisli S, Ali B, Saleem MH and Babalola OO. Foliar application of seaweed extracts enhance yield and drought tolerance of soybean. *Front. Plant Sci*. 2022; 13: 992880.

Yin D, Chen S, Chen F, Guan Z and Fang W. Morphological and physiological responses of two chrysanthemum cultivars differing in their tolerance to waterlogging. *Environ. Exp. Bot.* 2009; 67(1): 87-93.

Yoshida S, Orno DA, Cock JH and Gomez KA. Laboratory manual for physiological studies of rice. 3rd ed.. International Rice Research Institute, Manila, Philippines,1976.

Zeng F, Shaala L, Zhou M, Zhang G and Shabala S. Barley respnses to combined waterlogging and salinity stress: separating effects of oxygen deprivation and elemental toxicity. *Front. Plant Sci.* 2013; 4: 313.

J. Bangladesh Acad. Sci. 47(2); 169-180: December 2023 DOI:https://doi.org/10.3329/jbas.v47i2.67665

Journal of Bangladesh Academy of Sciences

Journal homepage: http://www.bas.org.bd/publications/jbas.html

Research Article

Requirement and use efficiency of nitrogen in transplanted Aman rice at Ganges tidal water flooded coastal ecosystem

Samsunnahar Pranto, Mohammad Asadul Haque* and Md Fazlul Hoque

Department of Soil Science, Patuakhali Science and Technology University, Dumki, Patuakhali, Bangladesh

ARTICLE INFO

Article History

Received:16 July 2023
Revised: 14 August 2023
Accepted: 17 August 2023

Keywords: Bangladesh, Chlorophyll content, Nitrogen use efficiency, Nutrient uptake, Tidal water

ABSTRACT

Transplanted (T) Aman rice covers most of the arable land in the south coastal region of Bangladesh, where nitrogen fertilizer requirement in the Ganges tidal water flooded ecosystem yet not determined. The on-farm experiment was conducted at Dumki Upazila, Patuakhali district of Bangladesh, during T. Aman rice season 2020. The three replicated randomized complete block design was used in the experiment. There were eight treatments with different rates of nitrogen, e.g., control (no nitrogen fertilizer), 18, 36, 54, 72, 90, 108, and 126 kg N ha^{-1}, which was equivalent to 0, 20, 40, 60, 80, 100, 120 and 140% of the current recommended rate, respectively. The test variety of rice was BR23. An increase in nitrogen rates progressively increased the grain yield of rice. The highest yield of 5.04 t ha^{-1} was found in 54 kg N ha^{-1} rate. However, using a quadratic equation, the most optimum rate was 75 kg N ha^{-1}, 17% lower than the current recommendation. Nitrogen amendment could increase T. Aman rice grain yield by only 35% over control under tidal water flooded conditions. The agronomic efficiency, recovery efficiency, and physiological efficiency of nitrogen were higher in lower rates of N and gradually decreased with the increase of the rate of N application. The present study recommends 75 kg N ha^{-1} for cultivating T. Aman rice (BR23) in tidal water flooded the south coastal ecosystem of Bangladesh.

Introduction

Rice is the staple food for approximately 163 million people in Bangladesh (BBS, 2019). Almost 16.5 million farm families (48% rural employment) cultivate rice (Akter et al., 2019). Especially in the south coastal region, most of the arable lands are occupied by T. Aman rice in the wet season (Kharif II). Although a big coverage, the yield potentiality of the traditionally grown T. Aman rice crop is very low.

While agronomic research has appeared to neglect cropping systems in environmentally challenging coastal areas, increasing T. Aman rice productivity is critical in efforts to improve food security. The location of farmers' fields in relation to the landscape is a key factor determining T. Aman's productivity in those areas. Increasing macro and micronutrients may be the most common technique for enhancing crop yields (Howlader et al., 2013; Hania et al., 2013; Begum et al., 2015). Nitrogen is the most limiting element, but the ecosystem usually loses more than half of the applied nitrogen (Haque et al., 2023a). In flooded rice, water depth may fluctuate during the growing season due to tidal water submergence; improving nitrogen performance is especially problematic (Ladha et al., 2005). Rice has

*Corresponding author: <masadulh@yahoo.com, masadulh@pstu.ac.bd>

recorded the low efficiency of nitrogen recovery by above-ground biomass (Haque and Jharna, 2008). Denitrification and volatilization, which impact farmers' water and crop management practices, may also induce fewer efficiencies under some circumstances due to leaching, seepage, and/or runoff (Choudhury and Kennedy, 2005).

To achieve optimal lowland rice grain yields, nitrogen is usually a crucial component. Among the mineral nutrient elements, nitrogen is the highest required element, which considerably improves the yield and quality of rice (Peng et al., 2021). However, if it is misused, it will pollute groundwater. Farmers generally apply excess nitrogen fertilizer, which is an optimum requirement for rice's rapid and vigorous growth. The over-application of nitrogen fertilizer in the soil causes underground water and environmental pollution and promotes soil acidification (Ma et al., 2021).

Modern crop production technology includes using appropriate fertilizer rates and fertilizer application methods to improve crop yield per unit area (Haque et al., 2023b). The optimal rate of nitrogen fertilization has traditionally been the rate that yields the highest economic yield. The required optimum nitrogen rate varies depending on soil type, cultivar yield potential, phosphorus and potassium levels, water management methods, disease, pest, and weed strength. In Bangladesh, fertilizer recommendations are made based on the agro-ecological zones with high heterogeneity in land type and soil fertility (FRG, 2018). Moreover, soil fertility status decreases daily due to increasing cropping intensity and introduction of high-yielding crops and crop varieties in the coastal cropping systems (Haque, 2020). The reduced fertility status signifies the update of nitrogen fertilizer recommendations. An updated recommendation is therefore needed for growing rice, especially in coastal tidal water-flooded ecosystems. Using an acceptable nitrogen rate is critical for maximizing economic returns and reducing emissions of chlorofluorocarbon gas (Fageria and Baligar, 2003).

Improved nitrogen use efficiency to achieve both high yield and grain quality needs close consideration of the rate of nitrogen fertilizer applications (Haque and Hoque, 2023). The current research work, therefore, is undertaken to determine the optimum nitrogen rate for T. Aman rice cultivation at the south coastal Ganges tidal water flooded ecosystem.

Materials and Methods

Experimental site and soil

The experiment was conducted at the farmers' field of Dumki upazila of Patuakhali district, Bangladesh, in the Kharif-II season 2020. Geographically, the experimental sites were located at 22.46328° north latitude and 90.39665° east longitude, typical of a non-saline Ganges tidal water flooded coastal ecosystem. Texturally, the soil (0-15 cm) was silt loam (80 sand:755 silt:165 clay, g kg^{-1}) with pH (water) 6.6, EC (dS/m) 0.92, Walkley & Black organic carbon 5.6 g kg^{-1}, total N (Kjeldahl N) 0.45 g kg^{-1}, Olsen P 5.75 mg kg^{-1}, NH_4OAc exchangeable K 0.33cmol (+) kg^{-1} and $CaCl_2$ extractable S 17.5 mg kg^{-1}. Soil physical and chemical analysis was done according to the methods described by Page et al. (1982).

Treatments and design

There were eight treatments with different rates of nitrogen, e.g., control (no nitrogen fertilizer), 18, 36, 54, 72, 90, 108, and 126 kg N ha^{-1}, which was equivalent to 0, 20, 40, 60, 80, 100, 120 and 140% of the current agro-ecological zone (AEZ) based recommended rate of nitrogen (FRG 2018), respectively. The statistical design of the study was a single randomized complete block design, having been replicated thrice. In each block, the treatments were randomly distributed to the plots.

Crop and Variety

The tested crop was rice, and the variety was BR23. The rice variety was developed by the Bangladesh Rice Research Institute for the Kharif-II season. This

is a late variety for the T. Aman season and is very popular in coastal regions. This variety can be transplanted up to the last week of September.

Raising seedling

Healthy seeds of BR23 were immersed in water for 24 hours. The seeds were then taken into a gunny bag. The bag was covered with a polythene sheet to improve the temperature inside the gunny bag. By 48 hours, the seeds started to sprout. After 72 hours, most of the seeds were fully germinated. A seedbed was prepared on high land for raising seedlings. The sprouted seeds of BR23 were sown on 3rd August 2020 in the seed bed.

Field preparation

The main field was tilled with a tractor one week prior to transplanting. Three plowing and cross plowing followed by laddering were done to make optimum puddled condition and to level the field. Individual small plots were prepared according to the layout and design of the experiment. Each plot had a size of 4m × 3m, and the unit plots were surrounded by 30 cm wide and 10 cm high earthen embankment. In between two blocks, a one-meter space was kept free of crops.

Fertilizer application

Every plot received equal P and K fertilizers (15 and 50 kg ha^{-1} P and K, respectively). Sulfur, zinc, or other nutrients were not applied in the field because, in our earlier experiments, we found no response to those elements in rice (Haque et al., 2023a). Urea, triple super phosphate, and muriate of potash were the sources of N, P, and K, respectively. One-third of urea and full TSP and MoP were broadcasted during tilling. The rest of the urea was top-dressed at 20 and 35 days after transplanting.

Uprooting and transplanting of seedlings

A light irrigation was made in the seedbed before the uprooting of the seedlings. Seedlings were then uprooted carefully so that no injury occurred in the seedlings. The seedling age was thirty days during transplanting, and plant-to-plant and row-to-distance was 20 cm × 20 cm. Each hill is comprised of 3-4 healthy seedlings. Transplanting of seedlings was done on 2nd September 2020.

Intercultural operations

Crops were grown under rainfed conditions; therefore, no irrigation was done. Rice plants enjoyed tidal water flooding during their growth period. However, there are fifteen days of spring tide and fifteen days of neap tide. During the neap tide period, water drains out from the field, and fields are inundated with water during the spring tide. Urea fertilizers were top-dressed during the neap tide period, a common practice in the coastal region. The experimental plots were weeded three times. A popular insecticide named Virtako was sprayed to control rice stem borer infestation.

Harvesting and data collection

The rice crop was harvested separately on 25th December 2020 in every unit plot. The grain was separated from the straw by threshing immediately after harvesting, and the fresh weight of each plot's grain was collected at the time of harvest. During weighing grain, moisture content was determined using a moisture meter. Grain yield was expressed on a 14% moisture content basis, whereas straw yield was expressed on a sundry basis. Growth and yield contributing data were recorded from five randomly selected plants. The grain and straw yield data were recorded by harvesting crops from 4 m^2 area. The harvest index and nitrogen use efficiencies were calculated using the following formula:

Harvest index (%)

The Harvest index was calculated by the following formula:

$$\text{Harvest index (\%)} = \frac{\text{Grain Yield}}{\text{Grain Yield + Straw Yield}} \times 100$$

Agronomic efficiency of N (AEN)

The agronomic efficiency of nitrogen was calculated as follows:

$$AEN=\frac{Y_{NA}-Y_{NO}}{R_N}$$

Where, AEN= Agronomic efficiency of nitrogen

$Y_{NA=}$ Yield (kg ha^{-1}) due to N addition

$Y_{NO=}$ Yield (kg ha^{-1}) due to N omission

R_N= Rate of N addition (kg ha^{-1})

Recovery efficiency of N (REN)

Recovery efficiency can be calculated as follows:

$$\text{Recovery efficiency} = \frac{NU_{NA}-NU_{NO}}{R_N}$$

Where,

NU_{NA}: Nutrient uptake (kg ha^{-1}) due to nutrient addition

NU_{NO}: Nutrient uptake (kg ha^{-1}) due to nutrient omission

R_N: Rate of nutrient addition (kg ha^{-1})

Physiological efficiency of N (PEN)

Physiological efficiency was calculated as follows:

$$\text{Physiological efficiency}=\frac{Y_{NA}-Y_{NO}}{NU_{NA}-NU_{NO}}$$

Where,

Y_{NA}: Yield (kg ha^{-1}) due to nutrient addition

Y_{NO}: Yield (kg ha^{-1}) due to nutrient omission

NU_{NA}: Nutrient uptake (kg ha^{-1}) due to nutrient addition

NU_{NO}: Nutrient uptake (kg ha^{-1}) due to nutrient omission

Plant sample analysis

The micro-Kjeldahl method determined the total N content in grain and straw samples (Page et al., 1982). The top third leaf was used to determine chlorophyll concentration following the method described by Coombs et al. (1985).

Statistical analysis

Data recorded on plant parameters were analyzed through the computer-based statistical program STAR (Statistical Tool for Agricultural Research). The significant effect of treatments was determined by analysis of variance (ANOVA) using a one-way randomized complete block design model. The treatment means were compared at a 5% significance level by Duncan's Multiple Range Test (DMRT).

Results and Discussion

Growth and yield attributing characters

The plant height of the T. Aman rice varied significantly due to different nitrogen doses (Table 1). The plant height was greatly affected by the application of different doses of N, and plant height increased with increasing rate of N. Plant height varied from 127.3 to 144.1 cm. The tallest plant was found both in 108 kg N ha^{-1} (120% recommended rate) and 126 kg N ha^{-1} (140% recommended rate) rate, which was statistically similar to 90 kg N ha^{-1} (100% recommended rate) rate (143.5 cm). The shortest plant of 127.3 cm was found in the control treatment. The 18 kg N ha^{-1} recorded statistically similar plant height of the control treatment. However, in the experiment, the increased rate of N progressively increased the plant height of T. Aman rice up to 90 kg N ha^{-1}. Thereafter, plant height attained a plateau. Increased plant height with the nitrogen treatments in sufficient amounts for the rice plant throughout the life cycle might have favored increased cell division and cell enlargement, which ultimately contributed to higher plant height and the number of effective tillers $hill^{-1}$of rice (Jahan et al., 2020).

Table 1. Effects of different rates of nitrogen application on growth and yield contributing characters of T. Aman rice (BR23)

Treatments	Plant height (cm)	Effective tillers hill^{-1} (no.)	No. of filled grains panicle^{-1}	1000-grain wt. (g)
T_1: N control	127.3 c	4.9 c	78.9 c	24.1
T_2: 18 kg N ha^{-1}	132.0 c	5.9 bc	110.5 b	24.4
T_3: 36 kg N ha^{-1}	137.3 b	6.7 abc	131.6 ab	25.1
T_4: 54 kg N ha^{-1}	137.9 b	7.3 ab	135.3 ab	25.4
T_5: 72 kg N ha^{-1}	140.2 ab	7.7 ab	137.1 ab	25.4
T_6: 90 kg N ha^{-1}*	143.5 a	8.2 ab	142.1 a	25.1
T_7: 108 kg N ha^{-1}	144.1 a	8.0 ab	128.1 ab	25.6
T_8: 126 kg N ha^{-1}	144.1 a	9.0 a	126.7 ab	25.5
% CV	1.29	11.36	8.76	7.31
Pr (> F)	0.0000	0.0005	0.0001	0.9550

Means with the same letter are not significantly different at the 5% level by DMRT; * indicate recommended rate (FRG, 2018)

Different nitrogen doses significantly influenced the number of effective tillers per hill (Table 1). Results showed that 126 kg N ha^{-1}(140% recommended rate) produced the highest number of tillers per hill (9.0). The lowest number of tillers per hill, 4.9, was recorded in T_1, which was statistically similar to the treatments T_2 and T_3. Table 1 shows that an increased level of N progressively increased the tiller production of T. Aman rice, although a higher rate of N had no significant improvement. The improved efficiency in tillers hill^{-1} observed in those treatments was attributed to positive root development and increased nitrogen mobility in soil solution and plant root absorption. The results conform with those of Tripathi and Jaishwal (2006).

Different nitrogen doses significantly affected the number of filled grains per panicle (Table 1). The highest number of grains per panicle (142.1) was obtained from 90 kg N ha^{-1}(100% recommended rate). The results clearly showed that with theincrease in the nitrogen dose, the number of grainsper panicle progressively increased to a certain level. After that, it sharply decreased. It indicates that excess N reduced rice fertility, which ultimately negativelyimpacted achieving higherrice yields (Zhao et al., 2022). It was found that 90 kg N ha^{-1}(100% recommended rate) treatment had 80% higher grain production over control. This might be because of the interaction between the source and sink, indicating that the maximum N source percentage is used per panicle and grain filling to create maximum spikelets (Ghoneim et al., 2018).

Thousand-grain weight of T. Aman rice did not vary significantly due to different N doses (Table 1). It probably happened due to the genetic characteristics of rice because rice coleoptile size did not vary to a greater extent by any management practices.

Yield parameters

Different nitrogen doses significantly affected the grain yield of T. Aman rice (Table 2). The lowest grain yield of 3.74 t ha^{-1} was recorded in the control treatment. The grain yield was progressively increased up to 54 kg N ha^{-1} with the increase of the rate of N application, and the highest yield of 5.04 t ha^{-1} was found at 54 kg N ha^{-1}rate, and yield decreased with increasing N rate. From the crop response curve, grain yield attained a static level up to 72 kg N ha^{-1}, and after that, grain yield decreased with increasing N rates under tidal flooded conditions. All the grain yield data were fitted into a quadratic equation of crop response curve to find out the optimum rate of N for growing T. Aman rice. It was found from Fig. 1 that 75 kg N ha^{-1} was the optimum rate of N for growing T. Aman rice (BR23) under tidal water flooded conditions of the coastal

region of Bangladesh. This rate is 83% of the current recommended rate. Therefore, there is a scope to reduce the N rate by about 17% from the AEZ-based recommendation made by the Fertilizer Recommendation Guide (FRG, 2018). Improved root and canopy functions and a morecoordinated source-sink relationship increased yield associated with yield-contributing characters (Ju et al., 2021). The less severe effects of N deficiency for T. Aman rice may be related tolower yield and, therefore decreased demand and to The supplementary supply of N from tidal water inundation (Rahman et al. 2013). Tidal water contains a huge amount of suspended silt and clay particles, which contribute to the N nutrition of the plant (Haque et al. 2008; Haque 2010, 2012). In the experiment, the initial soil contained only 0.45 g kg^{-1} N and 5.6 g kg^{-1} organic carbon, indicating a very low level of N. However, crop response was not obtained in higher N doses because of dissolved N in tidal water. According to Rahman et al. (2013), a 10 cm depth of tidal water can supply 0.05 to 0.46 kg ha^{-1} nitrate, 0.02 to 0.38 kg ha^{-1} ammonium, and 0.05 to 0.42 kg phosphate ha^{-1} daily.

Table 2. Effects of different rates of nitrogen application on yield of T. Aman rice (BR23)

Treatments	Grain yield (t ha^{-1})	Straw yield (t ha^{-1})	Harvest index (%)
T_1: N control	3.74 ^{b}	4.48 ^{b}	45.6 ^{ab}
T_2: 18 kg N ha^{-1}	4.48 ^{ab}	4.97 ^{ab}	47.3 ^{ab}
T_3: 36 kg N ha^{-1}	4.99 ^{a}	5.17 ^{ab}	49.4 ^{a}
T_4: 54 kg N ha^{-1}	5.04 ^{a}	5.07 ^{ab}	49.6 ^{a}
T_5: 72 kg N ha^{-1}	4.76 ^{a}	5.13 ^{ab}	48.2 ^{ab}
T_6: 90 kg N ha^{-1}*	4.55 ^{ab}	5.46 ^{a}	45.3 ^{ab}
T_7: 108 kg N ha^{-1}	4.36 ^{ab}	5.57 ^{a}	43.9 ^{ab}
T_8: 126 kg N ha^{-1}	4.30 ^{ab}	5.73 ^{a}	42.9 ^{b}
% CV	7.50	6.07	4.47
Pr (> F)	0.0075	0.0068	0.0095

Means with the same letter are not significantly different at the 5% level by DMRT;*indicate recommended rate (FRG, 2018)

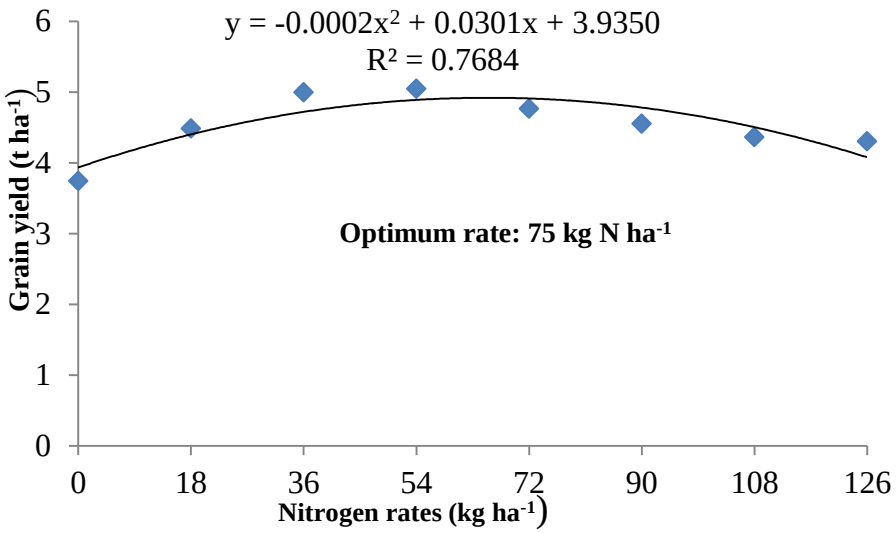

Fig. 1. Crop response curve to identify the optimum rate of N for growing T. Aman rice (BR23) at Ganges tidal water flooded the ecosystem

Optimum N rate = $\frac{-b}{2c} = \frac{-0.0301}{2 \times (-0.0002)}$ = 75 kg ha^{-1}

The straw yield varied significantly due to the application of different doses of nitrogen (Table 2). Results showed that increasing the N dose progressively increased the straw yield of rice; the highest (5.73 t ha^{-1}) was found in 126 kg N ha^{-1}(140% recommended rate), which was statistically similar to 90 and 108 kg N ha^{-1} with the value of 5.46 t ha^{-1} and 5.57 t ha^{-1}, respectively. The lowest straw yield (4.48 t ha^{-1}) was obviously achieved from the control treatment. The results found in grain yield were quite different from straw yield data. Increasing the N rate proportionately increases the vegetative growth of rice; interestingly, excessive vegetative growth does not favor a higher yield; rather, grain yield decreases due to an increase in the sterility of rice. Higher availability of nitrogen in the field at the vegetative growth stage when the primary, secondary, and tertiary tillers are initiated, and the accumulation of dry matter is probably favored to produce the higher straw yield. The results showed that the higher dose of nitrogen influenced vegetative growth in terms of plant height and total tillers per hill, resulting in differences in straw yield (Haque et al., 2003).

The different nitrogen doses significantly influenced the harvest index (HI) (Table 2). No N fertilizer was added in the control treatment, and HI was 45.6. The HI value progressively increased with the increase in the rate of N up to 54 kg N ha^{-1} (49.6 %); after that, it gradually decreased with increasing rate of applied N. The lower HI was found in higher rates of N due to higher straw yield in these treatments. Similar findings also found that the harvest index increased with increasing doses of N fertilizer, but after a certain level, it decreased (Siddique et al., 2014).

Grain and straw N contents

Different nitrogen doses had remarkable effects on the grain N content of T. Aman rice, though the effects on grain N contents were not significantly different (Table 3). Grain N content varied from 1.13 to 1.49 % over the treatments, with the highest value found in 126 kg N ha^{-1} rate and the lowest in the control treatment. It is observed from Table 3 that increasing the applied N rate proportionately increases the grain N content. Unfortunately, a higher rate of N in grain could not contribute to achieving a higher grain yield of rice. It means that rather than excess, a certain level of N in grain is required to attain the maximum rice yield. Various nitrogen doses significantly affect straw nitrogen content (Table 3). Like grain, the straw N content also progressively increased with the increased rate of applied N. The Highest nitrogen content (1.33%) was obtained from the T_8 (126 kg N ha^{-1}) treatment, and the lowest straw nitrogen content (0.95%) was found in the control treatment. However, there was found no significant difference in straw N contents in all the N doses except control.

Table 3. Effects of different rates of nitrogen application on N content and uptake of T. Aman rice (BR23)

Treatments	Grain N content (%)	Straw N content (%)	Grain N uptake (kg ha^{-1})	Straw N uptake (kg ha^{-1})	Total N uptake (kg ha^{-1})
T_1: N control	1.13	0.95^{b}	42.14^{b}	42.84^{d}	84.89^{b}
T_2: 18 kg N ha^{-1}	1.39	1.18^{a}	62.40^{a}	58.38^{c}	120.78^{a}
T_3: 36 kg N ha^{-1}	1.44	1.21^{a}	72.32^{a}	62.49^{bc}	134.81^{a}
T_4: 54 kg N ha^{-1}	1.41	1.22^{a}	70.20^{a}	61.69^{bc}	131.89^{a}
T_5: 72 kg N ha^{-1}	1.43	1.25^{a}	67.97^{a}	63.85^{abc}	131.82^{a}
T_6: 90 kg N ha^{-1}*	1.46	1.23^{a}	66.56^{a}	67.35^{abc}	133.91^{a}
T_7: 108 kg N ha^{-1}	1.48	1.31^{a}	64.70^{a}	72.98^{ab}	137.68^{a}
T_8: 126 kg N ha^{-1}	1.49	1.33^{a}	64.11^{a}	76.21^{a}	140.32^{a}
% CV	10.36	6.14	10.56	6.88	7.08
Pr (> F)	0.1375	0.0008	0.0023	0.000	0.0001

Means with the same letter are not significantly different at the 5% level by DMRT; * indicate recommended rate (FRG, 2018).

Nitrogen uptake

Grain nitrogen uptake varied significantly with different nitrogen doses (Table 3). It varies from 42.14 kg ha^{-1} to 64.11 kg ha^{-1} over the treatments. Different nitrogen doses also significantly influenced straw nitrogen uptake (Table 3). The highest straw nitrogen uptake (76.21 kg ha^{-1}) takes place in the T_8 (126 kg N ha^{-1}) treatment, and the lowest straw nitrogen uptake (42.84 kg ha^{-1}) takes place in the T_1 (no nitrogen) treatment. Total nitrogen uptake also varied due to different N doses (Table 3). It varies from 84.89 kg ha^{-1} to 140.32 kg ha^{-1}. The highest was found in T_8 (126 kg N ha^{-1}), and the lowest was in T_1 (no nitrogen) treatment.

Agronomic use efficiency of N

Nitrogen doses had a tremendous effect on agronomic efficiency of N (AEN; Fig. 2). The AEN varied from 4.5 to 41.1 kg grain per kg added N. In lower N application doses, agronomic efficiency was found to be higher, and agronomic efficiency was found to be lower in higher N application doses. Haque and Hoque (2023) reported that the progressively increased rate of N application increased both grain yield and N concentration in plants following quadratic model, therefore, at a lower rate of N application, the N use efficiency parameters were higher, and at a higher rate, the N use efficiency was lower. At low doses of N fertilizer application, Saleque et al. (2005) also indicated that AEN generally is higher.

Recovery efficiency of N (REN)

Nitrogen doses greatly affected recovery efficiency (Fig. 3). The REN varied from 0.174 to 1.125 kg grain per kg added N. In lower N application doses, the recovery efficiency was higher, and similarly, in higher N application doses, the recovery efficiency was lower.

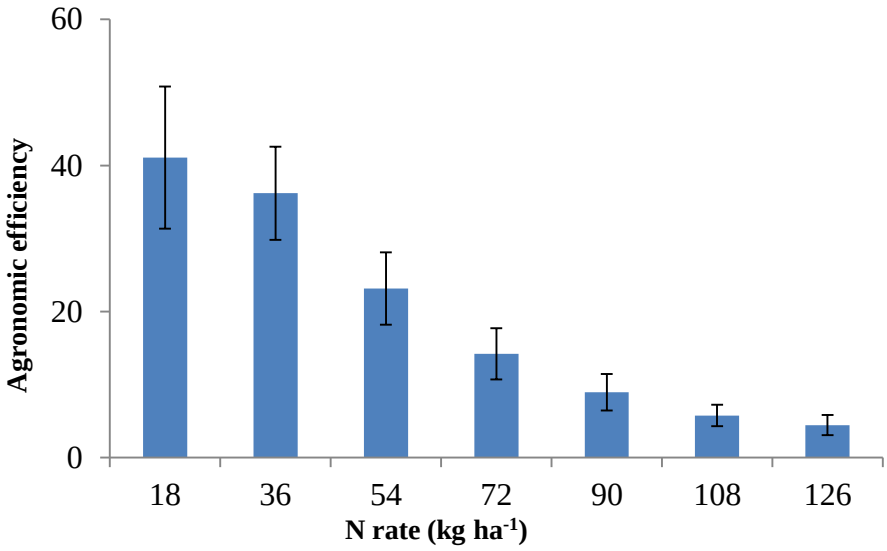

Fig. 2. Agronomic efficiency (kg grain kg^{-1}N) of nitrogen for growing T. Aman rice (BR23) at Ganges tidal water flooded coastal ecosystem of Bangladesh; vertical lines in bars indicate standard error of the mean.

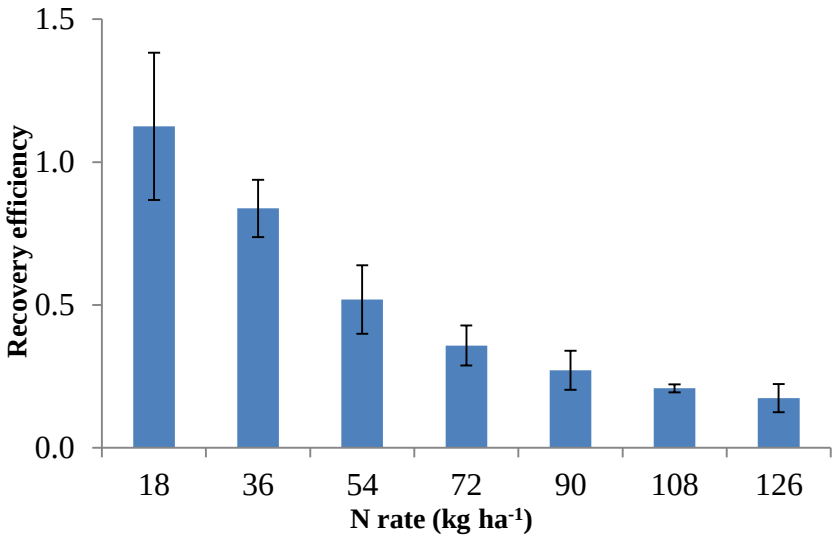

Fig. 3. Recovery efficiency (kg N uptake kg^{-1} added N) of nitrogen for growing T. Aman rice (BR23) at Ganges tidal water flooded coastal ecosystem of Bangladesh; vertical lines in bars indicate standard error of the mean.

Physiological efficiency of N (PEN)

Nitrogen doses had an interesting effect on the physiological efficiency of N (Fig. 4). The PEN varied from 27.5 to 44.5 kg grain per kg N uptake. Firstly, in lower N application doses, the PEN was found to be lower; similarly, in higher N application doses, the PEN was higher. Physiological efficiency was found to be highest at a 54 kg N ha^{-1} rate but gradually decreased after an increase in nitrogen rate.

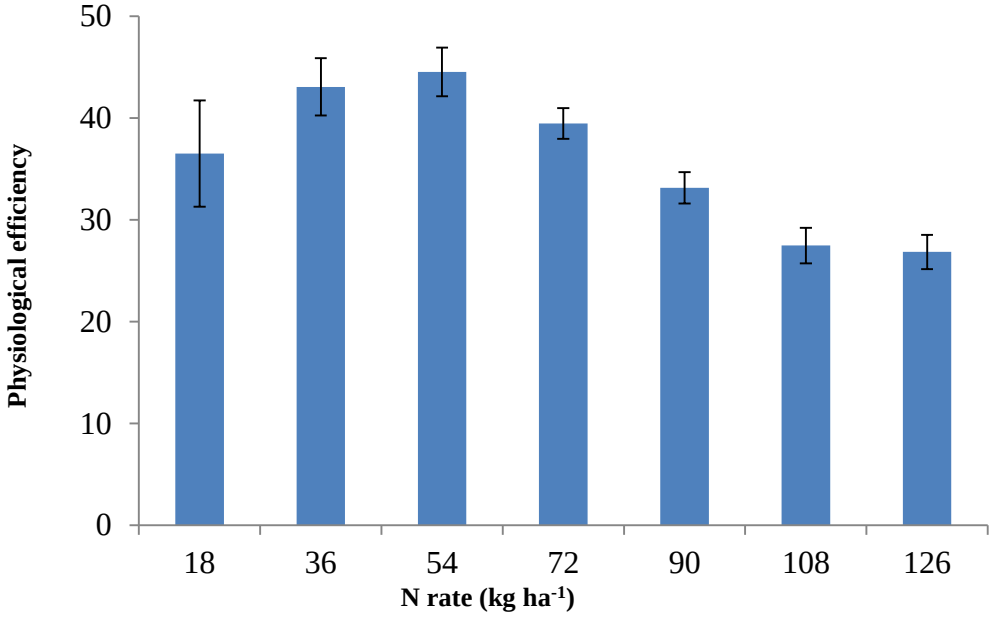

Fig. 4. Physiological efficiency (kg grain kg^{-1} N uptake) of nitrogen for growing T. Aman rice (BR23) at Ganges tidal water flooded coastal ecosystem of Bangladesh; vertical lines in bars indicate standard error of the mean.

Chlorophyll content of leaf

Chlorophyll-a, chlorophyll-b, and total chlorophyll content varied significantly with different nitrogen doses (Table 4). Increased N levels progressively increased the chlorophyll content of the leaf. Over the treatments, chlorophyll-a, chlorophyll-b, and totalchlorophyll content varied from 2.48 to 3.36, 0.52 to 0.77 and 3.01 to 4.13 mg g^{-1} fresh leaf, respectively. Overall results indicated that the application of N increases the chlorophyll contentof rice, and it was progressively increased with the increase of the rate of N. The use of nitrogen immediately increased the content of chlorophyll and leaf surface, leading to higher photosynthesis (Verma et al., 2004). The findings of this study revealed that a suitable nitrogen rate may increase photosynthesis, but excess nitrogen was not favorable for photosynthesis. Nitrogen is one of the major nutrients in chlorophyll biosynthesis (Razaq et al., 2017).

Conclusion

Increasing nitrogen levels caused an increase in plant growth and development up to a certain level of nitrogen application; after that, crop growth decreased. One of the essential factors to enhance N efficiency in rice cultivars is the application of an adequate quantity of N fertilizers. Optimum N application rate enhances the efficiency of N usage. It was found that 75 kg N ha^{-1} is an optimal N rate for producing a higher grain yield of T. Aman rice. This optimum rate is 83% of the current recommended rate for T. Aman rice in the study area. Therefore, there is a scope to reduce the N rate by about 17% from the Fertilizer Recommendation Guide (FRG-2018) recommend-dation. Further study is suggested to validate the findings by including more areas and other rice varieties.

Table 4. Effects of different rates of nitrogen application on chlorophyll content of leaf of T. Aman rice (BR23)

Treatments	Chlorophyll-a (mg g^{-1} fresh leaf)	Chlorophyll-b (mg g^{-1} fresh leaf)	Total chlorophyll (mg g^{-1} fresh leaf)
T_1: N control	2.48^{b}	0.52^{b}	3.01^{b}
T_2: 18 kg N ha^{-1}	2.82^{ab}	0.63^{ab}	3.45^{ab}
T_3: 36 kg N ha^{-1}	2.86^{ab}	0.64^{ab}	3.5^{ab}
T_4: 54 kg N ha^{-1}	2.88^{ab}	0.66^{ab}	3.53^{ab}
T_5: 72 kg N ha^{-1}	3.08^{ab}	0.69^{ab}	3.77^{ab}
T_6: 90 kg N ha^{-1}*	$3.21a^{b}$	0.75^{a}	3.96^{ab}
T_7: 108 kg N ha^{-1}	3.36^{a}	0.77^{a}	4.13^{a}
T_8: 126 kg N ha^{-1}	3.27^{ab}	0.77^{a}	4.04^{a}
% CV	9.25	11.23	9.33
Pr (> F)	0.0277	0.0173	0.0202

Means with the same letter are not significantly different at the 5% level by DMRT; *indicate recommended rate (FRG, 2018)

Acknowledgments

The research work was funded by the "Nutrient Management for Diversified Cropping in Bangladesh (NUMAN) project" jointly funded by ACIAR Australia (LWR/2016/136) and KGF Bangladesh (ICP-II). Especial thanks to Richard W Bell (Project leader), Murdoch University, Australia, for his suggestion and criticism of the project research. The first author expresses gratitude to the NUMAN project for offering the MS fellowship.

Author contributions

Samsunnahar Pranto experimented and wrote the first draft of the manuscript. Mohammad Asadul Haque planned and supervised the research work, edited, improved, and submitted the manuscript. Md Fazlul Hoque helped in the chemical analysis of soil and plant samples.

Conflict of interests

The authors declare that there is no conflict of interest regarding the publication of this paper.

References

Akter T, Parvin MT, Mila FA and Nahar A. Factors determining the profitability of rice farming in Bangladesh. *J. Bangladesh Agric. Univ*. 2019; 17: 86-91.

BBS. *Yearbook of Agricultural Statistics of Bangladesh.* Statistics and Informatics Division, Bangladesh Bureau of Statistics. Ministry of Planning, Government of the People's Republic of Bangladesh. 2019; p. 39.

Begum R, Jahiruddin M, Kader MA, Haque MA and Hoque ABMA. Effects of zinc and boron application on onion and their residual effects on mungbean. *Progress. Agric.* 2015; 26(2): 90-96.

Choudhury ATMA and Kennedy IR. Nitrogen fertilizer losses from rice soils and control of environmental pollution problems. *Commun. Soil Sci. Plant Anal.* 2005; 36:1625-1639.

Coombs J, Hind G, Leegood RC, Tieszen LL and Vonshak A. Analytical Techniques. In: *Techniques in Bioproductivity and Photos-ynthesis*. Coombs J, Hall DO, Long SP, Scurlock JMO (Editors), 2nd edition, Pergamon Press, 1985; p. 219-228.

Fageria NK and Baligar VC. Methodology for evaluation of lowland rice genotypes for nitrogen use efficiency. *J. Plant Nutr*. 2003; 26: 1315-1333.

FRG. *Fertilizer Recommendation Guide*, Bangladesh Agricultural Research Council (BARC), Farmgate, Dhaka. 2018; p 56.

Ghoneim AM, Gewaily EE and Osman MM. Effects of nitrogen levels on growth, yield and nitrogen use efficiency of some newly released Egyptian rice genotypes. *Open Agric.* 2018; 3(1): 310-318.

Hania U, Rabbani MG, Haque MA, Choudhury MSH, Sultana MN and Jahiruddin M. Micronutrient requirements for onion cultivation at old Brahmaputra floodplain soil. *Bangladesh J. Environ. Sci*. 2013; 24:191-95

Haque MA and Hoque MF. Nitrogen fertilizer requirement and use efficiency in sunflower at Ganges delta coastal salt-affected soils. *Commun. Soil Sci. Plant Anal.* 2023; 54(16): 2248-2262.

Haque MA and Jharna DE. Effects of nitrogen in different planting date on yield, yield component and nitrogen use efficiency of rice cultivation. *Intl. J. Sustain. Agril. Tech*. 2008; 4(3): 23-28.

Haque MA, Husain MM, Jharna DE, Uddin MN and Hussain ASMI. A comparative study of leaf color chart based and farmer's practice of nitrogen fertilizer application on rice under on-farm conditions of Bangladesh. *Pakistan J. Biol. Sci*. 2003; 6 (19): 1685-1688.

Haque MA, Jahiruddin M, Hoque MF, Islam MS, Hossain MB, Satter MA, Haque ME and Bell RW Increasing the use efficiency of fertilizer phosphorus for maize in low-P Ganges delta soils. *J. Plant Nutr*. 2023b; 46(10): 2257-2275.

Haque MA, Kabir ME, Akhter S, Hoque MF, Sarker BC, Anik MFA, Ahmed A, Pranto S, Sima AS, Lima F, Jahiruddin M, Hossain MB, Haque ME, Satter MA and Bell RW. Crop nutrient limitations in intensified cropping sequences on

the Ganges delta coastal floodplains. *J. Soil Sci. Plant Nutr*. 2023a; 23: 1996-2006.

Haque MA, Khatun A, Jharna DE and Saleque MA. Effect of tidal water flooding on growth and nitrogen uptake of rice. *Intl. J. Bio. Res.* 2008; 5(2): 1-5.

Haque MA. Contribution of tidal submergence to phosphorus nutrition and yield of rice. *J. Bangladesh Agric. Univ*. 2010; 8(2): 207-212.

Haque MA. Effects of tidal submergence on potassium nutrition and yield of rice. *Bangladesh J. Agric. Res.* 2012; 37(3): 433-439.

Haque MA. Increasing yield of maize through potash fertilizer management in saline soil. *J. Bangladesh Agric. Univ*. 2020; 18(2): 362-366.

Howlader P, Jahiruddin M, Islam MR and Haque MA. Requirement of micronutrients for yield maximization of rice in old Brahmaputra floodplain soil. *Bangladesh J. Crop Sci*. 2013; 24: 187-192.

Jahan A, Islam A, Sarkar MIU, Iqbal M, Ahmed MN and Islam MR. Nitrogen response of two high yielding rice varieties as influenced by nitrogen levels and growing seasons. *Geol. Ecol. Landsc.* 2020; 6(1): 1-8.

Ju C, Liu T and Sun C. Panicle nitrogen strategies for nitrogen-efficient rice varieties at a moderate nitrogen application rate in the lower reaches of the Yangtze River, China. *Agron.* 2021; 11(2): 1-11.

Ladha JK, Pathak H, Krupnik TJ, Six J and van Kessel C. Efficiency of fertilizer nitrogen in cereal production: retrospects and prospects. *Adv. Agron.* 2005; 87: 85-156.

Ma P, Lan Y, Lyu T, Li F, Yang Z, Sun Y and Ma J. Nitrogen: fate and efficiency of fertilizer application under a rapeseed–wheat–rice rotation system in southwest China. *Agron.* 2021; 11(2): 258.

Page AL, Miller RH and Keeney DR. *Methods of Soil Analysis. Part 2. Chemical and Microbiological Properties.* American Society of Agronomy. In Soil Science Society of America, Madison, Wisconsin. 1982: vol. 1159.

Peng J, Feng Y, Wang X, Li J, Xu G, Phonenasay S, Luo Q, Han Z and Lu W. Effects of nitrogen application rate on the photosynthetic pigment, leaf fluorescence characteristics, and yield of indica hybrid rice and their interrelations. *Sci. Rep*. 2021; 11(1): 7485.

Rahman SMB, Sarder L, Rahman MS, Ghosh AK, Biswas SK, Siraj SMS, Huq KA, Hasanuzzaman AFM and Islam SS. Nutrient dynamics in the Sundarbans mangrove estuarine system of Bangladesh under different weather and tidal cycles. *Ecol. Process,* 2013;2:29.

Razaq M, Zhang P, Shen HI and Salahuddin. Influence of nitrogen and phosphorous on the growth and root morphology of *Acer mono*. *PLoS ONE.* 2017; 12(2): e0171321.

Saleque MA, Naher UA, Choudhury NN and Hossain ATMS. Variety-specific nitrogen fertilizer recommendation for lowland rice. *Commun. Soil Sci. Plant Anal.* 2005; 35(13-14): 1891-1903.

Siddique MA, Islam N, Islam MZ, Islam SMM and Hussain J. Effect of N level on growth and yield of T. aman rice cv. Surjomoni. *Int. J. Sustain. Crop Prod.* 2014; 9(2): 33-37.

Tripathi HP and Jaishwal LM. Effect of nitrogen on yield and yield attributes of rice hybrids under irrigated conditions. *Oryza.* 2006; 43(3): 249-250.

Verma AK, Pandey N and Tripathy RS. Leaf growth, chlorophyll, nitrogen content and grain yield of hybrid rice as influenced by planting times and N levels. *Ann. Agric. Res. New Series.* 2004; 24(3): 456-458.

Zhao C, Liu G, Chen Y, Jiang Y, Shi Y, Zhao L, Liao P, Wang W, Xu K, Dai Q and Huo Z. Excessive nitrogen application leads to lower rice yield and grain quality by inhibiting the grain filling of inferior grains. *Agriculture.* 2022; 12(7): 962.

J. Bangladesh Acad. Sci. 47(2); 181-193: December 2023 DOI:https://doi.org/10.3329/jbas.v47i2.67851

Journal of Bangladesh Academy of Sciences

Journal homepage: http://www.bas.org.bd/publications/jbas.html

Research Article

In silico analysis of deleterious SNPs of human *DCDC2* gene and their impacts on subsequent protein-protein interactions

Nure Asma Lata, Nahid Parvez and Sumaiya Farah Khan*

Department of Genetic Engineering and Biotechnology, Faculty of Life and Earth Science, Jagannath University, Dhaka, Bangladesh

ARTICLE INFO

Article History

Received: 25 July 2023
Revised: 08 August 2023
Accepted: 14 August 2023

Keywords: DCDC2, Dyslexia, Microtubules, Single nucleotide polymorphism (SNP), Computational analysis

ABSTRACT

DCDC2 is a clinically significant protein causing a number of neurological disorders and, hence, is an important protein for analysis. In this study, multiple tools were employed to identify missense SNPs that are harmful to the protein itself and destabilize the interaction of this protein with tubulin subunits. After analyzing all 378 missense SNPs retrieved from the dbSNP database, thirteen were found to have harmful effects on the protein, which are L20P, R23L, G25W, G25R, D26E, I36N, G60E, P68S, G83R, T174I, L179R, R186G, V208E. Among these, four SNPs- T174I, L179R, R186G, and V208E were suggested to be significantly destabilizing for the interaction of the C-DC domain with microtubule, and three SNPs- L20P, D26E, and G83R for the interaction of N-DC domain with microtubule. Based on the total ΔΔG value, SNP R186G and L20P seem most destabilizing for the interaction of the C-DC and N-DC domains. These SNPs are found to affect the protein negatively by analysis using several computational tools. Genetic association and protein-protein interaction studies focused on these SNPs can reveal new findings about dyslexia or other neurodevelopmental disorders.

Introduction

DCDC2 (Doublecortin Domain Protein 2) is a member of the superfamily of proteins that include doublecortin domains (DC). This domain was discovered in an X-linked gene called *Doublecortin (DCX),* which is found to be associated with neural development (Liu et al., 2012). The protein encoded by this gene, *Doublecortin (DCX),* is crucial for brain growth and the formation of the layers of the cerebral cortex in the embryonic stage (Kim et al., 2003; Manka and Moores, 2020). Most of the understanding of doublecortin-related genes' molecular function (or malfunction) comes from the DCX protein and its aptitude for microtubule binding (Dijkmans et al., 2010). DCX are traditional microtubule (MT) associated proteins (MAPs), having two conserved tandems in two terminal domains that contribute to tubulin-binding over evolutionary time (Reiner et al., 2006) and is linked with MT stabilization, which regulates the cytoskeleton and is essential for neuronal migration, differentiation, maturation, and postmitotic neurons (Kim et al., 2003; Conde and Caceres, 2009). DCX can be divided into two functional parts: the N-terminal 30 kDa part is the protein's microtubule (MT) binding portion and comprises two homologous, 11 kDa DC domains. DCX contributes to brain development by stabilizing microtubules in the leading process of migrating neurons and other neuronal processes (Horesh et al., 1999). Recently, electron microscopy has shown that a single DC

*Corresponding author: <sumaiyafarah@yhaoo.com>

domain binds to microtubules at the vertex of four tubulin subunits in the groove between protofilaments (Fourniol et al., 2010).

Microtubule-associated proteins (MAPs) are indispensable to neurons at the embryonic stage, administering neuronal migration, dendrites, and axon development (Gleeson et al., 1998). Numerous studies on the effects of DCX on microtubules in neurons have revealed cooperative binding effects, modifications to MT structure, and control over molecular motors (Gleeson et al., 1999; Moores et al., 2006). Several studies reported the dysfunction of MT binding by mutant DCX consequences in inappropriate brain development and evolving diseases like lissencephaly, dyslexia, etc. (Moores et al., 2004; Gabel et al., 2011; Bechstedt and Brouhard, 2012).

α/β-tubulin heterodimers that assemble into protofilaments (PFs) make up microtubules. Doublecortin preferentially induces the construction of 13 protofilament microtubules and binds to them (Tilney et al., 1973; Chaaban and Brouhard, 2017). The nucleation and stabilization of this physiological 13-PF architecture are highly influenced by doublecortin. DCX contains N-terminal (N-DC) and C-terminal domain (C-DC), which have a considerable contribution to microtubule binding via PFs (Bechstedt and Brouhard, 2012; Bechstedt et al., 2014; Burger et al., 2016). MT nucleation seems to be facilitated by the conformationally plastic C-DC module, which also appears to stabilize tubulin-tubulin interactions while N-DC conducts MT stabilization (Manka and Moores, 2020). However, DC domain tandem is necessary for this function because DC domains alone do not induce MT polymerization (Taylor et al., 2000). Missense changes in the DC domains can be divided into two groups: those that occur at surface residues and those at hydrophobic residues ensconced in the heart of the ubiquitin fold. It is anticipated that the latter group will result in DCX misfolding. Bechstedt showed three consequences: loss of 13-PF selectivity, loss of cooperative contacts, and decreased microtubule binding are the first two kinds of biochemical defects in mutant DCX, while decreased turbidity assay performance is the third in their study (Bechstedt and Brouhard, 2012). Other studies reported that point mutation in N-DC, C-DC, and tandem alters DCX binding to MT or forms inappropriate fold and contributes to disease mechanism (Kim et al., 2003; Manka and Moores, 2020). Over and above deafness in humans was caused by a missense mutation in the doublecortin protein's C-terminal region (Grati et al., 2015).

The current study is focused on *DCDC2* of chromosome 6, which also has DC domains like DCX. Having DC domains, DCDC2 should also interact with microtubules and probably have functions in neural development. Studies reported mutation in our targeted gene *DCDC2* involved in renal-hepatic ciliopathy, neonatal sclerosing cholangitis with developmental delay, nephronophthisis, human recessive deafness, dyslexia, etc. (Gabel et al., 2011; Schueler et al., 2015; Girard, 2016; Srivastava et al., 2018; Syryn et al., 2021). Polymorphism in DCDC2 was reported to emerge in learning disability and speech difficulty (Lind et al., 2010; Zhong et al., 2013; Zhang et al., 2016).

No X-ray crystallography structure is available for the DCDC2 protein under study. The predicted tertiary structure of the DCDC2 protein is available in the AlphaFold database (ID: AF-Q9UHG0-F1), and it shows that this protein, like DCX protein, also contains two DC domains: one is N-terminal (17-100 aa) and another is C-terminal (139-222aa). Each of the domains should interact at the groove between two protofilaments. The rest of the region has no defined structural motif and is indicated as disordered. It has been stated that DC domain-containing proteins are involved in neural development through their interaction with microtubules. It is worth mentioning that association studies of the DYX2 locus on 6p21.3 have already identified altered DCDC2 as involved in common neurogenetic disorder reading disability (RD) or

dyslexia (Meng et al., 2011). The mentioned association studies identified 14 missense SNPs, each part of either N-terminal DC or C-terminal DC domains.

SNPs (Single nucleotide polymorphism), a molecular marker, refers to the variation or substitution of a single nucleotide at a specific position in DNA sequence among individuals (Vignal et al., 2002). SNPs can either be silent (synonymous), modify the encoded amino acids, or appear in non-coding areas. Missense SNPs result in the substitution of the wild-type amino acid. They are reported to be involved in the diversity of people, the evolution of the genome, and the most prevalent familial features, interindividual variations in drug response, as well as complicated and widespread illnesses like diabetes, obesity, hypertension, and mental health issues. They may have an impact on messenger RNA (mRNA) structure (stability), subcellular localization of mRNAs and/or proteins, and promoter activity (gene expression), and hence may result in illness (Shastry, 2009).

Though polymorphisms in DCDC2 cause several cases of diseases, no SNP-based computational analysis has been conducted yet. *Silico* SNP analysis will reveal risky SNP candidates' functional and structural importance. As a MAP-associated protein-coding gene, *DCDC2* has a distinct importance as a target of the experiment. The study will identify the most damaging and disease-causing missense SNP, alteration of protein stability, and evolutionary conservation to evaluate the potential for causing disease in the selected candidate. Moreover, maintaining protein-protein interactions is important for the usual function of the protein, and any mutation altering that interaction can cause disease. Accurate prediction of the effect of missense SNPs in protein binding is crucial for carrying out genome-wide studies. Therefore, in this study, the effect of missense SNPs on the protein-protein interaction of DCDC2 has also been explored.

Materials and Methods

Retrieving missense SNPs

All the required data of the human *DCDC2* gene, such as FASTA sequence and SNP, were retrieved from UniProtKB (https://www.uniprot.org/) and the National Centre for Biological Information (NCBI) (https://www.ncbi.nlm.nih.gov/) respectively. For this study, our main concern was missense SNPs. The missense SNP information, including protein accession number, missense rsID, allele change, position, and residue change, was collected from the NCBI dbSNP database (http://www.ncbi.nlm.nih.gov/nsNSSNP/).

Identifying the most damaging missense SNPs

The functional effect of missense SNPs of human *DCDC2* gene was identified using five tools, PolyPhen2 (http://genetics.bwh.harvard.edu/pph2/) (Adzhubei et al., 2010), PROVEAN [http://provean.jcvi.org/index.php] (Choi and Chan, 2015), SNPnexus (https://www.nsNSSNP-nexus.org/v4/) (Oscanoa et al., 2020), SNAP2 (https://www.rostlab.org/servces/snap/) (Johnson et al., 2008), Pon-P2 (http://structure.bmc.lu.se/PON-P2/) (Niroula et al., 2015).

PolyPhen-2 (Polymorphism Phenotyping v2) is an automatic tool that predicts the impacts of a missense SNP based on the sequence, biological process, and structural information characterizing the substitution.

PROVEAN is a tool similar to PolyPhen2, which predicts the impact of amino acid substitution.

SNPnexus tool uses the major gene annotation system to bring out essentially yields two results: tolerated and deleterious for SIFT prediction, and PolyPhen-2 prediction comes out as benign, perhaps damaging, and probably damaging (Oscanoa et al., 2020).

The SNAP2 server classifies the variations as having an effect or being neutral and provides a confidence score (Johnson et al., 2008).

PON-P2 is a pathogenic missense SNP identifier that groups the output into neutral, pathogenic, or unknown depending on the random forest probability score (Niroula et al., 2015).

In the case of PolyPhen-2, score 1 indicates the most damaging SNPs (http://genetics.bwh.harvard.edu/pph2/). For PROVEAN and SNPnexus, deleterious SNPs are indicated by scores lower than -2.5 and -0.5, respectively (http://provean.jcvi.org/index.php, https://www.nsNSSNP-nexus.org/v4/). The lower the score from the threshold, the more deleterious the SNPs are. In the case of SNAP2 (https://www.rostlab.org/servces/snap/) and PON-P2 (http://structure.bmc.lu.se/PON-P2/), SNPs are identified as deleterious if their scores are higher than 0 and 0.5 respectively. A higher score indicates more deleterious SNP. All the collected missense SNPs from dbSNP went through these five identifier tools to predict the most deleterious missense SNPs. SNPs, determined deleterious by at least four tools, were used for further investigation.

Results and discussions

Identification of disease-associated missense SNPs

SNPs&GO (http://snps-and-go.biocomp.unibo.it/snps-and-go/) and PMut (http://mmb.pcb.ub.es/PMut/) were applied to predict the association of SNPs with disease. The tool SNPs&GO is based on a supporting vector machine that classifies human disease correspondent single amino acid substitution with 82% accuracy, and results are classified into disease and neutral (Calabrese et al., 2009). Protein sequence, evolutionary information, and other information from gene ontology are used to predict (https://snps-and-go.biocomp.unibo.it/snps-and-go/). PMut is also a classifier that discovers possible disease-associated missense SNPs utilizing the manually curated variation database SwissVar. SNPs, sorted as a disease by both tools, were considered significant and selected as final short-listed SNPs for additional studies.

Protein evolutionary conservation analysis

A visual image was generated where "f" denoted a functional residue that is highly conserved and exposed, and "s" denoted a predicted structural residue that is highly conserved and buried. Color gradient showed the variable region to a highly conserved region. From this prediction, the SNPs and positions were found with conservation scores as color intensity.

Amino acid residues that are highly conserved are generally part of an important functional domain of a protein. ConSurf(https://consurf.tau.ac.il/), a Bayesian inference-based tool, was used for the conservation analysis of the DCDC2 protein sequence to detect highly conserved regions (Ashkenazy et al., 2010). It creates a phylogenetic tree based on the relationships between homologous sequences (Pupko et al., 2002). A conservation score of 1 to 4 was considered variable, a score of 5 to 6 was considered moderate, and a score of 7 to 9 was considered conserved (Jia et al., 2014).

Analysis of protein stability

The mutation causes an increase or decrease in protein stability, which causes an alteration of protein function. Changes in the stability of the protein due to point mutation were computed by two software, I-Mutant 2.0 (http://folding.biofold.org/i-mutant/i-mutant2.0.html) and MUpro.

I-Mutant2.0 is a tool that predicts protein stability changes depending on support vector machine (SVM) utilizing data from ProTherm. It calculates ΔΔG value by subtracting the wild protein's unfolding free energy value from the mutant protein's folding Gibbs free energy (Bava and Gromiha, 2004; Capriotti et al., 2005). MUpro also utilizes ΔΔG value to predict the stability change resulting from missense SNPs (Baldi, 2005).

Protein-protein interaction analysis

Based on the available experimental structures of N-DC domain and C-DC domain of DCX protein with tubulin subunits (6rev, 6RF2), two homology models have been generated using SWISS-MODEL (https://swissmodel.expasy.org/). Model No. 1 contains the N-DC domain of DCDC2 in complex with two monomers of tubulin alpha-1B chain and two monomers of tubulin beta-2B chain. Model no. 2 contains the C-DC domain of DCDC2 in a complex with identical tubulin monomers. Both models are larger than 500 amino acids, and no available *in silico* tool can refine and analyze the protein-protein interaction of such large models. So, each model was divided into two models: Model 1a containing N-DC

domain of DCDC2 and two monomers of tubulin alpha-1B chain, Model 1b containing N-DC domain of DCDC2 and two monomers of tubulin beta-2B chain, Model 2a containing C-DC domain of DCDC2 and two monomers of tubulin alpha-1B chain and Model 2b containing C-DC domain of DCDC2 and two monomers of tubulin beta-2B chain. These four models were refined with the Galaxy refine server (https://galaxy.seoklab.org/cgi-bin/submit.cgi?type=REFINE). Later, the refined versions were analyzed with three different tools (MCSM-PPI2, SAMBE-3D, and Beat-Music) to determine each complex's binding free energy change (ΔΔG) due to missense SNPs. The final short-listed SNPs were considered for predicting binding energy change (ΔΔG). mCSM-PPI2 is a novel machine-learning computational tool that exploits graph-based structural signatures to model the effects of variations on the inter-residue interaction network for more accurately predicting the effects of missense mutations on protein-protein interaction binding affinity (Dijkmans et al., 2010).

SAAMBE-3D is another machine learning-based approach for fast and accurate protein-protein interaction predictions (Pahari et al., 2020).

BeAtMuSiC is a coarse-grained predictor of the changes in binding free energy induced by point mutations. It relies on a set of statistical potentials derived from known protein structures and combines the effect of the mutation on the strength of the interactions at the interface and on the overall stability of the complex (Dehouck et al., 2013).

Table 1. Short-listed 13 SNPs and scores of those SNPs in seven tools

No	SNP	PolyPhen2[a]	PROVEAN[b]	SNPnexus[c]	SNAP2[d]	PON-P2[e]	SNPs&GO[f]	PMut[g]
1	R23L	1	-5.33	0.03	83	0.758	0.619	0.83
2	G83R	1	-6.48	0.02	62	0.805	0.674	0.77
3	G60E	1	-4.19	0	84	0.054	0.897	0.83
4	I36N	0.99	-5.36	0	60	0.582	0.820	0.84
5	R186G	0.998	-4.50	0	81	0.484	0.589	0.80
6	L179R	0.997	-4.39	0	76	0.759	0.606	0.64
7	G25W	1	-7.12	0	90	0.656	0.803	0.89
8	G25R	0.733	-7.08	0.02	86	0.626	0.716	0.16
9	P68S	1	-6.06	0	48	0.679	0.625	0.87
10	V208E	1	-5.33	0	80	0.717	0.652	0.65
11	L20P	0.979	-3.44	0	63	0.576	0.580	0.88
12	D26E	0.999	-3.58	0.03	72	0.481	0.512	0.86
13	T174I	1	-4.30	0	59	0.677	0.619	0.83

[a]PolyPhen2 predicts damaging if score is less than or equal to 1, [b]PROVEAN predicts deleterious if score is less than -2.5, [c]SNPnexus predicts deleterious if score is between 0-0.05, [d]SNAP2 predicts effect if score is greater than 0, [e]PON-P2 predicts pathogenic if score is less than 0.5, [f]SNPs&GO predicts disease if score is higher than 0.5, [g]PMut predicts disease if score is less than 1.

Analysis of evolutionary conserved regions

Evolutionary conserved regions are essential in proteins as they are more involved in biological processes and mechanisms (Asthana et al., 2007). As a result, SNPs located in highly conserved regions are more prone to cause disease. ConSurf web server was used to examine the conserved regions of DCDC2 and the location of the 13 short-listed SNPs (Supplementary Fig. 1). All the thirteen short-listed SNPs were classified as conserved ones (Table. 2). It implies that these SNPs are part of an essential functional or structural domain of the protein and their presence may significantly affect the protein function and stability.

Analysis of protein stability

Stability changes for the mutation in amino acid sequence was predicted by I-Mutant and MUpro predicted stability changes for the mutation in the amino acid sequence. When protein stability increases, it works more efficiently, but a decrease in stability causes the hindrance of protein action by degradation, misfolding, and aggregation (Du et al., 2005; Schoorman et al., 2007; Platek and Singh, 2010). For both tools, ΔΔG value less than zero indicates a decrease in stability. All thirteen short-listed SNPs reduced the protein's stability (Table 2).

Table 2. Analysis of and stability alteration due to short-listed 13 SNPs and conserved status of respective amino acid positions

SNP	Stability alteration		Conservation analysis
	ΔΔG[#] (I-Mutant)	**ΔΔG[#]** (MUpro)	**Score of each residue position[*]** (ConSurf)
R23L	-1.26	-0.65	9
G83R	-0.91	-0.58	9
G60E	-0.14	-0.17	9
I36N	-1.29	-1.65	8
R186G	-1.06	-1.32	9
L179R	-2.49	-2.57	8
G25W	-0.49	-0.94	9
G25R	-0.82	-1.01	
P68S	-2.01	-1.51	9
V208A	-1.56	-1.92	9
L20P	-1.72	-1.37	6
D26E	-2.24	-1.26	9
T174I	-0.57	-0.17	9

[#]ΔΔG<0 indicates decreased stability

[*]ConSurf scores are given on a scale from 1-9, where 1 means variable and 9 means highly conserved.

Analysis of protein-protein interaction

The DCDC2 protein (UniProt ID: Q9UHG0) contains two DC domains: one is N-terminal (17-100 aa), and the other is C-terminal (139-222aa). All the thirteen short-listed SNPs are part of either of those domains. It has been mentioned previously that DC domains of other proteins bind 13-protofilaments of microtubules at grooves surrounded by four tubulin monomers (Manka and Moores, 2020). Homology modeling was used to prepare Models 1 and 2 (Fig. 1).

Each model was divided into two and refined, resulting in four 3D models of DC domains and two tubulin monomers. These models were used to analyze the effect of thirteen short-listed SNPs on DCDC2 and tubulin interaction. Model 1, a and 1, b were used for SNPs of the N-DC domain (17-100aa), whereas Model 2,a and 2,b were used for SNPs of the C-DC domain (139-222aa) (Fig. 2). ΔΔG values calculated by three different tools of the considered SNPs are listed in Table 3 and 4. A positive value of ΔΔG indicates that the SNP lowers the binding energy of the DC domain with respective tubulin subunits. Among the considered six SNPs of the C-DC domain, four showed positive ΔΔG change in all three tools and for models 2a and 2b. These SNPs have been considered significant in case of destabilizing the interaction of the C-DC domain of DCDC2 with tubulin alpha-1B dimer and beta-2B dimer (Table. 5). Similarly, among the seven SNPs of N-DC domains, three were considered as significant (Table. 6).

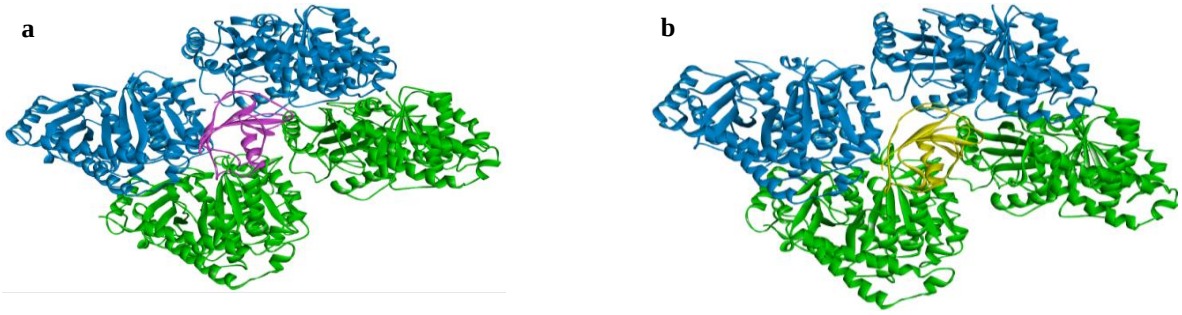

Fig. 1. a) Model 1- Complex of N-DC domain of DCDC2 with four tubulin subunits, b) Model 2- Complex of C-DC domain of DCDC2 with four tubulin subunits. N-DC domain, C-DC domain, tubulin alpha-1B subunits, and tubulin beta-2B subunits are indicated by purple, yellow, green, and blue color, respectively.

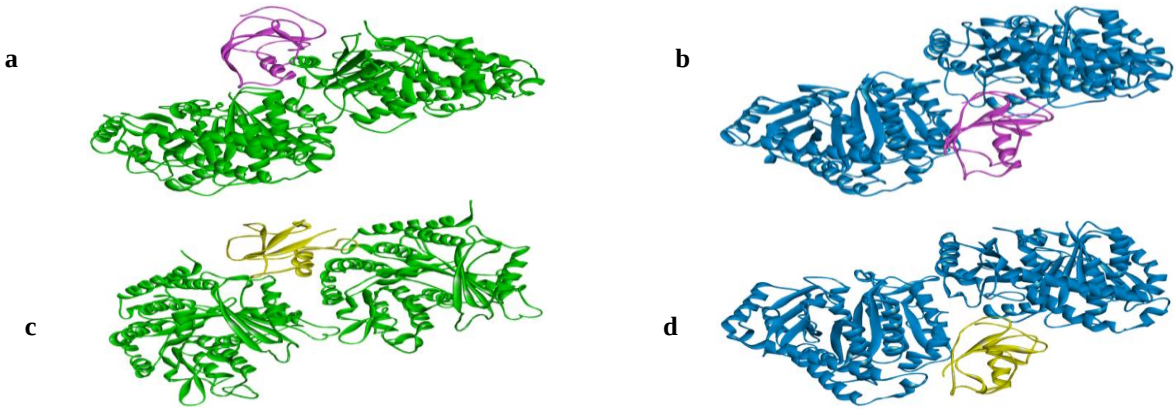

Fig. 2. a) Model 1a- Complex of N-DC domain with two tubulin alpha-1B subunits, b) Model 1b- Complex of N-DC domain with two tubulin beta-2B subunits, c) Model 2a- Complex of C-DC domain with two tubulin alpha-1B subunits, d) Model 2b- Complex of C-DC domain with two tubulin beta-2B subunits. The n-DC domain, C-DC domain, tubulin alpha-1B subunits, and tubulin beta-2B subunits are indicated by purple, yellow, green, and blue colors, respectively.

Table 3. Alteration of interaction of C-DC domain with α-1B pair and β-2B pair of tubulin 13-protofilament

Wild type	Residue No[b]	Mutant	Model 2a C_DCDC2_α-1B tubulin pair ΔΔG[a]			Model 2b C_DCDC2_β-2B tubulin pair ΔΔG[a]		
			MCSM-PPI2	SAAMBE-3D	Beat-Music	MCSM-PPI2	SAAMBE-3D	Beat-Music
P	152	A	0.106	0.22	*-0.06*	0.483	0.61	1.48
T	174	I	0.462	0.16	0.56	0.056	0.05	0.13
L	179	R	0.809	0.61	0.48	0.728	0.89	0.47
S	181	R	0.305	0.68	0.32	*-0.182*	0.14	0.34
R	186	G	1.339	0.92	1.41	0.354	0.80	0.65
V	208	E	0.453	0.09	1.33	0.42	0.09	1.61

[a]Positive ddG value indicates decreasing binding energy
[b]SNPs that create positive ddG value in all three tools are written in bold.

Table 4. Alteration of interaction of N-DC domain with α-1B pair and β-2B pair of tubulin13-protofilament

Wild	Residue No[b]	Mutant	Model 1a N_DCDC2_ α-1B tubulin pair ΔΔG[a]			Model 1b N_DCDC2_ β-2B tubulin pair ΔΔG[a]		
			MCSM-PPI2	SAAMBE-3D	Beat-Music	MCSM-PPI2	SAAMBE-3D	Beat-Music
L	**20**	**P**	**0.254**	**1.25**	**0.92**	**0.328**	**1.25**	**1.25**
R	23	L	0.253	0.53	*-0.04*	0.803	0.81	*-0.08*
G	25	w	0.419	-0.20	0.47	1.569	0.13	*-0.38*
G	25	R	0.199	-0.20	0.48	1.101	0.69	0.85
D	**26**	**E**	**0.140**	**0.9**	**0.44**	**0.549**	**1.00**	**0.99**
G	60	E	1.407	0.44	2.43	-0.169	0.24	1.14
G	**83**	**R**	**0.245**	**0.20**	**0.48**	**0.278**	**0.29**	**0.53**

[a] positive ddG value indicates decreasing binding energy
[b]SNPs that create positive ddG value in all three tools are written in bold.

The DCDC2 protein contains a doublecortin (DC) domain. This domain was found in the doublecortin (DCX) protein that binds microtubules. doublecortin (DCX) has been shown to stabilize microtubules and cause bundling in both *in vivo* and *in vitro* assays. Doublecortin, a basic protein, has an isoelectric point of 10, typical of microtubule-binding proteins.

In this *in silico* study, thirteen SNPs were short-listed after analysis with seven tools (L20P, R23L, G25W, G25R, D26E, I36N, G60E, P68S, G83R, T174I, L179R, R186G, V208E). These SNPs have not been reported to be associated with neurological or other physiological disorders before. All thirteen SNPs were either in N-terminal (17-100 aa) or C-terminal (139-222aa) DC domains. This corresponds to the finding that they are classified to be highly conserved in the ConSurf server. All thirteen SNPs have been found to lower the stability of the protein too. It indicates that these particular SNPs can compromise the structural integrity of the protein. As regions except N-DC and C-DC domains are disordered and no significant SNPs were found in the disordered regions, protein interaction analysis was focused only on N-DC and C-DC domains. Protein-protein interaction analysis revealed that four SNPs of the N-DC domain and three SNPs of the C-DC domains should hamper the interaction between the DC domains of DCDC2 and the microtubule. Inside the cell, microtubule-bound DC domains have been reported to be at the vertex of four tubulin subunits, two of which are alpha-1B monomers and the other two are beta-2B monomers (6rev, 6RF2) (Manka and Moores, 2020). The simultaneous interaction of the DC domain with four different subunits makes it very complicated to perform molecular docking analysis. Recently, the SWISS-MODEL server has extended its functionality to the modeling of homo- and heteromeric complexes (Waterhouse et al., 2018). It is based on the fact that, like homology modeling of monomeric proteins, the information of a protein's quaternary structure can be transferred to another model of homologous protein complex through homology (Szilagyi and Zhang, 2014). So, to avoid the problem with molecular docking, homology modeling via SWISS-MODEL was utilized to construct the structure of a single DC domain bound to two monomers of tubulin alpha chain and two monomers of tubulin beta chain simultaneously. Only one homology domain was generated for each of the DC domains. To improve the quality, the structures needed refinement, but the 3D structure of the complex is enormous and unsuitable for computational analysis. So, each of the complexes was divided into two structures; one has a DC domain with two monomers of tubulin alpha chain, and another has a DC domain with two monomers of tubulin beta chain. As homology modeling outputs are devoid of water molecules and contain H-atoms, these models were directly submitted to interaction analysis software.

ΔΔG values of model 2,a indicate the binding energy change of C-DC with alpha-1B dimer, and model 2,b indicates that of beta-2B dimer. So, for each SNP, the summation of the average ΔΔG values of both models can suggest the total binging energy change of the C-DC domain with four tubulin subunits. Table 5 shows that SNP R186G can be considered most destabilizing for interaction as it has the highest positive total ΔΔG value. Similarly, the summation of the average ΔΔG values of models 1,a and 1,b from Table 5 indicates the total binding energy change of the N-DC domain with four tubulin subunits. Among the three SNPs considered significant in altering the N-DC domain and tubulin interaction, L20P SNP can be considered as having the most destabilizing effect on the interaction of the N-DC domain, with four tubulin subunits for having the largest total positive ΔΔG value (Table 6). Positions of these SNPs in the tertiary structure of C-DC domain and N-DC domain are shown in Fig. 3.

Table 5. Order of missense SNPs of C-DC domain based on ΔΔG value

SNP	Average ΔΔG of C-DC with α-1B pair[#]	Average ΔΔG of C-DC with β-2B pair[*]	Sum of ΔΔG of C-DC domain[$]	Significance
R186G	1.223	0.601	1.824	
V208E	0.624	0.706	1.33	
L179R	0.633	0.696	1.33	
T174I	0.394	0.078	0.472	

[#]ΔΔG values indicating interaction alteration of C-DC domain with α-1B sub-unit pair
[*]ΔΔG values indicating interaction alteration of C-DC domain with β-2B sub-unit pair
[$]Total ΔΔG values indicating interaction alteration of C-DC domain with both α-1B pair and β-2B pair

Table 6. Order of missense SNPs of N-DC domain based on ΔΔG value

SNP	Average ΔΔG of N-DC with α-1B pair[#]	Average ΔΔG of N-DC with β-2B pair*	Sum of ΔΔG of N-DC domain[$]	Significance
L20P	0.808	0.942	1.75	
D26E	0.493	0.846	1.34	
G83R	0.308	0.366	0.674	

[#]ΔΔG values indicating interaction alteration of N-DC domain with α-1B subunit pair
*ΔΔG values indicating interaction alteration of N-DC domain with β-2B subunit pair
[$]Total ΔΔG values indicating interaction alteration of N-DC domain with both α-1B pair and β-2B pair

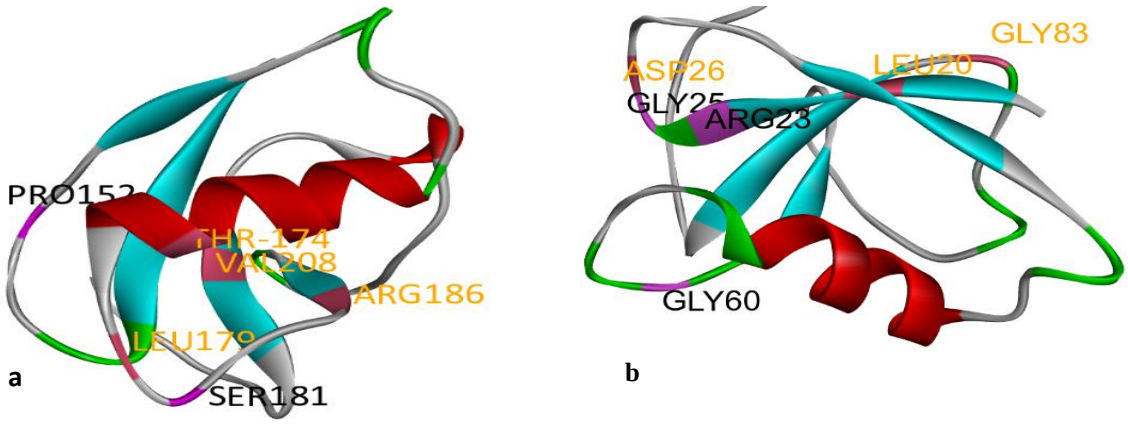

Fig. 3. a) C-DC domain structure with significant SNPs' amino positions. b) N-DC domain with amino positions of significant SNPs. Helices are red, beta sheets are cyan, turns are green, and coils are white. Residues written in yellow are significant for microtubule interaction.

Conclusion

Being implicated in several neurological disorders makes DCDC2 an important protein for analysis. This study utilized multiple tools to identify missense SNPs that are deleterious to the protein itself and destabilizing to the interaction of this protein with tubulin subunits. Thirteen SNPs were found to have deleterious effects on the protein, which are L20P, R23L, G25W, G25R, D26E, I36N, G60E, P68S, G83R, T174I, L179R, R186G, V208E. All are part of either the N-DC domain or C-DC domain. No SNP of the disordered region was found to be deleterious. Among these, four SNPs, T174I, L179R, R186G, and V208E, were suggested to be significantly destabilizing for the interaction of the C-DC domain with microtubule, and three SNPs- L20P, D26E, and G83R were suggested to be significantly destabilizing for the interaction of N-DC domain with microtubule. Based on the total ΔΔG value, SNP R186G and L20P seem most destabilizing for the interaction of the C-DC and N-DC domains. These SNPs have been identified for negatively affecting the protein in several types of analysis performed via tools of different algorithms. As *in-vitro* studies are yet to be performed on these SNPs, this study proposes a few potential deleterious SNPs worth looking into. Genetic association and protein-protein interaction studies focused on these SNPs can reveal new findings about dyslexia or other neurodevelopmental disorders.

Conflicts of Interest

The authors declare that they have no conflicts of interest regarding the publication of this article.

References

Adzhubei IA, Schmidt S, Peshkin L, Ramensky VE, Gerasimova A, Bork P, Kondrashov AS and Sunyaev SR. A method and server for predicting damaging missense mutations. *Nat. Methods.* 2010; 7(4): 248-249.

Ashkenazy H, Erez E, Martz E, Pupko T and Ben-Tal N. ConSurf 2010: calculating evolutionary conservation in sequence and structure of proteins and nucleic acids. *Nucleic Acids Res.* 2010; 38: 529-533.

Asthana S, Roytberg M, Stamatoyannopoulos J and Sunyaev S. Analysis of sequence conservation at nucleotide resolution. *PLoS Comput. Biol*. 2007; 3(12): 1-10.

Baldi JCARP. Prediction of protein stability changes for single-site mutations using support vector machines. *Proteins.* 2005; 62(4):1125-1132.

Bava KA and Gromiha MM. ProTherm, version 4.0: thermodynamic database for proteins and mutants, *Nucleic Acids Res.* 2004; 32(90001): D120-D121.

Bechstedt S and Brouhard GJ. Doublecortin recognizes the 13-protofilament microtubule cooperatively and tracks microtubule ends. *Dev. Cell.* 2012;23(1):181-192.

Bechstedt S, Lu K and Brouhard GJ. Doublecortin recognizes the longitudinal curvature of the microtubule end and lattice. *Curr. Biol.* 2014;24(20): 2366-2375.

Burger D, Stihle M, Sharma A, Lello PD, Benz J, D'Arcy B, Debulpaep M, Fry D, Huber W, Kremer T, Laeremans T, Matile T, Ross A, Rufer AC, Schoch G, Steinmetz MO, Steyaert J, Rudolph MG, Thoma R and Ruf A. Crystal structures of the human doublecortin C- and N-terminal domains in complex with specific antibodies. *J. Biol. Chem.* 2016; 291(31):16292-16306.

Calabrese R, Capriotti E, Fariselli P, Martelli PL and Casadio R. Functional annotations improve the predictive score of human disease-related mutations in proteins. *Hum. Mutat.* 2009; 30(8): 1237-1244.

Capriotti E, Fariselli P and Casadio R. I-Mutant2.0: predicting stability changes upon mutation from the protein sequence or structure. *Nucleic Acids Res.* 2005; 33: 306-310.

Chaaban S and Brouhard GJ. A microtubule bestiary: structural diversity in tubulin polymers. *Mol. Biol. Cell*. 2017; 28(22): 2924-2931.

Choi Y and Chan AP. PROVEAN web server: a tool to predict the functional effect of amino acid

substitutions and indels. *Bioinformatics.* 2015; 31(16): 2745-2747.

Conde C and Caceres A. Microtubule assembly, organization and dynamics in axons and dendrites. *Nat. Rev. Neurosci.* 2009;10: 319-332.

Dehouck Y, Kwasigroch JM, Rooman M and Gilis D. BeAtMuSiC: prediction of changes in protein–protein binding affinity on mutations. *Nucleic Acids Res.* 2013; 41(W1): 333-339.

Dijkmans T, Hooijdonk LWA, Fitzsimons CP and Vreugdenhil E. The doublecortin gene family and disorders of neuronal structure. *Cent. Nerv. Syst. Agents Med. Chem.* 2010; 10(1): 32-46.

Du K, Sharma M and Lukacs GL. The ΔF508 cystic fibrosis mutation impairs domain-domain interactions and arrests post-translational folding of CFTR. *Nat. Struct. Mol. Biol.* 2005; 12(1): 17-25.

Fourniol FJ, Sindelar CV, Amigues B, Clare DK, Thomas G, Perderiset M, Francis F, Houdusse A and Moores CA. Template-free 13-protofilament microtubule-MAP assembly visualized at 8 A resolution. *J. Cell Biol.* 2010; 191(3): 463-470.

Gabel LA, Marin I, LoTurco JJ, Che A, Murphy C,Manglani M and Kass S. Mutation of the dyslexia-associated gene Dcdc2 impairs LTM and visuo-spatial performance in mice. *Genes, Brain Behav.* 2011; 10(8): 868-875.

Girard M. DCDC2 mutations cause neonatal sclerosing cholangitis. *Hum. Mutat.* 2016; 37(10): 1025-1029.

Gleeson JG, Allen KM, Fox JW, Lamperti ED, Berkovic S, Scheffer I, Cooper EC, Dobyns WB, Minnerath SR, Ross ME and Walsh CA. Doublecortin, a brain-specific gene mutated in human X-linked lissencephaly and double cortex syndrome, encodes a putative signaling protein. *Cell*. 1998; 92(1): 63-72.

Gleeson JG, Lin PT, Flanagan LA and Walsh CA. Doublecortin is a microtubule-associated protein and is expressed widely by migrating neurons. *Neuron*. 1999; 23(2): 257-271.

Grati M, Chakchouk I, Ma Q, Bensaid M, Desmidt A, Turki N and Yan D. A missense mutation in DCDC2 causes human recessive deafness DFNB66, likely by interfering with sensory hair cell and supporting cell cilia length regulation. *Hum.Mol. Genet.* 2015; 24(9): 2482-2491.

Horesh D, Sapir T, Francis F, Wolf SG, Caspi M, Elbaum M, Chelly J and Reiner O. Doublecortin, a stabilizer of microtubules. *Hum. Mol. Genet*. 1999; 8(9): 1599-1610.

Jia M, Yang B, Li Z, Shen H, Song X and Gu W. Computational analysis of functional single nucleotide polymorphisms associated with the CYP11B2 gene. *PLoS ONE.* 2014; 9(8): e104311.

Johnson AD, Handsaker RE, Pulit SL, Nizzari SM, O'Donnell CJ and Bakker PIW. SNAP: a web-based tool for identification and annotation of proxy SNPs using Hap Map. *Bioinformatics*. 2008; 24(24): 2938-2939.

Kim MH, Cierpicki T, Derewenda U, Krowarsch D, Feng Y, Devedjiev Y and Dauter Z. The DCX-domain tandems of doublecortin and doublecortin-like kinase. *Nat. Struct. Mol. Biol.* 2003; 10(5): 324-333.

Lind PA, Luciano M, Wright MJ, Montgomery JW, Martin NG and Bates TC. Dyslexia and DCDC2: normal variation in reading and spelling is associated with DCDC2 polymorphisms in an Australian population sample. *Eur. J. Hum. Genet*. 2010; 18(6): 668-673.

Liu JS, Schubert CR, Fu X, Stultz CM, Moores CA and Walsh CA. Molecular basis for specific regulation of neuronal kinesin-3 motors by doublecortin family proteins. *Mol. Cell*. 2012; 47(5): 707-721.

Manka SW and Moores CA. Pseudo-repeats in doublecortin make distinct mechanistic contributions to microtubule regulation. *EMBO Rep.* 2020; 21(12): e51534.

Meng H, Powers NR, Tang L, Cope NA, Zhang PX and Fuleihan R. A dyslexia-associated variant in DCDC2 changes gene expression. *Behav. Genet.* 2011; 41(1): 58-66.

Moores CA, Perderiset M, Francis F, Chelly J, Houdusse A and Milligan RA, mechanism of microtubule stabilization by doublecortin. *Mol. Cell.* 2004;14(6): 833-839.

Moores CA, Perderiset M, Kappeler C, Kain S, Drummond D and Perkins SJ. Distinct roles of doublecortin modulating the microtubule cytoskeleton. *EMBO J.* 2006; 25(19): 4448-4457.

Niroula A, Urolagin S and Vihinen M. PON-P2: Prediction method for fast and reliable identification of harmful variants. *PLoS ONE*. 2015; 10(2): e0117380

Oscanoa J, Sivapalan L, Gadaleta E, Ullah AZD, Lemoine NR and Chelal C. SNPnexus: a web server for functional annotation of human genome sequence variation. *Nucleic Acids Res*. 2020; 48(W1): W185-W192.

Pahari S, Li G, Murthy AK, Liang S, Fragoza R,Yu H, and Alexov E. SAAMBE-3D: Predicting effect of mutations on protein-protein interactions. *Int. J. Mol. Sci.*2020; 21(7): 2563.

Platek SM and Singh D. Optimal waist-to-hip ratios in women activate neural reward centers in men. *PLoS ONE*. 2010; 5(2):1-5.

Pupko T, Bell RE, Mayrose I, Glaser F and Ben-Tal N. Rate4Site: an algorithmic tool for the identification of functional regions in proteins by surface mapping of evolutionary determinants within their homologues. *Bioinformatics*. 2002; 18(Suppl 1): S71-S77.

Reiner O, Coquelle FM, Peter B, Levy T, Kaplan A, Sapir T and Orr I. The evolving doublecortin (DCX) superfamily. *BMC Genom*. 2006; 7(1): 188.

Schoorman FD, Mayer RC and Davis JH. An integrative model of organizational trust: past, present, and future. *Acad. Manage. Rev*. 2007; 32(2):344-354.

Schueler M, Braun DA, Chandrasekar G, Gee HY, Klasson TD, Halbritter J, Bieder A, Porath JD, Airik R, Zhou W, LoTurco JJ, Che A and Otto EA. DCDC2 mutations cause a renal-hepatic ciliopathy by disrupting wnt signaling. *Am. J. Hum. Genet*. 2015; 96(1): 81-92.

Shastry BS. *Single Nucleotide Polymorphisms*. 2nd ed. Springer; 2009;p 3-22.

Srivastava S, Molinari E, Raman S and Sayer JA. Many genes—one disease? Genetics of Nephronophthisis (NPHP) and NPHP-associated disorders. *Front. Pediatr*.2018;5:287.

Syryn H, Hoorens A, Grammatikopoulos T, Deheragoda M, Symoens S and Velde SV. Two cases of related neonatal sclerosing cholangitis with developmental delay and literature review. *Clin. Genet.* 2021; 100(4): 447-452.

Szilagyi A and Zhang Y. Template-based structure modeling of protein-protein interactions. *Curr. Opin. Struct. Biol.* 2014; 24: 10-23.

Taylor KR, Holzer AK, Bazan JF, Walsh CA and Gleeson JG. Patient mutations in doublecortin define a repeated tubulin-binding domain. *J. Biol. Chem.* 2000; 275(44): 34442-34450.

Tilney LG, Bryan J, Bush DJ, Fujiwara K, Mooseker MS, Murphy DB and Snyder DH. Microtubules: evidence for 13 protofilaments. *J. Cell Biol.*1973; 59(2): 267-275.

Vignal A, Milan D, SanCristobal M and Egge A. A review on SNP and other types of molecular markers and their use in animal genetics.*Genet. Sel. Evol.* 2002; 34(3): 275-305.

Waterhouse A, Bertoni M, Bienert S, Studer G, Tauriello G, Gumienny R andHeer FT. SWISS-MODEL: homology modelling of protein structures and complexes. *Nucleic Acids Res.*2018; 46(W1): W296-W303.

Zhang Y, Li J,Song S,Tardif T,Burmeister M,Villafuerte SM,Su M,McBride C and Shu H. Association of DCDC2 polymorphisms with normal variations in reading abilities in a chinese population. *PLoS ONE*. 2016; 11(4): e0153603.

Zhong R, Yang B, Tang H, Zou L, Song R, Zhu LQ and Miao X. Meta-analysis of the association between DCDC2 polymorphisms and risk of dyslexia. *Mol. Neurobiol.*2013; 47(1): 435-442.

J. Bangladesh Acad. Sci. 47(2); 195-203: December 2023 DOI:https://doi.org/10.3329/jbas.v47i2.67950

Journal of Bangladesh Academy of Sciences

Journal homepage: http://www.bas.org.bd/publications/jbas.html

Research Article

Catalytic pyrolysis of waste high-density (HDPE) and low-density polyethylene (LDPE) to produce liquid hydrocarbon using silica-alumina catalyst

Mahmudur Rahman*, Bijoy Kumar Mondal[1], Nafees Ahmed and Md. Delwar Hossain

Department of Chemistry, Jagannath University, Dhaka, Bangladesh

ARTICLE INFO

Article History

Received: 30 July 2023
Revised: 03 September2023
Accepted: 04 September 2023

Keywords: Pyrolysis, High-density polyethylene (HDPE), Low-density polyethylene (LDPE), Catalyst

ABSTRACT

Catalytic pyrolysis of waste HDPE and LDPE polyethylene was successfully carried out using a silica-alumina catalyst at 450 °C under N_2 atmosphere. The synthesized silica-alumina is mesoporous and shows type IV isotherm. Thermal pyrolysis (without any catalyst) provided 47% wax-like hydrocarbons at 485 °C. On the other hand, more than 80% liquid yield was achieved using silica-alumina catalysts from waste HDPE and LDPE. The highest liquid yield was obtained from LDPE (87.69%) than HDPE (83.25%) at a catalyst-to-plastic ratio of 1:25. The ^{1}H NMR shows that the liquid product does not contain any aromatic compound. The GC-MS, ^{1}H NMR, and FTIR confirmed that the liquid contains linear and branched alkanes and alkenes.

Introduction

Plastics are extensively used in our day-to-day life. For this reason, a significant amount of plastic waste is generated globally (Rahman et al., 2022). In 2018, 360 million metric tons of plastics were produced (Yang et al., 2022; Fu et al., 2023). About 6300 million metric tons of plastic waste have been generated globally from 1950 to 2015 (Geyer et al., 2017; Fu et al., 2023). Only 9% of these plastic wastes are recycled, 12% are incinerated, and the remaining 79% are disposed of in landfills (Geyer et al., 2017; Fu et al., 2023). As a developed country, the USA generated around 35.4 million tons of plastics in 2017 (Rahman et al., 2022). The USA recycled only 8.4% of plastics, incinerated 16%, and the remaining 40% was landfilled (Rahman et al., 2022). Thus, plastic waste is causing significant environmental pollution.

Plastic wastes can be converted to liquid fuel using suitable catalysts. Catalytic pyrolysis occurs at low temperatures and takes a shorter time than thermal pyrolysis (without using any catalysts). Over the years, numerous catalysts have been developed for obtaining better gasoline selectivity and converting waste plastics to liquid fuel. Catalysts developed so far for the degradation of polyolefins are mostly based on zeolite HZSM-5 (Aguado et al., 1997;Lin et al., 2004; López et al., 2011; Sivagami et al., 2022), Zeolite-Y(Manos et al., 2001; Shoaib et al., 2021), silica-alumina (SiO_2-Al_2O_3) (Aguado et al., 1997; Uddin et al., 1997), mesoporousaluminosilicate (MCM-41) (Aguado et al., 1997; Lin et al., 2004), FCC catalysts and clays (Manos et al., 2001; Rahman et al., 2022).

The catalytic activity of polyolefin degradation increases with increasing number of acid sites. However, a highly acid catalyst will provide more gaseous products than liquid. For example, HZSM-5 zeolite, which is highly acidic, mostly gives gaseous hydrocarbon (C_2-C_4, 50% of the product) (Aguado et al., 1997). On the other hand, catalysts with medium acid sites (SiO_2-Al_2O_3, MCM-41) result in gasoline

*Corresponding author: <mm_rahman1978@yahoo.co.uk>

[1]*Dhaka University of Engineering and Technology, Gazipur, Bangladesh*

(C_5-C_{12}) and middle distillates (C_{13}-C_{22}) (Aguadoet al., 1997). Aguado et al. (1997) pyrolyzed model virgin HDPE and LDPE pellets obtained from REPSOL by ZSM-5, MCM-41, and SiO_2-Al_2O_3 catalysts. They found that ZSM-5 catalysts provided a significant amount of gaseous hydrocarbons (C_2-C_4) (50% is gaseous product), whereas MCM-41 and amorphous SiO_2-Al_2O_3 catalysts provided mostly liquid products with boiling points in the range of gasoline (C_5-C_{12}) and middle distillates (C_{13}-C_{22}).

Zeolites are microporousaluminosilicates and are used as catalysts and adsorbents. Serrano et al.(2002)used nano-crystalline ZSM-5 zeolite for pyrolysis of HDPE and LDPE and found that 100% of the gaseous hydrocarbons (C1-C5) are produced at a temperature of 340 °C. The nano-crystalline ZSM-5 zeolite is found to be more active than ZSM-5 in producing gaseous products.

Lin et al. (2004). pyrolyzed HDPE (MW 75, 000) using MCM-41, ZSM-5, and a mixture of MCM-41/ZSM-5. They found that the HZSM-5 catalyst produced higher amounts of gaseous hydrocarbon than MCM-41 and a mixture of MCM-41/ZSM-5. For example, pyrolysis of HDPE by MCM-41catalyst provided 87.88% gaseous hydrocarbon and 3.04% liquid product. The ZSM-5 catalyst provided 94.21% gaseous products and only 1.26% liquid. The combination of ZSM-5/MCM-41 catalyst provided less gaseous product (91.45% gaseous product and 3.58% liquid) than only using ZSM-5 (Lin et al., 2004).

Shoaib et al. (2021) pyrolyzed HDPE and LDPE using zeolite Y and found that pyrolysis of both HDPE and LDPE provided 71% liquid at 450 ℃ at a catalyst-to-plastic ratio of 1:5.

Manos et al. (2001) used clay and ultrastable Y zeolite to crack HDPE and found that clay catalysts can provide higher amounts of liquid than Y zeolite. The clay catalyst provided 68% liquid, whereas ultrastable Y zeolite provided 44% (Manos et al., 2001). The milder acidity of clays is believed to provide a higher amount of liquid. The strong acidity of ultrastable Y zeolite promotes cracking, leading to the formation of more gaseous products.

Achilias et al. (2007) investigated the pyrolysis of polyethylene (LDPE and HDPE) and polypropylene (PP) in a laboratory fixed-bed reactor with an FCC catalyst. They found that pyrolysis of the plastic bag made from LDPE leads to mainly gasoline region C_7–C_{12} hydrocarbons. A series of hydrocarbons (alkanes and alkenes) are present in the liquid product.

Traditionally, zeolite catalysts provide less liquid products and more gaseous hydrocarbons in plastic pyrolysis due to the acidity of the catalysts. However, mesoporous silica-alumina catalysts have a higher acidity than zeolite catalysts. This study aims to understand the effect of less acidic mesoporous silica-alumina (SiO_2-Al_2O_3) catalysts on real-life single-used waste HDPE and LDPE plastic pyrolysis.

Experimental

Materials and Methods

Tetraethyl orthosilicate, aluminum isopropoxide, HCl, isopropyl alcohol, and aqueous ammonia were purchased from Sigma Aldrich, Germany. Waste HDPE (bottles) and LDPE (polyethylene bags) were collected from Dhaka city. The melting points of HDPE and LDPE are 126 ℃ and 110 ℃, respectively. The carbon and hydrogen content of HDPE are 66.10 wt% and 26.93 wt%. The carbon and hydrogen content of LDPE are 77.72 wt% and 21.67 wt%.

Synthesis of silica-alumina (Aguadoet al., 1997)

The amorphous silica-alumina was prepared by the sol-gel route following a two-step method. In the first one, 16 g of tetraethyl orthosilicate was hydrolyzed with 10 g of 0.2 M aqueous HCl at room temperature for 45 min. Once the initially two-phase system became monophasic, a solution containing 0.523 g of aluminum isopropoxide in 7 g of isopropyl alcohol was added, and the mixture was stirred for 10 min to complete the hydrolysis of the Si and Al alkoxides. In the second step, the gel point was reached by drop-wise addition of 21

wt% aqueous ammonia solution. The cogel obtained was dried at 110 °C overnight and activated by calcination at 550 °C for 14 h.

Characterization of catalysts

The scanning electron microscopy (SEM-EDX) images were recorded on a JEOL-SEM, VERSION 3, 7600F, equipped with an energy-dispersive X-ray spectrometry detector at 5 kV. The BET-specific surface area and pore volume were determined by measuring nitrogen adsorption-desorption isotherms at liquid N_2 temperature (-196 °C) with a BELSORP MINI-11 (BEL Japan) apparatus. Belsorp Adsorption/Desorption Data Analysis Software-Ver. 6.1.0.8 was used to analyze and evaluate BET surface area and pore size distribution. Before each measurement, the samples were pretreated at 165 °C for 1.5 h under N_2 gas flow.

Characterization of liquid products

GC-MS, FTIR, and ^{1}H NMR spectroscopy analyzed the liquid products. For FTIR analysis, the Shimadzu 8400S, Japan, with KBr (heated at 100 ° C for 1 day before analysis) pellets in the 400-4000 cm^{-1} range were used. The Shimadzu GC-MS-TQ8040 with a quadrupole mass analyzer for GC-MS/MS analysis and electron impact ionization technique for MS detection (full scan mode 50-550 m/z) were used. A liquid sample of 0.5 µL was injected in splitless mode (flow rate of 1 mL/min and run time of 30 min) capillary column Rxi-5ms of 30 m length × 0.25 mm id at 250 ° C. The oven temperature was set to 50 ° C for 1 min and increased to 150 ° C at the rate of 5 ° C/min and then to 300 ° C at 15 ° C/min. Different compounds were identified using the computer-assisted mass spectral search by NIST-MS Library 2009. The^{1}H NMR of liquid products was conducted by the Bruker model (AVANCE III HD, 400 MHz).

Pyrolysis of waste high-density polyethylene (HDPE) and low-density polyethylene (LDPE)

The pyrolysis of waste HDPE and LDPE was investigated in a locally developed stainless steel reactor with a dimension of length, internal diameter, and outer diameter of 100, 75, and 77 mm, respectively (Fig. 1). The reactor consists of an electric furnace, thermocouple, temperature controller, condenser, and liquid collection vessel. 50.0 g of HDPE or LDPE were taken in each pyrolysis. In each catalytic pyrolysis experiment, a mixture of silica-alumina catalyst and HDPE or LDPE plastic (catalyst to plastics ratio 1:10, 1:15, and 1:25) was taken in the reactor and heated up to 450 °C under a nitrogen atmosphere. The reaction mixture was stirred by a mechanical stirrer. The condensable liquid products were collected through the condenser and weighed. The duration of each experiment was 30 min. Some coke was deposited on the catalysts after the completion of each catalytic reaction. Hence, each catalyst was used only once.

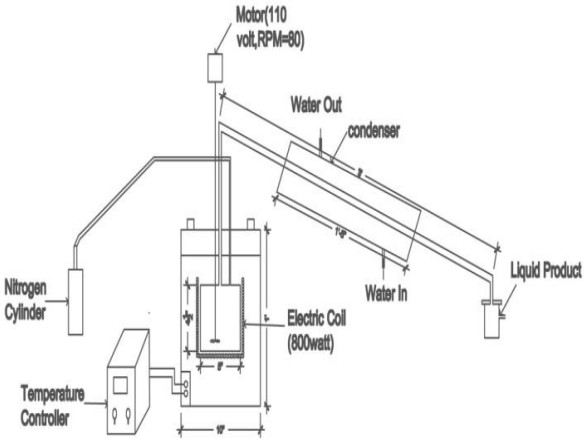

Fig. 1. Reactor setup for plastic pyrolysis

Results and discussion

The silica-alumina scanning electron micrograph (SEM) (Fig. 2) shows the morphological features. The micrographs indicate the disaggregation of the particles. The particle size is a few nanometers that are almost the same size. Fig. 3 displays an EDX spectrum for silica-alumina catalyst, and Table 1 shows silicon and oxygen are the most common elements making up the catalysts, with aluminum also being prevalent. The silica-alumina contained silicon and oxygen in SiO_4 tetrahedra, with a meager amount of aluminum. The Si/Al ratio of the silica-alumina is 98.5.

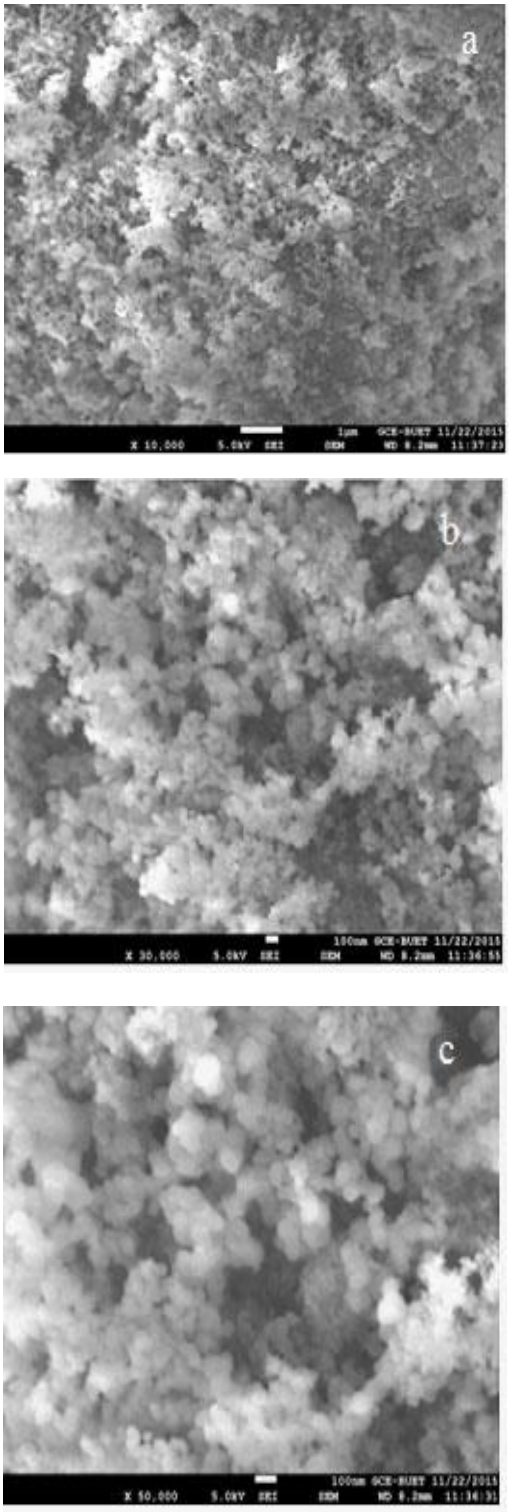

Fig. 2. SEM of silica-alumina (a) 10,000, (b) 30,000, and (c) 50,000 magnification.

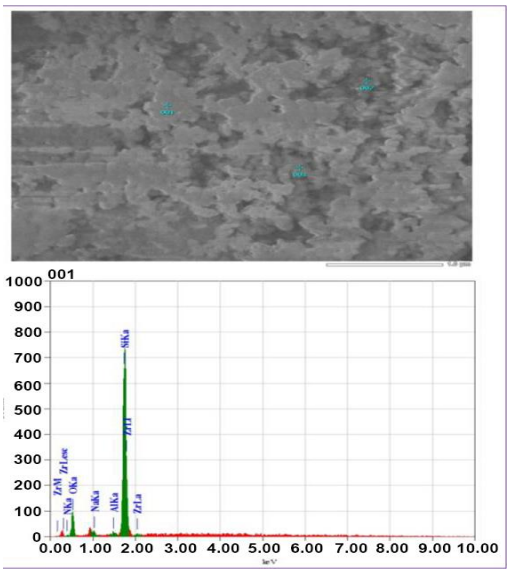

Fig. 3. EDX of silica-alumina

Table 1. Average weight % and atom % of each element in the catalyst sample

	N	O	Na	Al	Si	Zr	Si/Al
Atom%	4.51	31.71	0.60	0.63	62.06	0.49	98.5
Mass%	2.64	21.23	0.58	0.71	72.96	1.88	

The N_2 adsorption-desorption isotherms of the silica-alumina are shown in Fig. 4. The isotherms of these samples are classified as type IV based on IUPAC recommendations; this isotherm type is typical of mesoporous structures. The hysteresis loop of these samples is similar to type H3, typical of agglomerates of plate-like particles containing slit-shaped pores (Temuujin et al., 2001; Thommes, 2010). The isotherms also suggest the presence of some micro and macroporosity.

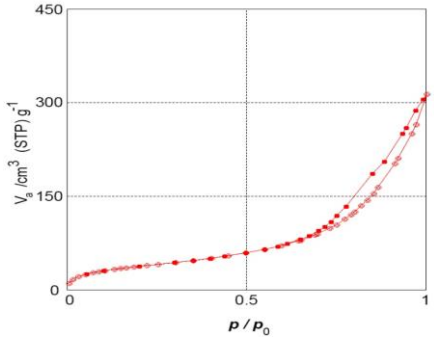

Fig. 4. N_2 adsorption/desorption isotherm of silica-alumina.

Table 2. Properties of $SiO_2 - Al_2O_3$ catalyst

Si/Al	BET			BJH		
	$a_{s'BET}$ $[m^2g^{-1}]$	T. Pore Vol.$[cm^3g^{-1}]$	Pore Dia.[nm]	V_p $[cm^3g^{-1}]$	Peak area[nm]	a_p $[m^2g^{-1}]$
98.5	1.4151E+02	0.4551	12.865	0.4832	4.03	181.95

BET= Brunauer-Emmett-Teller: BJH=Barrett-Jovner-Halenda

The BJH pore size distribution is given in Fig. 5, and pore volume and BET surface area are summarized in Table 2. It has been found that the BET surface area is 141.51 m^2g^{-1}, the mean pore diameter is 12.865 nm, and the total pore volume is $(p/p_0 = 0.990)\,0.4551 cm^3g^{-1}$ which is a typical feature of the uniform mesoporosity of this catalyst.

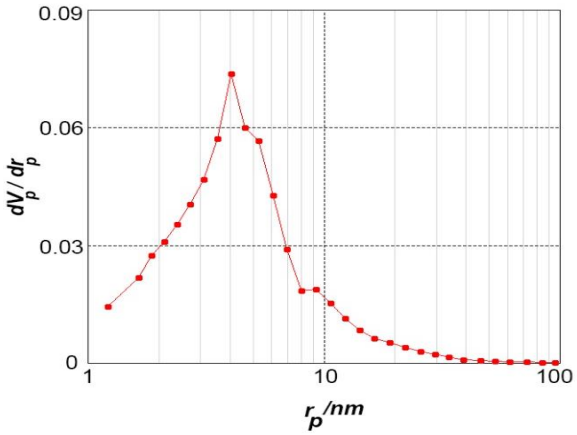

Fig. 5. BJH pore size distribution plot of silica-alumina

The amorphous SiO_2-Al_2O_3 exhibits a wide distribution of pore sizes. This material presents pores with sizes in the whole range between 1.3 and 40 nm, with two maxima around 4 and 9 nm, denoting the irregularity of its pore structure.

Catalytic pyrolysis of waste LDPE and HDPE using silica-alumina

As a control experiment, without any catalyst, the thermal pyrolysis of 50 g polyethylene provided 47% wax-like hydrocarbons at 485 °C. The wax was solidified at room temperature. In order to understand the effect of silica-alumina catalyst on pyrolysis ofboth single-used waste high-density polyethylene (HDPE) and low-density polyethylene (LDPE), we have carried out polyethylene pyrolysis at 450 °C inthe batch reactor under nitrogen atmosphere at various catalyst/plastic ratios of 1:10, 1:15 and 1:25. The gaseous hydrocarbon was vented off after pyrolysis and a small amount of coke was depositedonto the catalyst after pyrolysis. Hence, each catalyst was useda single time only. The durationof each experiment was 30 min. Table 3 summarizes the results obtained in the catalytic cracking of HDPE and LDPE over the silica-alumina catalyst.

Table 3. Pyrolysis of waste LDPE and HDPE using a silica-alumina catalyst. (450 °C, 30 min).

Catalyst	Plastics	Catalyst/Plastic ratio	Yield of liquid %
Silica-alumina	LDPE	1:10	70.56
		1:15	79.34
		1:25	87.69
Silica-alumina	HDPE	1:10	64.45
		1:15	75.67
		1:25	83.25

Table 3 shows that pyrolysis of LDPE at a catalyst-to-plastic ratio of 1:10 provided 70.56% liquid. An increased trend of liquid yield is observed with an increase in plastic ratio. For example, liquid yield increased from 79.34% to 87.69%, with the catalyst-to-plastic ratio increasing from 1:15 to 1:25 respectively. The liquid yield was higher in the pyrolysis of LDPE than HDPE. Similar to LDPE, an increased trend of liquid yield was observed with pyrolysis of HDPE. The pyrolysis of HDPE at a catalyst-to-plastic ratio of 1:10 provided 64.45%

liquid, which increased to 83.25% with the catalyst toplastic ratio of 1:25. Aguado et al., 1997 also found thatamorphous silica-alumina catalyst effectively produces liquid hydrocarbon from the pyrolysis of LDPE and HDPE. They pyrolyzed model virgin LDPE and HDPE pellets and obtained liquid hydrocarbons. The Si/Al of the catalyst was 35.6, and catalyst to plastic ratio was 1:36. Whereas, using ZSM-5 catalysts, they got 50% gaseous product from pyrolysis of both HDPE and LDPE (Aguado et al., 1997). Uddin et al. (1997) investigated the pyrolysis of HDPE and LDPE polyethylene using a silica-alumina catalyst. They achieved 80.2% liquid from LDPE and 77.4% from HDPE at 430 °C. FTIR, NMR, and GC-MS characterized the liquid product.

The FTIR spectrum of liquid obtained from pyrolysis of LDPE (Fig. 6) shows that the liquid contains linear alkanes and branched alkanes and alkenes. The observed peaks were assigned as follows: 2956 cm^{-1} C-H stretching of alkane; 1651cm^{-1} C=C stretching of alkene; 1458 cm^{-1} $>CH_2$ scissoring; 970 cm^{-1} C-H bending of alkane; 889 and 738 cm^{-1} C-H rocking from alkane. A similar FTIR spectrum was found in the liquid from pyrolysis of HDPE.

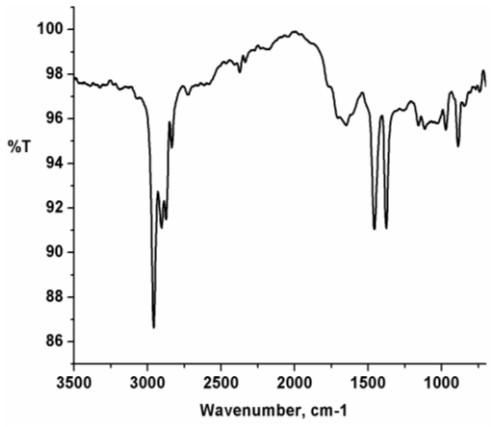

Fig. 6. FTIR spectrum of liquid obtained from pyrolysis of LDPE.

The ^{1}H NMR of liquid obtained from pyrolysis of LDPE (Fig. 7) shows peaks only in the range of 1-1.9ppm, which correspond to alkyl (methyl) and alkylene (methylene) protons originating from alkane compounds. A similar ^{1}H NMR spectrum was found in liquid from pyrolysis of HDPE.

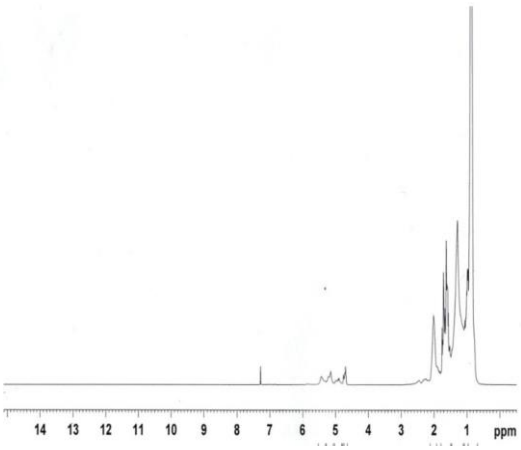

Fig. 7. The ^{1}H NMR of liquid obtained from pyrolysis of LDPE.

The GC-MS of the liquid was carried out to understand the composition of the liquid product.

Compounds were identified using the computer-assisted mass spectral search by NIST-MS Library 2009.The GC-MS of liquid obtained fromLDPE and HDPE (Tables 4 and 5) shows that the liquid contains mostly n-pentane, 2-methyl-2-pentene, 3-methyl-2-pentene, 2,4-dimethyl-1-pentene, 2,3-dimethyl-2-heptene, 2,2-dimethyl-3-heptene.

Conclusions

Catalytic pyrolysis of waste HDPE and LDPE was successfully carried out at 450 °C under N_2 atmosphere. The surface area of the silica-alumina catalyst is 141.51m^2g^{-1}, and the mean pore diameter is 12.865 nm. The synthesized silica-alumina is mesoporous and shows type IV isotherm. The hysteresis loop of the silica-alumina is type H3. More than 80% liquid yield was achieved using a silica-alumina catalyst. The highest liquid yield was obtained from LDPE (87.69%) than HDPE (83.25%) at a catalyst-plastic ratio of 1:25. The GC-MS and FTIR show that liquid product contains linear and branched alkanes and alkenes. The ^{1}H NMR shows that the liquid contains no carcinogenic compound like benzene.

Table 4. GC-MS of liquid obtained from waste LDPE by silica-alumina catalyst at 450 °C

Retention time (min.)	Compound	Chemical formula	Retention time (min.)	Compound	Chemical formula
1.550	2-methyl- Propene,	C_4H_8	5.106	2,3-Dimethyl-3-hexene	C_8H_{14}
1.721	n-Pentane	$n-C_5H_{12}$	5.197	2,3,3-Trimethyl-1,4-pentadiene	C_8H_{14}
1.7753	cis-2-Pentene	C_5H_{10}	5.272	3-Ethyl-2-hexene	C_8H_{16}
1.785	2-Methyl-2-butene	C_5H_{10}	5.363	2-Methyl-2-heptene	C_8H_{16}
1.924	cis-3-Methyl -2-pentene	C_6H_{12}	5.583	1,3-Dimethyl-1-cyclohexene	C_8H_{14}
1.967	2-Methylpentane	C_6H_{14}	5.652	3,3, 5-Trimethyl-1-hexene	C_9H_{18}
2.085	2-Methyl-1-pentene	C_6H_{12}	5.978	2,3,5-Trimethylhexane	C_9H_{20}
2.154	3-Methyl-2-pentene	C_6H_{12}	6.369	2,3-Dimethyl-2-heptene	C_9H_{18}
2.202	2-Methyl-2-pentene	C_6H_{12}	6.476	Cyclohexane	C_6H_{12}
2.298	cis-3-Methyl -2-pentene	C_6H_{12}	6.690	cis-2-Nonene	C_9H_{18}
2.389	2,3-Dimethyl-2-butene	C_6H_{12}	6.823	trans-2,2-Dimethyl-3-heptene	C_9H_{18}
2.438	1,3-Pentadiene	C_5H_8	6.930	trans-3-Nonene	C_9H_{18}
2.475	1,4-Hexadiene	C_6H_{10}	7.053	4-Ethyl-3-hep tene	C_9H_{18}
2.518	2,4-Dimethyl-1-pentene	C_7H_{14}	7.171	1,2,4-trimethylcyclohexane	C_9H_{18}
2.593	3,4-Dimethyl-2-pentene	C_7H_{14}	7.267	6-methyl-1-octene	C_9H_{18}
2.646	2,3-Dimethyl-1-pentene	C_7H_{14}	7.417	2,3-Dimethyl-3-heptene	C_9H_{18}
2.721	cis-4-Methyl-2-hexene	C_7H_{14}	7.604	2,6-Dimethyl-3-heptene	C_9H_{18}
2.978	2-Methyl-1-hexene	C_7H_{14}	7.920	5-Undecene	$C_{11}H_{22}$
3.208	cis-3-Methyl-3 -Hexene	C_7H_{14}	8.984	3-Methyl-4-undecene	$C_{12}H_{24}$
3.325	cis-3-Methyl-2 -Hexene	C_7H_{14}	10.541	2,4,6-Trimethyl-3-heptene	$C_{10}H_{20}$
3.290	2,3-Dimethyl-2-pentene	C_7H_{14}	11.049	cis-3-Decene	$C_{10}H_{20}$
3.951	2,3-Dimethyl-2-hexene	C_8H_{16}	11.733	cis-4-Decene	$C_{10}H_{20}$
4.080	2-Methyl-1-heptene	C_8H_{16}	12.825	2,6-Dimethyl-2-octene	$C_{10}H_{20}$
4.149	3-Methyl-3-heptene	C_8H_{16}	13.846	cis-5-Undecene	$C_{11}H_{22}$
4.224	4-Methyl-2-heptene	C_8H_{16}	14.402	2,3,6-Trimethyl-4-octene	$C_{11}H_{22}$
4.336	2,5-Dimethyl-2-hexene	C_8H_{16}	15.253	2,6-Dimethylnonane	$C_{11}H_{24}$
4.411	4-Methylheptane	C_8H_{18}	15.515	4-Methyl decane	$C_{11}H_{24}$
4.572	cis-2-Octene	C_8H_{16}	18.863	2,4-Dimethyl-2-decene	$C_{12}H_{24}$
4.652	3-Methyl-1,4-heptadiene	C_8H_{14}	19.788	1-Dodecene	$C_{12}H_{24}$
4.743	2,4-Dimethyl-1,3-pentadiene	C_7H_{12}	4.919	2,5-Dimethyl-2-hexene	C_8H_{14}

Table 5. GC-MS of liquid obtained from waste HDPE by silica-alumnia catalyst at 450 °C

Retention time (min.)	Composition	Chemical formula	Retention time (min.)	Composition	Chemical formula
1.550	2-methyl- Propene,	C_4H_8	5.053	3-Methyl-3-heptene	C_8H_{16}
1.721	n-Pentane	$n-C_5H_{12}$	5.106	4-Methyl-3-heptene	C_8H_{16}
1.753	2-Methyl-1-butene	C_5H_{10}	5.197	5,5-Dimethyl-1,3-hexadiene	C_8H_{14}
1.790	2-Methyl-1-butene	C_5H_{10}	5.272	cis-4-Octene	C_8H_{16}
1.924	1-Hexene	C_6H_{12}	5.363	2-Methyl-2-heptene	C_8H_{16}
1.972	2-Methyl-2-pentene	C_6H_{12}	5.583	1,3-Dimethyl-1-cyclohexene	C_8H_{14}
2.085	2-Methyl-1-pentene	C_6H_{12}	5.657	3,3,5-Trimethyl-1-hexene	C_9H_{18}
2.202	2,3-Dimethyl-2-butene	C_6H_{12}	5.738	2,6-Dimethyl-3-heptene	C_9H_{18}
2.256	cis-2-Hexene	C_6H_{12}	5.978	2,3,3-Trimethylhexane	C_9H_{20}
2.304	3-Methyl-2-pentene	C_6H_{12}	6.363	2,3-Dimethyl-3-heptene	C_9H_{18}
2.389	4-Methyl-trans-2-pentene	C_6H_{12}	6.465	n-Propylcyclohexane	C_9H_{18}
2.438	4-Methyl-1,3-pentadiene	C_6H_{10}	6.690	2,4-Dimethyl-1-heptene	C_9H_{18}
2.475	1,3-Hexadiene	C_6H_{10}	6.823	4-Ethyl-3-heptene	C_9H_{18}
2.518	2,4-Dimethyl-1-pentene	C_7H_{14}	6.930	cis-3-Nonene	C_9H_{18}
2.593	3,4-Dimethyl-2-pentene	C_7H_{14}	7.048	trans-3-Nonene	C_9H_{18}
2.651	3-Methyl-trans-3-hexene	C_7H_{14}	7.171	1,2,4-trimethylcyclohexane	C_9H_{18}
2.721	4-Methyl-2-hexene	C_7H_{14}	7.267	5-Methyl-1-heptane	$C_8H_{18}O$
2.892	5-Methyl-2-hexene	C_7H_{14}	7.604	2,6-Dimethyl-2-heptene	C_9H_{18}
2.983	2-Methyl-1-Hexene	C_7H_{14}	7.920	2-Nonene	C_9H_{18}
3.101	3-Methyl-2-Hexene	C_7H_{14}	8.198	4-Nonene	C_9H_{18}
3.149	cis-3-Heptene	C_7H_{14}	8.984	1,2,3-trimethyl-Cyclohexane	C_9H_{18}
3.208	2-Methyl-2-hexene	C_7H_{14}	9.097	2,3-Dimethyl-2-heptene	C_9H_{18}
3.325	3-Methyl-3-hexene	C_7H_{14}	9.166	2-Methyl-2-octene	C_9H_{18}
3.390	3,4-Dimethyl-2-pentene	C_7H_{14}	10.541	2,4,6-Trimethyl-3-heptene	$C_{10}H_{20}$
3.834	3-Ethyl-4-methyl-2-pentene	C_8H_{16}	11.054	cis-4-Decene	$C_{10}H_{20}$
3.957	2,3-Dimethyl-2-hexene	C_8H_{16}	11.193	3-Ethyl-2-methyl-2-heptene	$C_{10}H_{20}$
4.021	3, 5-Dimethyl-2-hexene	C_8H_{18}	11.536	trans-5-Decene	$C_{10}H_{20}$
4.085	2,5-Dimethyl-1-hexene	C_7H_{14}	11.701	trans-3-Decene	$C_{10}H_{20}$
4.154	3-Methyl-3-heptene	C_7H_{14}	12.054	2,6-Dimethyl-4-octene	$C_{10}H_{20}$
4.224	4-Methyl-2-heptene	C_8H_{16}	12.825	2,6-Dimethyl-2-octene	$C_{10}H_{20}$
4.277	cis-3-Octene	C_8H_{16}	13.242	cis-3-Decene	$C_{10}H_{20}$
4.336	2,5-Dimethyl-2-hexene	C_8H_{16}	14.119	Trans-2-Decene	$C_{10}H_{20}$
4.411	4-Methyl heptane	C_8H_{18}	15.515	2,4,4-Trimethyl-1-hexene	C_9H_{18}
4.577	3-Methyl-3-heptene	C_8H_{16}	18.687	2,4-Dimethyl-2-decene	$C_{12}H_{24}$
4.652	5-Methyl-2-heptene	C_8H_{16}	18.869	2,3, 7-Trimethyl-2-octene	$C_{11}H_{22}$
4.732	2-Methyl-2,4-hexadiene	C_7H_{14}	19.783	8-Methyl-3 undecene	$C_{12}H_{24}$

References

Achilias DS, Roupakias C, Megalokonomos P, Lappas AA and Antonakou EV. Chemical recycling of plastic wastes made from polyethylene (LDPE and HDPE) and polypropylene (PP). *J. Hazard. Mater.* 2007; 149(3): 536-542.

Aguado J, Sotelo JL, Serrano DP, Calles JA and Escola JM. Catalytic conversion of polyolefins into liquid fuels over MCM-41: Comparison with ZSM-5 and amorphous SiO_2–Al_2O_3. *Energy Fuels.*1997; 11(6): 1225-1231.

Fu Z, Hua F, Yang S, Wang H and Cheng Y. Evolution of light olefins during the pyrolysis of polyethylene in a two-stage process. *J. Anal. Appl. Pyrol.* 2023; 169: 105877.

Geyer R, Jambeck JR and Law KL. Production, use, and fate of all plastics ever made. *Sci. Adv.* 2017; 3(7): e1700782.

Lin YH, Yang MH, Yeh TF and Ger MD. Catalytic degradation of high density polyethylene over mesoporous and microporous catalysts in a fluidised-bed reactor. *Polym. Degrad. Stab.* 2004; 86(1): 121-128.

López A, de Marco I, Caballero BM, Laresgoiti MF, Adrados A and Aranzabal A. Catalytic pyrolysis of plastic wastes with two different types of catalysts: ZSM-5 zeolite and Red Mud. *Appl. Catal. B: Enviorn.* 2011; 104(3-4): 211-219.

Manos G, Yusof IY, Papayannakos N and Gangas NH. Catalytic cracking of polyethylene over clay catalysts. Comparison with an ultrastable Y zeolite. *Ind. Eng. Chem. Res.* 2001; 40(10): 2220-2225.

Rahman M, Shuva ZM, Rahman MA, Ahmed N, Sharmin A, Laboni AA, Khan M, Islam MW, Al-Mamun M, Roy SC and Saha JK. Catalytic pyrolysis of single-use waste polyethylene for the production of liquid hydrocarbon using modified bentonite catalyst. *Eur. J. Inorg. Chem.* 2022; 2022(34): e202200409.

Serrano DP, Aguado J, Escola JM and Rodríguez JM. Nano-crystalline ZSM-5: a highly active catalyst for polyolefin feedstock recycling. *Stud. Surf. Sci. Catal.* 2002; 142: 77-84.

Shoaib M, Subeshan B, Khan WS and Asmatulu E. Catalytic pyrolysis of recycled HDPE, LDPE, and PP. *Prog. Rubber Plast. Recycl.* 2021; 37(4): 264-278.

Sivagami K, Kumar KV, Tamizhdurai P, Govindarajan D, Kumar M and NambiI. Conversion of plastic waste into fuel oil using zeolite catalysts in a bench-scale pyrolysis reactor. *RSC Adv.* 2022; 12(13): 7612-7620.

Temuujin J, Burmaa G, Amgalan J, Okada K, Jadambaa T and MacKenzie KJD. Preparation of porous silica from mechanically activated kaolinite. *J. Porous. Mater.* 2001; 8(3): 233-238.

Thommes M. Physical adsorption characterization of nanoporous materials. *Chem. Ing. Tech.* 2010; 82(7): 1059-1073.

Uddin MA, Koizumi K, Murata K and Sakata Y. Thermal and catalytic degradation of structurally different types of polyethylene into fuel oil. *Polym. Degrad. Stab.* 1997; 56(1): 37-44.

Yang RX, Jan K, Chen CT, Chen andWu KCW.Thermochemical conversion of plastic waste into fuels, chemicals, and value-added materials: A critical review and outlooks. *Chem. Sus. Chem.* 2022; 15(11): e202200171.

J. Bangladesh Acad. Sci. 47(2); 205-213: December 2023 DOI:https://doi.org/10.3329/jbas.v47i2.65134

Journal of Bangladesh Academy of Sciences

Journal homepage: http://www.bas.org.bd/publications/jbas.html

Research Article

Molecular analysis of the first reported hereditary lymphedema-distichiasis case in Bangladesh

Nahid Parvez[1], Md. Lutfar Rahman[2], Md. Mostafizur Rahman[2], Mohammad Ali[3]
A.F.M Helal Uddin[2] and Mustak Ibn Ayub[*]

Department of Genetic Engineering and Biotechnology, Dhaka University, Dhaka, Bangladesh

ARTICLE INFO

Article History

Received: 27 March 2023
Revised: 18 October 2023
Accepted: 18 October 2023

Keywords: Lymphedema, Distichiasis, Polymerase chain reaction, Sanger sequencing, Forkhead/winged-helix transcription factor FOXC2

ABSTRACT

Lymphedema–distichiasis syndrome (LD, OMIM 153400) is hereditary primary lymphedema with autosomal dominant nature of inheritance and variable expression. LD is characterized by late childhood or pubertal onset of lower limb lymphedema and an aberrant second row of eyelashes (distichiasis) arising from the meibomian glands. Among the molecular reasons behind this condition are the mutations in the *FOXC2* gene, a forkhead transcription factor, that plays a role in the formation of lymphatic and vascular systems. In this study, we report the first case of LD from Bangladesh with classical lymphedema–distichiasis syndrome with an eight-base-pair deletion in the *FOXC2* gene. ClinVar accession code for this deletion is RCV000007679.3. FOXC2 protein is 501 amino acids long. This deletion of 8 bp (ACGCCGCC) causes frameshift of codons after amino acid number 304. The frameshift creates an altered truncated protein with 154 new amino acids after codon 304. We assume that these changes in the protein may affect its function contributing to the disease manifestations. Further research may confirm these assumptions.

Introduction

Lymphedema-distichiasis syndrome (LD) [MIM 153400]) is a form of hereditary lymphedema in which lymphedema, primarily of the limbs, with variable age at onset, is seen together with distichiasis, or double rows of eyelashes. The extra eyelashes grow from the meibomian glands and may protrude into the cornea, producing severe corneal abrasions. Various additional complications such as cleft palate, cardiac defects, abnormal curvature of the spine, droopy eyelids, etc (Szuba and Rockson, 1998) have also been observed.

The disease has been mapped to 16q24.3 (Mangion et al., 1999) where the forkhead/winged-helix transcription factor *FOXC2* is located. Studies showed that dominant mutations in the *FOXC2* gene (MIM602402), cause lymphedema with variable age of onset (range: 7-40 years), often associated with distichiasis (Fang et al., 2000). Key roles of FOXC2 include regulating differentiation of lymphatic endothelial cells, formation of smooth muscle cell layers, and morphogenesis of lymphatic valves. Along with VEGFR-3, FOXC2 acts to establish distinct features of the lymphatic vascular architecture (Sabine and Petrova, 2014).

In both humans and mice, FOXC2 is highly expressed in the developing lymphatic vessels, as well as in the adult lymphatic valves (Kriederman et al., 2003). Its critical role in lymphatic vascular development has been discovered by the manifestation of abnormal lymphatic patterning and the absence of proper lymphatic valves in Foxc2-deficient mice. LD patients develop similar defects characterized by lymph and venous reflux, indicating failure or absence of lymphatic and venous valves (Mellor et al., 2007).

[*]Corresponding author:<miayub@du.ac.bd>

[1]*Department of Genetic Engineering and Biotechnology, Jagannath University, Dhaka, Bangladesh*
[2]*Department of Medicine Sir Salimullah Medical College Mitford Hospital, Dhaka, Bangladesh*
[3]*Department of Biochemistry & Molecular Biology, Directorate General of Health Services, Dhaka, Bangladesh*

FOXC2 is transcribed to a 2.2 kb transcript containing a 1.5 kb single exon coding region. The FOXC2 protein contains 501 amino acids. The most characterized region in the gene (Fig. 1) is the fork-head DNA binding domain (FHD, amino acids 71 to 162). It also contains a nuclear localization signal (NLS1, amino acids 78-93). At the N-terminal, there is a transactivation domain 1 (AD-1) starting from the first amino acid until the FHD (amino acid 71). In the C-terminal, a second transactivation domain (AD-2, amino acids 395-494) and an inhibitory region (ID-2, amino acids 495-501) have been identified (Lam et al., 2013). In the central region of FOXC2 protein, after the nuclear localization signal 2 (NLS2, amino acids 168-176), some phosphorylation and SUMOylation conserved sites have been recently identified (Danciu et al., 2012; Ivanov et al., 2013).

Fig. 1. Structural domains of FOXC2 protein: transactivation domain 1 (AD-1), fork-head DNA binding domain (FHD), nuclear localization signal 1(NLS1), nuclear localization signal 2 (NLS2), transactivation domain 2 (AD-2), inhibitory region 2 (ID-2).

In LD patients, almost 70 different *FOXC2* mutations have been reported to date, scattered randomly along the whole coding sequence. The majority of *FOXC2* mutations are small insertions or deletions and nonsense mutations causing truncated proteins (Brice et al., 2002). It probably creates a haploinsufficiency condition which explains the dominant nature of LD. The *FOXC2*- haploinsufficient state is associated with hyperplasia and distichiasis in mice (Kriederman et al., 2003). Mutations responsible for the disease greatly vary among affected families and the secondary phenotypes differ among families. Nonetheless, any strong correlation has not yet been established between allelic variants and phenotypes. The disease exhibits variable penetrance of among the family members carrying the same allelic variant.

In this study, the *FOXC2* gene of an individual diagnosed positive for lymphedema distichiasis was analyzed by targeted Sanger Sequencing. The whole exon of 1501 bp was amplified through primer walking using five sets of primers. Due to the high GC percentage of the gene, the primers were not efficient and the PCR reaction mixture needed the addition of certain additives and nested PCR was performed. It is the first molecular study of a Bangladeshi lymphedema distichiasis patient and a homozygous 8 base pair deletion has been identified.

Materials and methods

The case

A 32-year-old normotensive, non-diabetic, male presented with a history of bilateral below knee swelling since the age of twelve. He also noted foreign body sensation in both eyes for the last 10 years and the recent appearance of whitish spots on the left eye with impairment of vision of the same eye for about a month. Patient's father and one of his younger brothers also showed the above-mentioned clinical features of eye lashes in the inner side of the eye lids and swelling of the lower limbs, albeit relatively milder. His sister is normal and does not exhibit any of the clinical problems. These characteristics indicated that the patient may be suffering from a certain type of hereditary lymphedema.

Mutational analysis of *FOXC2* gene

Genomic DNA isolation

Genomic DNA was isolated from a 200 µl blood sample of the patient using GeneJet™ DNA extraction kit following the standard isolation protocol. Concentration and purity of DNA was sufficiently good for PCR and sequencing.

DNA amplification

Due to absence of any reported mutational hot spot and presence of only one exon in this gene, it was planned to sequence the whole gene using a method called primer walking. Five sets of primers were designed to amplify 5 products that overlap each other to cover the whole gene (Table 1, Fig. 5[c]).

All PCR reactions were performed using NEB PCR kit following standard reagent composition and reaction condition except template amount, annealing temperature and extension time. These were variable

based on genomic DNA concentration, Tm of primer and product size of each PCR reaction.

It was also necessary to add DMSO (5% of volume) considering the high GC percentage of the target region. Detailed reagent composition and reaction condition of the PCR reactions are mentioned in Table: 2 and Table: 3. For retrieving full sequence, the following forward and reverse primer combinations were used: F1+R1, F2+R2, F3+R3, F4+R4, F5+R5, F1+R5, F2+R4. As the Tm value of each primer was very close, the annealing temperature of those primer combinations was set as 60 ^{0}C (Table 1, Table 3). PCR products were purified using ATP PCR/Gel DNA extraction kit following standard protocol.

Sanger sequencing of PCR products

At first, cycle sequencing was performed with the purified PCR amplified DNA. Big Dye Terminatorv1.1 Cycle Sequencing Kit and the forward or reverse primer of the respective product were utilized. Conditions for this cycle sequencing on thermocycler were: 1 minute for an initial denaturation of the DNA at 96 ^{0}C, followed by 35 cycles of a 10-second denaturation at 96 ^{0}C, variable annealing temperature based on the primers used for 5 seconds, and the extension step at 60 ^{0}C for 4 minutes. After this, capillary electrophoresis was performed on the 3130 Genetic Analyzer. The full process of sequencing was conducted in Advanced Molecular Biotechnology Laboratory, Department of Genetic Engineering and Biotechnology of University of Dhaka.

Results and Discussion

Clinical features and diagnosis

The patient was admitted with characteristics indicating a certain type of hereditary lymphedema. All the parameters of the general examination including the vitals were normal. Examination of lower limbs revealed bilateral edema of legs and feet (Fig. 2[a]) with dryness and hyperpigmentation of the overlying skin. Examination of the eye revealed partial ptosis on the left side, an extra partial set of eyelashes on both eyes (Fig. 2[c] and Fig. 2[d]), and left corneal opacity with reduced visual acuity on the left eye. Slit-lamp examination of both eyes showed bilateral distichiasis, epithelial and stromal opacity in the center of the cornea, and superficial corneal vascularization on the left eye. Results of other systemic examinations were normal. Isotope Lymphoscintigraphy (Fig. 2[b]) of both lower limbs revealed grade-1 and grade-2 lymphedema on the left and right sides respectively. Findings of Serum Creatinine, ALT, Prothrombin Time, Urine R/M/E, ECG, Echocardiogram, and CXR were normal. ICT for filaria was also negative. A Duplex study of both lower limbs found no evidence of deep vein thrombosis and no evidence of arterial insufficiency.

Table 1. Primers for PCR amplification of *FOXC2* gene

Primers	sequence	length	Tm(^{0}C)	Size(bp)
F1	GAGCCGTCTCGGAAGCAG	18	60.66	401
R1	TCGTTGAGCGAGAGGTTGTG	20	60.32	
F2	TTCATCATGGACCGCTTCCC	20	60.11	524
R2	ATGTTCTCCACGCTGAAGCC	20	60.47	
F3	CAAGGAGGCCGAGAAGAAG	19	60.1	564
R3	GTGGTGCTGGTGGTGGTG	18	62.2	
F4	ATCATGACCCTGCGAACG	18	60.7	598
R4	TGCCACTCACCTGGGACT	18	60.3	
F5	GCCTCCTGGTATCTCAACCA	20	60.1	328
R5	TCTCTGCAGCCCCTTAATTG	20	60.3	

Table 2. PCR reagent composition

Reagents	volume (µl)
10X Reaction Buffer	2.5
dNTP solution	0.5
Forward primer	0.5
Reverse primer	0.5
Template	Volume required for 60 ng genomic DNA
Taq Polymerase (5U/ µl)	0.125
DMSO	1.25 (5%)
Nuclease free H_2O	19.625 25 µl
Total	25

Table 3. PCR reaction conditions

Step	Temperature (^{0}C)	Duration	Cycle
Initial denaturation	95	4 min	1
Denaturation	95	30 sec	35
Primer annealing	60	30 sec	
Extension	72	Variable (1 min for 1kb)	
Final Extension	72	5 min	1

Based on these clinical features and the patient statement of his father and younger brother having the similar illness, he was diagnosed with a rare hereditary disease, Lymphedema distichiasis syndrome. After necessary documentation, blood sample from the patient was collected to test for the presence of *FOXC2* mutations.

PCR results of *FOXC2* gene

PCR amplification of the 5 primer sets showed specific bands only for pair numbers 1 and 5 (Fig. 3[a]). Regions covered by primer pairs one and five were sequenced (Fig. 4).

To reveal the sequence between, several modifications were tried. Interestingly, gel electrophoresis indicated amplification from primer combination of F1 and R5 with 5% DMSO (Fig. 3[b]). Annealing and extension temperatures were 60 ^{0}C and 72 ^{0}C respectively for this reaction. Later, this product was used as a template to perform nested PCR with primer combination of F2 and R4. In this nested PCR reaction mix, the annealing temperature was 60 ^{0}C and 3% DMSO was added. Nested PCR with primer combination of F2 and R4 resulted in better amplification but nonspecific products were present (Fig. 3[c]).

The band of the desired size of 1120 bp was isolated using Gel extraction after electrophoresis. This 1120 bp DNA was sequenced using the Sanger method from both primers. PCR products of primer pair F1+R1, F2+R4, and pair F5+R5 overlap each other and cover the whole coding region of the *FOXC2* gene. So, these three products were sequenced to get the complete sequence of the gene (Fig. 4).

Sequence analysis of *FOXC2* gene and locating deletion mutation

Primer pairs of PCR products that provided good quality sequence are F1+R1, F5+R5 and F2+R4. When blast search against the NCBI nucleotide database were performed, no mutation was found in the sequence derived from pair F1+R1 and F5+R5. Product of primer combination F2+R4 was sequenced with both F2 and R4 primer to get the sequence of the whole segment. Sequence from R4 was reverse-complemented and after trimming they were assembled in full 1120 bp sequence. When the assembled sequence was blast searched, an 8 bp deletion (ACGCCGCC) was identified (Fig. 5[a]). The chromatogram also indicates that the patient is homozygous for this deletion (Fig. 5[b]). This

deletion is identified to be between base no 6423 and 6431 of RefSeqGene on chromosome 16, (which refers to mRNA position between 914 and 921). This mutation had been reported before for the same disease. ClinVar accession code for this deletion is RCV000007679.3. Although most other mutations of this gene are unique among different families, as of October, 2021 only this 8 bp deletion has been reported four times in four independent studies for families from different geographical region (Bell et al., 2001; Erickson et al., 2001; Bahuau et al., 2002; Brice et al., 2002). These changes resulted in the production of a premature stop codon that terminated the predicted protein earlier than the wild-type and produced novel C-termini. Codons after 304 are disrupted for this mutation and new 154 amino acids are added.

In contrast to most other mutations, which appear to be unique, the eight-base-pair deletion reported in this study was observed in four additional unrelated pedigrees with lymphedema and distichiasis, suggesting that it is recurrent. One study reported this deletion in a French family showing autosomal-dominant segregation of upper- and lower-eyelid distichiasis in seven affected relatives over three generations, in addition to below-knee lymphedema of pubertal onset in three (Bahuau et al., 2002). Two children had cleft palate as well as distichiasis, but without any association with the Pierre–Robin sequence. Divergent strabismus and early-onset myopia were other ophthalmologic anomalies. Another study reported this deletion in a British family with the father and all three of his children being affected with both distichiasis and bellow-knee lymphedema (Bell et al., 2001). Another study reported this mutation in fourteen-year-old boy with distichiasis, cleft palate webbed neck and very early onset (6 week) lymphedema (Erickson et al., 2001). The patient of this study stated he developed lymphedema during his puberty. He had distichiasis in the lower lids of his both eyes. He did not have myopia or cleft palate like some other LD patients with this deletion. Being reported in this study makes this 8 bp deletion the only *FOXC2* mutation that has been found in five totally unrelated LD affected families. The reason behind the recurrence of this 8-base-pair-deletion is not fully clear. It indicates that the region is prone to DNA polymerase slippage during replication process. In fact, high GC percentage has been reported to make DNA more prone to deletion through polymerase slippage and recombination which partly explains why most of the *FOXC2* mutations are frameshift deletions. Elucidating the reason behind this particular deletion being relatively more frequent might shed light on to important features that make a sequence prone to deletion and has implications in mutational hotspot identification.

(a)

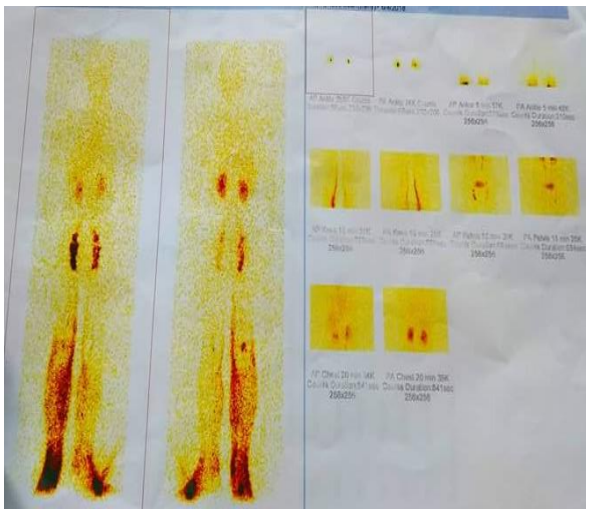

(b)

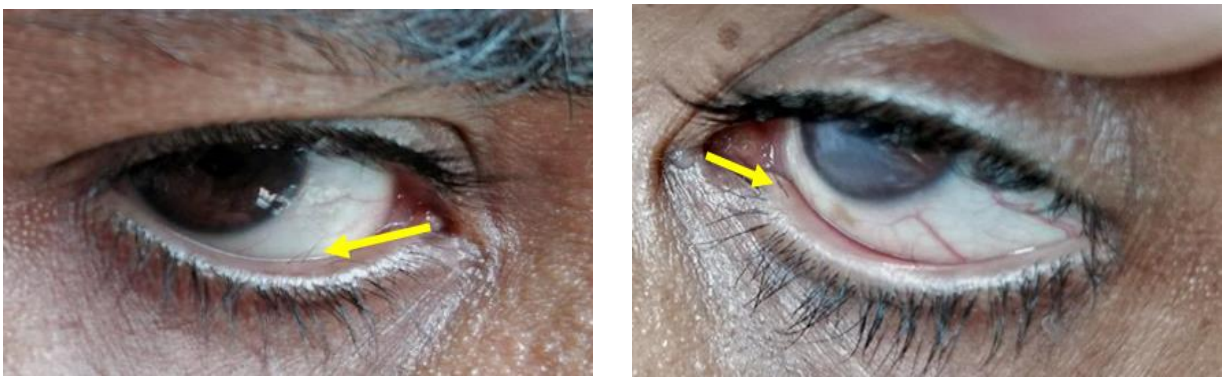

(c) (d)

Fig. 2. Clinical presentation of a 32-year-old Bangladeshi male with lymphedema distichiasis, (a) the lymphedema of the legs and feet, (b) Lymphoscintigraphy image of both legs, (c, d) Distichiasis in lower eye lids of the left and right eye respectively.

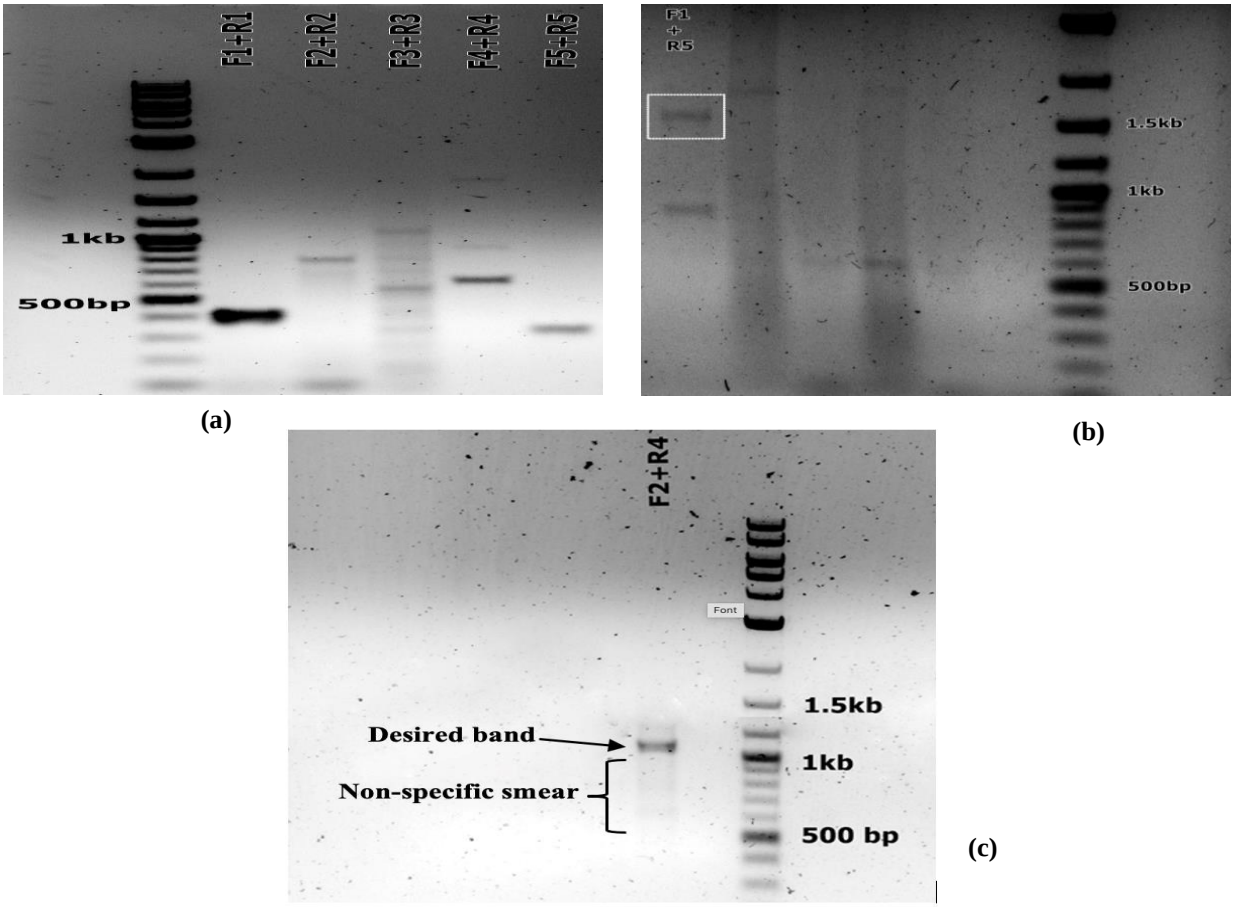

(a) **(b)** **(c)**

Fig. 3. (a) PCR amplification with all FOXC2 primer pairs. Among these, good quality sequence was determined from pair 1 and pair 5; (b) Gel electrophoresis of PCR amplification with DMSO, band was visible only for primer pair: F1+R5. The band of 1.5 kb size (indicated by the white box) was extracted from gel to use as template for nested PCR; (c) Nested PCR with product of F1+R5 as template, PCR product of primer F2+R4 was loaded in the gel and band of 1120 bp is visible with some nonspecific smears.

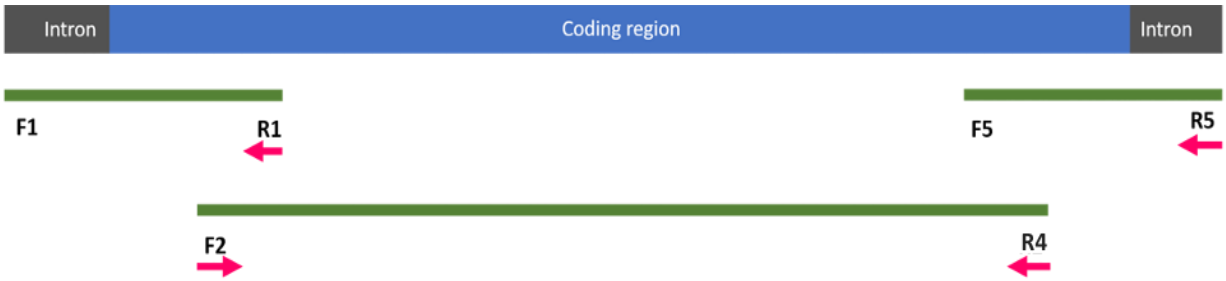

Fig. 4. PCR amplification maps of the FOX2 gene. F:forward primer, R: reverse primer, numbers after F/R means pair number, green bars indicate sequenced region, pink arrows indicate primers used during cycle sequencing.

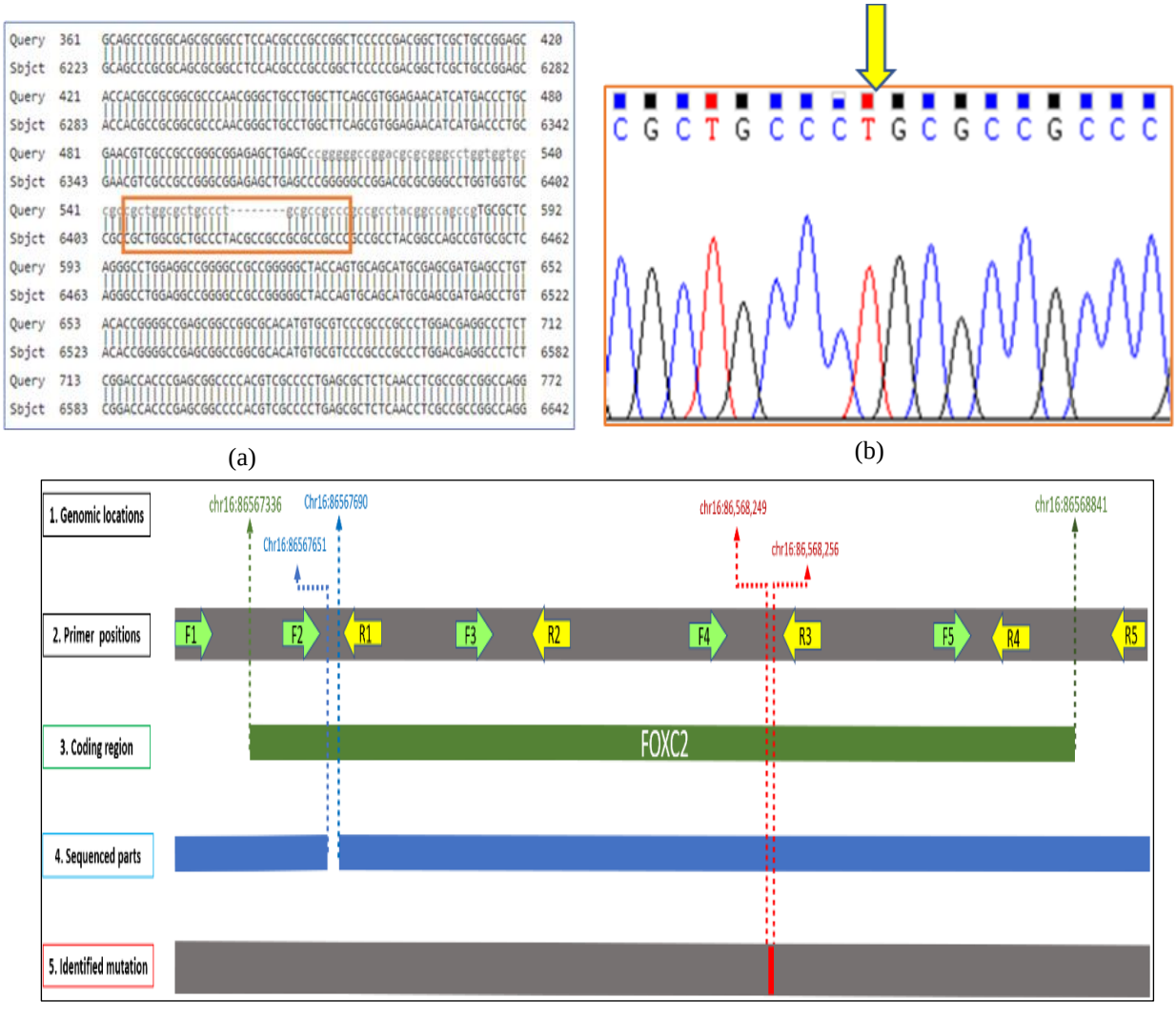

Fig. 5. (a) Blast result showing 8-base pair deletion, (b) Chromatogram of patient's DNA, yellow arrow indicates site of mutation. (c) Genomic locations [1] and the relative position of primer pairs [2], locations of *FOXC2* coding region [3], sequence gap [4] and identified mutation [5]; genomic locations are given according to GRCh38.

Conclusion

This is the first reported case of LD in Bangladesh. Although Hereditary lymphedemas are rare, analysis and investigation of such disease bear significance. The patient diagnosed in this study draws special attention due to the relatively low expressivity of the disease even though he is homozygous for the deletion in *FOXC2*. The deletion disrupts codons after 304. It means that the C-terminal activation domain and inhibitory domain are disrupted but the amino acid sequence for the N-terminal activation domain, nuclear localizing segment, and forkhead DNA binding domain remains identical to the native protein. As the homozygous deletion did not result in serious health complications for the patient, the mutated protein probably retains most of its native functions. Although the proper function of the protein might depend on the interactions among its domains, the function of the N terminal activation domain and forkhead DNA binding domain was not fully disrupted otherwise no native function would have been retained. A study found eight proline-directed Ser/Thr phosphorylation sites in FOXC2 clustered in a relatively short region of the protein encompassing amino acids 219 to 367. Phosphorylation at these sites was found to be important for FOXC2-induced vascular remodeling in vivo. It indicates that this eight-base-pair deletion probably hampers the proper regulation of the protein, but its major functional domains maintain their functions.

Unfortunately, the sequence of a 40 bp segment could not be clearly read from the chromatograms due to the limitation of Sanger sequencing to produce peaks of good resolution at the ends of the DNA molecule (Fig. 5[c]). Extensive literature search has ensured that there is no report of mutation in this region and no LD patients were found to simultaneously carry two different mutations of *FOXC2* gene until now.

Declarations

Ethics approval and consent to participate: Provided by patient.

Consent for publication: Attached

Availability of data and materials: All data are included in this manuscript.

Competing interests

The authors declare no competing interests

Funding

The molecular study was partially supported from Dr. Mustak Ibn Ayub's grant of the University Grants Commission of Bangladesh.

Authors' contributions: The clinical assessments were conducted by Md. Lutfar Rahman, Md. Mostafizur Rahman, Mohammad Ali and A.F.M Helal Uddin. The molecular study was planned and supervised by Dr. Mustak Ibn Ayub and bench work was conducted by Nahid Parvez.

Acknowledgements

We acknowledge the help of Dr. Abu Ashfaqur Sajib, Professor of the Department of Genetic Engineering and Biotechnology, University of Dhaka for his generous time, reagents and space during the first phase of this study.

References

Bahuau M, Houdayer C, Tredano M, Soupre V, Couderc R and Vazquez MP. FOXC2 truncating mutation in distichiasis, lymphedema, and cleft palate. *Clin Genet.* 2002; 62(6): 470-473.

Bell R, Brice G, Child AH, Murday VA, Mansour S and Sandy CJ. Analysis of lymphoedema-distichiasis families for FOXC2 mutations reveals small insertions and deletions throughout the gene. *Hum Genet.* 2001; 108(6): 546-551.

Brice G, Mansour S, Bell R, Collin JRO, Child AH and Brady AF. Analysis of the phenotypic abnormalities in lymphoedema-distichiasis syndrome in 74 patients with FOXC2 mutations or linkage to 16q24. *J Med Gene*t. 2002; 39(7): 478-483.

Danciu TE, Chupreta S, Cruz O and Fox JE, Whitman M, Iniguez-Lluhi JA. Small ubiquitin-like modifier (SUMO) modification mediates function of the inhibitory domains of

developmental regulators FOXC1 and FOXC2. *J Biol Chem.* 2012; 287(22): 18318-18329.

Erickson RP, Dagenais SL, Caulder MS, Downs CA, Herman G and Jones MC. Clinical heterogeneity in lymphoedema-distichiasis with FOXC2 truncating mutations. *J Med Genet.* 2001; 38(11): 761-766.

Fang J, Dagenais SL, Erickson RP, Arlt MF, Glynn MW and Gorski JL. Mutations in FOXC2 (MFH-1), a forkhead family transcription factor, are responsible for the hereditary lymphedema-distichiasis syndrome. *Am J Hum Genet.* 2000;67(6):1382-1388.

Ivanov KI, Agalarov Y, Valmu L, Samuilova O, Liebl J and Houhou N. Phosphorylation regulates FOXC2-mediated transcription in lymphatic endothelial cells. *Mol Cell Biol.* 2013; 33(19): 3749-3761.

Kriederman BM, Myloyde TL, Witte MH, Dagenais SL, Witte CL and Rennels M. FOXC2 haploinsufficient mice are a model for human autosomal dominant lymphedema-distichiasis syndrome. *Hum Mol Genet.* 2003; 12(10): 1179-1185.

Lam EW-F, Brosens JJ, Gomes AR and Koo C-Y. Forkhead box proteins: tuning forks for transcriptional harmony. *Nat Rev Cancer.* 2013; 13(7): 482-495.

Mangion J, Rahman N, Mansour S, Brice G, Rosbotham J and Child AH. A Gene for Lymphedema-Distichiasis Maps to 16q24.3. *Am J Hum Genet.* 1999; 65(2): 427-432.

Mellor RH, Brice G, Stanton AWB, French J, Smith A and Jeffery S. Mutations in FOXC2 are strongly associated with primary valve failure in veins of the lower limb. *Circulation.* 2007; 115(14): 1912-1920.

Sabine A and Petrova T V. Interplay of mechanotransduction, FOXC2, connexins, and calcineurin signaling in lymphatic valve formation. *Adv Anat Embryol Cell Biol.* 2014; 214: 67-80.

Szuba A and Rockson SG. Lymphedema: classification, diagnosis and therapy. *Vasc Med.* 1998; 3(2): 145-156.

J. Bangladesh Acad. Sci. 47(2); 215-222: December 2023 DOI:https://doi.org/10.3329/jbas.v47i2.66977

Journal of Bangladesh Academy of Sciences

Journal homepage: http://www.bas.org.bd/publications/jbas.html

Research Article

Stereoselectivity of thiazolidine, malonamides and bicyclic tetramates with isopropyl NH and SH protecting group

Halima Bagum* and Mark G. Moloney[1]

Department of Chemistry, University of Barishal, Bangladesh

ARTICLE INFO

Article History

Received: 18 June 2023
Revised: 14 September 2023
Accepted: 17 October 2023

Keywords: Tetramate, Cyclization, Heterocycle, Stereoselectivity

ABSTRACT

The stereochemistry of the routes to two different bicyclic tetramates are reported which enables to synthesize highly functionalized systems. An analysis of the structure shows that the tetramates permit ready incorporation of three to five functionality at different positions. This work demonstrates that novel bicyclic tetramates can be synthesized via stereoselective cyclization. The resulting heterocycles were studied with the help of NMR techniques.

Introduction

The tetramate moiety occurs in a diverse range of natural products which demonstrate a wide range of biological activity (Petermichl and Schobert, 2017; Schobert and Schlenk, 2008). Bicyclic tetramates, which may exhibit biological activity, are accessible by stereoselective Dieckmann ring closure reaction. We have shown this cyclization (Scheme 1) to get **4** and utilization of the cyclized product **4** to synthesize a library of compounds for a number of systems (Andrews et al., 1998; Bagum et al., 2019a, 2019b, 2020; Saney et al., 2023).

Alternative C7-methyl tetramate **8** was developed following the methodology reported by Andrews and co-workers (Andrews et al., 1994). The thiazolidine **2** was *N*-acylated by ethyl α-methylmalonyl chloride **6** and pyridine to afford *cis*-2,5 malonamide **7** (Scheme 2). The *trans*-2,5 malonamide was also formed as a minor product but only *cis*-2,5 malonamide **7** was isolated. Dieckmann cyclization at basic condition furnished in C7-methyl tetramates **8** and **9** which were inseparable at this stage. The structures of these novel compounds were determined by NMR and MS analysis. Previous works (Anwar et al., 2010; Bagum et al., 2019a, 2020; Saney et al., 2023) on this field has extensive examples with different NH and SH protecting groups including *t*-Bu and aryl systems. Herein, we have examined thiazolidine, malonamides and bicyclic tetramates with isopropyl NH and SH protecting group.

Of interest we studied the products of cyclization pathways (Scheme 1 and 2) by using spectroscopic techniques and herein we report the results of that exploration.

Materials and Methods

Starting materials were obtained from Sigma Aldrich, Apollo Scientific, Alfa Aesar, Fluorochem or Acros Organics. Reactions were carried out in oven-dried glassware and under an inert medium of nitrogen. Minutes (min), hours (h) and days (d) were used to record reaction times. Light petroleum ether of boiling point 40-60℃ was used, without further purification, as purchased from the commercial suppliers. Solvents were evaporated under reduced pressure at 40 ℃. Büchi R-210 and RE 111 rotary evaporator, attached to

*Corresponding author: <halimaju35@gmail.com>

[1]*Department of Chemistry, University of Oxford, United Kingdom*

a Vacuubrand CVC2 pump and pressure control system, were used to evaporate solvents.

Merck aluminium foil backed sheets precoated with 0.2 mm Kielselgel 60 F_{254} was used to perform Analytical thin-layer chromatography (TLC). Kielselgel 60 silica gel (230-400 mesh particle size) was used to accomplish flash column chromatography. The eluents are identified clearly for each column.

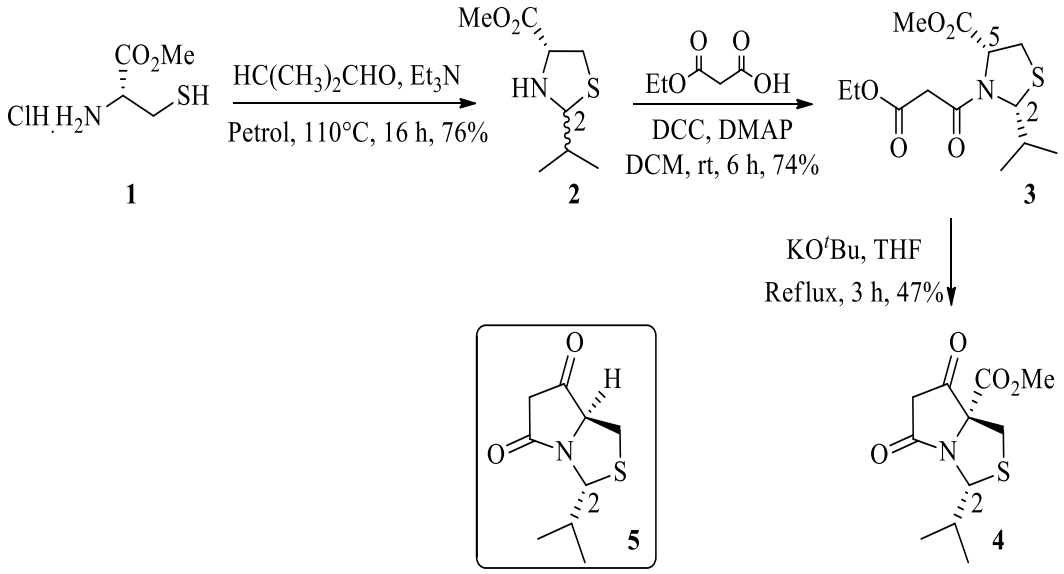

Scheme 1. Synthesis of tetramate 4.

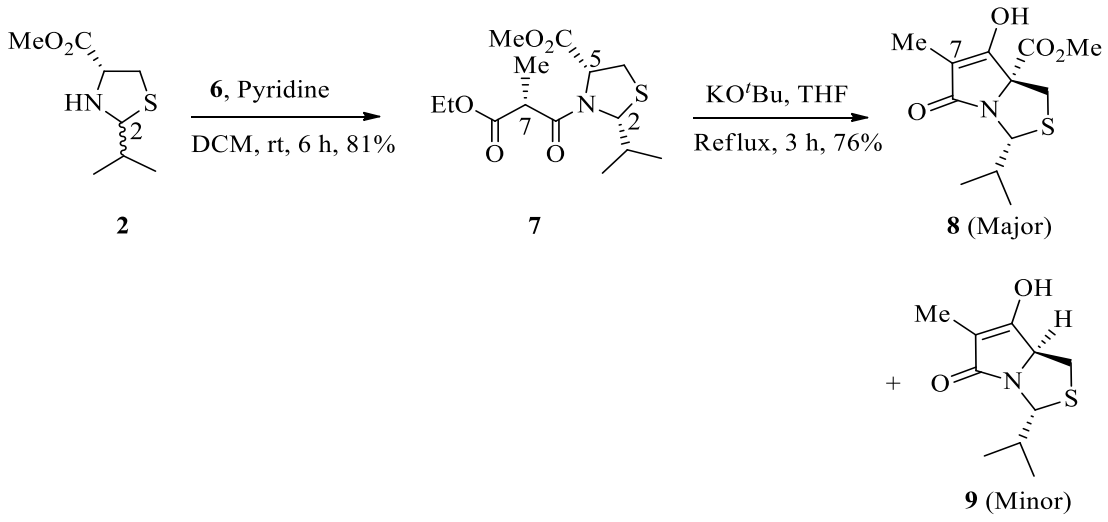

Scheme 2. Synthesis of C7-Me Tetramate 8 with isopropyl NH and SH-protecting group.

Bruker DPX200 (200 MHz), AVF400 (400 MHz), AVG400 (400 MHz), AVH400 (400 MHz), AVB500 (500 MHz), AVC500 (500 MHz) and AVX500 (500 MHz) were used to record NMR spectra by the internal assistance at the Chemistry Research Laboratory, Department of Chemistry, University of Oxford. Confirmation of stereochemistry was made using NOESY. In the circumstances where products subsist as a mixture of diastereomers, rotamers or tautomers, ^{1}H NMR spectrum was used to calculate the ratio of the mixtures.

Synthesis of Methyl Ester Hydrochloride 1 (Chaudhari and Bari,2015)*: General Method A*

To stirring anhydrous MeOH (2 M) at 0°C, $SOCl_2$ (1.5 eq) was added dropwise. L-cysteine (1 eq) was added portion-wise. The mixture was warmed up to 40°C and stirred at this temperature for 3 h. Then the solvent was evaporated under reduced pressure to produce the ester hydrogen chloride of the L-cysteine **1**.

Synthesis of Thiazolidine Compound 2 (Andrews et al., 1998; Seebach and Aebi, 1984)*: General Method B*

L-Cysteine methyl ester hydrogen chloride **1** (1.0 eq) was added in petroleum ether (50-100 mL). Then triethylamine (1.5 eq) and 2-methylpropanal (1.2 eq) were added. The reaction mixture was refluxed with continuous removal of water using a Dean-Stark apparatus for 18 h. The white precipitate was then filtered and washed with Et_2O. The combined filtrates were concentrated under reduced pressure to result the thiazolidine **2**.

N-Acylation of Thiazolidine 2 (Andrews et al., 1998)*: General Method C*

To a solution of thiazolidine **2** (1.0 eq) in anhydrous DCM, 4- dimethylaminopyridine (0.05 eq) and N,N'-dicyclohexylcarbodiimide (1.05 eq) were added. The mixture was cooled to 0°C followed by the addition of ethyl hydrogen malonate (1.05 eq). At 0°C, the reaction mixture was stirred for 30 minutes and at room temperature, the mixture was stirred for 5-6 h. A white precipitate was resulted, which was filtered and washed with dichloromethane. The combined filtrates were concentrated *in vacuo* and purified by flash column chromatography to furnish the expected products, *N*-acyl thiazolidines **3, 7**.

Dieckmann Cyclization (Andrews et al., 1998)*: General Method D*

Potassium *tert*-butoxide (1.05 eq) was added to a solution of *N*-acyl thiazolidine **3** or **7** (1.0 eq) in anhydrous tetrahydrofuran (THF). The reaction mixture was refluxed for 3 h. The mixture was separated between diethylether (Et_2O) and water. The aqueous phase was acidified with 2 M HCl and extracted with ethylacetate (EtOAc). 1 M aqueous solution of NaH_2PO_4 and brine was used to wash the organic layer. The organic layer was then dried over anhydrous Na_2SO_4 and concentrated under reduced pressure to produce the methyl ester tetramic acids **4** or **8**.

Results and Discussion

Products of cyclization pathways

The following thiazolidine, malonamide and bicyclic tetramate derivatives (Fig. 1) were obtained from the cyclization pathways using isopropyl NH and SH protecting group. The stereochemistry of the thiazolidine **2**, malonamides **3, 7**, and tetramates **4, 8** were assigned by NOE analysis (Fig. 2).

C2 Epimerisation and Rotameric Behaviour of Malonamide 3: Rationalisation.

A mixture of two different species, even after careful column chromatography, was apparent in the ^{1}H NMR spectra of malonamide **3**. These mixtures could have been rotamers due to the presence of the *N*-protecting group or an inseparable mixture of diastereomers (Fig. 3).

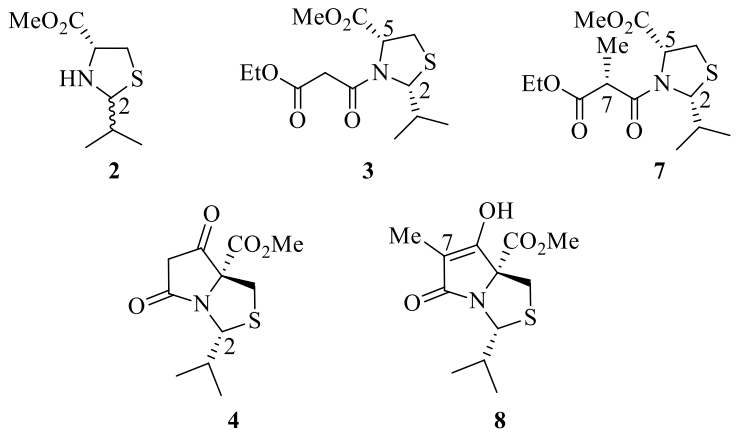

Fig 1. Products of cyclization pathways.

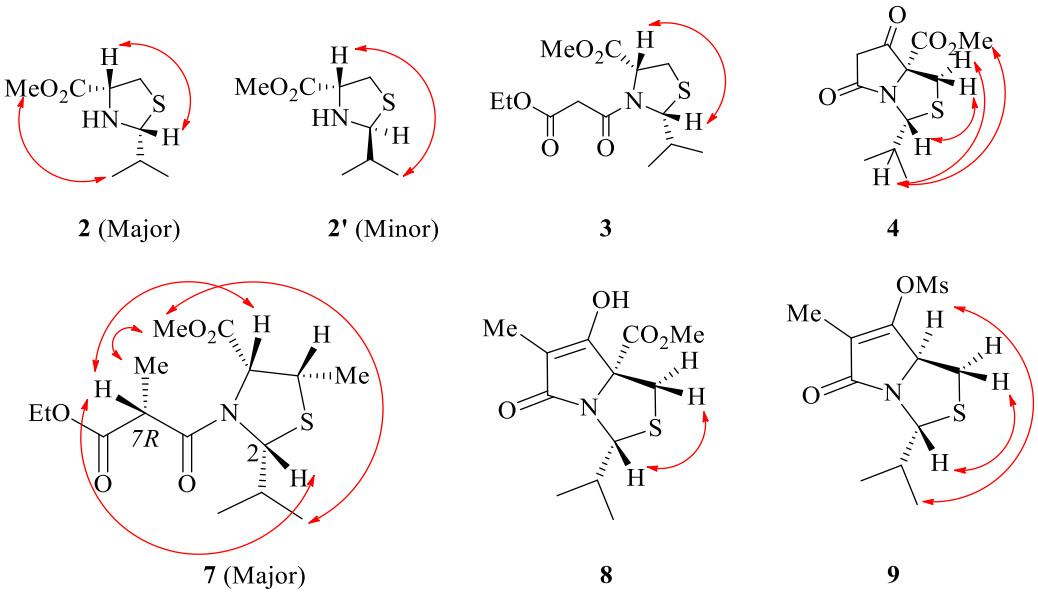

Fig. 2. Nuclear Overhauser Effect (NOE) analysis of thiazolidine 2, malonamides 3,7, and tetramates 4,8.

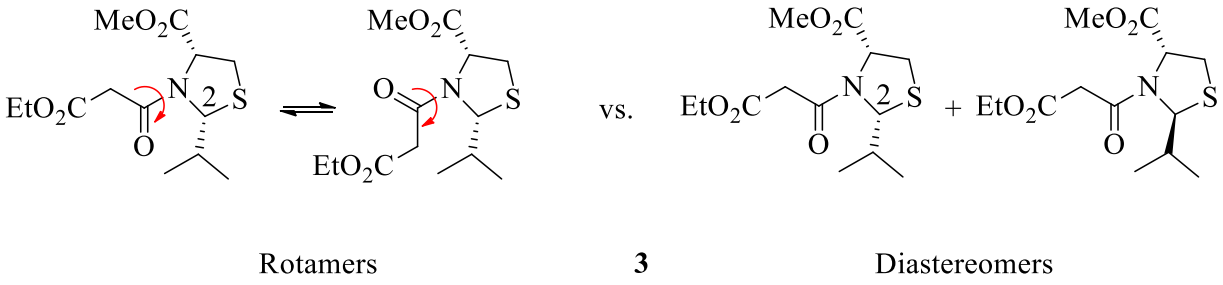

Fig. 3. Structure of rotamers and diastereomers for malonamide 3.

The rate of rotameric exchange is fast and can be examined by using variable temperature (VT) ^{1}H NMR, 1D selective chemical exchange NMR experiment or 2D gradient NOE experiment. In the VT NMR experiment, ^{1}H signals from rotameric species would coalesce. On the other hand, proton signals for the rotameric species would exhibit similar behaviour in a 1D gradient NMR experiment or exchange peaks would appear in 2D gradient NOE experiment.

The *cis*-2,5 malonamide **3** was found to exist as a mixture of rotamers detected by a 1D gradient selective NOE NMR experiment (Fig. 4). Selective

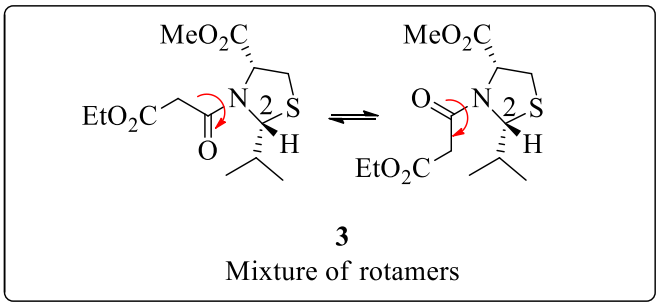

3
Mixture of rotamers

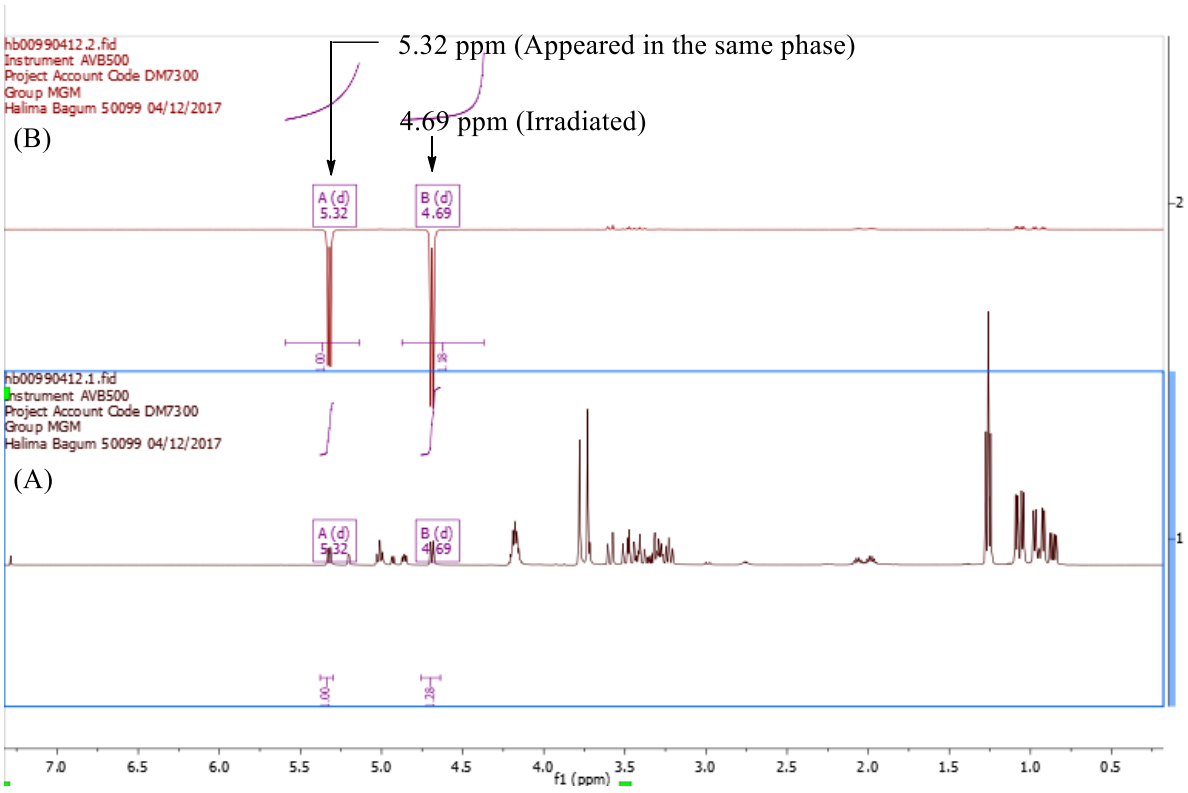

Fig. 4. (A) ^{1}H NMR of *cis*-2,5 malonamide 3; (B) 1D gradient NOE showing selective irradiation at H2.

irradiation of signal at 4.69 ppm in 1D gradient NOE experiment provided a spectrum (B) with two negative signals at 4.69 ppm and 5.32 ppm. This experiment revealed the rotameric exchange in *cis*-2,5 malonamide **3**.

Following the remarkable success in the synthesis of bicyclic teramate motif **4,** easy and cost efficient access to tetramate derivative, it was of interest to investigate the preparation and reactions of C7-methyl bicyclic tetramate with an isopropyl NH and SH-protecting group. This would permit access to 3, 4-substituted tetramate, pyrrolinone and pyrroglutaminol derivatives.

***Stereochemistry of Intermediate* 7**

The *cis*-2,5 malonamide **7** was obtained as a mixture of C7 epimers with *7R* as a major one and 1D gradient NMR spectropscopy revealed the presence of rotameric exchange (Fig. 5). The stereochemistry of the major malonamide analogue **7** was assigned confidently by NOE analysis (Fig. 2). Nuclear Overhouser Effect (NOE) analysis was used to determine the stereochemistry of the major tetramic acid **8**, whereas the stereochemistry of minor one was assigned by NOE analysis of mesylate derivative **9.**

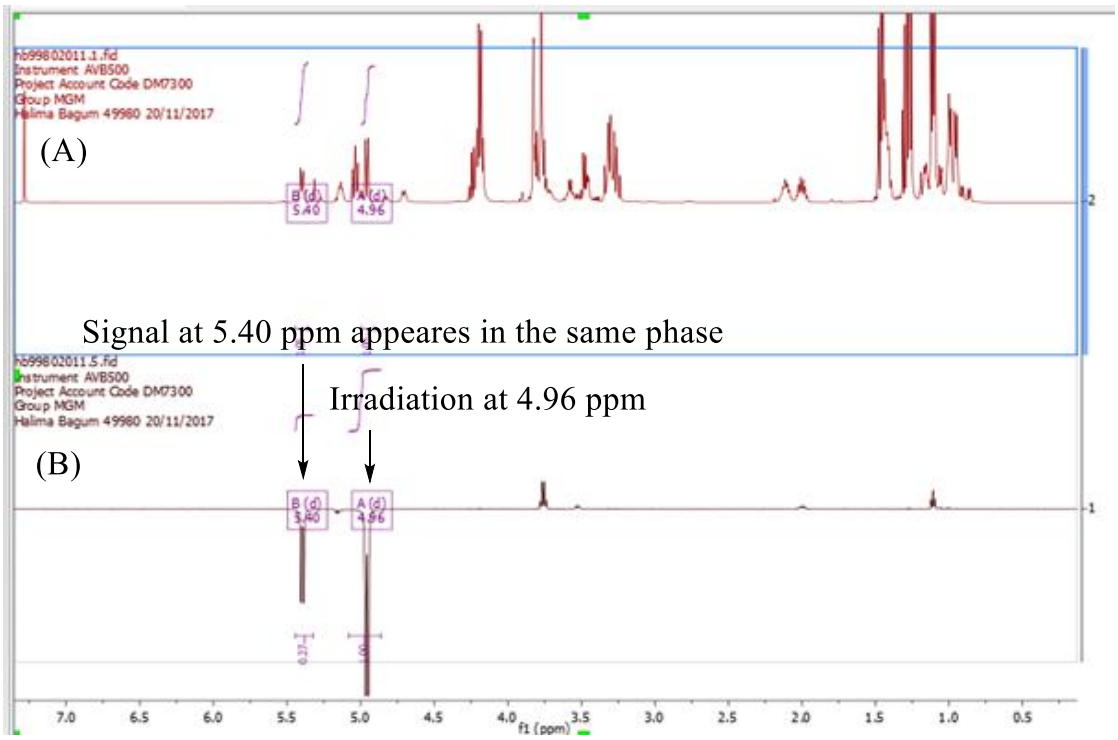

Fig. 5. (A) ^{1}H NMR of *cis*-2,5 malonamide 218b; (B) 1D gradient NOE showing selective irradiation at H2

Regioselectivity and Diastereoselectivity in Dieckmann Cyclization

Andrews and co-workers (Andrews et al., 1994, 1998) have reported a comprehensive study on the regioselectivity, diastereoselectivity and enantioselectivity of the Dieckmann ring closure of *N*-acyl oxazolidines. Similarly, the regioselectivity, diastereoselectivity and enantioselectivity of the Dieckmann ring closure of *N*-acyl thiazolidine can be described (Scheme 3). The steric bulk from the isopropyl group plays a vital role in the observed regioselectivity and diastereoselectivity in Dieckmann cyclization.

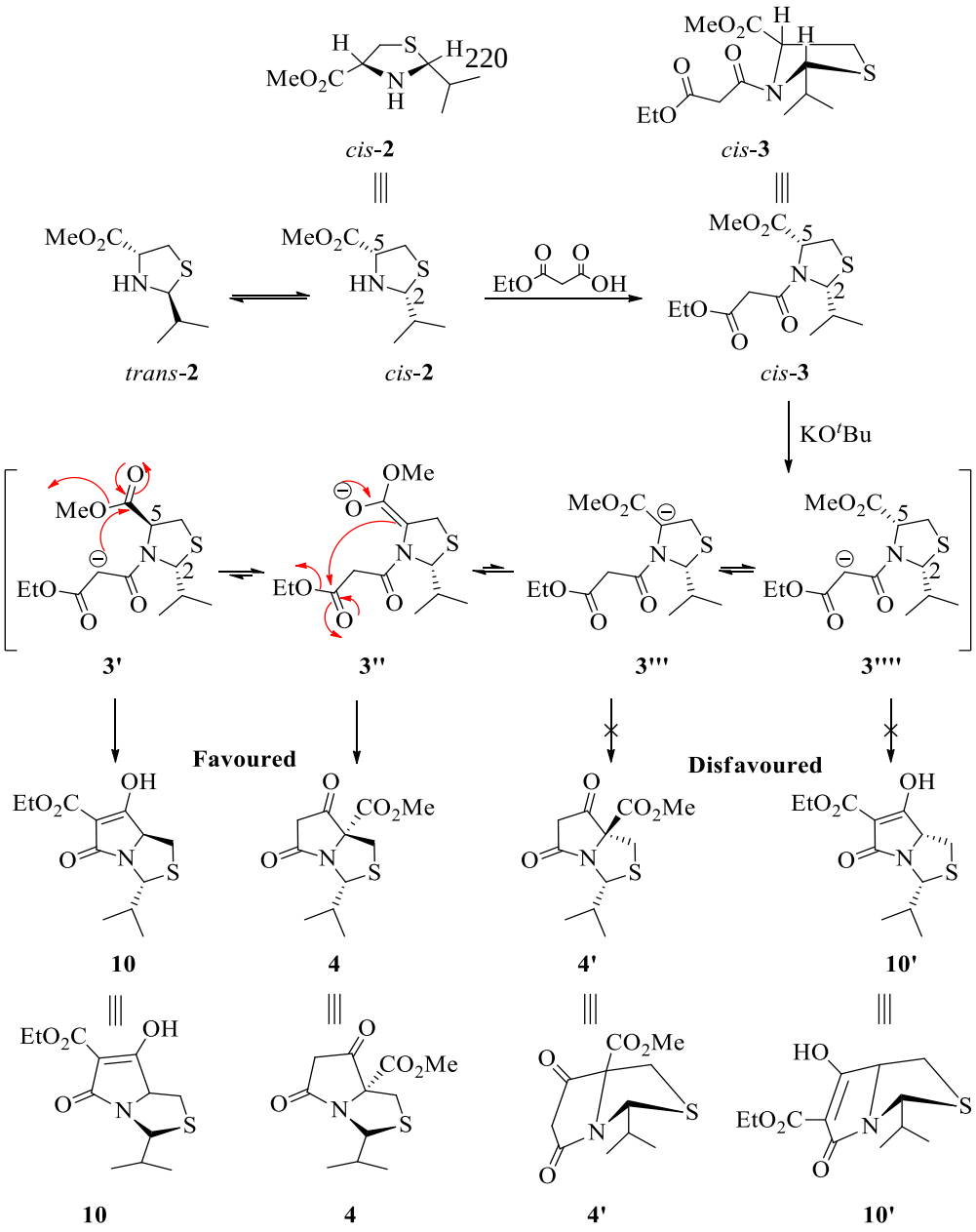

Scheme 3. Mechanism and possible outcomes for the Dieckmann cyclization.

Deprotonation of *cis*-**3** results in four possibilities for cyclization among which only two are favoured as the bulky isopropyl group is placed on the less obstructed *exo*-face of the bicyclic ring system and consequently, the major product comes from the more stable enolate **3’’**. The other two structures, **3’’’** and **3’’’’**, set the isopropyl group in the more obstructed *endo*-face of the bicyclic ring system and thereby cannot be formed. Jeong *et al.*(Jeong et al., 2011) have examined the chemoselectivity in Dieckmann cyclisation. Seebach’s substrate-controlling protocol ‘Self Regeneration of Stereocentres’(Seebach et al., 1996; Seebach and Aebi, 1984) allows this route to avoid racemization in the formation of chiral tetramates **4** and **10**. The optical purity of products for *O*-system was also

examined by Andrews (Andrews et al., 1998). These results clearly demonstrate that this three-step route to tetramate proceeds with regio- and chemoselectivity and develops tetramates **4** of excellent enantiomeric purity.

Conclusion

The stereochemistry of thiazolidine **2**, malonamides **3, 7** and bicyclic lactams **4, 8**, prepared from cysteine and 2-methylpropanal, were studied extensively with the help of different NMR techniques. It has shown that the products are stereoselective and in all cases the major products are of *cis*-configuration.

Acknowledgements

I would like to express my sincere gratitude to Professor M. G. Moloney for giving me the opportunity to carry out this work in his research group. This work was conducted with the financial support of the Commonwealth Scholarship Commission in the United Kingdom and the University of Oxford, United Kingdom.

Conflict of Interest

The authors of this manuscript declare that they have no conflict of interest.

Authors Contribution

Bagum H, with the help of Moloney MG, designed the experiment. Bagum performed the experiment. Moreover, Bagum H has prepared the manuscript and Moloney MG reviewed the manuscript.

References

Andrews MD, Brewster A and Moloney MG. A concise approach to functionalised, homochiral tetramic acids. *Tetrahedron: Asymmetry*, 1994; 5(8): 1477-1478.

Andrews MD, Brewster AG, Crapnell KM., Ibbett AJ, Jones T, Moloney MG, Prout K, and Watkin D. Regioselective Dieckmann cyclisations leading to enantiopure highly functionalised tetramic acid derivatives. *J. Chem. Soc., Perkin Transactions 1*, *2*, 1998; 223-236.

Anwar M, Cowley AR and Moloney MG. Novel chiral pyrrolidinone scaffolds derived from threonine with antibacterial activity. *Tetrahedron: Asymmetry*, 2010; 21(13-14): 1758-1770.

Bagum H, Christensen KE, Genov M, Pretsch A, Pretsch D and Moloney MG. Synthetic access to 3-substituted pyroglutamic acids from tetramate derivatives of serine, threonine, allo-threonine, and cysteine. *J. Org. Chem.*, 2019a*;* 84(16): 10257-10279.

Bagum H, Christensen KE, Genov M, Pretsch A, Pretsch D and Moloney MG. Synthetic access to 3,4-disubstituted pyroglutamates from tetramate derivatives from serine, allo-threonine and cysteine. *Tetrahedron*, 2019b*;* 75(40): 130561-130581.

Bagum H, Shire BR, Christensen KE, Genov M, Pretsch A, Pretsch D, and Moloney MG. Bicyclic lactams derived from serine or cysteine and 2-methylpropanal. *Synlett*, 2020; 31(4): 378-382.

Chaudhari P and Bari S. Efficient synthesis of N-sulfonyl β -arylmethylalaninates from serine via ring opening of N-sulfonyl aziridine-2-carboxylate. *Synth. Commun.*, 2015; 45(3): 391-402.

Jeong YC, Anwar M, Nguyen TM, Tan BSW, Chai CLL and Moloney MG. Control of chemoselectivity in Dieckmann ring closures leading to tetramic acids. *Org. Biomol. Chem.*, 2011; 9(19): 6663-6669.

Petermichl M and Schobert R. 3-Acyltetramic acids: A decades-long approach to a fascinating natural product family. *Synlett*, 2017; 28(06): 654-663.

Saney L, Panduwawala T, Li X, Christensen KE, Genov M, Pretsch A, Pretsch D and Moloney MG. Synthesis of fused tetramate-oxazolidine and -imidazolidine derivatives and their antibacterial activity. *Org. Biomol. Chem.*, 2023; 21(23): 4801-4809 .

Schobert R and Schlenk A. Tetramic and tetronic acids: An update on new derivatives and biological aspects. *Bioorg. Med. Chem.*, 2008; 16(8): 4203-4221.

Seebach D and Aebi JD. α-alkylation of serine with self-reproduction of the center of chirality. *Tetrahedron Letters*, 1984; 25(24): 2545-2548.

Seebach D, Sting AR and Hoffmann M. Self-regeneration of stereocenters(SRS)—Applica-tions, Llmitations, and abandonment of a synthetic principle. *Angew. Chem. Int. Ed. Engl.*, 1996; 35(2324): 2708-2748.

J. Bangladesh Acad. Sci. 47(2); 223-240: December 2023 DOI:https://doi.org/10.3329/jbas.v47i2.68555

Journal of Bangladesh Academy of Sciences

Journal homepage: http://www.bas.org.bd/publications/jbas.html

Research Article

Dissecting drought stress tolerance of soybean genotypes based on morphological and physiological attributes

Md. Karimul Ahsan, Md. Abdullah Al Mamun*, Toton Kumar Ghosh[1] and M. Abdul Karim

Department of Agronomy, Bangabandhu Sheikh Mujibur Rahman Agricultural University (BSMRAU), Gazipur, Bangladesh

ARTICLE INFO

Article History

Received: 03 September 2023
Revised: 16 October 2023
Accepted: 18 October 2023

Keywords: Drought, Morphology, Physiology, Tolerant, Yield.

ABSTRACT

Soybean genotypes G00006, BD2336, AGS383, PK472, BCS1, NCS1, BU Soybean1 and BARI Soybean6 were evaluated under 20% (drought) and 80% (control) of field capacity based on morpho-physiological and yield response to drought. The results revealed that plant height, leaf number, chlorophyll content, photosynthesis, stomatal conductance, transpiration rate, relative water content and water uptake capacity of soybean drastically reduced due to drought. However, root: shoot ratio increased under drought condition. Across the genotypes, the root : shoot ratio ranged from 0.20 to 0.47 in control, while 0.22 to 59 in drought condition. Genotypes BD2336, AGS383 and G00006 produced higher number of pods and seeds, whereas minimum yield reduction was recorded in AGS383 under drought. Based on drought tolerance index, AGS383 ranked 1st, while BD2336 and PK472 ranked 2nd and 3rd position, respectively. High grain yielding ability of AGS383 suggested that it could be cultivated in drought prone environment.

Introduction

Drought, scarcity of water, is the single most vital factor distressing the agricultural production and world food security. It hampers normal plant growth, alter phenotypic characters resulting decreasing of yield significantly (Mannan et al., 2022; Ku et al., 2013). Water shortage also affects physiological and developmental processes of plants that alter the yield of a crop (Allahmoradi et al., 2011). The development of high yield potential crop cultivars with drought tolerance ability has a great significance for increasing yield in dry land condition.

Globally, soybean (*Glycine max* L. Merrill) is a vital grain legume (Kumar et al., 2008; Ahmed et al., 2010). Hundred years ago, it was domesticated in East Asia. The management and production technology of soybean have been improved immensely throughout the world due to its nutritional value (Liu et al., 2005). It is a remarkable source of oil, protein, carbohydrate, minerals and vitamins (Mannan and Mamun, 2018; Dola et al., 2022). It is also very useful in improving the soil, because it has capability to fix atmospheric nitrogen for itself and other plants also (Kumar et al., 2008; Purcell et al., 2000; Ahmed et al., 2010; Mugendi et al., 2010). Drought negatively affects soybean growth and causes less crop growth and substantial reductions in yield (Akand et al., 2018; Fatema et al., 2023; Chowdhury et al., 2017; Mannan et al., 2023). The reproductive and grain filling stage of soybean is very sensitive to drought stress (Wijewardana et al., 2019; Liu et al., 2004). However, long-term water stress during vegetative phase also causes substantial yield loss. The scar city of water reduces stomatal conductance (Gs), lower photosynthesis (Pn),

*Corresponding author: <aamamun@bsmrau.edu.bd>

[1]*Department of Crop Botany, BSMRAU, Gazipur, Bangladesh*

chlorophyll (Chl) content, and transpiration rate (Tr). Biomass production negatively affected due to low leaf area under drought condition (Brown et al., 1985). Yield of grain legume depends on dry matter production in shoot (Saxena et al., 1990). Drought negatively affected the production of shoot and root biomass in soybean grown under water stress condition (Fatema et al., 2023). Roots play a vital role in drought tolerant because they uptake water and nutrient from soil (Eureka et al., 2000).

The climatic and the edaphic conditions allows soybean to grow throughout the year in Bangladesh. The area of soybean cultivation has been expanded dramatically from only 5000 ha in 2005 to 62508 ha in 2018-2019 (BBS, 2020; Mamun et al., 2022). The expansion of cultivation of soybean occurred mainly in the districts of Noakhali, Luxmipur, Bhola, Patuakhali, Faridpur, and even in the northern Bangladesh due to its high demand for making animal feed. Though, soybean can be cultivated throughout the year, but it is difficult to fit with existing cropping patter in rabi and kharif II due to high crop competition. Aman rice is popularly cultivated in kharif II, while winter crops in rabi season. However, only few field crops are grown during kharif I and this season may be a good option for growing soybean.

But, scarcity of water and high temperature hamper a harvest of good crop in kharif I season. Therefore, it is necessary to screen out soybean genotypes which would be well adapted to that low moisture regime. Miah et al. (2020) recommended dwarf variety BU Soybean1 that gave higher yield in rabi season when plant suffer for the scarcity of water due to less or no rainfall. G00006, BD2350, Shohag, BD2336, AGS383 and GMOT22 were found fairly drought tolerant as reported by Akand et al. (2018). Considering the above facts, this study was conducted to analyze the effect of drought on the changes in growth and productivity of soybean, and to determine the morpho-physiological mechanisms of drought tolerance in soybean.

Materials and methods

Experimental site

A pot experiment was conducted in a vinyl house of the Department of Agronomy, BSMRAU, Gazipur, Bangladesh during kharif I, 2018. The site is located in Madhupur Tract (Agroecological Zone 28).

Pot preparation

Total 80 pots were used in this experiment and they were filled with soil collected from Kodda, Gazipur. The soil was sandy loam and each pot contained 12.0 kg of soil. Urea, triple super phosphate, muriate of potash and gypsum was applied at 0.15, 0.18, 0.36 and 0.1 g pot^{-1}, respectively before sowing seeds.

Experimental treatment and design

A randomized complete block design with five replications was followed to conduct the experiment. The experimental treatments consisted of two factors, viz. Factor A (8 soybean genotype) included G00006, BD2336, AGS383, PK472, BCS1, NCS1, BU Soybean1 and BARI Soybean6; and Factor B (growing condition) drought (20% of field capacity (FC) and control (80% of FC).

Sowing soybean seeds and imposition of drought treatments

Five healthy seeds were sown in each pot uniform spacing on 03 May, 2018. After sowing of seeds, light irrigation was given for uniform seed germination. Before imposition of drought treatment, extra seedlings were removed by keeping one healthy plant pot^{-1}. Water stress treatments were imposed after trifoliate stage of the crop (15 days after sowing, DAS). To maintain equal soil moisture content in all pots, irrigation was applied one day before treatment imposition. Water stress condition was induced by withholding water until wilting symptom was observed in plants and irrigation was applied in each pot at the first appearance of wilting symptom in plants to maintain 20% of FC.

However, irrigation water was applied after 3-5 days of the previous application. A soil moisture meter

was used to determine the soil moisture level before applying irrigation. At FC, the experimental soil contains 30% moisture. Therefore, 6% of soil moisture was maintained to ensure 20% of FC of the soil. Further, about 24% soil moisture was maintained for control treatment, where 80% of FC was ensured.

Phenological attributes

Data on days to emergence, flowering, and pod formation were recorded for each genotype under both treatments. Days to first emergence were counted when at least one radical emerge throughout the seed coat in each genotype. Days to 50% emergence were counted when most of the plants of each genotype had more than 50% radical emergence. Days to first and 50% flowering were counted when at least one and more than 50% flowers opened, respectively. Days to first pod and 50% pod formation were counted when at least one pod and more than 50% pod was developed in most of the plants of each genotype, respectively. A plant was considered to have maturity when majority of the plant leaves turned yellow and color of pods became brownish and hard.

Collection of morphological parameters

Plant height was measured by a meter scale (100 cm) at 25 and 50 DAS. The height of plant was taken from the base to the tip of the plants. The height of the five plants was averaged. To record leaves number plant^{-1}, the leaves of sample plants were count down as 1, 2, 3, 4 and so on at 25 and 50 DAS. Leaves per plant of the five plants was averaged. The growth duration was determined from gap between date of seed sowing to date of physiological maturity of each genotype.

Quantification of physiological traits

At 50 DAS, Chl was determined on fresh weight (FW) basis extracting with 80% acetone by using double beam spectrophotometer according to Talukder et al. (2022). The formulae for computing Chl a, b and total chl were-

$$\text{Chl a (mg g}^{-1}\text{ FW)} = [\{12.7\ (D663) - 2.69\ (D645)\} \times \{V/(1000\times W)\}]$$

$$\text{Chl b (mg g}^{-1}\text{ FW)} = [\{22.9\ (D645) - 4.68\ (D663)\} \times \{V/(1000\times W)\}]$$

$$\text{Total chl (mg g}^{-1}\text{ FW)} = [\{20.2\ (D645) + 8.02\ (D663)\} \times \{V/(1000\times W)\}]$$

Where, D (663,645) = Optical Density of the chl extract at wavelength of 663 and 645 nm, respectively. V = Final volume (ml) of the 80 % acetone with chl extract and W = Weight of fresh leaf sample in g. Leaf temperature was recorded at flowering stage of the crop. The average value was recorded. The Pn, Gs and Tr were determined during flowering stages of the crop with a portable Pn system (LiCOR-6400, Lincoln, Nebraska). Measurement was taken in a clear sunny day. For determining FW, sampling was done at flowering stage of each genotype. Fully expanded leaves of each genotype were collected from both control and drought condition at noon. After collecting leaves from pot, they are transferred to the laboratory and FW was taken immediately. The leaves were soaked in distilled water for 24 hours to record the turgid weight (TW). Dry weight (DW) of leaf was obtained after oven drying for 72 h at 70 ºC. The relative water content (RWC) was calculated in following equation according to (Schonfeld et al. (1988).

$$RWC = \frac{FW - DW}{TW - DW} \times 100$$

Water saturation deficit (WSD) and water retention capacity (WRC) was calculated following Sangakkara et al. (1996).

$$WSD = \frac{TW - FW}{TW - DW} \times 100$$

$$WUC = \frac{FW - DW}{DW}$$

Where, FW= fresh weight, DW= dry weight and TW= turgid weight of the sample.

The root and shoot weight were taken at 50 DAS. From both treatments of control and drought, a soybean plant of each genotype was cut just above the soil surface. The weight of stem and leaves were obtained after oven drying for 72 h at 70 ºC. All the roots were collected carefully by hand and washed them in running tap water on a sieve. After washing, the roots were soaked with a cotton towel. Roots were dried in electric oven and weight of root were recorded after oven drying for 72 h at 70 ºC. The root and shoot ratio were determined from their weight.

$$\text{Root : shoot} = \frac{\text{Root weight}}{\text{Shoot weight}}$$

Yield and yield contributing data

Data on total number of pods per plant, total number of seeds per plant, number of seeds per pod, 100-seed weight and yield per plant were recorded. To measure yield per plant, total seeds from the sample plants were weighted by an electrical balance. The moisture content of seeds was measured by a hand-held moisture meter. The grain yield was adjusted to 14% moisture content using the following formula:

$$\text{Adjusted weight} = \frac{W \times (100 - M_1)}{(100 - M_2)} \times 100$$

Where, W is the fresh grain weight; and M_1 and M_2 were the fresh and adjusted moisture percent of the grain, respectively.

Data analysis

Computer software package "CropStat 7.2" version was used to analyze the collected data. The treatment means were separated using Duncan's Multiple Range Test (DMRT) at 5% level of significance (Gomez and Gomez, 1984). Some calculations and graphs were prepared using Excel software (Microsoft Corporation, Redmond, WA, USA). Using cluster analysis, soybean genotypes were scored on multiple agronomic parameters simultaneously. Drought tolerance index was determined as the observations under drought divided by the means of the controls. Cluster analysis was done according to Khrais et al. (1998) and cluster group rankings were obtained based on Ward's minimum variance. The cluster groups were identified in dendrogram and rankings were obtained from the average of means over multiple parameters in each cluster group. A sum was obtained by adding the numbers of cluster group ranking in each genotype. The genotypes were finally ranked based on the sums in order that those with the smallest sums were ranked as the most tolerant and those with the largest sums were ranked as the least tolerant in terms of relative drought tolerance.

Results and discussion

Phenological attributes

First emergence occurs within 2 DAS. For 50% emergence, the lowest time required for AGS383, PK472 and NCS1, while the highest for G00006 and BCS1 (Table 1). Under control, BU Soybean1 took 27, 30 days for first and 50% flowering, respectively. Similarly, this variety needed 35 and 42 days for first and 50% pod formation, respectively under control condition. On the contrary, BU Soybean1 flowered and pod produced 2-4 days earlier under drought conditions than control. Similarly, all the genotypes needed longer time for flowering and pod formation in control than drought condition. Among the genotypes, NCS1 and BCS1 took more time for flowering and pod development in both treatments. Akand et al. (2018) and Fatema et al. (2023) also reported that soybeans needed less time for flowering and maturity when they are grown in water deficit condition. For maturity, BU Soybean1 required 96 days in control condition and 92 days in drought condition (Fig. 1). However, the growth duration of NCS1 and BCS1 were the highest both control (144

days) and drought (140 days) conditions. Highly positive correlation was reported between days to flowering and days to maturity (Malek et al., 2014). Similarly, yield showed a positive association with days to maturity (Liu et al., 2005). Fenta et al. (2014) proved that drought exposure generally causes faster plant maturation.

Morphological parameters

Water stress inserted negative impact on root and shoot biomass. However, AGC383 produced the highest root biomass, which was followed by NCS1 under drought. On the other hand, BU Soybean1 gave the lowest root biomass, which was followed by BARI Soybean6. However, genotype G00006 produced the highest shoot biomass under control and drought condition, which was followed by BD2334 (Table 2). The root: shoot ratio increased due to drought stress. The root: shoot was increased in BCS1 and NCS1 on 50 DAS under drought condition as compare to control. Irrespective of soybean genotypes, the root : shoot ratio ranged from 0.20 to 0.47 in control, while the ratio was 0.22 to 59 in drought stress.

Drought decreased the plant height of soybean at both 25 and 50 DAS (Fig. 2). At 25 DAS, the height of PK472 was 70 cm in control, which decreased to 57.60 in drought. Similarly, the height of genotype PK472 was decreased by 19% under drought condition at 50 DAS. Rest of the genotypes also exhibited similar trend of reduction in plant height. Khan et al. (2014) reported that the height of soybean plant decreased due to water stress. Hamid et al. (1990) stated that water stress induced reduction in plant height due to lower Pn.

Drought caused decreased in number of leaves compared to control on 25 and 50 DAS in all soybean genotypes (Fig. 3). Regarding leaf production, the genotypic variation was obvious in soybean. On 25 DAS, PK472 showed lowest leaf reduction and BU Soybean1 showed highest leaf reduction. PK472 produced 7 mean leaf number in control which decreased to 6.80 mean leaf number in drought condition and BU Soybean1 produced 23 mean leaf number in control which decreased to 13.40 mean leaf number in drought condition. On 50 DAS, G00006 showed lowest leaf reduction and BARI Soybean6 showed highest leaf reduction. G00006 produced 25.40 mean leaf number in control which decreased to 23.60 mean leaf number in drought condition and BARI Soybean6 produced 39 mean leaf number in control which decreased to 21.80 mean leaf number in drought condition. Wu et al. (2008) and Fatema et al. (2023) reported similar results. Under water stress condition, the initiation of new leaf is hampered and senescence of existing leaves are accelerated in plants as reported by Chowdhury et al. (2015).

Physiological traits

There was a significant decrease in Chl content under drought stress in soybean leaves as reported by Makbul et al. (2011). Drought stress decreased leaf Chl a content. However, minimum reduction in Chl a content was recorded in the case of genotypes AGS383. Othe other hand, the higher amount of Chl a was obtained in the leaf of BD2336, while G00006 showed the minimum. Similarly, genotype AGS383 showed the highest Chl a under drought condition, followed by BCS1.

G00006 showed the lowest amount of Chl a. Photosynthetic pigments Chl a capture sunlight. However, Chl a more cope with in drought condition than Chl b. Reactive oxygen species were developed under water stress condition, which damaged chloroplast of plant cell resulting decreased Chl content.

Fatema et al. (2023) also reported similar results. Like Chl a, drought stress also decreased Chl b content of leaf to a large extent. However, Chl b was reduced more than Chl a. Among the eight genotypes, G00006 showed minimum decrease in Chl b content and followed by AGS383 (Fig. 4).

Table 1. Phenological changes due to drought in eight soybean genotypes

Soybean genotypes	FPE (days)		FF (days)		FPF (days)		FPoF (days)		FPPoF (days)	
	Cont.	Drout.	Cont.	Drout.	Cont.	Drout.	Cont.	Drout.	Cont.	Drout.
G00006	6	6	30	30	37	34	41	39	48	45
BD2336	5	5	31	30	39	35	45	42	51	48
AGS383	4	4	33	32	37	33	43	41	49	47
BU Soybean1	5	5	27	26	30	28	35	32	42	38
PK472	4	4	38	36	43	40	50	46	55	51
NCS1	4	4	60	57	66	62	70	67	75	70
BCS1	6	6	60	57	66	62	70	67	75	70
BARI Soybean6	5	5	55	54	62	56	66	61	71	67

FPE = 50% emergence, FF = First flowering, FPF = 50% flowering, FPoF = First pod formation, FPPoF = 50% pod formation, Cont. = Control, Drout. = Drought.

Table 2. Root and shoot weight of soybean genotypes under control and drought

Soybean genotypes	Root weight (g plant^{-1})		Shoot weight (g plant^{-1})		Root : shoot	
	Control	Drought	Control	Drought	Control	Drought
G00006	1.72±0.42	1.36±0.33	8.58±2.2	6.16±1.1	0.20±1.2	0.22±1.0
BD2336	1.29±0.16	1.23±0.12	5.16±0.34	4.25±0.31	0.25±0.1	0.29±1.1
AGS383	1.29±0.15	1.04±0.11	5.29±0.22	3.40±0.19	0.24±0.6	0.31±1.3
BU Soybean1	1.96±0.52	1.82±0.51	7.41±2.9	5.36±1.0	0.26±1.4	0.34±1.1
PK472	1.84±0.48	1.78±0.49	5.26±2.8	3.90±1.2	0.35±1.2	0.46±1.2
NCS1	1.76±0.51	1.80±0.54	5.42±2.0	3.31±1.2	0.32±1.0	0.54±1.3
BCS1	1.54±0.42	1.71±0.38	3.29±2.2	2.92±1.1	0.47±1.2	0.59±1.2
BARI Soybean6	1.65±0.11	1.15±0.10	4.92±0.26	4.09±0.22	0.34±1.0	0.28±1.1

Data are means±standard error of three replications.

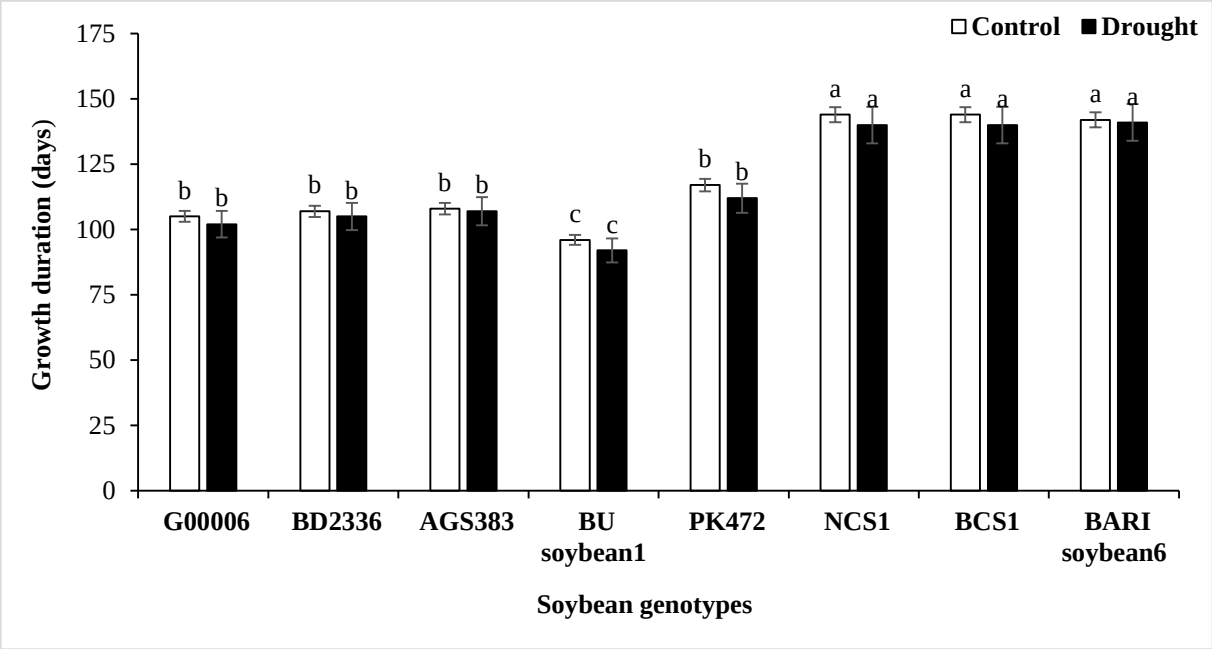

Fig. 1. Growth duration of soybean genotypes under drought and control

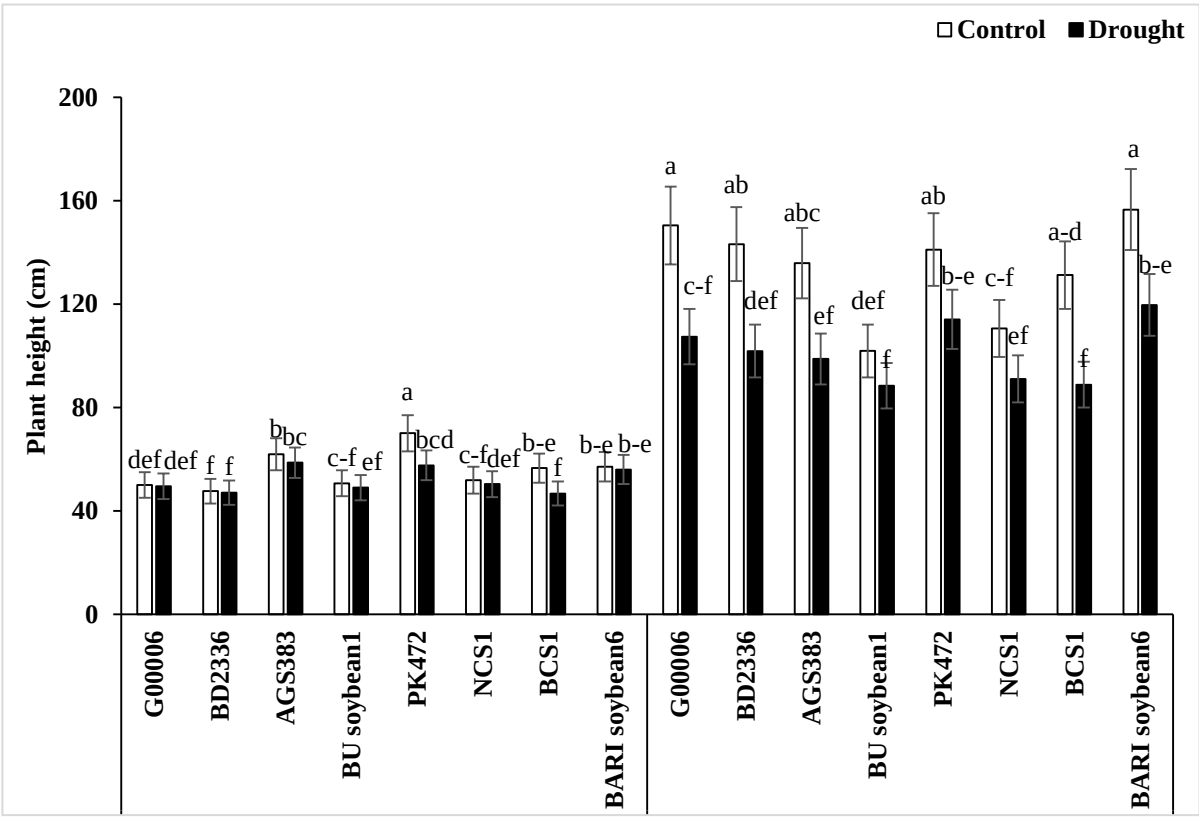

Fig. 2. Plant height of soybean genotypes under drought and control

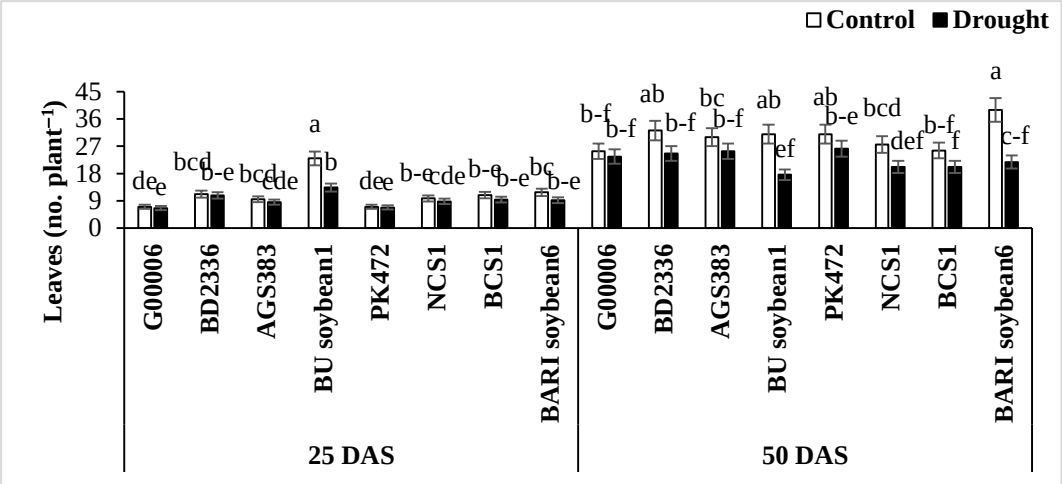

Fig. 3. Leaf production of soybean genotypes under drought and control

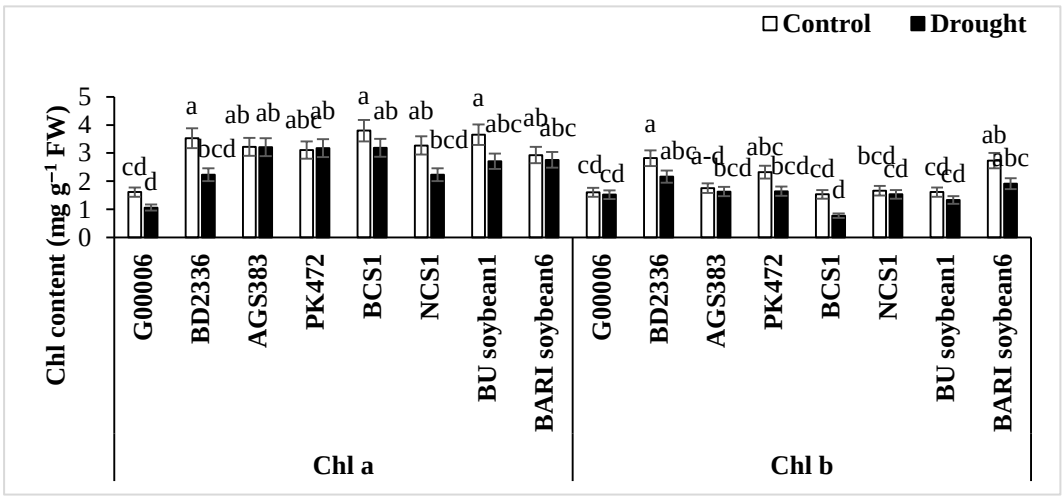

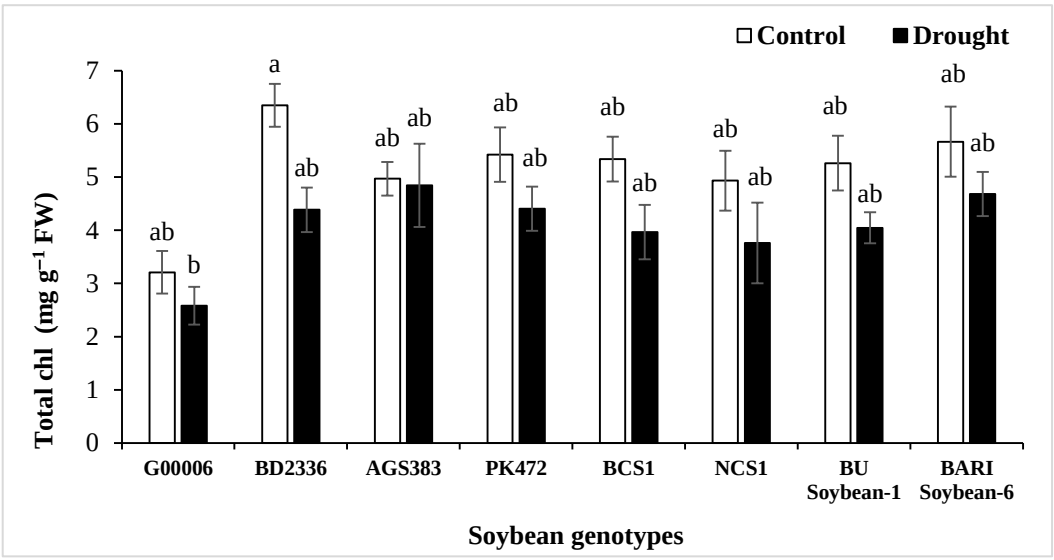

Fig. 4. Chlorophyll content of soybean genotypes at flowering stage under drought and control

The higher amount of Chl b was obtained in the leaf of genotype BD2336, while BCS1 showed the minimum under both growing conditions. Drought stress reduced total Chl content in leaves of soybean genotypes (Fig. 4). However, the content of total Chl was higher in the leaves of BD2336, which was followed by BARI Soybean6 and PK472. The minimum total Chl was obtained in the leaves of G00006. Interestingly, the maximum amount of total Chl (4.84 mg g^{-1} FW) content was determined in the genotype AGS383 in drought condition. Chl content reduced under drought condition also stated by Fatema et al. (2023).

Photosynthetic traits

Under water deficit condition, leaf Pn reduced in all the soybean genotypes (Fig. 5). The highest Pn reduction was found in BU Soybean1 where Pn value was 40.11 and 21.59 μ mol CO_2 m^{-2} s^{-1} in control and drought conditions, respectively. The lowest Pn reduction was found in AGS383 where Pn value was 30.54 and 30.39 μ mol CO_2 m^{-2} s^{-1} in control and drought condition respectively and the reduction was non-significant. Under drought stress, the stomata remain closure resulting lower Pn (Mahajan and Tuteja, 2005). Reduction of leaf number area vis a vis reduced Pn under drought is an important cause for reduced crop yield. Under water deficit condition, leaf Gs reduced in all soybean genotypes (Fig. 5).

The Gs was significantly affected by drought in BARI Soybean6, NCS1, BU Soybean1 and PK472. On the other hand, the Gs did not reduced significantly in the case of G00006, BD2336, AGS383 and BCS1. The RWC regulate the stomatal opening and closing and lower Gs under drought due to decreased RWC. Makbul et al. (2011) reported that Gs decreased during the drought period in leaves. About 42% lower Gs was obtained in drought condition as compared to control. The Tr significantly reduced under drought in all the soybean genotypes (Fig. 5). The Tr was 11.43 m mol m^{-2} s^{-1} in control which was reduced to 3.74 m mol m^{-2} s^{-1} in drought for genotype G00006. Similar trend was also observed for other genotypes. Zhang et al. (2016) and Fatema et al. (2023) also found lower Tr in leaves under water stress condition.

Plants under drought stress showed high leaf temperature compared to control condition in most of the soybean genotypes (Fig. 5). Under control condition AGS383 showed the highest leaf temperature which was 31 °C, and BARI Soybean6 showed the lowest leaf temperature which was 26 °C. Under drought condition BU Soybean1 showed the highest leaf temperature which was 33 °C followed by AGS383 and NCS1 where both the genotypes showed 32 °C and the differences among them were non-significant. BARI Soybean6 showed the lowest leaf temperature under drought condition which was 28 °C. As the drought continued, leaf temperature of the soybean increased earlier in the day and decreased later in the afternoon as was reported by Jung and Scott (1980). A significant difference in leaf temperature was also found between drought and control as reported by Winter et al. (1988).

Water related parameters

The RWC of eight soybean genotypes varied significantly and non-significantly due to water stress at flowering stage (Fig. 6).

RWC content was higher in BU Soybean1 under both control and drought stress condition. RWC of BU Soybean1 was 79.93% and 74.89% in control and drought condition respectively, which was statistically similar. Under drought condition, reduced RWC was found in soybean leaf as reported by Chowdhury et al. (2017). The water content of soil in drought treatment was 20% of FC, which was not enough for plants and cause dehydration of leaf tissue. Many earlier studies also showed that leaves exhibited a reduction of RWC when subjected to drought (Nayyar and Gupta, 2006) or salinity (Tareq et al., 2022). The WSD of eight soybean genotypes varied significantly and non-significantly due to water stress at flowering stage (Fig. 6).

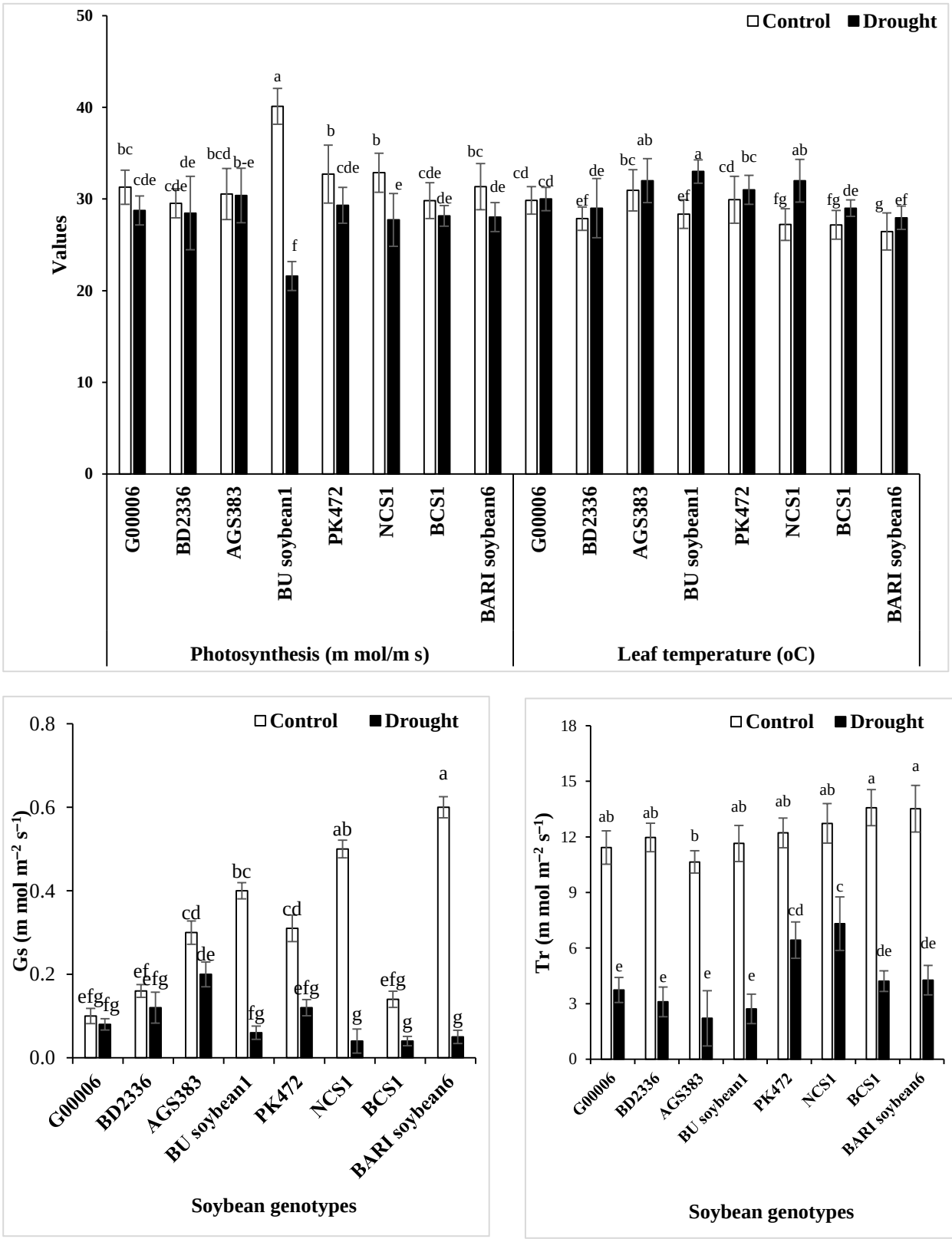

Fig. 5. Photosynthetic traits of soybean genotypes at flowering stage under drought and control

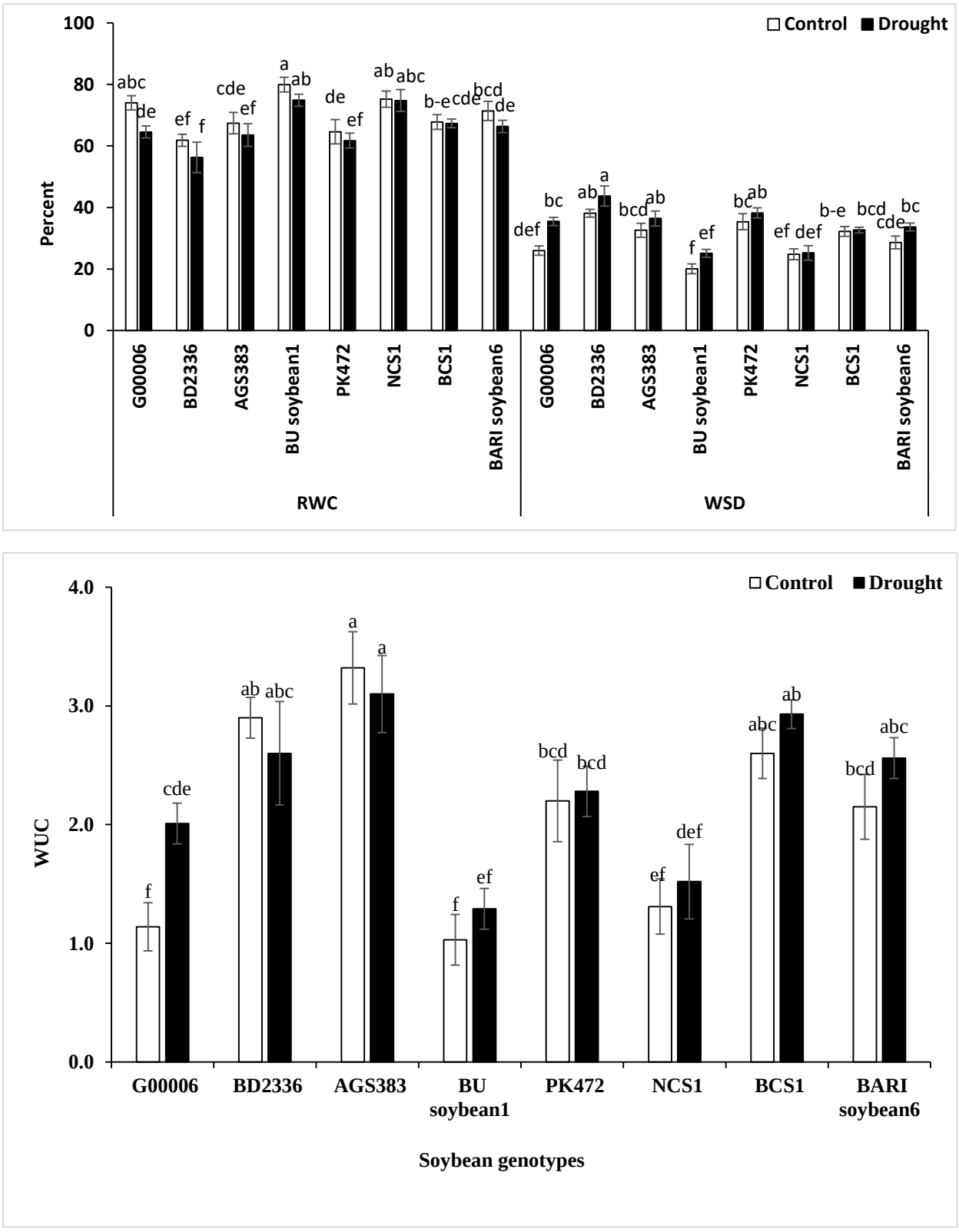

Fig. 6. Relative water content of soybean genotypes at flowering stage under drought and control

Under drought condition BU Soybean1 showed the lowest WSD followed by NCS1 and the relationship between them were non-significant. BD2336 showed highest WSD followed by AGS383 and PK472 under drought condition which was also non-significant. Chowdhury et al. (2017) also reported that WSD of soybean increased under water stress. Drought increased leaf WUC in most of the tested soybean genotypes (Fig. 6). AGS383 showed highest WUC under both control and drought condition, and the relationship between control and drought treated plant of AGS383 was statistically similar. The water use is maintained by drought tolerant genotypes under less water condition.

Yield attributing parameters

Water stress caused significant differences in pods plant^{-1} (Fig. 7). BD2336 produced the highest number of pods plant^{-1} (116), which was followed by BCS1 and AGS383. The lowest number of pods plant^{-1} (21) was produced by BU Soybean1. Similar results also reported by Akand et al. (2018). The number of fertile pods plant^{-1} reduced due to scarcity of water in seed filling stage. The findings of the present study is also supported by the findings of earlier studies in French bean (Omae et al., 2005), in soybean (Kokubun et al., 2001; Liu et al., 2004) and in mungbean (Islam, 2008).

The abortion of flowers and pods under water stress condition might be the possible reason for reduction of the number of pods plant^{-1} (Maleki et al., 2013).

Drought stress reduced the number of seed production per plant in all the tested soybean genotypes (Fig. 7). The highest number of seeds plant^{-1} (204) was recorded in BCS1, which was followed by BD2336 and AGS383. The lowest number of seeds plant^{-1} was produced by BU Soybean1. Under control condition, the highest number of seeds plant^{-1} (204) was found in BCS1 which was closely followed by BD2336 and AGS383 while the lowest number of seeds plant^{-1} was produced by BU Soybean1. Under drought conditions, AGS383 had maximum number of seeds plant^{-1} (81.16) followed by G00006 and BD2336 while NCS1 had the minimum (3.72 plant^{-1}) which was closely followed by BU Soybean1 and BARI Soybean6. Akand et al. (2018) and Fatema et al. (2023) also stated that soybean plants exposed to drought produced reduced number of seeds per plant. Drought stress reduced the number of seed production pod^{-1} in all the tested soybean genotypes (Fig. 7). Under control condition, NCS1 produced significantly highest number of seeds (2.1 pod^{-1}) than other genotypes and the lowest was produced by BD2336.

Under drought conditions, BCS1 had maximum number of seeds (1.42 pod^{-1}) followed by BARI Soybean6, AGS383 and PK472 while BD2336 had the minimum seeds (1.04 pod^{-1}) which was closely followed by BU Soybean1 and NCS1. The seeds number pod^{-1} and individual seed weight are genetically controlled and comparatively stable character. They are also less affected by environmental stress (Tera'n and Sigh 2002). In case of 100-seed weight, AGS383 produced significantly higher seed weight (15.4 g) than other genotypes followed by PK472 and BARI Soybean6 in control condition (Fig. 7). AGS383 produced the seeds of highest 100-seed weight (12.49 g), while NCS1 had the minimum 100-seed weight (3.27 g). Compared with the control, drought stress significantly reduced the 100-seed weight of soybean as reported by Du et al. (2020).

Seed yield

Seed yield of soybean reduced significantly under water stress in all soybean genotypes (Fig. 8). Among all the genotypes, seed production was minimum affected by drought in AGS383. It produced significantly highest seed yield under both control and drought condition which was 26 and 10.25 g plant^{-1} seed in control and drought stress, respectively. Under drought condition the genotype G00006 yielded 4.02 g plant^{-1} which was next to AGS383 followed by BD2336. The heavier grain size in AGS383 mostly contributed to the higher grain yield as compared to the other two genotypes. Regarding yield performance, AGS383 was the best under both well irrigated and waster stress condition as reported by Akand et al. (2018).

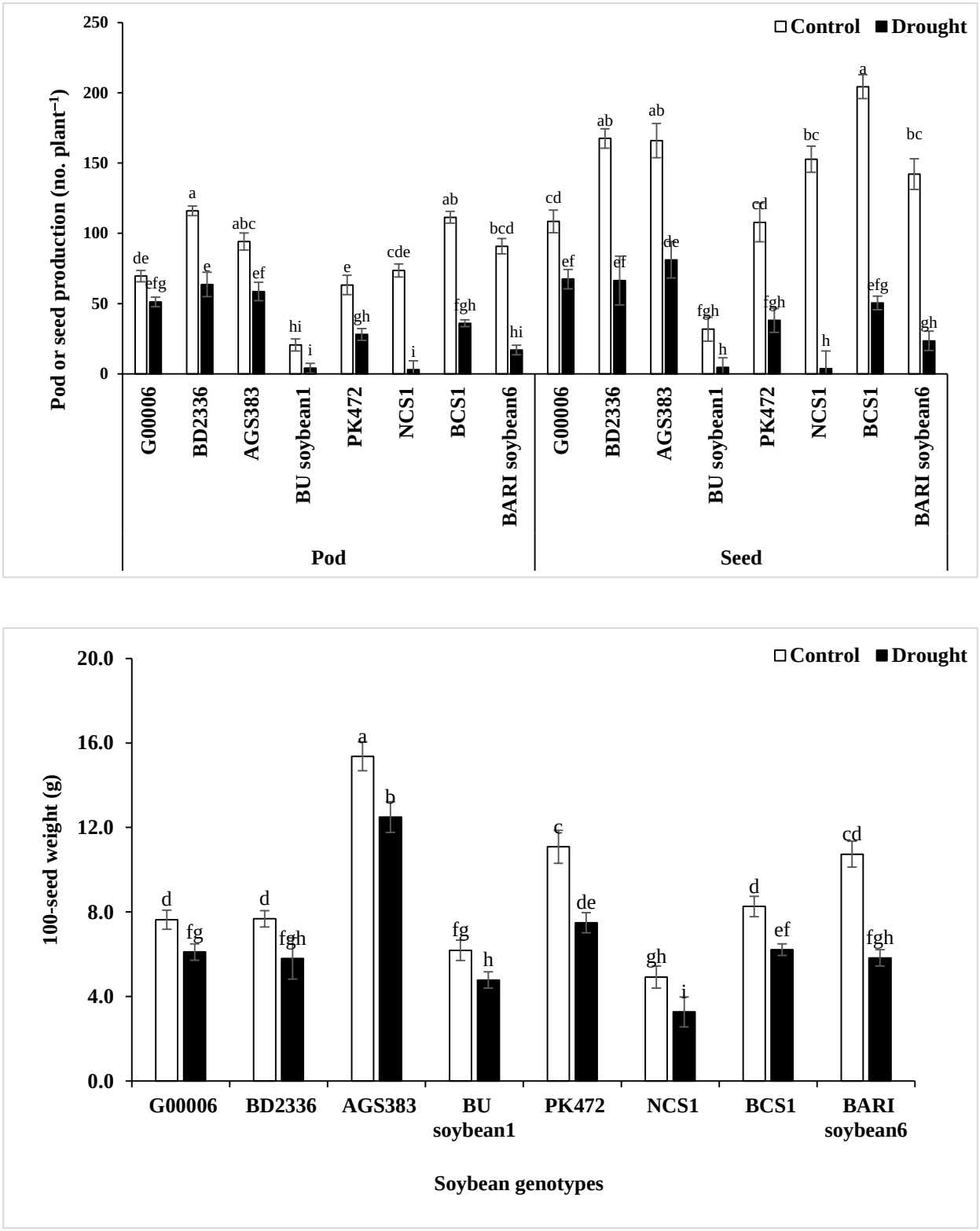

Fig. 7. Pod and seed production of soybean genotypes under drought and control.

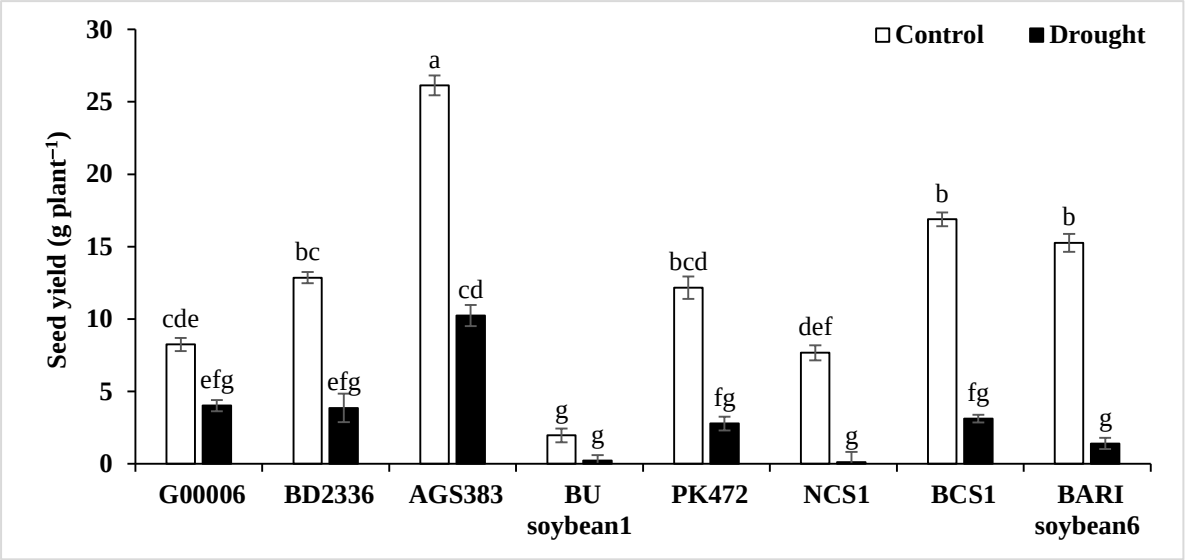

Fig. 8. Seed yield of soybean genotypes under drought and control

The photosynthetic efficiency of plants decreased under drought due to reduced number of leaves per plant which cause lower crop yield (Kramer, 1983). Similarly, the yield components like number of pods plant^{-1} and individual seed weight were also decreased, which induced lower grain yield of crop. In the present study, the lower yield under water stress condition due to decreased leaf area, lower photosynthetic rate, poor performance of yield components. These findings are supported by the previous findings of Taiz and Zeiger (2002), Liu et al. (2003) and Fatema et al. (2023). Low photosynthesis, decreased assimilates translocation, and flowers and pods abortion are the possible causes of lower yield under drought condition (Kukubun et al., 2001; Tera'n and Singh, 2002; Liu et al., 2003 and 2004;).

Drought tolerant soybean genotypes

Selection of drought tolerant soybean genotypes was done considering drought tolerance indexes in relation to genotypic performance on different agronomic parameters like height of plant; number of leaves, pods and seeds; 100-seed weight and seed yield (Table 3). AGS383, PK472 and BARI Soybean6 showed the best performance in case of plant height. In case of leaf production BU Soybean1 performed better than other genotypes. BD2336 performed better in pod production. AGS383 showed the best performance in case of total number of seeds, 100-seed weight and seed yield. In case of seeds per pod the genotype BCS1 performed better than other genotypes. Considering all the above-mentioned agronomic parameters, especially related to yield response, the genotype AGS383 performed better under drought stress than others. Based on agronomic parameters, AGS383 ranked 1 in all the parameters with the rank sum 7 (Table 4). BD2336 and PK472 ranked 2nd and 3rd positions, respectively in genotype ranking with rank sum 12 and 13. So in this experiment AGS383 perform better than all other genotypes under drought condition. The cluster analysis showed that the genotypes tended to group into two groups with 5 and 3 genotypes, respectively (Fig. 9). In this analysis, the second group performed better and was thus considered to be the most desirable cluster for both the growing conditions.

Table 3. Drought tolerance indexes based on agronomic parameters of the soybean genotypes

Soybean genotypes	Plant height	Leaf production	Pod production	Total seeds	Seeds per pod	100-seed weight	Seed yield
G00006	0.90	0.58	0.64	0.50	0.77	0.68	0.32
BD2336	0.84	0.96	0.80	0.49	0.62	0.65	0.31
AGS383	0.99	0.76	0.73	0.60	0.81	0.99	0.81
BU Soybean1	0.88	0.99	0.05	0.03	0.68	0.53	0.02
PK472	0.99	0.60	0.35	0.28	0.80	0.83	0.22
NCS1	0.90	0.78	0.04	0.03	0.73	0.36	0.01
BCS1	0.84	0.83	0.45	0.37	0.84	0.69	0.25
BARI Soybean6	0.99	0.81	0.21	0.17	0.82	0.65	0.11

Table 4. Ranking of soybean genotypes for their relative drought tolerance

Soybean genotypes	Cluster group ranking							Rank sum	Genotype ranking
	Plant height	Leaf number	Pod number	Total seeds	Seeds per pod	100-seed weight	Seed yield		
G00006	3	3	1	1	3	2	2	15	4
BD2336	2	2	1	1	2	2	2	12	2
AGS383	1	1	1	1	1	1	1	7	1
PK472	1	3	2	2	1	1	3	13	3
BCS1	2	4	2	2	1	2	3	16	5
BARI Soybean6	1	4	4	4	1	2	4	20	6
NCS1	3	1	3	3	3	4	4	21	7
BU Soybean1	4	2	3	3	4	3	4	23	8

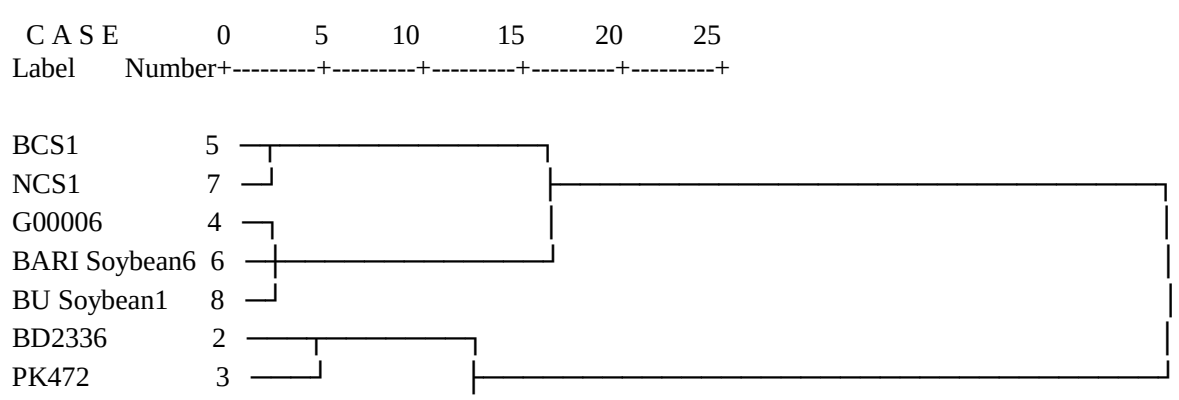

Fig. 9. Dendrogram of tested soybean genotypes using Ward's method

Conclusions

Morpho-physiological, yield and yield contributing characters of all soybean genotypes were reduced, while leaf temperature increased under drought condition. The genotype AGS383 produced heavier grains and gave improved grain yield under both growing conditions. A minimum yield reduction was occurred in AGS383 due to drought. A ranking of soybean genotypes based on relative drought tolerance index showed that AGS383 ranked 1st among all studied soybean genotypes. Due to high grain yielding ability of AGS383, it could be cultivated drought prone environment.

Author's contributions

Md. Abdullah Al Mamun contributed to the conceptualization, supervision, data analysis and manuscript drafting, Md. Karimul Ahsan carried out the field experiment and collect data, Toton Kumar Ghosh and M. Abdul Karim contributed in editing the manuscript.

Acknowledgements

The research work was funded by Research Management Committee, BSMRAU, Gazipur, Bangladesh.

Conflicting interest

The authors have no potential conflicts of interest regarding the publication of this article.

References

Ahmed MS, Alam MM and Mirza H. Growth of different soybean (*Glycine max* L. Merril) varieties as affected by sowing dates. *Middle East J. Sci. Res.* 2010; 5(5): 388-391.

Akand MMH, Mamun MAA, Ivy NA and Karim MA. Genetic Variability of soybean genotypes under drought stress. *Ann. Bangladesh Agri.* 2018; 22: 79-93.

Allahmoradi P, Ghobadi M, Taherabadi S and Taherabadi S. Physiological aspects of mungbean (*Vigna radiata* L.) in response to drought stress. In *Int. Conf. Food Eng. Biotechnol.* 2011; 9: 272-275.

BBS. Bangladesh Bureau of Statistics. Yearbook of Agricultural Statistics-2020. Bangladesh Bureau of Statistics. 2020.

Brown EA, Caviness CE and Brown DA. Response of selected soybean cultivars to soil moisture deficit 1. *Agron. J.* 1985; 77(2): 274-278.

Chowdhury JA, Karim MA, Khaliq QA, Ahmed AU and Mondol AM. Effect of drought stress on water relation traits of four soybean genotypes. *SAARC J. Agri.* 2017; 15(2): 163-175.

Chowdhury JA, Karim MA, Khaliq QA, Solaiman ARM and Ahmed JU. Genotypic variations in growth, yield and yield components of soybean genotypes under drought stress conditions. *Bangladesh J. Agril. Res.* 2015; 40(4): 537-550.

Dola DB, Mannan MA, Sarker U, Mamun MAA, Islam T, Ercisli S, Saleem MH, Ali B, Pop OL and Marc RA. Nano-iron oxide accelerates growth, yield, and quality of Glycine max seed in water deficits. *Front. Plant Sci.* 2022; 13:1-12.

Du Y, Zhao Q, Chen L, Yao X and Xie F. Effect of drought stress at reproductive stages on growth and nitrogen metabolism in soybean. *Agron.* 2020; 10(2): 302.

Eureka TM, Ocampo and Robles RP. Drought tolerance in mungbean II. Stomatal movement, photosynthesis and leaf water potential. *Philippine J. Crop Sci.* 2000; 25(1): 7-15.

Fatema MK, Mamun MAA, Sarker U, Hossain MS, Mia MAB, Roychowdhury R, Ercisli S, Alina Marc R, Babalola OO and Karim MA. Assessing Morpho-Physiological and Biochemical Markers of Soybean for Drought Tolerance Potential. *Sustainability*, 2023; 15: 1427.

Fenta BA, Beebe SE, Kunert KJ, Burridge JD, Barlow KM, Lynch JP and Foyer CH. Field phenotyping of soybean roots for drought stress tolerance. *Agron.* 2014; 4(3): 418-435.

Gomez KA and Gomez AA. Statistical procedure for agricultural research (2nd ed.). John Willey and Sons, Singapore. 1984; New York, p680.

Hamid A, Kubota F, Agata W and Morokuma M. Photosynthesis, transpiration, dry matter accumulation and yield performance of mungbean [*Vigna radiata*] plant in response to water stress. *J. Facul. Agri. Kyushu Uni. Japan*, 1990; 35(1-2): 81-92.

Islam MS. Water stress tolerance of mungbean [*Vigna radiata* L. Wilczek] genotypes as influenced by plant growth regulators. *A Ph. D Dissertation*, Dept. of Agronomy, Bangabandhu Sheikh Mujibur Rahman Agricultural University, Gazipur, Bangladesh. 2008.

Jung PK and Scott HD. Leaf Water Potential, Stomatal Resistance, and Temperature Relations in Field-Grown Soybeans 1. *Agron. J.* 1980; 72(6): 986-990.

Khan MSA, Karim MA and Haque MM. Genotypic differences in growth and ions accumulation in soybean under NaCl salinity and water stress conditions. *Bangladesh Agron. J.* 2014; 17(1): 47-58.

Khrais T, Leclerc Y and Donnelly DJ. Relative salinity tolerance of potato cultivars assessed by invitro screening. *Am. J. Potato Res.* 1998; 75(5): 207-210.

Kokubun M, Shimada S and Takahashi M. Flower abortion caused by preanthesis water deficit is not attributed to impairment of pollen in soybean. *Crop Sci.* 2001; 41(5): 1517-1521.

Kramer P. Water Relations of Plants. Academic Pres. *Inc New York*. 1983.

Ku YS, Au-Yeung WK, Yung YL and Li MW. Drought Stress and Tolerance in Soybean. *Licensee In Tech.* 2013; 209-225.

Kumar A, Pandey V, Shekh AM, Dixit SK and Kumar M. Evaluation of CROPGRO-Soybean (*Glycine max* L. Merrill) model under varying environment condition. *Europ. J. Agron.* 2008; 1: 34-40.

Liu F, Andersen MN and Jensen CR. Loss of pod set caused by drought stress is associated with water status and ABA content of reproductive structures in soybean. *Funcl. Plant Biol.* 2003; 30(3); 271-280.

Liu F, Andersen MN and Jensen CR. Root signal controls pod growth in drought-stressed soybean during the critical, abortion-sensitive phase of pod development. *Field Crops Res.* 2004; 85(2-3): 159-166.

Liu X, Jin J, Herbert SJ, Zhang Q and Wang G. Yield components, dry matter, LAI and LAD of soybeans in Northeast China. *Field Crops Res.* 2005; 93(1); 85-93.

Mahajan S and Tuteja N. Cold, salinity and drought stresses: an overview. *Arc. Biochem. Biophys.* 2005; 444(2): 139-158.

Makbul S, Güler NS, Durmuş N and Güven S. Changes in anatomical and physiological parameters of soybean under drought stress. *Turkish J. Bot.* 2011; 35(4): 369-377.

Malek MA, Rafii MY, Afroz SS, Nath UK and Mondal M. Morphological characterization and assessment of genetic variability, character association, and divergence in soybean mutants. *Scient. World J.* 2014; 968796.

Maleki A, Naderi A, Naseri R, Fathi A, Bahamin S and Maleki R. Physiological performance of soybean cultivars under drought stress. *Bull. Environ. Pharmacol. Life Sci.* 2013; 2(6): 38-44.

Mamun MAA, Julekha, Sarker U, Mannan MA, Rahman MM, Karim MA, Ercisli S, Marc RA and Golokhvast KS. Application of potassium after waterlogging improves quality and productivity of soybean seeds. *Life*, 2022; 12: 1816.

Mannan MA and Mamun MAA. Selection of vegetable soybean suitable for Bangladesh through multivariate analysis. *Ann. Bangladesh Agril.* 2018; 22(2): 51-57.

Mannan MA, Begum F, Mamun MAA and Habib MA. Evaluation of maize (*Zea mays*) genotypes for tolerance to drought using yield-based tolerance indices. *J. Agri. Crops,* 2023; 9(3): 329-337.

Mannan MA, Tithi MA, Islam MR, Mamun MAA, Mia S, Rahman MZ, Awad MF, ElSayed AI and Hossain MS. Soil and foliar applications of zinc sulphate and iron sulfate alleviate the destructive impact of drought stress in wheat. *Cereal Res. Commn.* 2022; *50: 1279-1289*.

Miah AA, Karim MA, Mamun MAA, Khan MAR, Akter N and Haque MM. Planting time effects on phenology and yield of early maturing dwarf soybean genotypes. *Bangladesh J. Ecol.* 2020; 2: 19-24.

Mugendi E, Gitonga N, Cheruiyot R and Maingi J. Biological nitrogen fixation by promiscuous soybean (*Glycine max* L. Merril) in the central highlands of Kenya: response to inorganic fertilizer soil amendments. *World J. Agril. Sci.* 2010; 6(4): 381-387.

Nayyar H and Gupta D. Differential sensitivity of C_3 and C_4 plants to water deficit stress: association with oxidative stress and antioxidants. *Environ. Expt. Bot.* 2006; 58(1-3): 106-113.

Omae H, Kumar A, Egawa Y, Kashiwaba K and Shono M. Midday drop of leaf water content related to drought tolerance in snap bean (*Phaseolus vulgaris* L.). *Plant Prod. Sci.* 2005; 8(4): 465-467.

Purcell LC, King CA and Ball RA. Soybean cultivar differences in ureides and the relationship to drought tolerant nitrogen fixation and manganese nutrition. *Crop Sci.* 2000; 40(4): 1062-1070.

Sangakkara UR, Hartwig UA and Nösberger J. Soil moisture and potassium affect the performance of symbiotic nitrogen fixation in faba bean and common bean. *Plant Soil,* 1996; 184(1): 123-130.

Saxena KB, Singh L and Gupta MD. Variation for natural out-crossing in pigeonpea. *Euphytica,* 1990; 46(2): 143-148.

Schonfeld MA, Johnson RC, Carver BF, and Mornhinweg DW. Water relations in winter wheat as drought resistance indicators. *Crop Sci.* 1988; 28: 526-531.

Taiz L, and Zeiger E. Photosynthesis: physiological and ecological considerations. *Plant Physiol.* 2002; 9: 172-174.

Talukder S, Mamun MAA, Hossain MS, Khan MAR, Rahman MM, Talukder MR, Haque MM and Biswas JC. Duration of low temperature changes physiological and biochemical attributes of rice seedling. *Agron. Res.* 2022; 20(S1): 1163-1176.

Tareq MS, Mannan MA, Rahman MM, Mamun MAA and Karim MA. Salinity-induced changes in growth, physiology and yield of soybean genotypes. *Ann. Bangladesh Agri.* 2022; 26(1): 29-48.

Terán H, and Singh SP. Comparison of sources and lines selected for drought resistance in common bean. *Crop Sci.* 2002; 42(1): 64-70.

Wijewardana C, Reddy KR and Bellaloui N. Soybean seed physiology, quality, and chemical composition under soil moisture stress. *Food Chem.* 2019; 278: 92-100.

Winter SR, Musick JT and Porter KB. Evaluation of screening techniques for breeding drought resistant winter wheat. *Crop Sci.* 1988; 28(3): 512-516.

Wu S, Mickley LJ, Jacob DJ, Rind D and Streets DG. Effects of 2000–2050 changes in climate and emissions on global tropospheric ozone and the policy-relevant background surface ozone in the United States. *J. Geophysic. Res.: Atmosp.* 2008; 113: D18312.

Zhang J, Terrones M, Park CR, Mukherjee R, Monthioux M, Koratkar N and Chen Y. Carbon science in 2016: Status, challenges and perspectives. *Carbon,* 2016; 98(70): 708-732.

J. Bangladesh Acad. Sci. 47(2); 241-248: December 2023 DOI:https://doi.org/10.3329/jbas.v47i2.68520

Journal of Bangladesh Academy of Sciences

Journal homepage: http://www.bas.org.bd/publications/jbas.html

Research Article

Interior regularity to the signed solution of the singular doubly nonlinear parabolic equations

Md Abu Hanif Sarkar

Department of Mathematics, Faculty of Science, Jagannath University, Dhaka, Bangladesh

ARTICLE INFO

Article History

Received: 31 August 2023
Revised: 17 October 2023
Accepted: 18 October 2023

Keywords: Energy estimate, Expansion of positivity, Intrinsic scaling, Singular equation.

ABSTRACT

We study doubly nonlinear parabolic equation with sign changing solutions. We establish the Hölder regularity of the singular parabolic equations within a parabolic domain.

Introduction

Let $\Omega \subset \mathbb{R}^N$ and for $T > 0$ define the cylindrical doamin $\Omega_T := \Omega \times (0, T]$. Consider the following doubly nonlinear parabolic equation

$$\partial_t(|u|^{p-2}u) - div(|Du|^{p-2}Du) = 0 \quad weakly\ in \quad \Omega_T \tag{1}$$

where $\Delta_p u := div(|Du|^{p-2}Du)$ is the p-Laplacian. For the case $p = 2$ then this operator transforms to well known heat equation. In this manuscript, the weak solution u is unknown and assumed to be locally bounded, real function which depends on both the time and space variables namely x and t in the cylindrical domain.

In our context, the term structural data indicates the parameters p and N. It is also

assumed that the constant $\gamma > 0$, need to be evaluated quantitatively apriori in terms of the structural data. In addition, deno te $\Gamma_T := \partial\Omega_T - \overline{\Omega} \times \{T\}$ to be the parabolic boundary of the cylindrical domain Ω_T. For $\theta > 0$, consider the follo wing backward cylinders of the form $(x_0, t_0) + Q_\varrho(\theta) = (x_0, t_0) + K_\varrho(0) \times (-\theta\varrho^p, 0] = K_\varrho(x_0) \times (t_0 - \theta\varrho^p, t_0]$.

For the case $\theta = 1$, we will call it as Q_ϱ.

The conclusions to be derived from the discoveries presented in this article are summarized as follows.

Theorem 1.1

Let's consider a bounded domain with a smooth boundary, denoted as $\partial\Omega$. Given that u constitutes a local weak solution bounded by (1) in Ω_T, it follows that u exhibits local Hölder continuity within Ω_T. Precisely, there exist constants $\gamma > 1$ and $\beta \in (0,1)$, predetermined based on the data, such that for any compact subset $C \subset \Omega_T$, the inequality

$$|u(x_1, t_1) - u(x_2, t_2)| \le \gamma \| u \|_{\infty,\Omega_T} \left(\frac{|x_1 - x_2| + |t_1 - t_2|^{\frac{1}{p}}}{dist_p(C, \Gamma_T)} \right)^\beta,$$

holds true for any pair of points $(x_1, t_1), (x_2, t_2) \in C$.

The following oscillation decay will be demonstrated as part of the proof of the

aforementioned theorem:

$$ess\ osc_{(x_0,t_0)+Q_r} u \le \gamma ess\ osc_{(x_0,t_0)+Q_\varrho} u \left(\frac{r}{\varrho}\right)^\beta,$$

*Corresponding author: <sarkarhanif@ymail.com>

for any pair of cylinders $(x_0, t_0) + Q_r \Subset (x_0, t_0) + Q_\varrho \Subset \Omega_T$. A typical covering

argument can be used to draw the conclusion of Theorem 1.1 at the end.

A weak solution is defined in Definition 3, and (Kuusi et al., 2021) examines the weak solution's global existence.

1.1 Originality and Importance

The standard equation (1) is referred to as Trudinger's equation. Because of the nonlinear nature of the solution as well as the gradient in its spatial domain, the equation is sometimes known as a doubly nonlinear parabolic equation. Our choice of this particular type of equation for study is particularly intriguing because of its excellent mathematical

structure, capable of producing mixed forms of degeneracy and/or singularity in partial differential equations. It also has connections to physical models, such as the dynamics of glaciers in (Mahaffy, 1976), shallow water flows in (Alanso et al., 2008; Feng and Molz, 1997; Hromadka et al., 1985), and friction-dominated flow in a gas network in (Leugering and Mophou, 2018). Another natural connection between the Trudinger equation and the non-linear eigenvalue issue $-\Delta_p u = \lambda |u|^{p-2} u$ (Lindgren and Lindqvist, 2022) is that it is crucial to nonlinear potential theory.V. B. Ogelein, F. Duzzar, and N. Liao examined the Hölder continuity of signed solutions for broader equations under structural constraints in (Bogelion et al., 2021). Through Moser's iteration, Trudinger (Trudinger, 1968b) investigates the Hölder regularity of this equation and finds that, similar to the heat equation, it has a Harnack inequality for non-negative weak solutions. This Harnack inequality is used in (Kussi et al., 2012a; Kuusi et al., 2012b) to prove the Hölder regularity of nonnegative weak solutions. Now, we have the opportunity to discuss our contribution. To ensure Hölder regularity, we remove the constraint of non-negativity from solutions and instead consider sign-changing solutions. The Harnack inequality (Giannnaza and Vespri, 2006, Urbano, 2008) is not applicable in our scenario as it only applies to non-negative solutions. Instead, we employ the positivity expansion to achieve our desired result.

By comparing the oscillation with the supremum/infimum of the solution, our demonstration of interior Hölder regularity unfolds in two primary cases: when the

solution approaches zero or when it significantly deviates from zero. Utilizing our equation's scaling invariant property, we can derive the positivity expansion in the first case. Without the use of intrinsic scaling procedures, Proposition 3.1 is analogous to the classical parabolic theory found in (Ladyzenskaja et al., 1968). On the other hand, the behavior of the solution in the latter case resembles that of the parabolic p-Laplacian equation, specifically $u_t = \Delta_p u$. Consequently, success in this second scenario depends on our ability to handle a degenerate case $(p > 2)$ or a singular case $(1 < p < 2)$ equation, for which we utilize the theory that has already been developed in (DiBenedetto, 1993; DiBenedetto et al., 2012). The paper (Nakamura and Misawa, 2018) illustrates the presence of a weak solution to equation (1). Additionally, research into the Hölder regularity of doubly nonlinear equations has been explored in (Ivanov, 1994, 1995; Ivanov and Mkrtychyan, 1994; Kinnunen and Kuusi, 2007; Sarkar, 2022; Vespri, 1992; Vespri and Vestberg, 2020). We want to implement the Theorem 1.1.

Preliminaries

We establish certain notations and tools for technical analysis that will be utilized subsequently. [cf.(Bogelion et al., 2021, DiBenedetto, 2016, 1993, 1986, 1983, Evans, 1998, Ladyzenskaja et al., 1968, Leugering and Mophou, 2018, Trudinger, 1968b)].

2.1 Notation

2.1.1 Concept of Local Weak Solution

Let u be a function belonging to

$$u \in C(0, T; L^p_{loc}(\Omega)) \cap L^p_{loc}(0, T; W^{1,p}_{loc}(\Omega)) \qquad (2)$$

It is considered a local weak sub(super)-solution to (1) if, for every compact subset C of Ω and each sub-interval $[t_1, t_2] \subset (0, T]$

$$\int_C |u|^{p-2}u\ \zeta\ dx|_{t_1}^{t_2} + \iint_{C\times(t_1,t_2)} [-|u|^{p-2}u\zeta_t + |Du|^{p-2}Du \cdot D\zeta]dx\,dt \leq (\geq)0 \quad (3)$$

holds for all non-negative test functions

$$\zeta \in W_{loc}^{1,p}(0, T; L^p(C)) \cap L_{loc}^{p}(0, T; W_0^{1,p}(C)).$$

ensuring the convergence of all integrals in (3). A function u satisfying both the conditions of being a local weak subsolution and a local weak supersolution to (3) is termed a local weak solution.

2.1.2 Function Spaces on a time-space area

We define several function spaces that operate in space-time domains. For $1 \leq p, q \leq \infty$, $L^q(t_1, t_2\ ;\ L^p(\Omega))$ represents a collection of measurable real-valued functions defined on$\Omega \times (t_1, t_2)$, encompassing a finite-region in both space and time and characterized by a norm that may not be bounded:

$$\| v \|_{L^q(t_1,t_2\ ;\ L^p(\Omega))}:$$
$$= \begin{cases} \left(\int_{t_1}^{t_2} \| v(t) \|_{L^p(\Omega)}^q\ dt\right)^{1/q} & \text{if} 1 \leq q < \infty \\ ess\ sup_{t_1\leq t\leq t_2} \| v(t) \|_{L^p(\Omega)} & \text{if} q = \infty \end{cases}$$

where

$$\| v(t) \|_{L^p(\Omega)}:$$
$$= \begin{cases} \left(\int_{\Omega} |v(x,t)|^p\ dx\right)^{1/p} & \text{if} 1 \leq p < \infty \\ ess\ sup_{x\in\Omega}|v(x,t)| & \text{if} p = \infty \end{cases}$$

For simplicity, we use $L^p(\Omega \times (t_1, t_2)) = L^p(t_1, t_2\ ;\ L^p(\Omega))$ when $p = q$. For $1 \leq p < \infty$, the Sobolev Space $W^{1,p}(\Omega)$ consists of weakly differentiable measurable real-valued functions whose weak derivatives are p-th integrable on Ω, with the norm

$$\| w \|_{W^{1,p}(\Omega)} := \left(\int_{\Omega} |w|^p + |\nabla w|^p\ dx\right)^{1/p}$$

where $\nabla w = (w_{x_1}, \ldots, w_{x_n})$ indicates, in a distribution sense, the gradient of w, and let $W_0^{1,p}(\Omega)$ denote the closure of $C_0^{\infty}(\Omega)$ with the norm $\|\cdot\|_{W^{1,p}}$. Additionally, we define $L^q(t_1, t_2\ ;\ W_0^{1,p}(\Omega))$ as a function space of measurable real-valued functions on a space-time region with a bounded norm:

$$\| w \|_{L^q(t_1,t_2\ ;\ W_0^{1,p}(\Omega))} = \left(\int_{t_1}^{t_2} \| w(t) \|_{W^{1,p}(\Omega)}^q\ dt\right)^{1/q} \quad (3)$$

Consider $\Omega \subset \mathbb{R}^n$ as a bounded domain. The truncation of a function v for a real number m can be expressed as

$$(v - m)_+ := \max\{(v - m), 0\}; \quad (v - m)_- := -\min\{(v - m), 0\}. \quad (4)$$

For a measurable function v in $L^1(\Omega)$ and real numbers $m < n$, we introduce the sets

$$\begin{cases} \Omega \cap \{v > n\} := \{x \in \Omega :\ v(x) > n\} \\ \Omega \cap \{v < m\} := \{x \in \Omega :\ v(x) < m\} \\ \Omega \cap \{m < v < n\} := \{x \in \Omega :\ m < v(x) < n\}. \end{cases}$$

2.2 Technical tools

Let's begin by recalling De Giorgi's inequality (refer to DiBenedetto, 1993).

Proposition 2.1 (Inequality of De Giorgi)

Consider $v \in W^{1,1}(B)$ and real numbers

$k, m \in \mathbb{R}$ satisfying $k < m$. Then there exists a positive constant C dependent solely on p as well as n in a way that

$$(k - m)|B \cap \{v > k\}| \leq C\frac{\rho^{n+1}}{|B\cap\{v<m\}|}\int_{B\cap\{k<v<m\}} |\nabla v|\ dx. \quad (5)$$

Following the approach in (DiBenedetto, 1993), we introduce the auxiliary function

$$\begin{cases} A^+(k, u) := +(p - 1)\int_k^u |s|^{p-2}(s - k)_+\ ds \\ A^-(k, u) := -\int_k^u |s|^{p-2}(s - k)_-\ ds \end{cases} \quad (6)$$

for $u, k \in \mathbb{R}$. In the special case of $k = 0$, we simplify as $A^+(u) = A^+(0, u)$ and $A^-(u) = A^-(0, u)$.

It's evident that $A^{\pm} \geqslant 0$. We introduce bold notation b^{α} to represent the signed α-exponent of b, as defined below

$$b^{\alpha} = \begin{cases} |b|^{\alpha-1}\, b, & b \neq 0, \\ 0, & b = 0. \end{cases}$$

We present a known lemma; cf. (Acerbi and Fusco, 1989, Sarkar, 2023: Lemma 2.2) and (Giaquinta and Modica, 2006) for $\alpha > 1$. This lemma is utilized in the proof of the subsequent lemma:

Lemma 2.2

For each positive value of α, there exists a specific constant β, denoted as β(α), for which the *inequality below holds for any pair of real numbers a, b:*

$$\frac{1}{\beta}|b^{\alpha} - a^{\alpha}| \leqslant (|a| + |b|)^{\alpha-1}|b - a| \leqslant \beta|b^{\alpha} - a^{\alpha}|.$$

Building upon the aforementioned lemma, we establish the following result.

Lemma 2.3

There exists a constant $\beta = \beta(p)$ such that the following inequality holds for all $w, k \in \mathbb{R}$ and $\alpha > 0$:

$$\frac{1}{\beta}(|w| + |k|)^{p-2}(w-k)_{\pm}^{2} \leqslant A^{\pm}(k, w \leqslant \beta(|w| + |k|)^{p-2}(w-k)_{\pm}^{2}$$

We introduce a type of time mollification for the solution u to enhance its time regularity: $[u]_h(x,t) \overset{def}{=} \frac{1}{h}\int_0^t e^{\frac{s-t}{h}} u(x,s)ds$ for any $u \in in\ L^1(\Omega_T)$

Lemma 2.4 (Properties of mollification)

(Kinnunen and Lindqvist, 2006)

1. If $u \in L^p(\Omega_T)$, then

$$\| [u]_h(x,t) \|_{L^p(\Omega_T)} \leqslant \| u \|_{L^p(\Omega_T)} \text{ and}$$

$$\frac{\partial [u]_h}{\partial t} = \frac{u - [u]_h}{h} \in L^p(\Omega_T).$$

Moreover, $[u]_h \to u$ in $L^p(\Omega_T)$ as $h \to 0$.

2. If, additionally, $\nabla([u]_h) = [\nabla u]_h$ componentwise,

$$\| \nabla([u]_h) \|_{L^p(\Omega_T)} \leqslant \| \nabla u \|_{L^p(\Omega_T)}$$

and $\nabla[u]_h \to \nabla u$ in $L^p(\Omega_T)$ as $h \to 0$.

3. Furthermore, if $u_k \to u$ in $L^p(\Omega_T)$, then

$$[u_k]_h \to [u]_h \ and\ \frac{\partial [u_k]_h}{\partial t} \to \frac{\partial [u]_h}{\partial t}$$

in $L^p(\Omega_T)$. and $\nabla[u]_h \to \nabla u$ in $L^p(\Omega_T)$ as $h \to 0$.

4. If $\nabla u_k \to \nabla u$ in $L^p(\Omega_T)$, then also $\nabla[u_k]_h \to \nabla[u]_h$ in $L^p(\Omega_T)$.

5. Similar results hold for weak convergence in $L^p(\Omega_T)$.

6. Lastly, if $\varphi \in C(\overline{\Omega}_T)$, then $[\varphi]_h(x,t) + e^{-\frac{t}{h}}\varphi(x,0) \to \varphi(x,t)$ uniformly in Ω_T as $h \to 0$.

Moving forward, we will employ the following energy estimate (as found in Sarkar, 2022).

We briefly outline the estimate before proceeding with the main proof.

Proposition 2.5

Assume that u serves as a subsolution in a local sense for equation (1). In this context, there exists positive constant $\gamma(p)$ in a way that for any cylinders $Q_{R,S} = K_R(x_0) \times (t_0 - S, t_0) \Subset \Omega_T$, the subsequent inequality is satisfied for every non-negative piecewise smooth cutoff function ζ that vanishes along $\partial K(x_0) \times (t_0 - S, t_0)$, as well as for any $k \in \mathbb{R}$:

$$\text{ess sup}_{t_0 - S < t < t_0} \int_{K_R(x_0)\times\{t\}} \zeta^p A^{\pm}(k,u)\, dx + \iint_{Q_{R,S}} \zeta^p |D(u-k)_{\pm}|^p\, dx\, dt$$

$$(7) \leqslant \gamma \iint_{Q_{R,S}} [|D\zeta|^p (u-k)_{\pm} + A^{\pm}(k,u)|\, \partial_t \zeta^p|]\, dx\, dt + \int_{K_R(x_0)\times\{t_0 - S\}} \zeta^p A^{\pm}(k,u)\, dx$$

Positivity expansion

Consider $K \subset \mathbb{R}^n$ and a cylinder $\mathcal{Q} \overset{\text{def}}{=} K \times (t_1, t_2) \subset \Omega_T$. Throughout this section, we will utilize the following notations:

$$\mu^+ \geq \text{ess sup}_{\mathcal{Q}} u, \quad \mu^- \leq \text{ess inf}_{\mathcal{Q}} u, \quad \omega = \mu^+ - \mu^-.$$

We also assume that $(x_0, t_0) \in \mathcal{Q}$ for defining the forward cylinder

$$K_{8\varrho}(x_0) \times (t_0, t_0 + (8\varrho)^p) \subset \mathcal{Q}. \qquad (9)$$

In this context, we present the proposition regarding the extension of positivity. The

complete proof can be found in (Sarkar, 2023).

Proposition 3.1

Given that u is locally limited and acts as a sub(super)solution on a local scale for equation (1) within the domain Ω_T, and for a specific point $(x_0, t_0) \in \Omega_T$, as well as for constants M, α, and ϱ, where $M > 0$, and α belongs to the interval (0,1), while $\varrho > 0$ the ensuing conditions are met: (9) and $|\{\pm(\mu^{\pm} - u(., t_0)) \geq M\} \cap K_{\varrho}(x_0)| \geq \alpha|K_{\varrho}|$.

Subsequently, constants ξ, δ, and η all falling within the range of (0,1), can be identified based solely on the provided information and the value of α. This leads to either

$$|\mu^{\pm}| > \xi M$$

or

$$\pm(\mu^{\pm} - u) \geq \eta M$$

$$\text{almost every where in} \quad K_{2\varrho}(x_0) \times (t_0 + \delta(\frac{1}{2}\varrho)^p, t_0 + \delta\varrho^p),$$

where

$$\xi = \begin{cases} 2\eta, & \text{if } p > 2, \\ 8, & \text{if } 1 < p \leq 2. \end{cases}$$

The proof of Proposition 3.1 follows directly from three lemmas presented in

subsequent sections. Here, we provide the statements of these lemmas, which collectively form the foundation for proving the expansion of positivity. For detailed proofs, please refer to (Sarkar, 2022).

3.1 Extension of Positivity in Measure

Lemma 3.2

Take any positive M and $\alpha \in (0,1)$ into account. Consequently, there are δ and ε within the range of (0,1), and their values are exclusively *determined by the provided information and the value of α. In cases where u functions as a locally*

restricted sub(super)-solution to equation (1) within Ω_T, adhering to the condition

$$|\{\pm(\mu^{\pm} - u(\cdot, t_0)) \geq M\} \cap K_{\varrho}(x_0)| \geq \alpha|K_{\varrho}|,$$

we have either

$$|\mu^{\pm}| > 8M$$

or

$$\left|\left\{\pm\left(\mu^{\pm} - u(\cdot, t)\right) \geq \varepsilon M\right\} \cap K_{\varrho}(x_0)\right| \geq \frac{\alpha}{2}\left|K_{\varrho}\right| \quad \text{for all } t \in (t_0, t_0 + \delta\varrho^p). \tag{10}$$

3.2 Lemma of shrinking

Lemma 3.3

Given the assumptions in Lemma 3.2, the second option (10) is true. Let $Q = K_{\varepsilon}(x_0) \times (t_0, t_0 + \delta\varepsilon^p]$ denote the corresponding cylindrical domain, and let $\widetilde{Q} = K_{4\varepsilon}(x_0) \times (t_0, t_0 + \delta\varrho^p] \subset \Omega_T$. A positive constant γ, which is exclusively dependent on the given data and α, exists. This constant is such that for any positive integer j_*, when $1 < p < 2$, the following inequality is legitimate:

$$\left|\left\{\pm(\mu^{\pm} - u) \leq \frac{\varepsilon M}{2^{j_*}}\right\} \cap \tilde{Q}\right| \leq \frac{\gamma}{j_*^{\frac{p-1}{p}}}|\tilde{Q}|,$$

Similarly, if $p > 2$, the same result holds when $|\mu^{\pm}| < \varepsilon M 2^{-j_*}$.

3.3 Lemma of the DeGiorgi type

Within this section, we introduce a Lemma resembling DeGiorgi's lemma, but it pertains to cylinders in the format of $Q_{\varrho}(\theta)$. In the scope of its application, the value of the parameter θ will be a constant universally determined by the provided data. Remarkably, this constant θ remains unaffected by changes in the solution and remains consistent.

Lemma 3.4

Examine a locally bounded function u, which serves as a local

sub(super)-solution to equation (1) within Ω_T. Consider the set $(x_0, t_0) + Q_{\varrho}(\theta) =$

$K_{\varrho}(x_0) \times (t_0 - \theta\varrho^p, t_0] \Subset \Omega_T$. A constant $\nu \in (0,1)$, relying solely on the given data and θ, is present. If the condition holds that

$$\left|\{\pm(\mu^{\pm} - u) \leq M\} \cap (x_0, t_0) + Q_{\varrho}(\theta)\right| \leq \nu|Q_{\varrho}(\theta)|,$$

then either $|\mu^{\pm}| > 8M$, or

$$\pm(\mu^{\pm} - u) \geq \frac{1}{2}M \quad \text{a.e. in} \quad (x_0, t_0) + Q_{\frac{1}{2}\varrho}(\theta).$$

Main Theorem Proof

Proof. Let's introduce the cylinder $Q_0 = K_{\varrho}(x_0) \times (t_0 - \varrho^p, t_0] \Subset \Omega_T$. For simplicity, we'll assume that

the origin and (x_0, t_0) coincide. We begin by noting that

$$\mu^+ = ess\ sup_{Q_0} u, \quad \mu^- = ess\ inf_{Q_0} u, \quad \omega = \mu^+ - \mu^-.$$

Our argument proceeds through two main scenarios, specifically,

$$\begin{cases} \text{when } u \text{ is near zero: } \mu^- \le \omega \text{ and } \mu^+ \ge -\omega, \\ \text{when } u \text{ is away from zero: } \mu^- > \omega \text{ or } \mu^+ < -\omega. \end{cases} \quad (11)$$

Notice that $(11)_1$ is equivalent to the condition $-2\omega \le \mu^- \le \mu^+ \le 2\omega$. Consequently,

$$|\mu^{\pm}| \le 2\omega.$$

4.1 A decrease in oscillation around zero

Within this section, we consider the scenario where the requirement specified in (11) is valid for the initial scenario. It's crucial to emphasize that one of the subsequent possibilities must hold:

$$|\{u(\cdot, -\tfrac{1}{2}\varrho^p) - \mu^- > \tfrac{1}{4}\omega\} \cap K_\varrho| \ge \tfrac{1}{2}|K_\varrho|, \quad (12)$$

or

$$|\mu^+ - \{u(\cdot, -\frac{1}{2}\varrho^p) > \frac{1}{4}\omega\} \cap K_\varrho| \ge \frac{1}{2}|K_\varrho|,$$

We confine ourselves to the case (12) as both cases can be handled similarly. Employing Proposition 3.1 provides η within the range of (0,1) determined solely by the provided information,in a way that

$$u \ge \mu^- + \eta\omega \ \ a.e.\ in\ \ Q_1 = K_{\varrho_1} \times (-\varrho_1^p, 0], \quad with\ \ \varrho_1 = \frac{1}{2}\varrho.$$

This results in a decrease in oscillation,i,e. we have

$$ess\ osc_{Q_1} u \le (1-\eta)\omega := \omega_1.$$

We can now proceed with the induction. Assume that up to $i = 1,2,\cdots, j-1$, we have constructed

$$\begin{cases} \varrho_i = \frac{1}{2}\varrho_{i-1}, \omega_i = (1-\eta\omega_{i-1}, Q_i = K_{\varrho_i} \times (-\varrho_i^p, 0], \\ \mu_i^+ = ess\ sup_{Q_i} u, \mu_i^- = ess\ inf_{Q_i} u, ess\ osc_{Q_i} u =\le \omega_i. \end{cases}$$

We consider the situation where the initial condition in (11) is valid for all indices

$i = 1,2,\cdots, j-1$, i.e.,

$$\mu_i^- \le \omega_i \ \ and \ \ \mu_i^+ \ge -\omega_i.$$

This allows us to reiterate the initial argument, which we have done for all $i = 1,2,\cdots, j$,

$$ess\ osc_{Q_i} u \le (1-\eta)\omega_{i-1} := \omega_i.$$

Thus, by repeating the aforementioned iterative inequality, we obtain the following for all values of i ranging from 1 to j.

$$ess\ osc_{Q_i} u \le (1-\eta)^i \omega := \omega(\tfrac{\varrho_i}{\varrho})^{\beta_0} \ \ where\ \ \beta_0 = \tfrac{-ln(1-\eta)}{ln2}. \quad (13)$$

4.2 A decrease in oscillation away from zero

Assuming that j is the smallest index in this section that satisfies the second condition in (11), meaning either $either\ \ \mu_j^- > \omega_j\ \ or\ \ \mu_j^+ < -\omega_j$, we will consider the case where $\mu_j^- > \omega_j$, as the opposite case follows similarly. Given that j marks the initial index for this scenario, it implies that $\mu_{j-1} < \omega_{j-1}$. Additionally, an estimation is made:

$$\mu_j^- \le \mu_{j-1}^- + \omega_{j-1} + \Omega_{j-1} - \omega_j \le 2\omega_{j-1} - \omega_j = \frac{1+\eta}{1-\eta}\omega_j.$$

Consequently, we have:

$$\omega_j < \mu_j^- \le \tfrac{1+\eta}{1-\eta}\omega_j. \quad (14)$$

Starting from index j, equation (1) exhibits resemblance to a parabolic p-Laplacian equation within Q_j, as indicated by condition (14). Hence, the ability to solve the parabolic p-Laplacian equation plays a role in determining the possibility of reducing oscillation. For this purpose, we temporarily omit the subscript j from our symbol and define $v = \frac{u}{\mu^-}$ across the region $Q = K_\varrho \times (-\varrho^p, 0)$. It can be readily confirmed that v fulfills:

$$\partial_t v^{p-1} - \mathrm{div}(|Dv|^{p-2}Dv) = 0 \ \ weakly\ in\ \ Q,$$

where $(x,t) \in Q$, $v \in \mathbb{R}$, and $\xi \in \mathbb{R}^N$. Additionally,

$$1 \le v \le 2 \ \ a.e., \ \ Q. \quad (15)$$

By leveraging the established regularity theory for the parabolic p-Laplacian (see DiBenedetto, 1993, DiBenedetto et al., 2012), the equation satisfied by $w := v^{p-1}$ turns out to be more amenable, namely,

$$\partial_t w - \mathrm{div} A(x,t,w,Dw) = 0 \ \ weakly\ in\ \ Q, \quad (16)$$

where for $(x,t) \in Q$, $w \in \mathbb{R}$, and $\xi \in \mathbb{R}^N$, we use

$$A(x,t,w,\xi) = \left(\frac{1}{p-1}\right)^{p-1} |w|^{\frac{(2-p)(p-2)}{p-1}} w|\xi|^{p-2}\xi.$$

It is evident that w occupies the identical functional space (2) as u and v because of (15), leading to $1 \le w \le 2^{p-1}$ in Q. Reapplying (15), it can be confirmed that there exist positive constants $\gamma_0(p)$ and $\gamma_1(p)$ such that

$$A(x,t,w,\xi).\xi \ge \gamma_0(p)|\xi|^p \ \ and \ \ |A(x,t,w,\xi)| \le \gamma_1(p)|\xi|^{p-1}, \quad (17)$$

for almost every $(x,t) \in Q$, and any $w \in \mathbb{R}$, and any $\xi \in \mathbb{R}^N$. This implies that w serves as a regional weak solution to the equation resembling the parabolic p-Laplacian.

Proposition 4.1

For p > 1, let w be a bounded, local, weak solution to (1) in Q: = Q_ϱ, and define

$$\widetilde{\omega} = \text{ess osc}_Q w.$$

If for some constants σ in (0,1), the condition

$$ess\ osc_{Q_{\sigma\varrho}(\theta)} w \le \widetilde{\omega} \ \ holds, \ where \quad \theta = \widetilde{\omega}^{2-p}, \quad (18)$$

then there exist constants $\beta_1 \in (0,1)$ and $\gamma > 1$ dependent solely on N, p, $\tilde{C}_0$, $\tilde{C}_1$, and σ, such that for all $0 < r < \varrho$,

$$ess\ osc_{Q_r(\theta)} w \le \gamma\widetilde{\omega}\left(\frac{r}{\varrho}\right)^{\beta_1}.$$

To apply this proposition suitably for cases where $1 < p < 2$, we initially verify the fulfillment of the condition (18). In fact, recollect that $v = \frac{u}{\mu^-}$, $w = v^{p-1}$, and

$\omega = ess\ osc_Q u$, using (15) and invoking the mean value theorem results in

$$(p-1)2^{p-2} ess\ osc_Q v \le \widetilde{\omega} = ess\ osc_Q w \le (p-1) ess\ osc_Q v.$$

As $ess\ osc_Q v = \frac{\omega}{\mu^-}$, this becomes

$$(p-1)2^{p-2}\frac{\omega}{\mu^-} \le \widetilde{\omega} \le (p-1)\frac{\omega}{\mu^-}.$$

Considering (14), we have

$$c \overset{\text{def}}{=} \frac{1-\eta}{1+\eta}(p-1)2^{p-2} \le \widetilde{\omega} \le (p-1) \le 1.$$

Since $\widetilde{\omega} \le 1$, we have $Q_\varrho(\theta) \subset Q_\varrho$, so the condition (18) in proposition 4.1 is fulfilled for $\sigma = 1$. This leads to the conclusion of Proposition 4.1. Furthermore, the set inclusion is actually obtained by the earlier bound on $\widetilde{\omega}$:

$$Q_r(\theta_0) \subset Q_r(\theta) \ \ where \ \ \theta_0 = c^{2-p}.$$

Utilizing this set inclusion and rewriting the oscillation decay in Proposition 4.1 in terms of u, we deduce that for any $0 < r < \varrho$,

$$ess\ osc_{Q_r(\theta_0)} u \le \gamma\omega\left(\frac{r}{\varrho}\right)^{\beta} \ \ with \ \ \beta = \min\{\beta_0, \beta_1\}.$$

For the case of $1 < p < 2$, appropriate rescaling produces the desired oscillation decay and finalizes the demonstration of Theorem 1.1.

References

Alonso R, Santillana M and Dawson C. on the diffusive wave approximation of the shallow water equations. *European J. Appl. Math.* 2008; 19(5): 575-606.

Acerbi E. and Fusco N, Regularity for minimizers of nonquadratic functionals: the case $1 < p < 2$, *J. Math. Appl*. 1989; 140(1): 115-135.

Bogelion V, Duzaar F, and Liao N. On the Hölder Regularity of Signed Solutions to a Doubly Nonlinear Equation. *J. Funct. Anal.*, 2021; 281(9):

DiBenedetto E, Gianazza U and Vespri V. The Harnack's Inequality for Degenerate and Singular Parabolic Equations. Springer Monographs in Mathematics; 2012.

DiBenedetto E. Continuity of weak solutions to a general porous medium equation. *J. Indiana Univ. Math.* 1983; 32:83-118.

DiBenedetto E. Degenerate Parabolic Equations (Universititext). 1st edition, Springer-Verlag; 1993.

DiBenedetto E. On the local behaviour of solutions of degenerate parabolic equations with measurable coefficients. *Ann. Sc. Norm. Super. Pisa-CI. Sci.* 1986; 13(3): 487-535.

DiBenedetto E. Real Analysis. Birkhäuser Springer; 2016.

Evans LC. Partial Differential Equations. *Graduate Studies in Mathematics*, Vol. 19, American Mathematical Society; 1998. pp. 1-695.

Feng F and Molz F. J. A 2-d diffusion based, wetland flow model. *J. Hydrol.* 1997; 196: 230-250.

Giannaza U and Vespri V. A Harnack inequality for solutions of doubly nonlinear parabolic equations. *J. Appl. Funct. Anal.* 2006; 1(3): 271-284.

Giaquinta M and Modica G. Remarks on the regularity of the minimizers of certain degenerate functionals. *J. Appl. Funct. Anal.* 2006; 1(3): 271-284.

Hromadka TV Berenbrock CE, Freckleton JR and Guymon GL. A two dimensional dam- break flood plain model. *Adv. Water Resour*. 1985; 8: 7-14.

Ivanov AV, and Mkrtychyan PZ. Regularity up to the boundary for generalized solutions to the first boundary-value problem for doubly degenerate quasilinear parabolic equations. *J. Math. Sci.* 1994; 70(6): 2112-2122.

Ivanov AV. Hölder estimates for equations of fast diffusion type. *Algebra I Analiz*. 1994; 6(4): 101-142.

Ivanov AV. The classes $B_{m,l}$ and Hölder estimates of weak solutions for quasilinear parabolic equations admitting doubly degeneracy. *Zap. Nauchn. S. Peterburg. Otdel. Mat. Inst. Steklov.* (POMI) 1992; 197: 42-70.

Kinnunen J and Kuusi T. Local behaviuor of solutions to doubly nonlinear parabolic equations. *Math. Ann.* 2007; 337(3): 705-728.

Kinnunen J and Lindqvist P. Pontwise behaviuor of semicontinuous supersolutions to a parabolic solutions to doubly nonlinear quasilinear parabolic equation. *Ann. Mat. Pura Appl.* 2006; 185(3): 411-435.

Kuusi T, Misawa M and Nakamura K. Global existence for the p-Sobolev flow. *J. Differ. Equ*. 2021; 279: 245-281.

Kuusi T, Siljander J and Urbano JM. Local Hölder continuity for doubly nonlinear parabolic equations. *J. Indiana Univ. Math.* 2012a; 61(1): 399-430.

Kuusi 1 T, Siljander J, Laleoglu R and Urbano JM. Hölder continuity for Trudinger's equations in mrasure spaces. *Calc. Var. Partial Differ. Equ.* 2012b; 45(1-2): 193-229.

Ladyzenskaja OA, Solonnikov VA and Ural'ceva N. Linear and quasilinear equations of parabolic type. *Math. Mono*.1968: 23; pp648.

Leugering G and Mophou G. Instantaneous optimal control of friction dominated flow in a gas-network, in "Shape Optimization, Homogenization and Optimal Control". International series of Numerical Mathematics. 2018;169, Birkhaüser, Cham.

Lindgren E and Lindqvist P. On a Comparison Principle for Trudingers equation. *Adv. Calc. Var.* 2022; 15(3): 401-415.

Mahaffy MW. A three dimensional numerical model of ice sheets: Tests on the Barnes ice cap, northwest territories. *J. Geophys. Res.* 1976; 81(6):1059-1066.

Nakamura K and Misawa M. Existence of weak solution to the p-Sobolev flow. *Nonlinear Anal*. 2018; 175: 157-172.

Sarkar A.H. Positivity expansion to signed solution for doubly nonlinear parabolic equations. Jagannath Univ. J. Sci. 2023 (in press).

Sarkar AH. Energy estimates of signed solution to the doubly nonlinear parabolic equations. *Jagannath. Univ. J. Sci*. 2022; 9(1): 43-49.

Trudinger NS. Pointwise estimates and quasilinear parabolic equations. Comm. *Pure Appl. Math.* 1968b; 21(7): 205-226.

Trudinger NS. Remarks concerning the conformal deformation of Riemannian structures on compact manifolds. Ann. *Schoula. Sup. Pisa.* 1968a; 22: 265-274.

Urbano JM. The Method of Intrinsic Scaling: A Systematic Approach to Regularity for Degenerate and Singular PDEs (Lecture Notes in Mathematics, 1930), Springer-Verlag; 2008.

Vespri V, and Vestberg M. An extensive study of the regularity properties of solution to doubly singular equations. *arXiv:2001.0414.1v1, 2020.*

Vespri V. On the local behaviour of solutions of a certain class of doubly nonlinear parabolic equations. *Manuscripta Math.* 1992; 75(1): 65-80.

J. Bangladesh Acad. Sci. 47(2); 249-265: December 2023 DOI:https://doi.org/10.3329/jbas.v47i2.68474

Journal of Bangladesh Academy of Sciences

Journal homepage: http://www.bas.org.bd/publications/jbas.html

Research Article

Wildlife diversity and community structure in northern deciduous forest of Bangladesh

Mohammad Firoj Jaman, Md. Fazle Rabbe, Arnob Saha, Ashikur Rahman Shome and Md. Mahabub Alam*

Wildlife Research Laboratory, Department of Zoology, University of Dhaka, Dhaka, Bangladesh

ARTICLE INFO

Article History

Received: 29 August 2023
Revised: 06 November 2023
Accepted: 08 November 2023

Keywords: Abundance, Cluster analysis, Diversity, Seasonal variation, Protected areas

ABSTRACT

Monitoring wildlife communities in protected areas is pivotal to successful conservation efforts. This study employed a direct observations-based approach to examine the diversity and community structure of wildlife in four protected deciduous national parks (Ramsagar, Birganj, Singra, and Nawabganj) in the northern Dinajpur district of Bangladesh. This study assessed the wildlife assemblage structures by measuring α diversity and β diversity. This research recorded a total of 159 wildlife species under 29 orders. Singra National Park displayed the highest species richness (N=73) and was found to be more diverse (H=3.36 ± 0.16) and even in distribution (J=0.9 ± 0.01). Analysis of Similarity test showed significant differences across all study sites (R=0.5216; p=0.0001). Whittaker Plot ranked *Dendrocygna javanica* as dominating, species making the community uneven. We found significant differences in species richness among seasons ($F_{2,\ 9}$=17.8, p=0.0001). For example, winter and rainy seasons were significantly richer over summer. This study identified profound human intrusions, which could potentially impact wildlife communities in the study area. Our findings underscore the conservation efforts to safeguard the threatened species in the study area.

Introduction

Bangladesh is characterized by diverse, intricate ecosystems, including hilly areas, wetlands, plain lands, evergreen forests, deciduous forests (locally known as *Sal* forests), and coastal regions. Notably, Bangladesh is distinguished by abundant plant species, which exhibit exceptional genetic, species, and ecosystem diversity, distributed among forests, village groves, and dwellings (IUCN Bangladesh, 2015). Forests and village groves are integral in providing various services, such as fruit and nuts, fuel and fodder, vegetables, medicinal plants, bamboo, numerous other non-wood forest products, and valuable timber and wood tree species. Forests are invaluable natural resources that serve numerous vital functions in nature. Among the major forest ecosystems, deciduous forests comprising dry-deciduous and moist deciduous forests are prominent landscapes in central and northern Bangladesh (Khan, 2015). Northern Bangladesh is home to only 14% of the *Sal* forest, with the remaining 86% in the central region (Alam et al., 2008).

Based on estimates from the Food and Agriculture Organization (FAO), it is reported that only 10% of *Sal* forest cover was present in 1990, down from an estimated 36% in 1985, indicating a significant reduction in *Sal* forest cover (Haque, 2007). The Sal forest has been identified as one of the most vulnerable ecosystems in Bangladesh (Alam et al., 2008). Various anthropogenic and natural threats, including overuse, deforestation, invasive species, habitat conversion for agriculture, and pollution, are causing critical ecosystems to deteriorate in certain

*Corresponding author: <mahabub.zoo@du.ac.bd>

forest areas. Consequently, at least 31 wildlife species have been extirpated in Bangladesh (IUCN Bangladesh, 2015). If these conditions persist, wildlife species will likely disappear continuously, leading to ecological imbalance and disaster. As a result, the flora and fauna of *Sal* forests might also be threatened with extinction risks.

Regarding biodiversity, Bangladesh is recognized as having a considerable abundance of wildlife. For example, this country harbors a diverse array of fauna, including approximately 133 mammal species, 711 bird species, 173 reptile species, and 64 amphibian species (IUCN Bangladesh, 2015; Khan, 2015; Khan, 2018; Shome et al., 2021). It is noteworthy that Bangladesh possesses diverse wildlife species due to its geographic location as a continental nation with a variety of habitats shared with neighboring countries (www.bforest.gov.bd). This also instigates the rich biodiversity of northern Bangladesh with various forms of microhabitats. Still, there is a lack of knowledge and research on the wildlife diversity and community structure in the existing *Sal* forests of that particular areas.

Several studies have been conducted on the diversity, status, distribution, threats, and conservation strategies of wildlife in different parts of Bangladesh at different times (Kabir and Ahmed, 2005; Jaman et al., 2015, 2020, 2021, 2022; Shome et al., 2020, 2021, 2022a, 2022b; Barkat et al., 2021; Rabbe et al., 2022a, 2022b, 2022c; Saha et al., 2022). The number of studies on deciduous forests of northern Bangladesh is very limited and done on a preliminary basis. For instance, Rimi et al. (2013) and Ali et al. (2020) assessed the biodiversity, conservation, and management activities in Ramsagar National Park and Singra National Park, respectively. Rabbe et al. (2022a, 2022b) conducted a study on the herpetofaunal diversity, abundance, human perception of the herpetofauna, threats to the herpetofauna, and conservation measures in Greater Dinajpur and Nilphamari districts of Bangladesh.

The present study was designed to address the research gaps in wildlife diversity and community structure in the *Sal* forests of northern Bangladesh. The main objective of this study was to quantify and compare the diversity, composition, and abundance of wildlife in the four deciduous protected areas (i.e., National Parks). In addition, this study aimed to provide baseline information on wildlife and conservation aspects in the study area.

Material and methods

Study areas

This study was conducted in four protected national parks, namely Ramsagar National Park, Birganj National Park, Singra National Park, and Nawabganj National Park, under northern Dinajpur district from July 2021 to August 2022 (Fig. 1, Table 1). These protected areas are dominated by deciduous forests, primarily consisting of *Sal* (*Shorea robusta*) trees. The forests differ in their composition of large and small *Sal* trees, grasslands (with a height of less than or equal to 2 m), bushes and thickets, small canals, roadside areas, and a permanent waterbody (*dighi* only in Ramsagar) (Akter et al., 2023; DoF, 2023).

The microhabitats of the study sites were identified through direct observations and classified into five distinct categories: Agricultural land (AL), which are actively farmed areas for rice, corn, and vegetables; Dense vegetation (DG), consisting of short, small grassy and bushy vegetation with a maximum height of ≤2 m; Homestead area (HA), which includes large and small trees around residential houses near the periphery of the protected area; Trees (T), which include plants with a minimum height of ≥2 m; and Waterbody (W), which encompasses shallow water channels, small and large ponds, and seasonal wetlands.

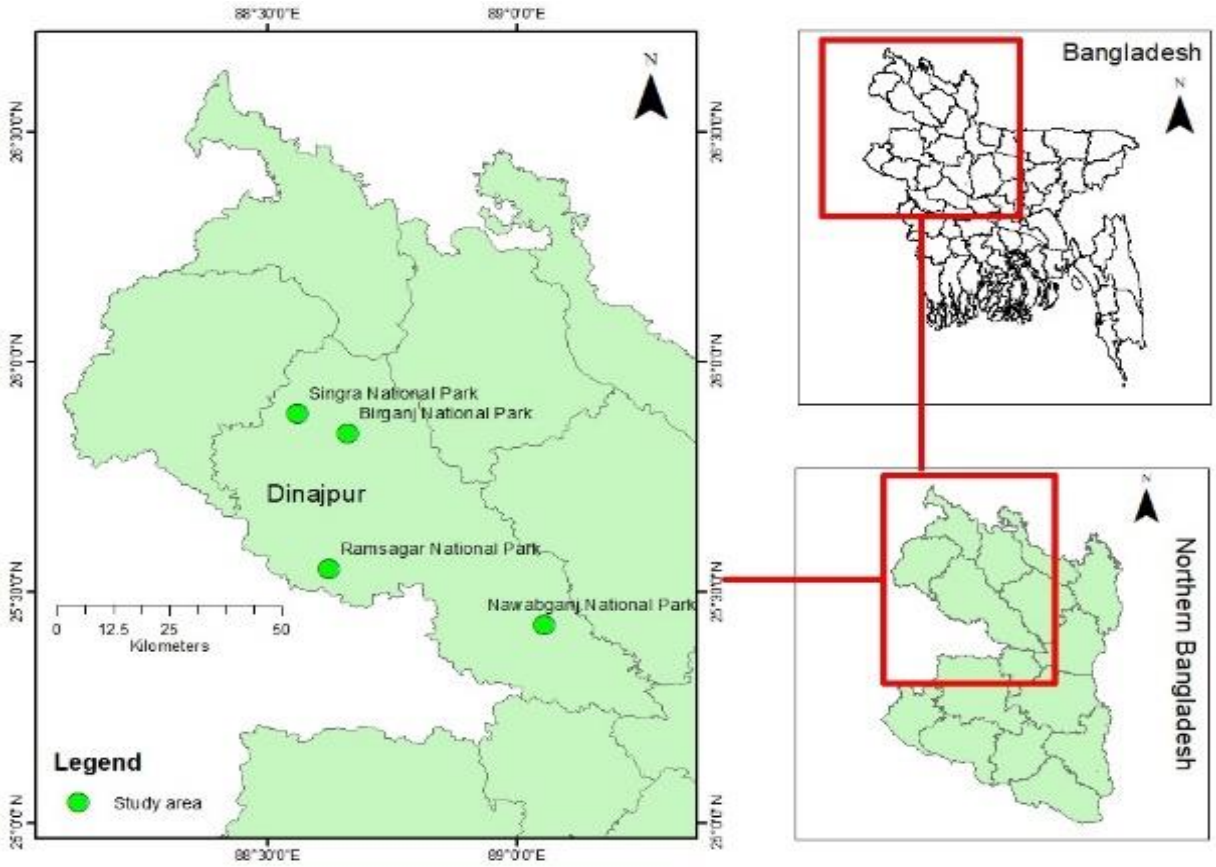

Fig. 1. Map of the study area showing the four national parks of northern Dinajpur district, Bangladesh.

Table 1. Major landscape features and characteristics of habitats in four national parks

Parameters	Ramsagar NP	Birganj NP	Singra NP	Nawabganj NP
Area(ha)	27.75	168.56	305.69	517.61
Latitude and Longitude	25°33′17″N 88°37′24″E	25°51'11"N 88°39'33"E	25°53'31"N 88°33'36"E	25.4517°N 89.0534°E
IUCN category	IV	IV	IV	IV
Declared in	2001	2011	2010	2010
Major tree	–	*Shorea robusta*	*Shorea robusta*	*Shorea robusta*
Waterbody	Permanent and large *dighi*	Permanent ponds & temporary ditches	Temporary canal	*Beel* and temporary ditches
Bushes	Present	Present	Present	Present
Human settlements	Periphery	Inside	Inside	Periphery
Microhabitats	Agricultural land, Dense vegetation, Homestead area, Trees, Waterbody			

Survey protocol

Data were systematically collected through direct field observations using the line transect method following Yallop et al. (2004). Surveys were conducted for a minimum of 10 hours each day. The whole day was divided into morning (06:00 to 10:00), afternoon (15:30 to 19:00), and night (21:30 to 24:00). Each transect had a length of 500 m and a width of 50 m. Each transect had five predetermined intervals, each spaced 100 meters apart, and approximately 20 minutes were allocated at each interval point for amphibians' and reptiles' observation. A pair of binoculars (Bushnell Power view 10x42) was used to facilitate observations of mammals and birds. Upon spotting any species, the individual count and microhabitat usage were recorded. Wildlife species hidden in the bushes, jungles, and branches of trees were detected by hearing their songs and calls, and then identification was confirmed by direct observation. In addition, local people were interviewed, and pictorial guides were shown to confirm the presence and abundance of wild animals, especially turtles and snakes. Species were occasionally photographed using NIKON D5300 with a 55–200 mm lens for identification. To evaluate seasonal changes in wildlife diversity, the entire study period was divided into three seasons: summer (March-June), rainy (July–October), and winter (November–February). The guidelines of IUCN Bangladesh (2015) and Khan (2018) was followed for the taxonomic identification of observed species.

Data analysis

To ensure adequate sampling, we constructed a species accumulation curve following the rarefaction method outlined by Magurran (2013).

We also calculated sampling completeness by following the formula:

$$\text{Sample completeness}=\frac{\text{Observed Number of species (n)}}{\text{Estimated Number of species }(x)}*100$$

To assess the α level of diversity status of wildlife in each site, we measured Margalef Species richness, Pielou's evenness, and the Shannon–Wiener index. The relative abundance (RA) of each species in each site was calculated using the formula RA = (number of individuals of a particular species) / (total number of individuals of all species)×100. We also presented the relative abundance of wildlife observed in different microhabitats as a stacked bar diagram for each study site. To assess β diversity (species turnover) between sites, we performed an Analysis of Similarities (ANOSIM). We used the 'adonis' function from the vegan R package (Oksanen et al., 2019).

A cluster analysis was conducted using the Bray–Curtis index (Everitt et al., 2011) in PAST version 3 (Hammer et al., 2001) to examine similarities among the different microhabitats. A Whittaker rank-abundance diagram was generated by plotting the relative abundance against their rank in each study site (Whittaker, 1965). To identify significant differences among study sites and the seasonal variation of wildlife, we performed one-way ANOVA followed by Dunn's post-hoc comparison test. We checked the normality of the data using Q-Q plots, the Shapiro–Wilk Test, and histograms. All statistical analyses were performed using relevant statistical packages in R 4.0.5 (R Core Team 2020), and the ggplot2 package was used for plotting (Wickham, 2016).

Results and Discussion

Sampling completeness, species diversity, and composition

A total of 159 wildlife species were recorded during the study period, belonging to 64 families under 23 orders. The species accumulation curves indicated that the survey was sufficiently comprehensive and that sampling efforts were adequate (Fig. 2).

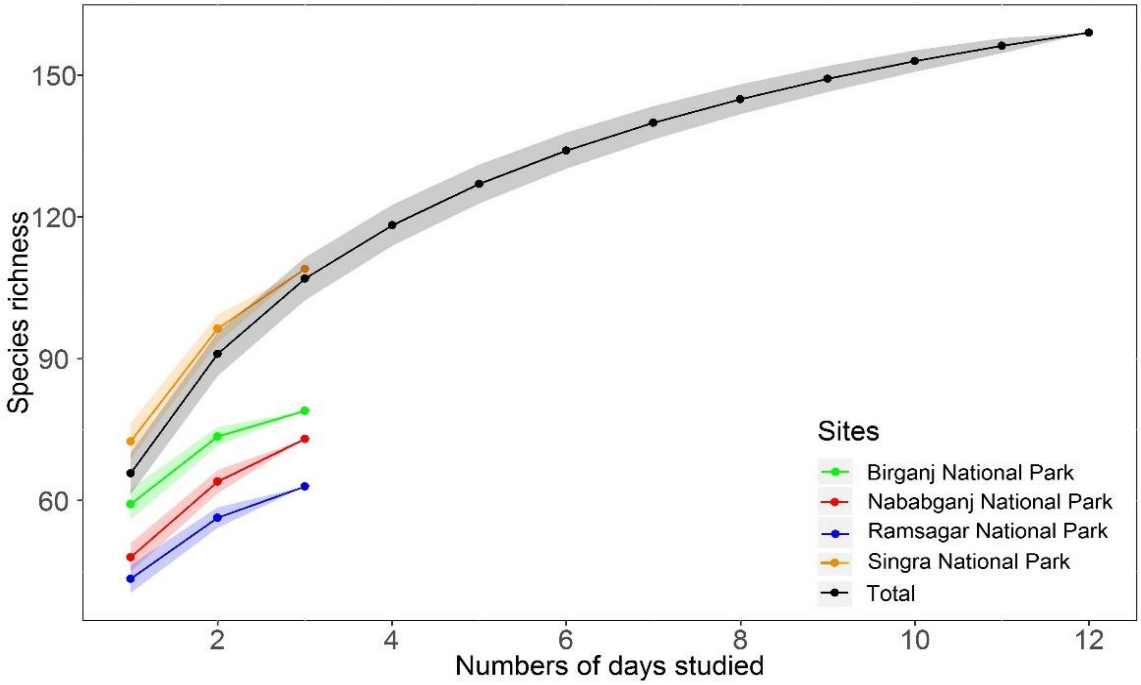

Fig. 2. Species accumulation curve of the study sites. The X-axis has been scaled to show the number of days studied.

Of the 159 wildlife species recorded during the study period, 119 were birds, 12 were amphibians, 10 were mammals, and 18 were reptiles (Table 3). A total of 2966 individuals of these 159 species were observed. Singra National Park had the highest species richness (N=73), followed by Ramsagar National Park (N=71), Nawabganj National Park (N=70), and the lowest in Birganj National Park (N=68). The average number of wildlife species observed per day did not differ significantly among study sites ($F_{3, 8}$=0.11, p = 0.95). Singra National Park had the highest average number of observed wildlife species per day (43±8.71), followed by Ramsagar National Park (40±13), Nawabganj National Park (40±10.44), and Birganj National Park (38.33±7.50) (Fig. 3). However, the relative abundances of wildlife varied among different microhabitats. Agricultural land was the most abundant in Birganj National Park. In contrast, the "Tree" microhabitat was relatively abundant in Nawabganj and Singra National Park. Lastly, wildlife inhabiting waterbodies was the most. abundant in Ramsagar National Park. (Fig. 4).

Shannon-Wiener diversity index (H) showed that Singra National Park had the highest species diversity (H=3.36±0.16), followed by Nawabganj National Park (H=3.25±0.28), Ramsagar National Park (H=2.77±0.86), and the lowest in Birganj National Park (H= 2.73±0.79). However, the average Shannon-Wiener diversity index did not vary significantly among study sites ($F_{3, 8}$=0.846, p=0.50) (Fig. 3). Pielou's Evenness further indicated that species in Singra National Park (J=0.9±0.01) and Nawabganj National Park (J= 0.89±0.08) were more evenly distributed compared to Birganj National Park (J=0.76±0.24) and Ramsagar National Park (J=0.75±0.19). This unevenness of species community was also illustrated in the Whittaker Plot (Fig. 5) and the most dominating species were *Dendrocygna javanica* (RA=40.314%) in Ramsagar National Park, *Euphlyctis cyanophlyctis* (RA=36.506%) in Birganj National Park and *Sturnus contra* in Nawabganj National Park (RA=18.526%) and Singra National Park (RA=8.998%).

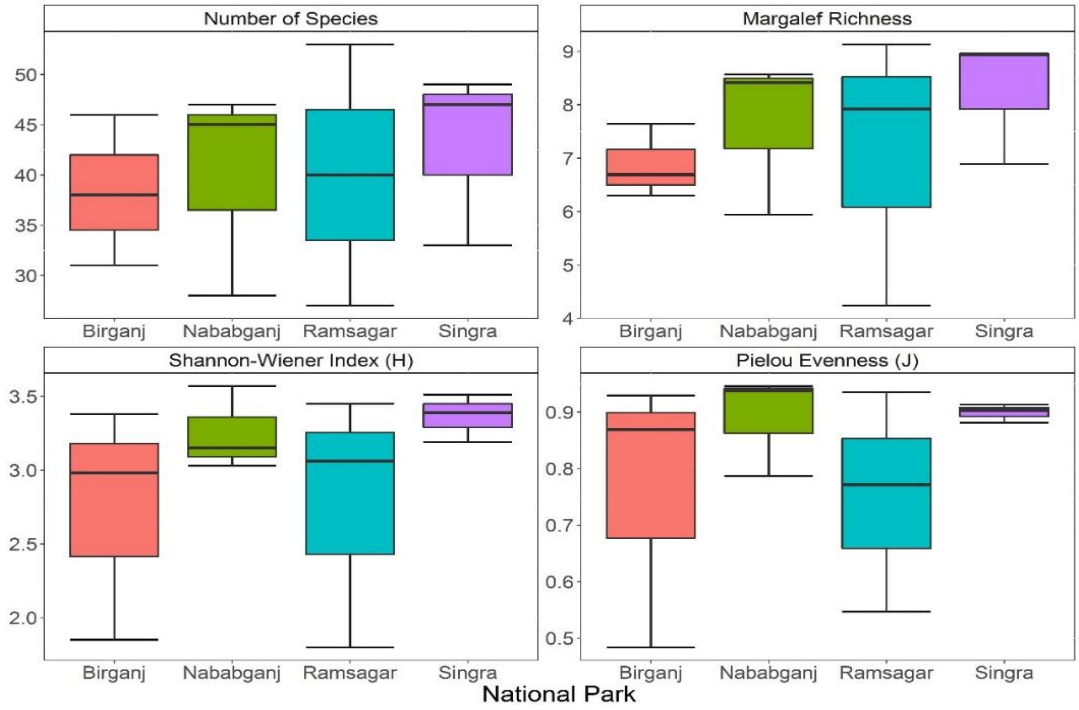

Fig. 3. Boxplot of Alpha-diversity indices, Margalef Richness, and number of observed species in four study sites A, Number of species; B, Margalef Richness C, Shannon-Wiener Index (H) D, Pielou's Evenness (J).

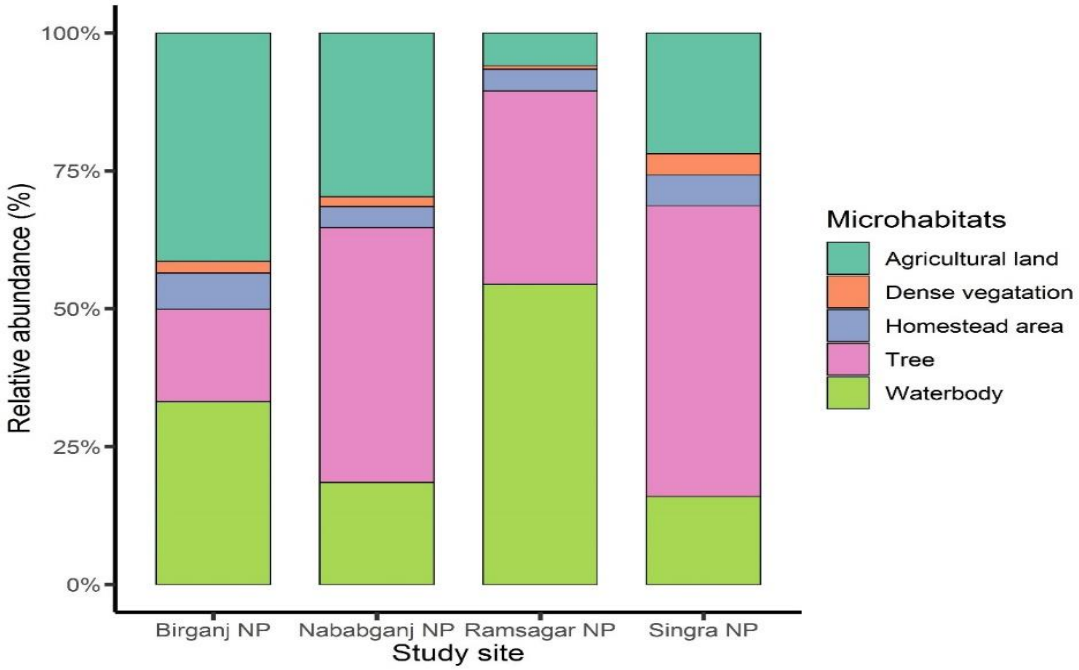

Fig. 4. Histogram of relative abundance of wildlife among study sites. The X-axis represents study sites, and the Y-axis represents the relative abundance of wildlife occupying different microhabitats.

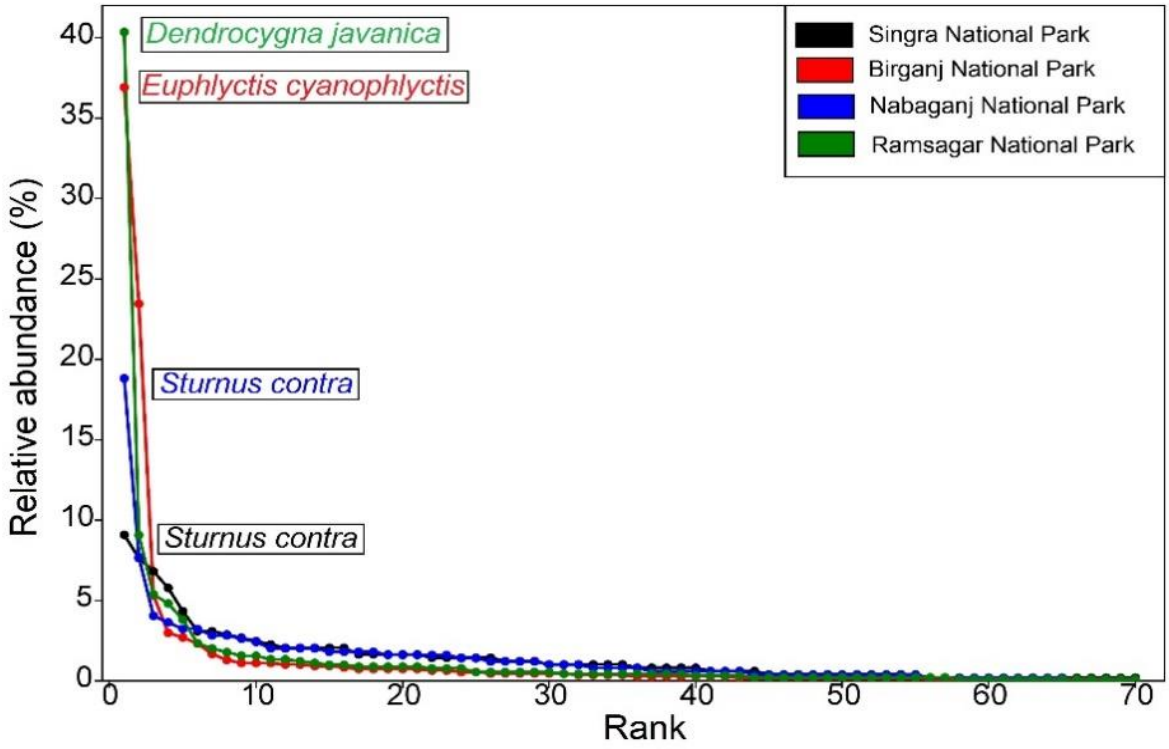

Fig. 5. Whittaker plot representing the abundance rank of wildlife species in the study sites.

The study revealed a seasonal variation in species composition; the winter season had the highest number of recorded wildlife species (115). Still, the number of individuals was highest in the rainy season (1316 individuals). ANOVA indicated a significant difference in wildlife species richness among seasons ($F_{2,9}$=17.8, p=0.0001), and the winter season (46.75±6.34) and the rainy season (44.5±3.10) were significantly richer than the summer season (29.75±2.75) (p<0.05). Similarly, significant variation was seen among seasons for Margalef Richness ($F_{2,9}$=9, p=0.001) and the winter season and summer season were significant over the summer season (p<0.05). Although the Shannon-Wiener index calculated the overall highest diversity in winter (H=3.845), it did not differ significantly ($F_{2, 9}$=0.57, p>0.05) among seasons (Fig. 6).

The beta diversity pattern was analyzed using the Analysis of Similarity (ANOSIM) test, demonstrating a statistically significant difference in wildlife communities across all sites (R=0.5216; p=0.0001). However, no significant differences were observed between sites in pairwise comparisons at p<0.05 (Table 2).

Cluster analysis showed one distinct cluster between "Tree" and "Agricultural land," indicating they shared the most species community. The dendrogram revealed that this group formed a tight cluster with the "Homestead area," which also had considerable similarities in the species community. In addition, the dendrogram demonstrated that the most distinct species communities were observed in "Waterbody" and "Dense vegetation" during the study period (Fig. 7).

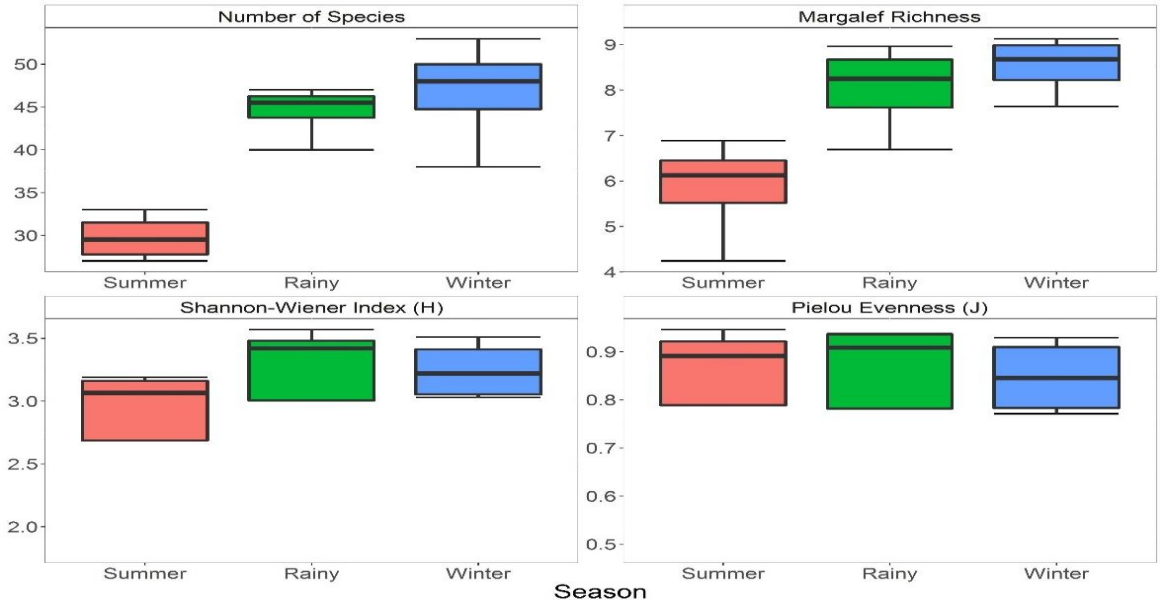

Fig. 6. Seasonal variation in diversity indices- A, Number of Species; B, Margalef species Richness; C, Shannon-Wiener Index; D, Pielou Evenness

Fig. 7. Dendrogram showing species community similarities among microhabitats based on Bray–Curtis Index

Table 2. Pairwise comparison among study sites based on the ANOSIM test. Bonferroni-corrected p values are used.

National parks	Birganj	Nawabganj	Ramsagar
Nawabganj	R=0.44; p=0.09		
Ramsagar	R=0.26; p=0.19	R=0.74; p=0.10	
Singra	R=0.40; p=0.10	R=0.81; p=0.10	R=0.85; p=0.09

Table 3. Class, family, species names, abundance (n), and relative abundance (RA) of observed vertebrate wildlife in four study sites

Family	Scientific name	Common name	n	RA (%)	Site-wise RA (%)			
					BNP	NNP	RNP	SNP
Class: Amphibia								
Bufonidae	*Duttaphrynus melanostictus*	Common Toad	28	0.90	1.30	0.00	0.80	1.40
Dicroglossidae	*Euphlyctis cyanophlyctis*	Skipper Frog	445	15.00	36.50	1.60	0.60	7.60
Dicroglossidae	*Euphlyctis kalasgramensis*	Kalasgram Skipper Frog	281	9.50	23.20	1.40	0.20	4.30
Dicroglossidae	*Fejervarya asmati*	Asmat's Cricket Frog	68	2.30	5.30	1.20	0.20	0.60
Dicroglossidae	*Fejervarya nipalensis*	Nepal Wart Frog	25	0.80	1.10	0.40	0.40	1.40
Dicroglossidae	*Fejervarya pierrei*	Pierre's Cricket Frog	10	0.30	0.50	0.60	0.00	0.40
Dicroglossidae	*Fejervarya teraiensis*	Terai Wart Frog	10	0.30	0.30	0.40	0.00	1.00
Dicroglossidae	*Hoplobatrachus crassus*	Jerdons Bullfrog	2	0.10	0.20	0.00	0.00	0.00
Dicroglossidae	*Hoplobatrachus tigerinus*	Indian Bullfrog	18	0.60	1.00	0.40	0.00	1.00
Microhylidae	*Microhyla sp*	Narrow-mouthed Frog	6	0.20	0.50	0.00	0.00	0.20
Rhacophoridae	*Polypedates maculatus*	Maculated Tree Frog	3	0.10	0.20	0.20	0.00	0.00
Rhacophoridae	*Polypedates leucomystax*	Common Tree Frog	6	0.20	0.20	0.60	0.00	0.20
Class: Reptilia								
Agamidae	*Calotes versicolor*	Common Garden Lizard	6	0.20	0.10	0.60	0.00	0.40
Colubridae	*Ahaetulla nasuta*	Common Vine Snake	2	0.10	0.20	0.00	0.00	0.00
Colubridae	*Dendrelaphis pictus*	Common Bronze-back	1	0.00	0.00	0.00	0.00	0.20
Colubridae	*Enhydris enhydris*	Common Smooth-scaled Water Snake	1	0.00	0.00	0.20	0.00	0.00
Colubridae	*Lycodon aulicus*	Common Wolf Snake	1	0.00	0.10	0.00	0.00	0.00
Colubridae	*Ptyas mucosa*	Indian Rat Snake	2	0.10	0.20	0.00	0.00	0.00
Colubridae	*Xenochrophis cerasogaster*	Painted Keelback	1	0.00	0.10	0.00	0.00	0.00
Colubridae	*Xenochrophis piscator*	Checkered Keelback	2	0.10	0.00	0.00	0.10	0.20
Elapidae	*Naja naja*	Binocellate Cobra	2	0.10	0.20	0.00	0.00	0.00
Gekkonidae	*Gekko gecko*	Tokay Gecko	1	0.00	0.00	0.20	0.00	0.00

Family	Scientific name	Common name	n	RA (%)	Site-wise RA (%)			
					BNP	NNP	RNP	SNP
Gekkonidae	*Hemidactylus brookii*	Brook's House Gecko	2	0.10	0.00	0.40	0.00	0.00
Gekkonidae	*Hemidactylus frenatus*	Common House Gecko	1	0.00	0.00	0.20	0.00	0.00
Scincidae	*Eutropis carinata*	Common Skink	2	0.10	0.00	0.00	0.00	0.40
Scincidae	*Eutropis macularia*	Bronze Grass Sking	1	0.00	0.10	0.00	0.00	0.00
Trionychidae	*Lissemys punctata*	Spotted Flapshell Turtle	1	0.00	0.10	0.00	0.00	0.00
Typhlopidae	*Argyrophis diardii*	Diard's Blindsnake	2	0.10	0.20	0.00	0.00	0.00
Varanidae	*Varanus bengalensis*	Bengal Monitor	1	0.00	0.00	0.00	0.00	0.20
Varanidae	*Varanus flavescens*	Yellow Monitor	1	0.00	0.10	0.00	0.00	0.00
		Class: Aves						
Accipitridae	*Accipiter badius*	Shikra	3	0.10	0.00	0.00	0.00	0.60
Accipitridae	*Buteo rufinus*	Long-legged Buzzard	1	0.00	0.00	0.00	0.10	0.00
Accipitridae	*Circus spilonotus*	Eastern Marsh-harrier	1	0.00	0.00	0.20	0.00	0.00
Accipitridae	*Clanga hastata*	Indian Spotted Eagle	1	0.00	0.00	0.00	0.10	0.00
Accipitridae	*Elanus caeruleus*	Black-winged Kite	1	0.00	0.00	0.00	0.10	0.00
Accipitridae	*Haliastur indus*	Brahminy Kite	2	0.10	0.00	0.00	0.20	0.00
Accipitridae	*Ichthyophaga ichthyaetus*	Grey-headed Fish-eagle	8	0.30	0.00	0.60	0.60	0.00
Accipitridae	*Milvus migrans*	Black Kite	3	0.10	0.00	0.00	0.00	0.60
Accipitridae	*Nisaetus cirrhatus*	Changeable Hawkeagle	1	0.00	0.00	0.00	0.10	0.00
Accipitridae	*Pernis ptilorhyncus*	Oriental Honey Buzzard	8	0.30	0.00	0.00	0.80	0.20
Accipitridae	*Spilornis cheela*	Crested Serpent Eagle	1	0.00	0.00	0.00	0.00	0.20
Aegithinidae	*Aegithina tiphia*	Common Iora	8	0.30	0.00	0.00	0.90	0.00
Alcedinidae	*Alcedo atthis*	Common Kingfisher	26	0.90	0.70	2.00	0.90	0.00
Alcedinidae	*Ceryle rudis*	Pied Kingfisher	2	0.10	0.00	0.40	0.00	0.00
Alcedinidae	*Halcyon smyrnensis*	White-breasted Kingfisher	28	0.90	0.70	1.80	1.20	0.00
Alcedinidae	*Pelargopsis capensis*	Stork-billed Kingfisher	1	0.00	0.00	0.00	0.10	0.00

Family	Scientific name	Common name	n	RA (%)	Site-wise RA (%)			
					BNP	NNP	RNP	SNP
Alcedinidae	*Psilopogon asiaticus*	Blue-throated Barbet	2	0.10	0.00	0.00	0.20	0.00
Anatidae	*Dendrocygna javanica*	Lesser Whistling Duck	360	12.10	0.00	0.00	40.30	0.00
Anatidae	*Nettapus coromandelianus*	Cotton Pygmy-goose	5	0.20	0.00	0.00	0.60	0.00
Anatidae	*Spatula querquedula*	Gargeny	1	0.00	0.00	0.00	0.10	0.00
Apodidea	*Apus nipalensis*	House Swift	2	0.10	0.00	0.40	0.00	0.00
Apodidea	*Cypsiurus balasiensis*	Asian Palm Swift	5	0.20	0.00	0.00	0.60	0.00
Ardidae	*Ardeola grayii*	Indian Pond Heron	62	2.10	1.70	2.80	1.80	2.90
Ardidae	*Bubulcus ibis*	Cattle Egret	8	0.30	0.00	1.60	0.00	0.00
Ardidae	*Egretta garzetta*	Little Egret	14	0.50	0.00	2.80	0.00	0.00
Ardidae	*Nycticorax nycticorax*	Black-crowned Night Heron	4	0.10	0.40	0.00	0.00	0.00
Artamidae	*Artamus fuscus*	Ashy Woodswallow	9	0.30	0.00	1.80	0.00	0.00
Campephagidae	*Coracina macei*	Large Cuckooshrike	8	0.30	0.00	0.00	0.00	1.60
Campephagidae	*Coracina melanoptera*	Black-headed Cuckooshrike	4	0.10	0.20	0.00	0.00	0.40
Campephagidae	*Coracina melaschistos*	Black-winged Cuckooshrike	3	0.10	0.00	0.00	0.30	0.00
Campephagidae	*Pericrocotus cinnamomeus*	Small Minivet	18	0.60	0.00	0.00	2.00	0.00
Campephagidae	*Tephrodornis pondicerianus*	Common Woodshrike	5	0.20	0.00	0.00	0.40	0.20
Caprimulgidae	*Caprimulgus macrurus*	Long-tailed Nightger	2	0.10	0.00	0.00	0.20	0.00
Chardridae	*Charadrius dubius*	Little Ringed Plover	3	0.10	0.00	0.60	0.00	0.00
Chardridae	*Tringa glareola*	Wood Sandpiper	3	0.10	0.00	0.60	0.00	0.00
Chardridae	*Vanellus cinereus*	Grey-headed Lapwing	2	0.10	0.00	0.40	0.00	0.00
Chardridae	*Vanellus indicus*	Red-wattled Lapwing	15	0.50	0.30	0.80	0.30	1.00
Ciconidae	*Anastomus oscitans*	Asian Openbill	15	0.50	0.00	0.00	0.00	3.10
Cicticolidae	*Cisticola juncidis*	Zitting Cisticola	5	0.20	0.30	0.40	0.00	0.00
Cicticolidae	*Prinia gracilis*	Graceful Prinia	4	0.10	0.00	0.00	0.00	0.80
Cicticolidae	*Prinia hodgsonii*	Grey-breasted Prinia	6	0.20	0.00	1.20	0.00	0.00
Cicticolidae	*Prinia inornata*	Plain Prinia	5	0.20	0.00	0.00	0.00	1.00
Columbidae	*Columba livia*	Rock Dove	13	0.40	0.50	0.80	0.40	0.00
Columbidae	*Spilopelia chinensis*	Eastern Spotted Dove	38	1.30	0.00	4.00	0.90	2.00
Columbidae	*Streptopelia decaocto*	Eurasian Collared Dove	17	0.60	0.60	0.00	0.00	2.00
Columbidae	*Streptopelia tranquebarica*	Red Turtle Dove	2	0.10	0.20	0.00	0.00	0.00
Columbidae	*Treron phoenicopterus*	Yellow Footed Green Pigeon	19	0.60	0.00	0.00	0.80	2.50
Coracidae	*Coracias benghalensis*	Indian Roller	3	0.10	0.00	0.20	0.00	0.40
Corvidae	*Corvus splendens*	House Crow	4	0.10	0.00	0.00	0.20	0.40

Family	Scientific name	Common name	n	RA (%)	Site-wise RA (%)			
					BNP	NNP	RNP	SNP
Corvidae	*Corvus levaillantii*	Jungle Crow	13	0.40	0.50	0.00	0.90	0.00
Corvidae	*Dendrocitta vagabunda*	Rufous Treepie	39	1.30	0.90	2.00	1.30	1.40
Cuculidae	*Centropus sinensis*	Greater Coucal	2	0.10	0.00	0.00	0.20	0.00
Cuculidae	*Eudynamys scolopaceus*	Western Koel	4	0.10	0.00	0.00	0.40	0.00
Cuculidae	*Hierococcyx varius*	Common Hawk-Cuckoo	20	0.70	0.00	1.80	0.00	2.20
Cuculidae	*Phaenicophaeus tristis*	Green-billed Malkoha	1	0.00	0.00	0.00	0.00	0.20
Dicaeidae	*Dicaeum erythrorhynchos*	Pale-billed Flowerpecker	9	0.30	0.00	0.80	0.60	0.00
Dicruridiae	*Dicrurus hottentottus*	Hair-crested Drongo	30	1.00	0.50	1.60	0.20	3.10
Dicruridiae	*Dicrurus leucophaeus*	Ashy Drongo	7	0.20	0.30	0.20	0.30	0.00
Dicruridiae	*Dicrurus macrocercus*	Black Drongo	25	0.80	0.00	3.20	1.00	0.00
Dicruridiae	*Dicrurus aeneus*	Bronzed Drongo	11	0.40	0.20	0.60	0.40	0.40
Estrilidae	*Lonchura malabarica*	White-throated Munia	2	0.10	0.00	0.00	0.20	0.00
Estrilidae	*Lonchura punctulata*	Scaly-breasted Munia	6	0.20	0.20	0.00	0.00	0.80
Estrilidae	*Lonchura striata*	White-rumped Munia	6	0.20	0.20	0.80	0.00	0.00
Falconidae	*Falco chicquera*	Red-headed Falcon	1	0.00	0.00	0.20	0.00	0.00
Herundinidae	*Hirundo rustica*	Barn Swallow	2	0.10	0.00	0.40	0.00	0.00
Jacanidae	*Hydrophasianus chirurgus*	Pheasant-tailed Jacana	13	0.40	0.00	2.60	0.00	0.00
Jacanidae	*Metopidius indicus*	Bronze-winged Jacana	5	0.20	0.00	1.00	0.00	0.00
Lanidae	*Lanius cristatus*	Brown Shrike	7	0.20	0.20	0.40	0.10	0.40
Lanidae	*Lanius schach*	Long-tailed Shrike	4	0.10	0.00	0.00	0.00	0.80
Lanidae	*Lanius tephronotus*	Grey-backed Shrike	2	0.10	0.00	0.20	0.10	0.00
Megalaimidae	*Psilopogon haemacephala*	Coppersmith Barbet	10	0.30	0.00	1.20	0.00	0.80
Meropidae	*Merops orientalis*	Asian Green Bee-eater	10	0.30	0.00	0.00	1.10	0.00
Monarchidae	*Terpsiphone paradisi*	Asian Paradise-Flycatcher	2	0.10	0.00	0.00	0.20	0.00
Motacilidae	*Anthus rufulus*	Paddyfield Pipit	2	0.10	0.10	0.00	0.00	0.20
Motacilidae	*Motacilla madaraspatensis*	White-browed Wagtail	4	0.10	0.00	0.00	0.10	0.60
Motacilidae	*Motacilla alba*	White Wagtail	17	0.60	0.00	1.40	0.00	2.00
Motacilidae	*Motacilla citreola*	Citrine Wagtail	2	0.10	0.00	0.20	0.10	0.00
Motacilidae	*Motacilla flava*	Yellow Wagtail	1	0.00	0.00	0.00	0.10	0.00
Muscicapidae	*Copsychus saularis*	Oriental Magpie-robin	45	1.50	1.10	1.60	1.30	2.70
Muscicapidae	*Culicicapa ceylonensi*	Grey-headed Canary-flycatcher	4	0.10	0.40	0.00	0.00	0.00
Muscicapidae	*Eumyias thalassina*	Verditer Flycatcher	2	0.10	0.00	0.00	0.00	0.40
Muscicapidae	*Ficedula albicilla*	Taiga Flycatcher	6	0.20	0.40	0.00	0.20	0.00
Nectarinidae	*Nectarinia asiatica*	Purple Sunbird	10	0.30	0.00	2.00	0.00	0.00
Pandionidae	*Pandion haliaetus*	Osprey	2	0.10	0.00	0.20	0.00	0.20

Family	Scientific name	Common name	n	RA (%)	Site-wise RA (%)			
					BNP	NNP	RNP	SNP
Paridae	*Parus major*	Great Tit	32	1.10	0.70	2.40	0.40	1.60
Passeridae	*Passer domesticus*	House Sparrow	19	0.60	0.70	0.00	0.40	1.40
Phalacrocoracidae	*Microcarbo niger*	Little Cormorant	106	3.60	0.60	1.80	9.10	2.00
Picidae	*Chrysocolaptes guttacristatus*	Greater Flameback	1	0.00	0.00	0.00	0.10	0.00
Picidae	*Dendrocopos macei*	Fulvous-breasted Woodpecker	6	0.20	0.00	0.00	0.00	1.20
Picidae	*Dinopium benghalense*	Black-rumped Flameback	27	0.90	0.70	0.00	1.00	2.00
Picidae	*Picus xanthopygaeus*	Streak-throated Woodpecker	6	0.20	0.00	0.00	0.00	1.20
Ploceidae	*Ploceus philippinus*	Baya Weaver	10	0.30	0.00	1.00	0.00	1.00
Pycnonotidae	*Pycnonotus cafer*	Red-vented Bulbul	71	2.40	0.80	0.00	3.80	5.70
Rallidae	*Amaurornis phoenicurus*	White-breasted Waterhen	9	0.30	0.40	1.00	0.00	0.00
Scolopacidae	*Actitis hypoleucos*	Common Sandpiper	1	0.00	0.00	0.20	0.00	0.00
Scolopacidae	*Calidris minuta*	Little Stint	2	0.10	0.00	0.40	0.00	0.00
Scolopacidae	*Calidris temminckii*	Temminck's Stint	5	0.20	0.00	0.00	0.60	0.00
Scolopacidae	*Gallinago gallinago*	Common Snipe	2	0.10	0.00	0.40	0.00	0.00
Scolopacidae	*Gallinago stenura*	Pin-tailed Snipe	1	0.00	0.00	0.00	0.10	0.00
Scolopacidae	*Tringa ochropus*	Green Sandpiper	1	0.00	0.00	0.20	0.00	0.00
Sturnidae	*Acridotheres fuscus*	Jungle Myna	9	0.30	0.50	0.00	0.40	0.00
Sturnidae	*Acridotheres tristis*	Common Myna	25	0.80	1.00	0.00	1.60	0.00
Sturnidae	*Acridotheres ginginianus*	Bank Myna	5	0.20	0.20	0.60	0.00	0.00
Sturnidae	*Sturnus malabaricus*	Chestnut-tailed Starling	68	2.30	2.70	3.60	2.40	0.00
Sturnidae	*Sturnus contra*	Asian Pied Starling	210	7.10	2.30	18.50	5.40	8.99
Sylvidae	*Acrocephalus dumetorum*	Blyth's Reed-warbler	1	0.00	0.00	0.00	0.00	0.20
Sylvidae	*Acrocephalus stentoreus*	Clamorous Reedwarbler	1	0.00	0.10	0.00	0.00	0.00
Sylvidae	*Megalurus palustris*	Striated Grassbird	2	0.10	0.00	0.40	0.00	0.00
Sylvidae	*Orthotomus sutorius*	Common Tailorbird	34	1.10	0.90	3.20	0.00	1.60
Sylvidae	*Phylloscopus fuscatus*	Dusky Warbler	4	0.10	0.10	0.00	0.20	0.20
Sylvidae	*Phylloscopus trochiloides*	Greenish Warbler	1	0.00	0.00	0.00	0.00	0.20
Timalidae	*Malacocincla abbotti*	Abbott's Babbler	10	0.30	0.30	0.00	0.00	1.40
Timalidae	*Turdoides striata*	Jungle Babbler	146	4.90	3.00	7.60	4.80	6.70
Turdidae	*Zoothera citrina*	Orange-headed Thrush	6	0.20	0.00	1.20	0.00	0.00
Turdidae	*Zoothera dauma*	Eurasian Scaly Thrush	1	0.00	0.00	0.00	0.00	0.20
Class: Mammalia								
Canidae	*Canis aureus*	Golden Jackal	9	0.30	0.30	0.00	0.40	0.40
Canidae	*Vulpes bengalensis*	Bengal Fox	11	0.40	0.30	0.00	0.00	1.60
Cercopithecidae	*Macaca mulatta*	Rhesus Macaque	4	0.10	0.20	0.00	0.00	0.40
Felidae	*Prionailurus viverrinus*	Fishing Cat	1	0.00	0.00	0.00	0.00	0.20
Megadermatidae	*Megaderma lyra*	Greater False Vampire	2	0.10	0.00	0.00	0.20	0.00
Muridae	*Bandicota bengalensis*	Lesser Bandicoot Rat	1	0.00	0.00	0.00	0.00	0.20
Muridae	*Bandicota indica*	Large Bandicoot Rat	2	0.10	0.00	0.00	0.20	0.00
Muridae	*Mus musculus*	House Mouse	1	0.00	0.00	0.00	0.10	0.00
Pteropodidae	*Pteropus giganteus*	Indian Flying Fox	11	0.40	0.60	0.00	0.00	0.80
Sciuridae	*Funambulus pennantii*	Five-striped Palm Squirrel	8	0.30	0.00	1.60	0.00	0.00

Abbreviations: n = number of individuals; RA = Relative Abundance; BNP = Birganj National Park; NNP = Nawabganj National Park; RNP = Ramsagar National Park; SNP = Singra National Park.

In discussion, wildlife is an essential indicator of ecosystem health and habitat heterogeneity (Pomeroy, 1992; Gonzalez-Gajardo et al., 2009; Lorenzón et al., 2016). It is frequently utilized in conservation planning and monitoring efforts (Kandel et al., 2018; Woldemariam et al., 2018; Priambodo et al., 2019), and serves as a crucial measure of habitat significance as the number of species and individuals present in a given area can provide valuable insights into potential biological hotspots that require conservation efforts (Mengesha and Bekele, 2008). Therefore, effective conservation efforts in biological hotspots and protected areas necessitate continuous monitoring of the wildlife community and identification of potential threats.

The current study provides valuable baseline data on wildlife that can lay the foundation for future monitoring efforts. The study by Rimi et al. (2013) revealed the presence of 38 birds and miscellaneous fauna in Ramsagar National Park, while Ali et al. (2020) documented 28 animal species in Singra National Park. In comparison, the current study recorded 159 species, indicating sampling gaps in prior research. To evaluate patterns of vertebrate diversity at alpha and beta levels, this study examined species richness, composition, and abundance within and between study sites and microhabitats. The results indicate that the highest species diversity was observed in Ramsagar National Park and Singra National Park. Ramsagar National Park, characterized by a large water body and dense vegetation, serves as an essential stopover and wintering ground for numerous migratory waterbird species, including Greylag Goose (*Anser anser*), as previously reported by Rimi et al. (2013). Additionally, we observed another migratory bird, Gargeny (*Spatula querquedula*), from the study site. On the other hand, Singra National Park, with its dense vegetation and forest patches containing various tree species, provides suitable habitat for wildlife species (Ali et al., 2020; Rabbe et al., 2022a). The large water body in Ramsagar National Park is enriched with benthic organisms, mollusks, crustaceans, and freshwater worms (Rimi et al., 2013), which serve as adequate food sources for many waterbird species. As a result, species such as *Dendrocygna javanica* (RA=40.30%, n=360) and *Microcarbo niger* (RA=9.10%, n=106) were found to be the most dominant. These species created an uneven wildlife community in Ramsagar National Park. In Singra National Park, however, there wasn't any single dominant species, and the species community was also evenly distributed according to Pielou's evenness (J=0.9±0.01) and Whittaker's Plot (Fig. 5). The most relatively abundant species in Singra National Park were *Sturnus contra* (RA=8.99%, n=44), *Euphlyctis cyanophlyctis* (RA=7.6%, n=37), and *Turdoides striata* (RA=6.7%, n=33). The Whittaker plot also showed high dominance and low evenness in the other two sites (Fig. 5). In the case of the Birganj National Park, most of the forest areas have been encroached on and turned into agricultural land for farming (Rahman et al., 2022). Thus, most amphibian species were observed near the agricultural fields (RA=41.82%) and nearby waterbodies used specially for breeding during this study. The most dominant species in this site were *Euphlyctis cyanophlyctis* (RA=36.5%, n=395) and *Euphlyctis kalasgramensis* (RA=23.20%, n=251). Finally, Nawabganj National Park, which had a similar habitat heterogeneity to the Singra National Park, didn't support any dominant species except a habitat generalist like *Sturnus contra* (RA=18.50%), and that's why the wildlife community was more evenly distributed compared to Ramsagar National Park and Nawabganj National Park.

Seasonal changes have been found to impact avian diversity significantly (Canepuccia et al., 2007; Neelgund and Kadadevaru, 2020), largely due to seasonal migrations that alter the composition of wildlife communities within a given study area. In addition, the foraging behavior of different avian species is also influenced by seasonal changes; insectivorous birds tend to consume more insects, fruit-eating birds forage for fruit, and nectar-feeding birds seek out nectar from blooming flowers during the winter season (Khan, 2015). Across all four study

sites, the number of observed species and Margalef species richness significantly increased during the winter, largely due to the influx of migratory birds to the study area. This pattern is consistent with findings from other studies conducted in various parts of Bangladesh, where species richness has been shown to increase during the winter months (Jaman et al., 2015; 2022; Saha et al., 2022) due to the presence of migratory birds, from both Central Asian and East Asia/Australasia flyways. Conversely, species richness decreased during the warmer months as migratory waterbirds left the area.

Based on the Analysis of Similarity (ANOSIM) performed on the study sites, significant differences were observed among the wildlife communities of all sites. Differences in habitat heterogeneity, microhabitats, and resource availability typically contribute to variations in wildlife communities (Jaman et al., 2022; Saha et al., 2022). However, since the four studied national parks are closely located and exhibit similar habitat structures and patches, the occupying wildlife communities were found to be not significantly different from one another in pairwise comparison.

The primary factors contributing to the loss of biodiversity are habitat degradation, including changes in land use, the conversion of agricultural lands, the priority of alien invasive species, urbanization, the expansion of road networks, and unplanned development (Khan, 2015). Most ecosystems have been harmed by artificial activities like embankments, overuse of resources, such as unauthorized fishing, illegal logging, encroachment, hunting, indiscriminate removal of non-timber forest products, and environmental pollution (IUCN Bangladesh, 2015). During the study period, some threats were identified in the study areas, like deforestation and anthropogenic developments in Singra National Park, agricultural expansion in Birganj National Park and Nawabganj National Park, and lastly, Sound and Water pollution in Ramsagar National Park. As these study sites harbor one near-threatened (*Hoplobatrachus crassus*), two vulnerable (*Vulpes bengalensis* and *Macaca mulatta*), and one endangered (*Prionailurus viverrinus*) species, it is crucial to implement appropriate conservation measures to minimize these perceived threats and protect these vibrant and diverse protected forests.

Conclusions

The present study provides valuable information on the diversity of vertebrate wildlife in four protected national parks in Bangladesh, which can serve as baseline data for future wildlife conservation efforts. The study examined these species' alpha and beta diversity patterns across different study sites and microhabitats. Human intrusion was identified as a major anthropogenic stressor that might threaten the species community in these protected areas. However, further research is needed to comprehend the full impact of these stressors. The study's results hold significant implications for future biodiversity surveys, monitoring programs, and the development a comprehensive management plan for the conservation of wildlife communities in these four national parks.

Acknowledgments

The authors are grateful to the Chairman of Zoology, University of Dhaka, for allocating space while conducting this research. The authors are also thankful to some anonymous volunteers of the Department of Zoology, University of Dhaka, and some local guides for their contribution to the field, particularly during data collection. The authors also thank the University of Dhaka authority. This work was financed by the “Centennial Research Grants” University of Dhaka, Bangladesh.

References

Akter F, Bashar MN, Rahman MA, Sultana MN, Rashid HA, Rahman MA and Aziz MA. Ecology of Bengal fox (*Vulpes Bengalensis*) in Northwest Bangladesh. *Bangladesh J. Zool.* 2023; 51(1): 35-45.

Alam M, Furukawa Y, Sarker SK and Ahmed R. Sustainability of Sal (*Shorea robusta*) forest in Bangladesh: past, present and future actions. *Int. For. Rev.* 2008; 10: 29-37.

Ali MM, Akter N, Kabir MR, Hasan MM, Rahman MM and Bari MS. The Biodiversity status and conservation activities of singra National Park (SNP) in the link of co-management strategy. *Int. J. Environ.* 2020; 10(10): 136-146.

Barkat AI, Liza FT, Akter S, Shome AR and Rabbe MF. Wildlife hunting practices of the *Santal* and *Oraon* communities in Rajshahi, Bangladesh. *J. Threat. Taxa.* 2021; 13(11): 19484-19491.

Canepuccia AD, Isacch JP, Gagliardini DA, Escalante AH and Iribarne OO. Waterbird response to changes in habitat area and diversity generated by rainfall in a SW Atlantic coastal lagoon. *Waterbirds.* 2007; 30(4): 541-553.

DoF. Department of Forest, Dinajpur. https://forest.dinajpur.gov.bd/. Accessed on 2 June 2023.

Everitt BS, Landau C, Leese M and Stahl D. Cluster analysis. 5th ed. Balding DJ, Cressie NAC, Fitzmaurice GM, Goldstein H, Molenberghs G, Scott D W, Smith AFM, Tsay RS, Weisberg S, eds., John Wiley & Sons, 2011.

González-Gajardo A, Sepúlveda PV and Schlatter R. Waterbird assemblages and habitat characteristics in wetlands: Influence of temporal variability on species-habitat relationships. *Waterbirds*. 2009; 32(2): 225-233.

Hammer Ø, Harper DAT and Ryan PD. PAST: Palaeontological Statistics software package for education and data analysis. *Palaeontologia Electronica.* 2001; 4: 1-9.

Haque N. Depletion of tropical forests with particular reference to Bangladesh. *Our Nature.* 2007; 8: 313-3321.

IUCN Bangladesh. Red List of Bangladesh, Volume 1-4: Reptiles and Amphibians, Aves, Mammals. IUCN, International Union for Conservation of Nature, Bangladesh Country Office, Dhaka, Bangladesh. 2015.

Jaman MF, Alam MM, Shome AR, Saha A, Rabbe M, Rana M and Rahman M. Diversity and community structure of wild vertebrates in the Sandwip Island of Bangladesh. *Trop. Ecol.* 2022; 64: 224-237

Jaman MF, Rabbe MF, Alam MM, Shome AR, Hossain MA and Sarker MAR. Students' perceptions on snake in Northwestern Bangladesh. Asian J. Ethnobiol. 2020; 3(2): 62-69.

Jaman MF, Sarker AR, Alam MM, Rahman M, Rabbe F, Rana AS, Shome AR and Hossain S. Species diversity, distribution and habitat utilization of urban wildlife in a megacity of Bangladesh. *Biodiver. J.* 2021; 12(3): 635-653.

Jaman MF, Uddin MM, Alam MM, Rahman MM, Khatun MT and Alam SMI. Species diversity and population status of wildlife in Keshabpur, Bangladesh.*J.Biodivers.Conserv. Bioresour. Manag.* 2015; 1(2): 9-21.

Kabir DS and Ahmed AZ. Wildlife biodiversity in Bhawal National Park: Management techniques and drawbacks of wildlife management and nature conservation. *Our Nature.* 2005; 3(1): 83-90.

Kandel P, ThapaI, Chettri N, Pradhan R and Sharma E. Birds of the Kangchenjunga Landscape, the Eastern Himalaya: Status, threats and implications for conservation. *Avian Res.* 2018; 9(9): 1-13.

Khan MAR. Wildlife of Bangladesh: checklist and guide. Chyabithi, Dhaka, Bangladesh. 2015.

Khan MMH. Photographic guide to the wildlife of Bangladesh. Arannayk Foundation, Dhaka, Bangladesh. 2018.

Lorenzón RE, Beltzer AH, Olguin PF and Ronchi-Virgolini, AL. Habitat heterogeneity drives bird species richness, nestedness and habitat selection by individual species in fluvial wetlands of the Paraná River, Argentina. *Austral. Ecol.* 2016; 41(7): 829-841.

Magurran AE. Measuring biological diversity.1st ed. *Blackwell Science*. 2013.

Mengesha G and Bekele A. Diversity and relative abundance of birds of Alatish National Park, North Gondar, Ethiopia. *Int. J. Ecol. Environ. Sci.* 2008; 34(2): 215-222.

Neelgund HD and Kadadevaru G. Avifaunal diversity of some selected water bodies of Khanapur Taluka, Belagavi District, Karnataka, India. *J. Threat. Taxa*. 2020; 12(5): 15572-15586.

Oksanen J, Blanchet FG, Friendly M, Kindt R, Legendre P, McGlinn D, Minchin PR, O'Hara RB, Simpson GL, Solymos P, Stevens MHM, Szoecs E and Wagner H. Vegan: Community ecology package, R Package Version 2.5-6. 2019.

Pomeroy D. Countng Birds: A guide to assessing numbers, biomass and diversity of Afrotropical birds. *African Wildlife Foundation*. 1992.

Priambodo B, Permana H, Akhsani F, Indriwati, SE, Wangkulangkul S, Lestari SR and Rohman F. Characteristic of water sources in Malang, based on the diversity, community structure, and the role of herpetofauna as bioindicator. *Eurasian J. Bio. Sci*. 2019; 13(2): 2279-2283.

R Core Team. R: A language and environment for statistical computing. Vienna, Austria: R Foundation for Statistical Computing. 2020.

Rabbe MF, Jaman MF, Alam MM, Rahman MM and Sarker MAR. Species diversity, composition, and distribution of the herpetofauna in the Northwestern region of Bangladesh. *Amphib. Reptile Conserv*. 2022a; 16(1): 226-234.

Rabbe MF, Jaman MF, Alam MM, Rahman MM, Sarker MAR and Jamee AR. Human perceptions toward herpetofauna in Northwestern Bangladesh. A*mphib. Reptile Conserv*. 2022b; 15(2): 210-227.

Rabbe MF, Mohammad N, Roy D, Roy D, Jaman MF and Naser MN. A rapid survey of herpetofaunal diversity in Nijhum Dwip National Park, Bangladesh. *Reptil. Amphib*. 2022c; 29(1): 9-16.

Rahman N, Sultana M, Rahman MS, Islam KK, Hoque MA and Saqee A. Floral composition of Birgonj National Park in Dinajpur district, Bangladesh. *Bull. Bangladesh National Herb.* 2022; 8: 77-91.

Rimi RH, Rahman F and Latif MB. Biodiversity status and its management at ramsagar National Park at Dinajpur in Bangladesh. *Int. J. Environ. Sci Nat. Resour*. 2013; 6(1): 21-32.

Saha A, Alam MM, Jaman MF, Saha N and Rahman MM. Avian community structure in human dominated landscape in Daudkandi, Bangladesh. *Community Ecol*. 2022; 310-313.

Shome AR, Jaman MF, Rabbe MF, Barkat AI, and Alam MM. New distribution record of *Rhabdophis subminiatus* (Schlegel, 1837; Squamata, Colubridae) from Madhupur National Park, Tangail, Bangladesh. *Herpetol. Notes*. 2020; 13: 549-551.

Shome AR, Alam MM, Rabbe MF, Mia T, Munira S, Ilma UH and Jaman MF. Ecology of Avifauna in Green Spaces of a Sub-Tropical Urban Landscape: Community Structure and Habitat Preference. *J. Biodivers. Conserv. Bioresour. Manag.* 2022a; 8(2): 37-50.

Shome AR, Jaman MF, Rabbe MF and Alam MM. Bird diversity, composition and response during COVID-19 in an urban landscape, Jamalpur, Bangladesh. *Dhaka Univ. J. Biol. Sci.* 2021; 30(2): 261-274.

Shome AR, Rabbe MFM, Alam M, Emon SF, Islam MM, Setu RS, Khan N, Biswas D and Jaman MF. Avifauna in an urban landscape of a lower Ganges district, Bangladesh: Community structure, seasonality, habitat preference and conservation issues. *Dhaka Univ. J. Biol. Sci.* 2022b; 31(2): 261-274.

Whittaker RH. Dominance and diversity in land plant com-munities numerical relations of species express the importance of competition in community function and evolution. *Science*. 1965; 147: 250-260.

Wickham H. *ggplot2 Elegant Graphics for Data Analysis*. Springer. 2016.

Woldemariam W, Mekonnen T, Morrison K and Aticho A. Assessment of wetland fora and avifauna species diversity in Kafa Zone, Southwestern Ethiopia. *J. Asia-Pac. Biodivers.* 2018; 11(4): 494-502.

Yallop ML, O'Connell MJ and Bullock R. Waterbird herbivory on a newly created wetland complex: potential implications for site management and habitat creation. *Wetl. Ecol. Manag*. 2004; 12(5): 395-408.

J. Bangladesh Acad. Sci. 47(2); 267-275: December 2023 DOI:https://doi.org/10.3329/jbas.v47i2.66872

Journal of Bangladesh Academy of Sciences

Journal homepage: http://www.bas.org.bd/publications/jbas.html

Research Article

Speciation of Cr(III) and Cr(VI) in aqueous solution and their removal by oyster mushroom biomass

M. N. M. Asif, Rashedul Islam, M. A. Goni[1], Sumon Ganguli[2], Ashok Kumar Chakraborty[3], Mahbub Kabir, and Md Abdus Sabur[*]

Department of Chemistry, Jahangirnagar University, Savar, Dhaka, Bangladesh

ARTICLE INFO

Article History

Received: 13 June 2023
Revised: 12 November 2023
Accepted: 14 November 2023

Keywords: Biosorption, Chromium removal, Adsorption isotherms, pH envelope.

ABSTRACT

This study investigates the effectiveness of oyster mushroom (*Pleurotus platypus*) for the removal of Cr(III) and Cr(VI) from aqueous solutions by conducting a series of batch adsorption experiments. Results from the adsorption pH envelope experiments show that while the adsorption of Cr(III) increases with increasing pH, the adsorption of Cr(VI) decreases as the pH rises. These two distinct pH envelope patterns for Cr(III) and Cr(VI) suggest that the adsorption processes are primarily driven by the electrostatic force of attractions followed by the ligand exchange process. Findings from the adsorption isotherm experiments demonstrate that chromium binding to the adsorbent surface is better described by the Freundlich model than the Langmuir model, underscoring the presence of multiple surface binding sites. The study highlights the significance of identifying dominant chromium species before they are subjected to adsorptive removal from contaminated waters.

Introduction

Heavy metals generally enter natural environments (e.g., water and soil) by weathering rocks and minerals (Bradl, 2005; Finlay et al., 2019). Nevertheless, anthropogenic activities including mining, smelting, combustion of fossil fuel, and the improper discharge of untreated industrial wastes can lead to excessive metal presence in various environmental compartments (Bradl, 2005; Wuana and Okieimen, 2011). Once heavy metals enter natural systems, the system's recovery becomes challenging, often relying on natural attenuation for restoration. Generally, organic and inorganic wastes often contaminate natural environments near industrial sites (Khan et al., 2011; Rahman et al., 2014). Therefore, reusing treated water is another option for reducing environmental pollution.

Conventional water treatment methods commonly used to remove heavy metals from contaminated waters include reverse osmosis, ion exchange, membrane filtration, electro-dialysis etc. (Azimi et al., 2017; Carolin et al., 2017). While ion exchange and membrane filtration methods are highly effective, they are costly and often impractical for commercial use. An alternative approach is the coagulation-precipitation method, which can effectively remove organic and inorganic pollutants from contaminated water. This method offers relative affordability and ease of design but may generate a substantial volume of sludge. Additionally, metal ions from contaminated waters can be successfully removed by adsorption filtration techniques (Bhatnagar and Sillanpää, 2010; Bhatti et al., 2007; Kumari et al., 2006; Nuhoglu et al., 2002; Reddy et al., 2011, 2010; Say et al., 2001; Vimala and Das, 2009).

[*]Corresponding author: <sabur@juniv.edu>

[1]*Department of Chemistry, Bangladesh University of Engineering and Technology, Dhaka, Bangladesh*

[2]*Department of Applied Chemistry and Chemical Engineering, University of Chittagong, Chittagong, Bangladesh*

[3]*Department of Applied Chemistry and Chemical Engineering, Islamic University, Khustia, Bangladesh*

Besides the typical chemical adsorption methods, biosorption has emerged as an attractive and viable alternative for mitigating environmental pollution from industrial wastewater (Alluri et al., 2007; Bhatnagar and Sillanpää, 2010; Kanamarlapudi et al., 2018; Say et al., 2001). Typical biosorbents consist of lignin, cellulose, and proteins with various surface functional groups such as hydroxyl, carboxyl, and amide (Shakoor et al., 2019). The presence of these functional groups on the surface of biological materials determines the potential binding capacity of biosorbents with a wide range of chemical contaminants, including cations and anions. Over the past two decades, numerous biosorbents have been investigated for their effectiveness in the removal of heavy metals from aqueous wastes (Alluri et al., 2007; Bhatnagar and Sillanpää, 2010; Kanamarlapudi et al., 2018; Say et al., 2001). Compared to other bio-sorbents, mushroom powder has demonstrated promise and effectiveness in removing pollutants from diverse sources (Das, 2005; Mathialagan et al., 2003; Prasad and Sachin, 2013; Vimala and Das, 2009).

Previous studies have extensively examined the capabilities of common biosorbents in removing chromium and other heavy metals (Gupta et al., 2011; Kanamarlapudi et al., 2018; Michalak et al., 2013; Sag and Kutsal, 2001; Vimala and Das, 2009). However, mechanisms governing the binding of both cationic and anionic chromium to the mushroom surface remain relatively unexplored (Chen et al., 2005; Das, 2005; Ertugay and Bayhan, 2008; Jing et al., 2011; Kanamarlapudi et al., 2018; Suseem and Mary Saral, 2014). Here, we use ground mushroom biomass to evaluate the potential mechanisms and optimal conditions for the adsorptive removal of Cr(III) and Cr(VI) using batch adsorption experiments. This study highlights the significance of understanding chromium speciation before their adsorptive removal from contaminated waters.

Materials and Methods

Preparation of biosorbent

Fruit bodies of oyster mushrooms (*Pleurotus platypus*) were collected from the National Mushroom Development and Extension Centre, Savar, Bangladesh. Mushrooms were washed thoroughly with deionized water to remove the dirt and other undesirable materials. Subsequently, the mushrooms were turned into smaller pieces and dried in an oven at 80 °C for 24 h. After drying, the fruit bodies were finely ground using a mortar and pestle.

Preparation of stock solution

Individual stock solutions of 1000 mM of Cr(III) and Cr(VI) were prepared separately by dissolving the solid powder of $CrCl_3$ (Merck, India, 158.35 g/mol) and $K_2Cr_2O_7$ (Guangdong Guanghua Chemical Factory Co, Ltd, China, 294.185 g/mol), respectively, in deionized water. The solutions were subsequently diluted to the appropriate concentrations based on the type of adsorption experiments.

Adsorption experiment

Batch adsorption experiments were conducted in Cr(III) or Cr(VI) solutions containing solid mushroom powder at 28±1°C on an orbital shaker. The effect of pH on the adsorption of chromium to adsorbent was investigated within the pH range from 2.0 to 8.0. Before starting the adsorption pH envelope experiment, pH in the chromium solutions (0.2 mM) was adjusted between pH 2.0 and 8.0 using HCl and NaOH solutions. The chromium solutions (100 mL each) with suitable pH adjustment were then equilibrated separately with the adsorbent (1.0 g/L) for 6 h in reagent bottles.

Kinetic studies for the adsorption of chromium with the adsorbent were conducted. Solutions of both chromium species (0.2 mM each) were agitated with the adsorbent (1.0 g/L) in six individual reactors. This experiment's initial pH (before adsorption) was adjusted separately for each chromium species based on the maximum adsorption pH condition, as revealed from the adsorption pH envelope experiment. The reactors were sacrificially removed at 10, 20, 30, 60, 120, 180, 240, and 300 min, respectively.

The effects of initial chromium concentrations (0.2 to 2 mM) for chromium adsorption on the mushroom surface were conducted for 180 min. The initial pH levels (before adsorption) for assessing the effect of adsorbent dosages and the initial concentrations were adjusted separately based on the maximum adsorption pH condition obtained from the pH envelope and adsorption kinetic studies.

After the adsorption experiments, the suspension samples from each reactor were filtered using 0.45 µM (Whatman) filter paper, and the filtrate was stored at 4 °C until analysis. Chromium concentrations in the samples were determined using atomic absorption spectroscopy before and after each adsorption experiment (AA-7000, Shimadzu, Japan) equipped with air acetylene flame. The adsorption data are presented in terms of surface coverage and removal percentage. The surface coverage (θ) by Cr(III) and Cr(VI) is estimated from the difference between the initial (C_0) and final (Ce) concentration of chromium and the amount of adsorbent (in grams) used in the adsorption experiments.

Results and discussion

Adsorption pH envelope

The effect of initial pH (before adsorption) on the adsorption of both Cr(III) and Cr(VI) onto the mushroom surface was evaluated within the pH range of 2.0 to 8.0. pH plays a vital role in determining the degree of ionization of sorbates, influencing the speciation of sorbent surfaces, and affecting the solubility of metal ions (Langmuir, 1997; Michalak et al., 2013). For instance, the adsorption of anions generally decreases with increasing pH, although the adsorption pH envelope depends on the sorbent's point of zero charge (PZC). Conversely, the adsorption characteristics of cations grow with increasing solution pH (Langmuir, 1997; Sabur, 2019). The calculation of aqueous speciation for Cr(III) and Cr(VI) relies on the reactions and their respective constants listed in Table 1, which are comparable to those documented in existing literature (Papassiopi et al., 2014; Szabó et al., 2018). Aqueous speciation of Cr(III) and Cr(VI) are computed by PHREEQC 3 (Parkhurst and Appelo, 2013) with the minteq.dat database (Fig. 1).

Table 1. Cr(III) and Cr(VI) speciation reactions and the corresponding reaction constants at 25 °C used to construct Fig. 1.

Species	Reaction	logK
Cr(III)	$Cr(OH)_2+ + 2H+ = Cr^{3+} + 2H_2O$	9.84
	$Cr(OH)_2^+ + H+ = Cr(OH)^{2+} + H_2O$	6.27
	$Cr(OH)^{2+} + H_2O = Cr(OH)_3 + H+$	-7.36
	$Cr(OH)^{2+} + 2H2O = Cr(OH)4- + 2H+$	-16.18
	$Cr(OH)^{2+} = CrO2- + 2H+$	-17.74
Cr(VI)	$CrO_4^{2-} + H^+ = HCrO^{4-}$	6.51
	$CrO4^{2-} + 2H^+ = H_2CrO_4$	5.65
	$2CrO4^{2-} + 2H^+ = Cr_2O_7^{2-} + H_2O$	14.56

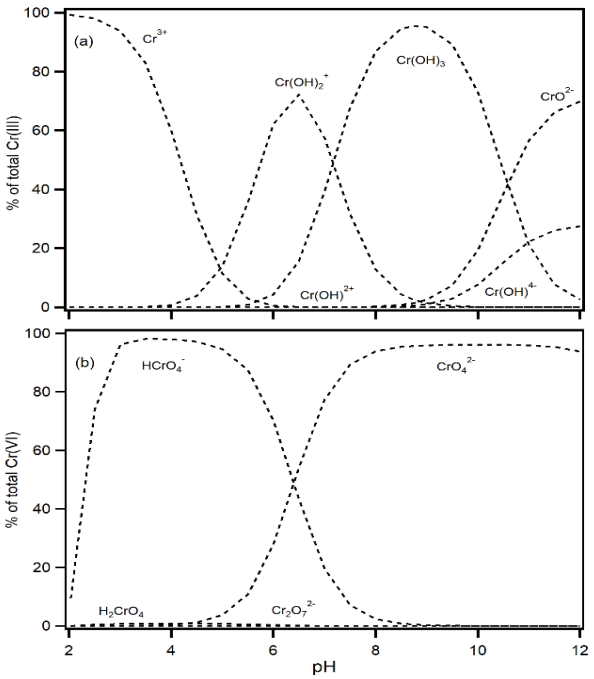

Fig. 1. The speciation of Cr(III) (a) and Cr(VI) (b) in aqueous solutions as a function of pH at 25°C. The speciation diagrams were constructed using 0.2 mM solutions of $CrCl_3$ and K_2CrO_7 for Cr(III) and Cr(VI), respectively. The diagrams were generated with the PHREEQC 3 computer program, incorporating reaction constants from the minteq.dat database, consistent with previous studies (Papassiopi et al., 2014; Szabó et al., 2018).

In an aqueous solution of $CrCl_3$, Cr^{3+} undergoes hydrolysis, and the hydrolytic products of chromium mostly exist as cations within the pH range of 2.0 to 8.0 (Fig. 1a). However, under alkaline conditions, typically above pH 8.0, the hydrolyzed product of Cr^{3+} transforms into negatively charged $Cr(OH)^{4-}$. When potassium dichromate ($K_2Cr_2O_7$) is dissolved in water, it forms several stable ions (Fig. 1b) contingent upon the concentration and pH in the solution. Notably, $HCrO_4^-$ predominates under acidic conditions, while CrO_4^{2-} prevails under alkaline conditions. $K_2Cr_2O_7$ can also generate $Cr_2O_7^{2-}$, however, the presence of this ion may be insignificant in our experimental system based on the concentration range used in the adsorption pH envelope experiments.

Fig. 2 shows the results of the adsorption pH isotherm studies reveal that the adsorption of chromium (III) on mushroom surface increases as the initial pH of the solution rises (Fig. 2). A similar adsorption isotherm pattern was found in the adsorption of Cr(III) on lichen biomass (Uluozlu et al., 2008) and is consistent with the adsorption of other metal cations on mushroom surface (Ertugay and Bayhan, 2010; Vimala and Das, 2009). Cr(III) ions exist primarily as positively charged ions with free Cr^{3+} ions or as hydrated Cr^{3+} ions with coordinated hydroxyl groups (OH^-) in aqueous solutions. Therefore, the speciation of the Cr(III) ion changes with the variation of pH in the solutions due to the changing coordination states of the metal ion (Fig. 1b). Increasing pH (e.g., increasing OH^- ion concentration) in the solution initially results in the neutralization of the positive charge carried by the Cr^{3+} ion. Subsequent rise of pH results in the negative charge buildup on the metal ion, primarily due to the binding of negatively charged OH^- groups.

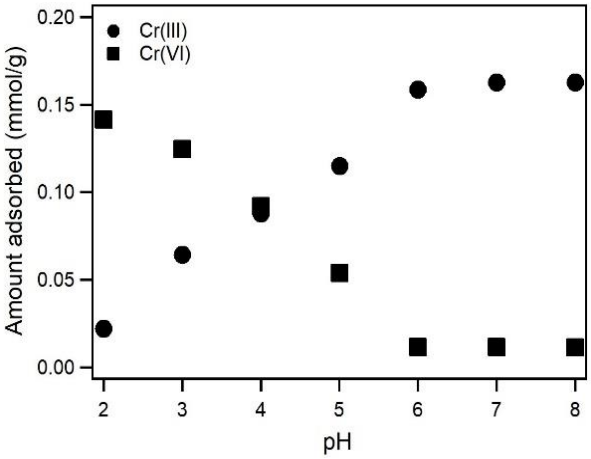

Fig. 2. Effect of pH on Cr(III) and Cr(VI) adsorption on the mushroom surface.

The predominant functional groups found in the typical biosorbents are hydroxyl, carboxylic acid, and amide (Shakoor et al., 2019). These functional groups at the surface may undergo acid-base reactions and can transform the biosorbent's surfaces with a negative charge under alkaline conditions (Michalak et al., 2013). The positively charged Cr(III) ions experience a greater electrostatic attraction with the solid surface, and this attraction increases with increasing pH, enhancing Cr(III) removal from the aqueous solution. Apart from the adsorptive removal of cationic chromium species, chromium removal from the aqueous phase might also occur via Cr(OH)3 precipitation on the adsorbent surface (Guimarães et al., 2020). The later process will likely be thermodynamically favorable at near neutral to alkaline conditions with increasing solution pH, e.g., pH > 6.0 (Fig. 1a).

The maximum adsorption for Cr(VI) was observed under strongly acidic conditions, followed by a sharp decline as the pH increased further (Fig. 2). This trend is consistent with prior research, including studies involving surfactant-modified mushroom and other biosorbents (Fernández-López et al., 2014; Jing et al., 2011). Additionally, Cr(VI) adsorption becomes minimal at or above a pH of approximately 6.0. This phenomenon can be

elucidated by the fact that Cr(VI) primarily exists as negatively charged chromate ions ($HCrO_4^-$ and CrO_4^{2-}) under the specified experimental conditions (Fig. 1b).

As the pH shifts from acidic to alkaline conditions, there is a notable increase in the concentration of singly deprotonated chromate species ($HCrO_4^-$), leading to the formation of CrO_4^{2-} (Fig. 1b). Therefore, the limited adsorption Cr(VI) at or above the pH 6.0 suggest that the adsorption of $HCrO_4^-$ on the mushroom surface primarily occurred from pH 2.0 to 6.0. The sharp decrease of Cr(VI) adsorption with further pH elevation beyond 6.0 implies that the mushroom surface undergoes a negative charge modification, likely attributed to either the deprotonation of the surface-active groups or the adsorption of hydroxyl (OH^-) groups onto the solid surface. These findings collectively suggest that an increase in solution pH leads to the deduction in electrostatic attraction between the deprotonated chromate ion (CrO_4^{2-}) and the negatively charged surface, resulting in diminished Cr(VI) adsorption onto the solid surface.

Effect of equilibrium time

Kinetic studies for the adsorption of Cr(III) and Cr(VI) are conducted using identical concentrations (0.2 mM each) and fixed chromium solution volume (100 mL). The amount of adsorbent also remained the same, with the only variation being the pH levels, set at 6.5 and 2.0 for Cr(III) and 2.0 for Cr(VI). Results show that the adsorption of Cr(III) and Cr(VI) progressively increases as the equilibration time lengthens (Fig. 3). The removal of chromium occurs rapidly, mostly within 100 min of the adsorption period. This rapid adsorption may be attributed to the higher availability of surface binding sites on the biomass. However, the adsorption rate gradually diminishes as the equilibration time extends. This deceleration in adsorption suggests a potential depletion of surface-active sites due to the continued adsorption process.

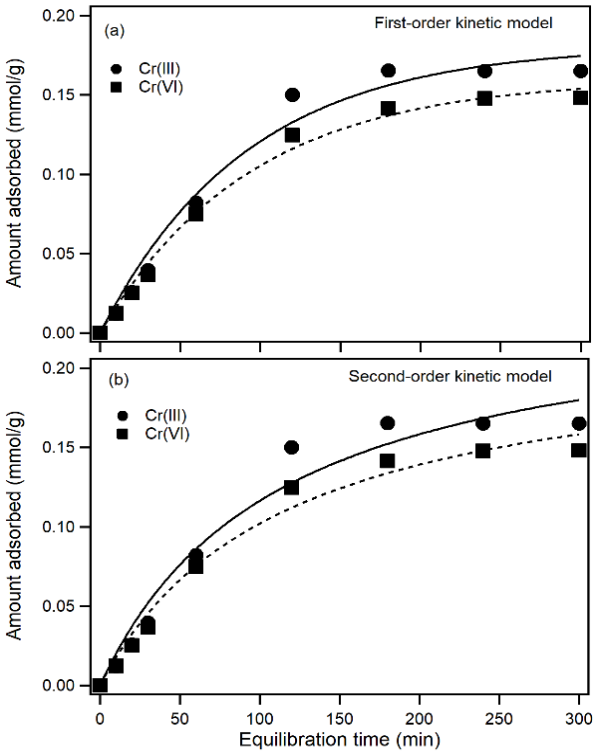

Fig. 3. The kinetic data (symbol) for the adsorption of Cr(III) and Cr(VI) on the mushroom surface. The dotted solid and dotted lines represent simulated kinetic data for Cr(III) and Cr(VI), respectively, according to the pseudo-first-order (a) and second-order (b) kinetic models.

Adsorption kinetic data are often fitted to first and second-order kinetic models to gain insights into the adsorption mechanism. Kinetic parameters for the adsorption of Cr(III) and Cr(VI) are extracted by fitting the experimental data using first and second-order adsorption kinetic models. The mathematical representation of pseudo first and second-order adsorption kinetics (Lima et al., 2015) can be expressed by Equation 1 and Equation 2.

$$\theta(t) = \theta(1 - e^{-k_1 \cdot t}) \quad \ldots\ldots\ldots\ldots\ldots\ldots\ldots\ldots\ldots\ldots\ldots\ldots \quad (1)$$

$$\theta(t) = \frac{k_2 \theta t}{1 + k\theta t} \quad \ldots\ldots\ldots\ldots\ldots\ldots\ldots\ldots\ldots\ldots\ldots\ldots \quad (2)$$

Where, $\theta(t)$ is the amount of Cr(III), or Cr(VI) sorbed onto the adsorbent surface (in mmol/g) at time t (h) with rate constants k_1 and k_2 for the first and second-order adsorption models, respectively.

Table 2. Kinetic parameters were extracted for the adsorption of Cr(III) (at pH 2.0) and Cr(VI) (at pH 6.5) by fitting the experimental data to Equation 1 and 2 with a 95% confidence limit. Chi-square (χ2) values illustrate the quality of the fit.

Species	θ (mmol/g)	*k*	χ^2
First-order			
Species	**θ (mmol/g)**	***k*** **(h^{-1})**	χ^2
Cr(III)	0.18±0.03	0.01±0.00	7.83×10^{-4}
Cr(VI)	0.16±0.01	0.01±0.00	2.35×10^{-4}
Second-order			
Species	**θ (mmol/g)**	***k*** **g/(mmol×h)**	χ^2
Cr(III)	0.25 ± 0.07	0.04 ± 0.03	1.27×10^{-3}
Cr(VI)	0.22 ± 0.04	0.04 ± 0.03	4.88×10^{-3}

Table 2 shows that the θ_1 values derived from the pseudo-first-order kinetic model for Cr(III) and Cr(VI) adsorption are aligned closely with the data point obtained at or near the equilibrium. Notably, the pseudo-second-order adsorption kinetic model estimates slightly higher θ_1 values than the measured values (Table 2). Furthermore, the pseudo-first-order kinetic model better fits the experimental data than the pseudo-second-order adsorption kinetic model, as evident from the respective chi-square values.

This result indicates the importance of available active sites on the adsorbent surface for binding both chromium species.

Effect of initial concentration

The initial concentration of sorbate, the adsorbent, and sorbate-to-adsorbent ratios play a significant role in shaping adsorption isotherm. The surface coverage increases with sorbate concentration for a given amount of sorbent. Adsorption mechanisms and the binding strength of surface species are often described in terms of Langmuir and Freundlich models (Lima et al., 2015). The Langmuir model assumes the homogeneous distribution of the surface-active sites by sorbate species, whereas the Freundlich predicts the heterogamous distribution of potentially active sites on surfaces (Lima et al., 2015). Equations 3 and 4 represent the mathematical models describing the nonlinear Langmuir and Freundlich adsorption isotherms (Langmuir, 1997; Lima et al., 2015) can be shown by Equations 3 and 4.

$$\theta = \theta_{max} \frac{K_L[A]}{1 + K_L[A]} \quad (3)$$

$$\theta = K_F * [A]^{1/n} \quad (4)$$

Where, θ in Equations 3 and 4 represents the quantity of chromium adsorbed onto the adsorbent surface (mmol/g) at a specific chromium concentration of $[A]$ and θ_{max} in Equation 3 is the maximum surface coverage of mushroom biomass by chromium. K_L and K_F denote the Langmuir and Freundlich adsorption constants, while 'n' in Equation 4 stands for the order of the surface reaction.

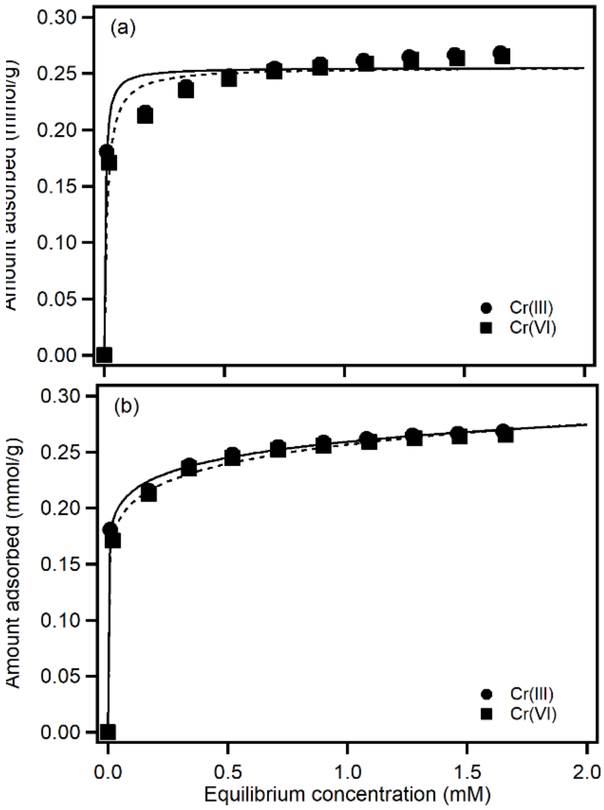

Fig. 4. Effect of initial concentration on removing Cr(III) and Cr(VI) by mushrooms. Experimental data and the predictions by Langmuir (a) and Freundlich (b) models are shown by the markers and dotted lines, respectively.

Experimental data in Fig. 4 shows that the adsorption of Cr (III) and Cr (VI) ions strongly influenced their initial concentrations. As observed in Fig. 4, the adsorption of chromium increases with rising initial chromium concentrations (Fig. 4), reaching a plateau near 0.5 mM of chromium, as anticipated. The experimental data are fitted to the Langmuir and Freundlich adsorption models in Fig. 4a and 4b, respectively, and the resulting adsorption isotherm parameters are presented in Table 3.

By comparing least square fits (chi-square values) for the experimental data, it is evident that the Freundlich adsorption model better fits the experimental data than the Langmuir model. However, the adsorption constant obtained by fitting the experimental data using the Langmuir and Freundlich models greatly depends on the experimental conditions. This implies that the values of K_L and K_F obtained from the present study cannot be compared with adsorption processes involving Cr(III) or Cr(VI) on different biosorbents, nor are they applicable to various other sorbates (e.g., lead, cadmium, arsenic, etc.) when considering the mushroom surface as the adsorbent. Even these values cannot be directly compared to the adsorption processes of Cr(III) or Cr(VI) on the same mushroom surface under different pH conditions. Notably, the values of K_L are similar for both Cr(III) and Cr(VI) adsorptions, accounting for the respective error bars (Table 3). This result indicates that the adsorption of Cr(III) and Cr(VI) to the mushroom surface occurs with similar chromium binding strengths, also reflected in K_F values (Table 3).

As discussed earlier, the values of reaction quotients for the adsorption of Cr(III) or Cr(VI) obtained by the two different adsorption models cannot be compared, but the respective chi-square values can demonstrate the relative performance of the models to explain the experimental data. Thus, the significance of adsorption constants ($K_L$and K_F) for comparing the binding strength of Cr(III) and Cr(VI) with the mushroom surface is limited, primarily because the adsorption isotherm experiments are conducted under distinct pH conditions. Nonetheless, the potential binding mechanisms can be partially elucidated for the adsorption of both Cr(III) or Cr(VI) by comparing the corresponding $K_L$and K_F values derived from the Langmuir and Freundlich models. Compared to the Langmuir model, the lower chi-square values obtained from fitting experimental data with the Freundlich model suggest that mushroom powder will likely provide multiple surface-active sites for adsorbing chromium species from aqueous solutions. The potential diffusion of chromium from the mushroom surfaces to the interior of the soil is also possible.

Table 3. Adsorption isotherm parameters were extracted by fitting the experimental data to the Langmuir (Equation 3) and Freundlich (Equation 4) adsorption models, respectively. The chi-square values (χ_c^2 = 4.87) represent the goodness of fit.

Langmuir model			
	K_L	θ_{max}	χ^2
Cr(III)	224±14	0.26±0.01	1.85×10^{-3}
Cr(VI)	88±43	0.26±0.00	1.31×10^{-3}
Freundlich model			
	K_F	n	χ^2
Cr(III)	0.26±0.00	12.22±1.25	1.03×10^{-4}
Cr(VI)	0.26±0.00	10.08±0.98	1.05×10^{-4}

Conclusion

Here, we evaluate mushroom surfaces' adsorption behavior for removing Cr(III) and Cr(VI) from aqueous solutions. The results from the pH envelope studies show that Cr(III) and Cr(VI) adsorption occur with two distinct pH envelope patterns. While anionic Cr(VI) removal is favored under acidic conditions, the maximum cationic Cr(III) removal occurs under alkaline conditions. These results indicate that removing aqueous chromium is primarily driven by the electrostatic attraction between the sorbate ions and the active functional groups on the adsorbent surface, followed by the surface complexation reactions. Adsorption isotherm studies for both chromium

species show that the experimental data align better with the Freundlich model than the Langmuir model. This result implies that mushroom surfaces possess multiple active sites for binding cationic and anionic chromium species. Therefore, mushroom powders hold potential as a low-cost adsorbent for removing chromium from contaminated waters with a prior understanding of the oxidation states of dissolved chromium.

Acknowledgments

The authors are grateful to the Wazed Miah Science Research Centre, Jahangirnagar University, Savar, Dhaka, for providing the analytical facility with the atomic absorption spectroscopy.

Disclosure statement

The authors do not have any conflict of interest regarding the publication of this manuscript.

References

Alluri HK, Ronda SR, Settalluri VS, Bondili JS, Suryanarayana V and Venkateshwar P. Biosorption: An eco-friendly alternative for heavy metal removal. *Afr. J. Biotechnol.* 2007; 6(25): 2924-2931.

Azimi A, Azari A, Rezakazemi M and Ansarpour M. Removal of heavy metals from industrial wastewaters: a review.*Chem.Bio.Eng. Rev*. 2017; 4(1): 37-59.

Bhatnagar Amit and Sillanpää M. Utilization of agro-industrial and municipal waste materials as potential adsorbents for water treatment-A review. *Chem. Eng. J.* 2010; 157(2-3): 277-296.

Bhatti HN, Mumtaz B, Hanif MA and Nadeem R. Removal of Zn(II) ions from aqueous solution using Moringa oleifera Lam. (horseradish tree) biomass. *Process Biochem*. 2007; 42(4): 547-553.

Bradl HB. 2005. Sources and origins of heavy metals. In: Interface Science and Technology. Elsevier. 2005; p.1-7.

Carolin CF, Kumar PS, Saravanan A, Joshiba GJ and Naushad M. Efficient techniques for the removal of toxic heavy metals from aquatic environment: A review. *J. Environ. Chem. Eng*. 2017; 5(3): 2782-2799.

Chen GQ, Zeng GM, Tu X, Huang GH and Chen YN. A novel biosorbent: characterization of the spent mushroom compost and its application for removal of heavy metals. J. Environ. Sci. 2005; 17(5): 756-760.

Das N. Heavy metals biosorption by mushrooms. *Nat. Prod. Radiance.* 2005; 4: 454-459.

Ertugay N and Bayhan YK. Biosorption of Cr (VI) from aqueous solutions by biomass of Agaricus bisporus. *J. Hazard. Mater*. 2008; 154(1-3): 432-439.

Ertugay N and Bayhan YK. The removal of copper (II) ion by using mushroom biomass (Agaricus bisporus) and kinetic modelling. *Desalination* 2010; 255(1-3): 137-142.

Fernández-López JA, Angosto JM and Avilés MD. Biosorption of hexavalent chromium from aqueous medium with opuntia biomass. *Sci. World J*. 2014; ID 670249: 1-8.

Finlay RD, Mahmood S, Rosenstock N, Bolou-Bi EB, Köhler SJ, Fahad Z, Rosling A, Wallander H, Belyazid S, Bishop K and Lian B. Biological weathering and its consequences at different spatial levels–from nanoscale to global scale. *Biogeosciences* 2020; 17(6): 1507-1533.

Guimarães T, Paquini LD, Ferraz BRL, Profeti LPR and Profeti D. Efficient removal of Cu (II) and Cr (III) contaminants from aqueous solutions using marble waste powder. *J. Environ. Chem. Eng.* 2020; 8(4): 103972.

Gupta VK, Shrivastava AK and Jain N. Biosorption of chromium (VI) from aqueous solutions by green algae Spirogyra species. *Water Res.* 2011; 35(17): 4079-4085.

Jing X, Cao Y, Zhang X, Wang D, Wu X and Xu H. Biosorption of Cr (VI) from simulated wastewater using a cationic surfactant modified spent mushroom. *Desalination* 2011; 269(1-3): 120-127.

Kanamarlapudi SLRK, Chintalpudi VK and Muddada S. Application of biosorption for removal of heavy metals from wastewater. *Biosorption* 2018; 18(69): 69-116.

Khan MKA, Alam M, Islam MS, Hassan MQ and Al-Mansur MA. Environmental pollution around Dhaka EPZ and its impact on surface and

groundwater. *Bangladesh J. Sci. Ind. Res*. 2011; 46(2): 153-162.

Kumari P, Sharma P, Srivastava S and Srivastava MM. Biosorption studies on shelled Moringa oleifera Lamarck seed powder: Removal and recovery of arsenic from aqueous system. *Int. J. Miner. Process*. 2006; 78(3): 131-139.

Langmuir D. Aqueous Environmental Geochemistry. Prentice-Hall. Inc., *New Jersey* 1997; p. 343-402

Lima ÉC, Adebayo MA and Machado F. Kinetic and equilibrium models of adsorption. In: Carbon Nanomaterials as Adsorbents for Environmental and Biological Applications. *Springer* 2015; p. 33-69.

Mathialagan T, Viraraghavan T and Cullimore, DR. Adsorption of cadmium from aqueous solutions by edible mushrooms (Agaricus bisporus and Lentinus edodes). *Water Qual. Res. J. Canada* 2003; 38(3): 499–514.

Michalak I, Chojnacka K and Witek-Krowiak A. State of the art for the biosorption process—a review. *Appl. Biochem. Biotechnol*. 2013; 170: 1389-1416.

Nuhoglu Y, Malkoc E, Gurses A and Canpolat, N. The removal of Cu (II) from aqueous solutions by Ulothrix zonata. *Bioresour. Technol*. 2002; 85(3): 331-333.

Papassiopi N, Vaxevanidou K, Christou, C, Karagianni E and Antipas GSE. Synthesis, characterization and stability of Cr (III) and Fe (III) hydroxides. *J. Hazard. Mater*. 2014; 264: 490-497.

Parkhurst DL and Appelo CAJ. Description of input and examples for PHREEQC version 3--a Computer program for speciation, batch-reaction, one-dimensional transport, and inverse geochemical calculations: U.S. Geological Survey techniques and methods, USGS 2013.

Prasad YL and Sachin DR. Biosorption of Cu , Zn , Fe , Cd , Pb and Ni by Non-Treated Biomass of Some Edible Mushrooms. *Asian J. Exp. Biol. Sci.* 2013; 4(2): 190-195.

Rahman MS, Saha N and Molla AH. Potential ecological risk assessment of heavy metal contamination in sediment and water body around Dhaka export processing zone, Bangladesh. *Environ. Earth Sci.* 2014; 71: 2293-2308.

Reddy DHK, Harinath Y, Seshaiah K and Reddy AVR. Biosorption of Pb(II) from aqueous solutions using chemically modified Moringa oleifera tree leaves. *Chem. Eng. J.* 2010; 162(2): 626-634.

Reddy DHK, Ramana DKV, Seshaiah K and Reddy AVR. Biosorption of Ni(II) from aqueous phase by Moringa oleifera bark, a low cost biosorbent. *Desalination* 2011; 268(1-3): 150-157.

Sabur MA. Interactions of Phosphate and Silicate with Iron oxides in Freshwater Environments. *University of Waterloo* 2019.

Sag Y and Kutsal T. Recent trends in the biosorption of heavy metals: A review. Biotechnol. *Bioprocess Eng.* 2001; 6: 376-385.

Say R, Denizli A and Arıca MY. Biosorption of cadmium (II), lead (II) and copper (II) with the filamentous fungus Phanerochaete chrysosporium. *Bioresour. Technol*. 2001; 76(1): 67-70.

Shakoor MB, Niazi NK, Bibi I, Shahid M, Saqib ZA, Nawaz MF, Shaheen SM, Wang H, Tsang DCW, Bundschuh J, Ok YS and Rinklebe J. Exploring the arsenic removal potential of various biosorbents from water. *Environ. Int.* 2019; 123: 567-579.

Suseem SR and Mary Saral A. Biosorption of heavy metals using mushroom Pleurotus eous. *J. Chem. Pharm. Res.* 2014; 6(7): 2163-2168.

Szabó M, Kalmár J, Ditrói T, Bellér G, Lente G, Simic N and Fábián I. Equilibria and kinetics of chromium (VI) speciation in aqueous solution–a comprehensive study from pH 2 to 11. *Inorganica Chim. Acta* 2018; 472: 295-301.

Uluozlu OD, Sari A, Tuzen M and Soylak M. Biosorption of Pb(II) and Cr(III) from aqueous solution by lichen (Parmelina tiliaceae) biomass. Bioresour. *Technol*. 2008; 99(8): 2972-2980.

Vimala R and Das N. Biosorption of cadmium (II) and lead (II) from aqueous solutions using mushrooms: A comparative study. *J. Hazard. Mater*. 2009; 168(1): 376-382.

Wuana RA and Okieimen FE. Heavy metals in contaminated soils: a review of sources, chemistry, risks and best available strategies for remediation. *Isrn Ecol*. 2011; ID 402647: 1-20.

J. Bangladesh Acad. Sci. 47(2); 277-278: December 2023 DOI:https://doi.org/10.3329/jbas.v47i2.67774

Journal of Bangladesh Academy of Sciences

Journal homepage: http://www.bas.org.bd/publications/jbas.html

Short Communication

A new addition of bright babul blue - *Azanus ubaldus* - stoll, 1782 (Lepidoptera: Lycaenidae) for Bangladesh

Akash Mojumdar*, Md. Naim Ur Rashid[1], Md. Imrul Kayes[2], Umma Kadija[3], Md. Najmul Hossain[4]

Department of Computer Science and Information Technology, Shanto-Mariam University of Creative Technology, Dhaka, Bangladesh

ARTICLE INFO

Article History

Received: 25 July 2023
Revised: 07 September 2023
Accepted: 18 October 2023

Keywords: Butterfly, Bright Babul Blue, *Azanus ubaldus*, New record, Distribution, Bangladesh.

ABSTRACT

The Bright Babul Blue, scientifically known as *Azanus ubaldus* (Stoll, 1782), has been observed for the first time in the Premtoli Social Forestation Area (N 24.387555, E 88.404246), Godagari Upazila, Rajshahi district, Bangladesh. This finding adds to our understanding of the butterfly's distribution and underscores the importance of conserving the unique biodiversity within the Premtoli Social Forestation Area.

Introduction

Bangladesh has a diverse and abundant butterfly fauna due to its tropical climate (Chowdhury and Hossain, 2013; Larsen, 2004). Edition 7 of the IUCN (2015) Red List for Bangladesh documented 305 butterfly species spanning 10 families. The recent identification of *Azanus ubaldus* (Stoll, 1782) belonging to the Lycaenidae family adds to the country's diverse butterfly records. On November 25th, 2022, a momentous discovery was made, recording the first sighting of the butterfly species at the Premtoli Social Forestation Area in Godagari Upazila, Rajshahi district, Bangladesh (N 24.387555, E 88.404246).

Bangladesh's diverse biogeography and abundant biodiversity make it a haven for butterflies, boasting remarkable species richness. Preserving their natural habitats is vital to protecting the country's ecological treasure. Godagari Upazila, situated in Rajshahi district, covers an area of approximately 472.13 square kilometers. It is geographically located between 24°21' and 24°36' north latitudes and between 88°17' and 88°33' east longitudes. This region's unique location and diverse geography contribute to its ecological significance and provide an ideal habitat for various plant and animal species, including the recently recorded butterfly species, *Azanus ubaldus*, from (N 24.387555, E 88.404246) (Fig. 1).

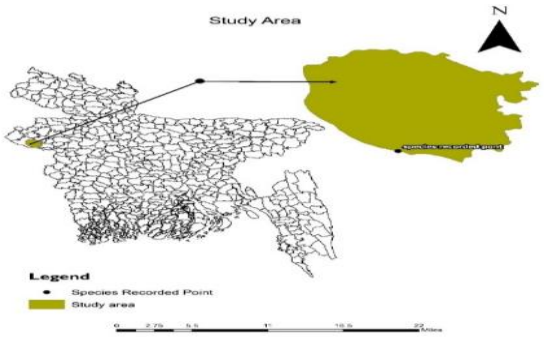

Fig. 1. Map of the study area

The Bright Babul Blue can be found in open, sunny habitats such as grasslands, scrublands, and coastal dunes. Its flight path is often irregular, and it is often seen darting between low-lying foliage and flowers (Fig. 2).

*Corresponding author:<akashmojumdar99@gmail.com>

[1]*Department of Environmental Science, Stamford University, Dhaka, Bangladesh;* [2]*Department of Ceramics and Sculpture, University of Rajshahi, Rajshahi, Bangladesh;* [3]*Department of Banking and Insurance, University of Rajshahi, Rajshahi, Bangladesh;* [4]*Department of Marketing University of Rajshahi, Rajshahi, Bangladesh*

Fig. 2. Habitat of *Azanus ubaldus* (Stoll, 1782)

Fig. 3. *Azanus ubaldus* (Stoll, 1782)

The study spanned three days, from November 23 to November 25, 2022. During this period, butterflies were systematically observed and documented, adhering to the prescribed methodologies outlined by Pollard (1977), Pollard and Yates (1993). Observations were conducted in the morning between 9:00 a.m. and 5:00 p.m. The identification of butterflies was primarily done through direct observation, and photo evidence was captured using a Nikon d7100 camera equipped with a 70–300 mm lens.

Members of the genus *Azanus*, belonging to the family Lycaenidae, are exceptionally rare in Bangladesh. Until the recent discovery, *Azanus ubaldus* (Stoll, 1782) had not been mentioned in any published literature or identified from collected preserved specimens in Bangladesh. However, on November 25th, 2022, at 12:40 pm +06 GMT, a significant event occurred as a single individual of *Azanus ubaldus* was first recorded in the Premtoli Social Forestation Area, located in Godagari Upazila, Rajshahi district, Bangladesh (N 24.387555, E 88.404246). This observation marks the first confirmed record of the species in the country's butterfly fauna and contributes to our understanding of the butterfly diversity in the region.

Azanus ubaldus has a modest wingspan of 25 to 30 mm, with rounded wings, a curled outer edge, and a long, slender tail protruding from the hindwing. Prominent white markings and a rare blueish-grey color can be seen on the wings (Kehimkar, 2016). The butterfly's venation follows the typical Lycaenidae family pattern, containing a prominent subcostal vein perpendicular to the costa and a brief discal cell. The butterfly's long, slender, black-tipped antennae with a white base are equipped with tiny, hair-like structures that resemble setae in males (Fig. 3).

The type is from India, but the species is also widespread in Arabia and Africa (Larsen, 2004).

The discovery of the *Azanus ubaldus* (Stoll, 1782) butterfly underscores the importance of conservation efforts in Bangladesh, a country abundant in diverse flora and fauna. Despite its biodiversity, many species in Bangladesh remain unidentified or need further study. This finding of a new butterfly species adds to the growing list of discoveries in the country, emphasizing the necessity for increased attention and protection of its unique natural heritage.

References

Chowdhury SH and Hossain M. *Butterflies of Bangladesh: A Pictorial Handbook.* 2nd ed. Dhaka, Bangladesh: Skylark Printers; 2013. p.260.

IUCN Bangladesh. *Red List of Bangladesh, Volume 7: Butterflies*, IUCN (International Union for Conservation of Nature Bangladesh) Bangladesh Country Office, Dhaka, Bagnaladesh; 2015, p. 400.

Kehimkar I. *Butterflies of Indian.* Mumbai: Bombay Natural History Society; 2016, p-519.

Larsen TB. *An annotated checklist of the butterflies of Bangladesh (lepidoptera, rhopalocera).* Dhaka, Bangladesh: IUCN (International Union for Conservation of Nature Bangladesh) Bangladesh Country Office; 2004. p.158.

Pollard E. A method for assessing changes in the abundance of butterflies. *Biol. Conserv.*, 1977; 12(2): 115-134.

Pollard E and Yates V. *Monitoring Butterflies for Ecology and Conservation.* Chapman and Hall, London, UK: Springer Dordrecht; 1993, p-292.

INSTRUCTION FOR AUTHORS

The Journal of Bangladesh Academy of Sciences is published four times a year in March, June, September and December. Original research articles, review articles, and short communications of high standards of all branches of Science and Technology are considered for publication in this journal. Review articles are generally by invited authors; however, the Editor welcomes suggestions of potential topics and potential authors.

The following instructions must be followed while preparing the manuscript intended for publication in this journal:

1. **Research Article:** Manuscripts should be concise and consistent with the style of the journal. The manuscript must be typed using Times New Roman font, size 12 on A4 size page, and wide (1 inch) margins on all four sides. The main text must be typed in a two-column format with 1.5 spacing, and for full papers, it should not exceed 10-20 typed pages, including figures, tables, and references. In general, an article may contain the following sub-titles in sequence: **Title, Abstract, Keywords, Introduction, Materials and Methods, Results and Discussion, Acknowledgement (**if any), and **References.**

A. Title: The first page of the paper, the title page, should have the title and the names of the authors. The title should be brief and specific. Abbreviations and formulae should be avoided where possible. The next line in italics should be the authors' affiliation addresses (where the actual work was done) below the names. Indicate all affiliations with a lowercase superscript letter immediately after the author's name and in front of the appropriate address. The corresponding author, along with email address, should be indicated at the footnote with a proper asterisk.

B. The second page should carry the Title of the paper, Abstract, and Keywords. Author(s) name must not be typed on this page.

(i) Abstract: It should not exceed 150 words and should briefly state the purpose of the research, the significant results, and meaningful conclusions. Nonstandard or uncommon abbreviations should be avoided, but if essential, they must be defined at their first mention in the abstract itself.

(ii) Keywords: Immediately after the abstract, provide a maximum of 6 keywords.

C. The next pages (a maximum of 15 printed pages), will contain the main text of the paper.

(i) Introduction: It should be concise and relevant to the objectives of the study. The importance of the research work described should be pointed out. An appropriate review of the current literature should be made to identify the frontier of existing knowledge and point out the need for further work. The knowledge contributed to the study should be mentioned.

(ii) Materials and Methods: Materials used should be mentioned precisely along with their sources and any pre-treatment undertaken.

The description of methods must be brief but clear enough to enable a reader to reproduce the results. References must be considered sufficient for methods described in earlier publications: only relevant modifications should be described.

It is recommended that authors use the nomenclature and symbols adopted by IUPAC document UIFII (S.U.N. 65-3) 1965, symbols, units, and nomenclature in Physics or by IUPAC Manual of Physiochemical symbols,

Terminology and similarly for other disciplines.

(iii) Results and Discussion: This section should include descriptions of results obtained with the help of figures, tables, graphs, and photographs as may be necessary. Tables should have a descriptive title. Large and cumbersome tables should be avoided. Figures and graphs should be prepared and should be properly labelled with bold solid lines such that no further size reduction will be necessary. The paper should contain a minimum number of **Tables, Graphs,** and **Figures.** The same data should not be depicted using both tables and figures. The photographs are to be submitted in JPEG format.

The discussion should include thorough analysis and interpretation of results, and comparison with existing relevant published results, if any, and self-evaluation of the new knowledge contributed, avoiding extensive citations and discussion of published literature.

(iv) Conclusions

The study's main conclusions may be presented in a short Conclusions section, which may stand alone or form a part of the Results and Discussion section.

(v) Acknowledgment: The following support for the research work should be acknowledged:

- Funding by any agency;
- The use of instruments in a laboratory other than those of the authors;
- Individual's help during the research (e.g., providing an interpretation of results, language help, writing assistance, or proofreading, etc.).

(vi) Author contributions

For transparency, we encourage authors to submit an author contribution statement outlining each author's contributions to the paper. The authors should have participated sufficiently in the work to take public responsibility for appropriate portions of the content.

(vii) References and Text Citations:

In the text, references should be cited within brackets quoting the first author's surname followed by et al. if necessary and the year of publication in the appropriate place, e.g. (Bhuiyan, 2020), Khan et al. (2021) or (Khan et al., 2021). In the case of only two authors, surnames of both need to be mentioned, e.g., (Khan and Rahman, 2021). A semi colon should separate two or more references when putting within the same bracket. At the end of the manuscript, references should be listed and arranged alphabetically according to the first author's surname according to the style described below:

(a) Journal article:

In each reference, names of all authors' will have to be given in the same style, e.g., surname followed by initials, lumped together without using a full stop. The names will be followed by the full title of the article and the journal's abbreviated title (in italics). The year of publication will be given next, followed by volume number (issue number) and page ranges. For abbreviations of the names of journals, authors are advised to follow the *World List of Scientific Periodicals.* For online publications, the URL address must be given. Note: Please list ALL authors' names in the list of references, do not use (et al.). **Examples:**

Islam S. The Induced Morphological and Root Anatomical Changes in Lentil. *J. Bangladesh Acad. Sci.* 2019; 43(2):107-112.

James BD and Bennett DA. Causes and Patterns of Dementia: An Update in the Era of Redefining

Alzheimer's Disease. *Annu. Rev. Public Health;* 2019; 40: 65-84.

Moniruzzaman M, Khatoon R and Qamruzzaman AKM. Influence of Plant growth Regulators on Vegetative Growth, Sex Expression and Yield of Summer Bottle Gourd. *Bangladesh J. Agril. Res*. 2019; 44(4): 577-590.

(b) Book or Chapter in a Book:

The place and name of the publisher, year of publication, will have to be given in addition to the name of the author(s), the title of the book (in italics), edition number (if not first), and the number of pages. In the case of an article or chapter in a book or proceedings of a conference, author(s) name and the title of the article or chapter will be followed by the title of the book (in italics), the names of the editors of the book, edition number (if not first), the place and name of the publisher, year of publication and page or page numbers of chapter. **Examples:**

Book:

Carlson BM. *Human Embryology and Developmental Biology*. 4th ed. St. Louis: Mosby; 2009. p. 541.

Cassese A, Acquaviva G, Fan M and Whiting A. *International Criminal Law: Cases and Commentary*. Oxford University Press; 2011, p. 600.

Chapter in an edited book:

Muhammad HFL and Dickinson KM. Nutrients, energy values and health impact of conventional beverages, Chapter 3. In: *The Science of Beverages*, *Volume 12: Nutrients in Beverages*. Grumezescu AM, Holban AM, eds., Elsevier Science; 2019; pp. 77-109.

Balsam KF, Martell CR, Jones KP, Safren SA. Affirmative cognitive behavior therapy with sexual and gender minority people. In: *Culturally Responsible Cognitive Behavior Therapy: Practice and Supervision*. Iwamasa GY, Hays PA, eds., 2nd edition, American Psychological Association. 2019; p. 287-314.

(c) Proceedings of a Conference:

Luca J and Tarricone P. Does emotional intelligence affect successful teamwork? In: *Meeting at the Crossroads*. Kennedy G, Keppell M, McNaught C (eds.), Proceedings of the 18th Annual Conference of the Australasian Society for Computers in Learning in Tertiary Education, 2001 Dec 9-12; Melbourne: Biomedical Multimedia Unit, The University of Melbourne; 2001. pp. 367-376.

(d) Reports:

Bangladesh Bureau of Statistics (BBS). Population census - 2011. Preliminary report. Bangladesh Bureau of Statistics, Ministry of Planning, Government of the People's Republic of Bangladesh, Dhaka, 2011.

Rowe IL and Carson NE. *Medical manpower in Victoria. East Bentleigh (AU)*: Monash University, Department of Community Practice; 1981. p. 35. Report No.: 4.

2. **Short communication:** Important research findings that may initiate further research in the relevant field may be published in the form of a short communication. This should not exceed three printed pages (900 words), including Graphs, Tables, and Figures. The presentation should be continuous and paragraphed, i.e., without headings like Introduction, Materials, and Methods, etc. A short communication paper should have an **Abstract** containing the gist of the article and should not exceed 60 words, followed by **Keywords.**

3. **Declarations:** While submitting, the corresponding **a**uthor will have to make a declaration mentioning the laboratory/laboratories in which the work was carried out and certifying that the contents of the paper were not published before or submitted for publication in any other journal and that all the co-authors have given their consent for the article to be considered by the Editorial Board for publication in the Journal of Bangladesh Academy of Sciences.

Declaration of conflicting interests

The corresponding author must provide a formal conflict of interest statement for all authors disclosing any financial and personal relationships with other people or organizations that could inappropriately influence (bias) their work. If no conflict exists, please state that 'The author(s) declare(s) that they have no conflicts of interest regarding the publication of this article.'

4. The manuscript should be submitted in pdf or MS Word or LaTex files through online at www.bas.org.bd/publications/jbas.html. Equations generated by using Math Type or Math ML should be incorporated in the text.

   Soft copies of manuscripts with tables, graphs, illustrations, and photographs placed correctly in a printable format are to be submitted. Authors wishing to publish coloured schemes/diagrams/ sketches/photographs in their papers need to pay for the printing charges of one format. This will be charged only after the acceptance of the manuscripts for publication in the JBAS.

   The manuscript submitted should also contain a separate list of tables, figures, illustrations, photographs, and sketches with appropriate captions.

5. Electronic versions of final galley proofs will be sent to authors. No alteration in the title or additions in the text is desirable at this stage.

6. All correspondence for publication should be made on www.bas.org.bd/publications/jbas.html to the **Editor, Journal of Bangladesh Academy of Sciences, National Science and Technology Complex, Agargaon, Dhaka 1207.**

N.B.: No paper will be accepted for publication if it does not conform to the style specified for the journal and approved by the Editorial Board, which has the authority to accept or reject the manuscript of a paper submitted without showing any reason.